✓VOLUME 77 MARCH 29, 1973 NUMBER 7

JPCHAx

THE JOURNAL OF PHYSICAL CHEMISTRY

PUBLISHED BIWEEKLY BY THE AMERICAN CHEMICAL SOCIETY

THE JOURNAL OF

PHYSICAL CHEMISTRY

AMERICAN CHEMICAL SOCIETY, *1155 Sixteenth St., N.W., Washington, D. C. 20036*

Books and Journals Division

JOHN K CRUM *Director*
RUTH REYNARD *Assistant to the Director*

CHARLES R. BERTSCH *Head, Editorial Processing Department*
D. H. MICHAEL BOWEN *Head, Journals Department*
BACIL GUILEY *Head, Graphics and Production Department*
SELDON W. TERRANT *Head, Research and Development Department*

 Published biweekly by the American Chemical Society at 20th and Northampton Sts., Easton, Pa. 18042. Second-class postage paid at Washington, D. C., and at additional mailing offices.

All manuscripts should be sent to *The Journal of Physical Chemistry*, Department of Chemistry, University of Minnesota, Minneapolis, Minn. 55455.

Additions and Corrections are published once yearly in the final issue. See Volume 76, Number 26 for the proper form.

Extensive or unusual alterations in an article after it has been set in type are made at the author's expense, and it is understood that by requesting such alterations the author agrees to defray the cost thereof.

The American Chemical Society and the Editor of *The Journal of Physical Chemistry* assume no responsibility for the statements and opinions advanced by contributors.

Correspondence regarding accepted copy, proofs, and reprints should be directed to Editorial Processing Department, American Chemical Society, 20th and Northampton Sts., Easton, Pa. 18042. Head: CHARLES R. BERTSCH. Assistant Editor: EDWARD A. BORGER. Editorial Assistant: JOSEPH E. YURVATI.

Advertising Office: Centcom, Ltd., 142 East Avenue, Norwalk, Conn. 06851.

Business and Subscription Information

Remittances and orders for subscriptions and for single copies, notices of changes of address and new professional connections and claims for missing numbers should be sent to the Subscription Service Department, American Chemical Society, 1155 Sixteenth St., N.W., Washington, D. C. 20036. Allow 4 weeks for change of address. Please include an old address label with the notification.

Claims for missing numbers will not be allowed (1) if received more than sixty days from date of issue, (2) if loss was due to failure of notice of change of address to be received before the date specified in the preceding paragraph, or (3) if the reason for the claim is "missing from files."

Subscription rates (1973): members of the American Chemical Society, $20.00 for 1 year; to nonmembers, $60.00 for 1 year. Those interested in becoming members should write to the Admissions Department, American Chemical Society, 1155 Sixteenth St., N.W., Washington, D. C. 20036. Postage to Canada and countries in the Pan-American Union, $5.00; all other countries, $6.00. Single copies for current year: $3.00. Rates for back issues from Volume 56 to date are available from the Special Issues Sales Department, 1155 Sixteenth St., N.W., Washington, D. C. 20036.

This publication and the other ACS periodical publications are now available on microfilm. For information write to MICROFILM, Special Issues Sales Department, 1155 Sixteenth St., N.W., Washington, D. C. 20036.

Notice to Authors last printed in the issue of November 23, 1972

THE JOURNAL OF
PHYSICAL CHEMISTRY

Volume 77, Number 7 March 29, 1973

JPCHAx 77(7) 863-972 (1973)

COMMUNICATIONS TO THE EDITOR

AUTHOR INDEX

In papers with more than one author the name of the author to whom inquiries about the paper should be addressed is marked with an asterisk in the by-line.

THE JOURNAL OF
PHYSICAL CHEMISTRY

VOLUME 77, NUMBER 7 MARCH 29, 1973

Reactions of O(^{1}D) with Methane and Ethane[1]

C.-L. Lin and W. B. DeMore*

Jet Propulsion Laboratory, California Institute of Technology, Pasadena, California 91103 *(Received October 6, 1972)*

Publication costs assisted by The California Institute of Technology

Gas-phase reactions of O(^{1}D) with CH_4 and with C_2H_6 were studied by the photolyses of N_2O–CH_4 and N_2O–C_2H_6 mixtures using 1849-Å light. Pressure effects and radical scavenging techniques were used to identify the sources of the products. At low pressures, where stabilization of excited alcohol intermediates did not occur, the main path of the O(^{1}D) + CH_4 reaction was to form CH_3 + OH radicals, which ultimately produce C_2H_6. Molecular elimination giving H_2 + CH_2O occurred to the extent of 9%, which is the same as when the reaction takes place in liquid Ar at 87°K. The main path of the O(^{1}D) + C_2H_6 reaction was to form C_2H_5 + OH and CH_3 + CH_2OH radicals, which ultimately produce n-C_4H_{10}, C_3H_8, and C_2H_6 as principal products. The total reaction does not proceed *via* ROH* intermediates. The OH radicals are produced both by fission of such intermediates and by direct abstraction of H atoms, in agreement with the results of Cvetanovic and coworkers. Comparison with previous results in liquid argon indicates that the condensed medium suppresses the abstraction reaction in favor of the insertion reaction. The molecular process giving CH_2O + H_2 also does not involve the CH_3OH* intermediate, as shown by the fact that this path contributes equally both in the gas and liquid phases.

Introduction

The reaction of the excited atomic oxygen O(^{1}D) with hydrocarbons has been a matter of great interest both in upper atmosphere chemistry and from the viewpoint of chemical kinetics. Yet even the simple reaction of O(^{1}D) with methane, which may be an important source of OH in the upper atmosphere,[2] is not fully understood, particularly in regard to the details of the primary processes. Different and even contradictory experimental results have been put out from several laboratories.[3-6] This reaction was first studied by Basco and Norrish[3a] who proposed that the abstraction reaction

$$O(^1D) + CH_4 \longrightarrow CH_3 + OH$$

is the primary process based on their observations of vibrationally excited OH in the photolyses of O_3–CH_4 mixtures in the gas phase.

In previous work in this laboratory, DeMore and Raper[3b] investigated this reaction by photolyzing O_3–CH_4 mixtures dissolved in liquid argon and found that the insertion leading to CH_3OH, *i.e.*

$$O(^1D) + CH_4 \longrightarrow CH_3OH$$

is the major path. In addition, both molecular elimination of hydrogen, *i.e.*

$$O(^1D) + CH_4 \longrightarrow H_2 + HCHO$$

and OH abstraction occurred to some extent. It was suggested by DeMore[3c] that the abstraction reaction could be viewed as occurring through the excited ROH* intermediate. This was inferred from studies of the reactions between O(^{1}D) and higher alkanes which indicated that the excited alcohols formed from the insertion of O(^{1}D) into the C–H bonds of ethane, propane, and isobutane could be completely stabilized in liquid argon medium at 87°K.

From a series of experiments on the reactions of O(^{1}D) with propane,[7a] isobutane,[7b] neopentane,[7c] and cyclopen-

(1) This paper presents the results of one phase of research carried out at the Jet Propulsion Laboratory, California Institute of Technology, under Contract No. NAS 7-100, sponsored by the National Aeronautics and Space Administration.

(2) (a) M. Nicolet, *Ann. Geophys.*, **26**, 531 (1970); (b) R. P. Lowe and D. McKinnon, *Can. J. Phys.*, **50**, 668 (1972).

(3) (a) N. Basco and R. G. W. Norrish, *Can. J. Chem.*, **38**, 1769 (1960); (b) W. B. DeMore and O. F. Raper, *J. Chem. Phys.*, **46**, 2500 (1967); (c) W. B. DeMore, *J. Phys. Chem.*, **73**, 391 (1969).

(4) J. N. Bradley, A. D. Edwards, and J. R. Gilbert, *J. Chem. Soc. A*, 326 (1971).

(5) R. I. Greenberg and J. Heicklen, *Int. J. Chem. Kinet.*, **4**, 417 (1972).

(6) F. I. Vilesov and A. M. Fravilov, *High Energy Chem.*, **4**, 475 (1970).

tane[7d] in the gas phase, Cvetanovic and his coworkers have concluded that the interactions of $O(^1D)$ with paraffins proceed in three distinct ways: (1) by insertion into the C-H bonds of paraffins to form vibrationally excited alcohols, which undergo fragmentation if not stabilized by collisions; (2) by abstraction of H atoms to form OH and alkyl radicals; and (3) molecular elimination of H_2, in accord with the findings of DeMore and Raper[3b] on methane. They also established that the lifetimes of the hot alcohols increase with the number of carbon atoms in the paraffin molecules (from about 10^{-11} sec for the hot propyl alcohols to 4×10^{-9} sec for the hot neopentyl alcohol).

A recent study by Bradley, *et al.*,[4] on the reaction of $O(^1D)$ and CH_4, by photolysis of N_2O–CH_4 mixtures with 1849-Å light, supported the correctness of the insertion reaction leading to CH_3OH^* as the major path. Yet it was necessary for them to postulate a nitrous oxide-photosensitized decomposition of methane to account for the excess H_2 formation over the oxygenated products, *i.e.*

$$N_2O + h\nu \longrightarrow N_2O^*$$

$$N_2O^* + CH_4 \longrightarrow CH_3 + H + N_2O$$

$$H + CH_4 \longrightarrow CH_3 + H_2$$

On the other hand, Greenberg and Heicklen[5] studied this reaction by photolyzing N_2O–CH_4 mixtures with the 2139-Å zinc resonance line and failed to detect H_2. They further asserted that the abstraction reaction producing exclusively CH_3 and OH radicals is the lone primary step and attributed the yield of CH_3OH to recombination of CH_3 and OH.

In their complex analysis of the data in the photolysis of O_2–CH_4 mixtures in the spectral range 1550–1925 Å, Vilesov and Pravilov[6] attributed the production of CH_3OH to the direct insertion of $O(^1D)$ to CH_4 and concluded that the excited CH_3OH^* molecules thus formed are easily deactivated, requiring less than 10 Torr of pressure for complete stabilization.

For the $O(^1D)$ reaction with ethane, in addition to the above-mentioned reaction paths, a reaction involving removal of two H atoms

$$O(^1D) + C_2H_6 \longrightarrow C_2H_4 + H_2O$$

also occurs to a small extent.[3c] This reaction was originally postulated by Castellion and Noyes[8a] and Murad and Noyes[8b] in their study of the photolysis of N_2O–C_2H_6 mixtures to account for the quantity of C_2H_4 in the products.

To further understand the reaction mechanism, to narrow down the above-quoted conflicting experimental results, and to bridge the gap between the gas- and liquid-phase reaction, we have extended the previous work in this laboratory into the gas phase. The technique was to photolyze the N_2O–CH_4 and N_2O–C_2H_6 mixtures with 1849-Å light and measure the reaction products gas chromatographically.

Experimental Section

The photolyses were carried out in a cylindrical stainless steel cell 2 cm i.d. and 5 cm long fitted with 10-mm thick quartz windows at each end and made vacuum tight by means of indium gaskets. The cell was designed to operate at pressures up to 3000 psi. All the experiments were done at room temperature (22°).

The source of 1849-Å light was a low-pressure mercury lamp used in the previous work.[3b,c] All data were taken without optical filtering or light collimation, except in some experiments an ozone filter made of a 1-cm path length cell filled with 25 psi O_2 and cooled to −15° by a circulating 2-propanol coolant was used to block the 2537-Å radiation. This was accomplished when O_2, absorbed the 1849-Å light, dissociated into O atoms, and recombined with O_2 to produce O_3. Under normal conditions, an optical density at 2537 Å greater than 3.3 could be achieved. The use of an ozone filter is necessary for the experiments using O_2 as the radical scavenger to prevent 2537-Å light from photolyzing O_3, thus producing additional $O(^1D)$ atoms. The O_3 was formed from the $O + O_2 + M$ reaction where O atoms were produced from the photolysis of O_2 by 1849-Å light. In addition, an iodine lamp powered by a microwave discharge was used as an alternative source. The 2062-Å iodine line was used primarily to check whether there was any mercury photosensitized reaction involved in the mercury lamp photolysis of N_2O–paraffin mixtures as well as to check the consistency of the experimental data.

Although the 1849-Å light (155 kcal/mol) has more than enough energy to produce $O(^1S)$ atoms from N_2O (135 kcal/mol), the works of Preston and Cvetanovic[9] and Greenberg and Heicklen[10] provided ample evidence that the photolysis of N_2O by 1849-Å light produces exclusively $O(^1D)$ atoms. This was clarified and explained in the semiempirical calculation on the potential curves of N_2O bv Chutjian and Segal[11] who showed that, in the Franck–Condon region, to excite the N_2O molecule to the $2^1\Sigma^+$ state which correlates to $N_2(X) + O(^1S)$ requires at least 8.43-eV energy, which is far greater than the available energy of 1849-Å light (6.71 eV). The experiments by Preston and Barr[12] also ruled out the importance of the process of nitrogen atom formation (*i.e.*, $N_2O + h\nu \rightarrow NO + N$) which only requires 4.93 eV.

The inert gases, He (Gardner Cryogenics) and Ar (Linde), were taken directly from cylinders. Research grade Matheson CH_4 with less than 15 ppm ethane as impurity and Phillips C_2H_6 of 99.99% purity were used without further purification. Gas chromatographic runs confirmed the factory specifications. The N_2O used was of 98% minimum purity which was further purified by slow passage over Ascarite and condensation at 77°K. Similar purification procedures were performed on SF_6 gas supplied by Allied Chemical.

Typical reactant mixtures used were 10 Torr of N_2O–760 Torr of CH_4 and 10 Torr of N_2O–300 Torr of C_2H_6. With these high alkane to N_2O ratios, the $O(^1D)$ produced from the 1849-Å irradiation reacted mainly with paraffins and the N_2 formed simultaneously served as an internal actinometer without complication from the reaction between $O(^1D)$ and N_2O. Calculations from known rate con-

(7) (a) H. Yamazaki and R. J. Cvetanovic, *J. Chem. Phys.*, **41**, 3703 (1964); (b) G. Paraskevopoulos and R. J. Cvetanovic, *ibid.*, **50**, 590 (1969); (c) G. Paraskevopoulos and R. J. Cvetanovic, *ibid.*, **52**, 5821 (1970); (d) P. Michaud and R. J. Cvetanovic, *J. Phys. Chem.*, **76**, 1375 (1972); (e) G. Paraskevopoulos and R. J. Cvetanovic, *J. Amer. Chem. Soc.*, **91**, 7572 (1969).
(8) (a) G. A. Castellion and W. A. Noyes, Jr., *J. Amer. Chem. Soc.*, **79**, 290 (1957); (b) E. Murad and W. A. Noyes, Jr., *ibid.*, **81**, 6405 (1959).
(9) K. F. Preston and R. J. Cvetanovic, *J. Chem. Phys.*, **45**, 2888 (1966).
(10) R. I. Greenberg and J. Heicklen, *Int. J. Chem. Kinet.*, **2**, 185 (1970).
(11) A. Chutjian and G. A. Segal, *J. Chem. Phys.*, in press.
(12) K. F. Preston and R. F. Barr, *J. Chem. Phys.*, **54**, 3347 (1971).

stants showed that less than 1% of the O(^{1}D) will react with N_2O. To prevent possible secondary reactions, the conversion of paraffins was kept well below 1%.

After irradiation the gases not condensable at liquid nitrogen temperature were collected in a large cylinder and forced, by a piston stroke, into a gas chromatograph column for analysis. The column, a 4 ft × 0.25 in. aluminum tube packed with 13X molecular sieve, was operated at room temperature using He or Ar as the carrier gas, the latter to increase the sensitivity for the detection of H_2. The condensable products were collected in a U-tube and analyzed either on an 8 ft × 0.25 in. Porapak Q or S column at 140°. Ethylene in the presence of excess ethane was analyzed on a silica gel column at room temperature. For the detection of formaldehyde, an 8 ft × 0.25 in. Porapak T column was used at 150°. The identification and quantitative determination were based on the retention times and peak area measurements by comparison with the authentic samples.

Results and Discussion

Reaction between O(^{1}D) and CH_4. For the 10 Torr of N_2O–760 of Torr CH_4 mixtures, the major products were ethane, water, hydrogen, carbon monoxide, and propane. The yields of these products (except water) relative to N_2 as unity are plotted in Figure 1 *vs.* the extent of photolysis expressed as the amount of N_2 produced. Because of the great uncertainty in its measurement, water was not determined quantitatively. The yield of CH_3OH was about 3% and C_2H_5OH 1.5%. Small quantities of CO_2 were also identified but not measured quantitatively. All data were taken without filtration of the light because the results were found to be independent of the presence of the O_3 filter. Some experiments were done using the 2062-Å iodine line instead of 1849-Å mercury light to ascertain that there was no mercury photosensitized reaction. We have also studied pressure effects in the O(^{1}D) + CH_4 reaction by adding more CH_4 to the 10 Torr of N_2O–760 Torr of CH_4 mixture. The CH_3OH yield is shown in Figure 2. The yields of C_2H_6 were not reported because these data were obscured by the C_2H_6 impurity in CH_4. Although the impurity only amounts to several ppm, it becomes an intolerable quantity at high pressures. The yields of noncondensables can not be measured at the high pressure of CH_4. However, some data of CO and H_2 yields were included in Figure 2 using SF_6 as the stabilizing gas, and assuming that the N_2 yield was the same as for irradiation of a 10 Torr of N_2O–760 Torr of CH_4 mixture using the same light intensity and irradiation time. From data presented above and the evidence which will be discussed later, it is appropriate to write the major steps for the photolysis of N_2O–CH_4 mixtures with 1849-Å light as follows

$$N_2O + h\nu \longrightarrow N_2 + O(^1D) \quad (M1)$$

$$O(^1D) + CH_4 \longrightarrow CH_3OH^* \quad (M2a)$$

$$\longrightarrow CH_3 + OH \quad (M2b)$$

$$\longrightarrow H_2 + HCHO \quad (M2c)$$

$$CH_3OH^* + M \longrightarrow CH_3OH + M \quad (M3)$$

$$CH_3OH^* \longrightarrow CH_3 + OH \quad (M4)$$

$$OH + CH_4 \longrightarrow CH_3 + H_2O \quad (M5)$$

$$CH_3 + CH_3 + M \longrightarrow C_2H_6 + M \quad (M6)$$

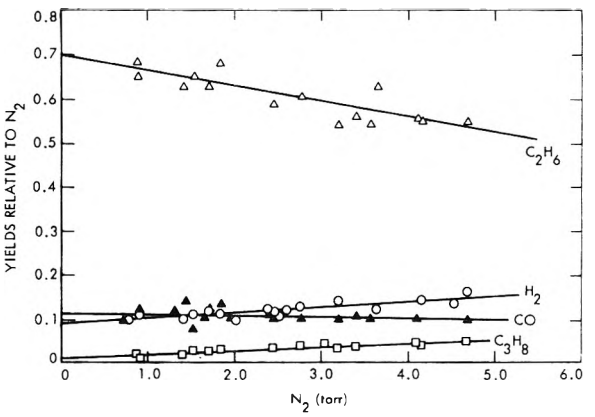

Figure 1. Dependence of major product yields on the extent of the O(^{1}D) + CH_4 reaction (10 Torr of N_2O–760 Torr of CH_4).

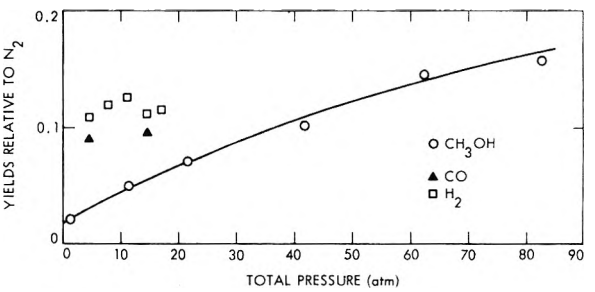

Figure 2. Pressure dependence of some product yields in the O(^{1}D)–CH_4 reaction. The pressurizing gases were CH_4 for the CH_3OH measurements and SF_6 for the H_2 and CO measurements.

The small amount of propane, shown in Figure 1, which increased with increasing extent of reaction, was undoubtedly formed from the recombination of CH_3 and C_2H_5 radicals. The latter resulted from the secondary reaction of OH with the major product, C_2H_6. Calculations from known rate constants[13] for OH + CH_4 ($k = 6.2 \times 10^6$ M^{-1} sec^{-1}) and OH + C_2H_6 (1.8×10^8 M^{-1} sec^{-1}) support this interpretation. The suggestion of Bradley, *et al.*,[4] that C_2H_5 originates from the reaction between O(^{1}D) and C_2H_6 is unlikely as the rate constant[3c] is only about twice that for reaction between O(^{1}D) and CH_4.

For the 10 Torr of N_2O–760 Torr of CH_4 mixture, the 3% yield of CH_3OH came neither from the stabilization of CH_3OH (reaction M3) nor from the recombination of CH_3 and OH radicals

$$CH_3 + OH\ (+M) \longrightarrow CH_3OH\ (+M) \quad (M7)$$

The pressure effect study showed that reaction M3 was not the source, since at the total pressure of 770 Torr, no appreciable amount of CH_3OH^* can be stabilized. This will be discussed further in conjunction with the lifetime estimation of CH_3OH^*. Steady-state calculations based on reactions M1 and M2b (assuming the reaction produced CH_3 + OH only) and the reactions M5 and M6 using a typical experimental absorption intensity of about 2 Torr of N_2/hr and known rate constants[5] ($k_{M2b} = 1.3 \times 10^{11}$, $k_{M5} = 6.2 \times 10^6$, and $k_{M6} = 2.4 \times 10^{10}$ M^{-1} sec^{-1}) showed that $[O(^1D)]_{ss} = 5.7 \times 10^{-18}$ M, $[CH_3]_{ss} = 1.2 \times 10^{-9}$ M, and $[OH]_{ss} = 1.2 \times 10^{-13}$ M. Thus the OH concentration was about four orders of magnitude smaller

(13) F. Kaufman, *Annu. Rev. Phys. Chem.*, **20**, 45 (1969).

TABLE I: Effect of Additions of NO, CO, and Isobutane on the Yields of N_2O–CH_4 Photolysis Products

CH_4 pressure, Torr	790	790	35[a]	35[a]	760	760	760
N_2O pressure, Torr	20	20	20	20	10	10	10
Additive, Torr	None	NO, 3	None	NO, 3	CO, 59	CO, 2	Isobutane, 10
Total pressure, Torr	810	813	35[a]	35[a]	829	772	780
N_2 yield, Torr	1.2	1.8	1.2	1.2	4.3	1.84	4.9
			Yields Relative to N_2[b]				
C_2H_6	0.635	0	~0.6	0	0.426	0.531	0.164
CO	0.110	Present	Present	Present	n.a.	n.a.	0.143
H_2	0.120	Present	Present	Present	0.113	0.128	0.160
C_3H_8	0.028	0	Present	0	0.026	0.018	0.007
CH_3OH	0.053	0.025	0.128	0.096	0.036	Present	Present
C_2H_5OH	0.023	0	0.070	0	Present	Present	Present
Neopentane	0	0	0	0	0	0	0.068

[a] Atmospheres. [b] Present indicates product was identified but not quantitatively determined; n.a., not analyzed.

than the CH_3 concentration and, therefore, reaction M7 could not compete with reaction M6 to produce as much as 3% CH_3OH, especially since we expect that the rate constant for reaction M7 will be smaller than that for reaction M6.

Further evidence against CH_3 + OH recombination as the source of CH_3OH was provided by NO scavenging experiments shown in Table I. With the additions of NO to the N_2O–CH_4 mixtures either at normal pressure or high pressure (35 atm), the CH_3OH yield was reduced only slightly while the C_2H_6 and C_3H_8 yields were reduced to zero, indicating essentially complete scavenging of CH_3 and C_2H_5 radicals by NO.

The 3% CH_3OH yield probably came from CH_2OH and CH_3O by abstraction of hydrogen atoms from CH_4, with possibly a trace contribution (<1%) from the secondary reaction of CH_3O_2. The fact that the CH_3OH yield decreased only partly upon NO addition may be due to incomplete scavenging of CH_3OH precursors such as CH_3O. The latter react with NO about two orders of magnitude slower than does CH_3.[5] Unfortunately, the rate of CH_2OH scavenging by NO is not known. CH_3O_2 results from the CH_3 radical scavenging by O_2,which is one of the products of the side reaction between $O(^1D)$ and N_2O. The radicals CH_2OH and CH_3O could come from the splitting of the hot CH_3OH^* by

$$CH_3OH^* \longrightarrow CH_2OH + H \qquad (M8)$$

$$\longrightarrow CH_3O + H \qquad (M9)$$

If this is the case, then these splittings can account for no more than about 4.5% (3% from the CH_3OH yield and 1.5% from the C_2H_5OH yield, see below) of the fragmentation processes of CH_3OH^*.

CH_2OH was probably also responsible for the formation of C_2H_5OH by recombination with CH_3 since no other likely channel was available. We ruled out the possible recombination between C_2H_5 and OH on the same grounds as the recombination between CH_3 and OH, especially for the reason that $[C_2H_5] < 0.1[CH_3]$. The possibility of C_2H_5OH coming directly from the insertion reaction between $O(^1D)$ and C_2H_6 was also ruled out as the lifetime of $C_2H_5OH^*$ is too short to be stabilized at normal pressure. The NO scavenging experiments gave strong evidence of radical recombintion as the source of C_2H_5OH. In all cases, the C_2H_5OH disappeared upon the addition of NO to the photolyzing N_2O–CH_4 mixtures (see Table I).

All experimental evidence pointed to the fact that in the absence of CH_3OH^* stabilization, the main decomposition process is reaction M4 producing CH_3 and OH radicals. The question of whether reaction M2b is a separate process or it is merely part of CH_3OH^* decomposition processes is resolved later in conjunction with the lifetime estimation of CH_3OH^*. Evidence for the existence of OH radicals was provided by experiments using CO as additive to the N_2O–CH_4 mixture. The CO, in competition with CH_4 (rate constant[13] for OH + CO is about 15 times greater than for OH + CH_4 reaction), removed part of the OH radicals and thus reduced the yield of C_2H_6 as shown in Table I. The reactions

$$CH_3OH^* \longrightarrow CH_2 + H_2O \qquad (M10)$$

and/or

$$O(^1D) + CH_4 \longrightarrow CH_2 + H_2O \qquad (M11)$$

are probably unimportant, but are difficult to detect. The isobutane addition experiments shown in Table I drastically reduced the yield of C_2H_6 and at the same time produced a new product, neopentane, which apparently resulted from the recombination between CH_3 and isobutyl radical.

To determine whether the H_2 molecules came from the direct molecular elimination (reaction M2c) or from secondary reactions of H atoms, an experiment was performed by adding 30 Torr of O_2 and 10.6 atm of SF_6 to the N_2O–CH_4 mixtures to scavenge H atoms. (The O_3 filter was used to cut off the 2537-Å line.) Under this experimental condition, we would expect that all of the radicals should be totally scavenged by O_2. The H_2 yield reduced only a little to a constant value of about 9% indicating the direct formation of H_2 at this amount. The slight increase in the yield of H_2 with the extent of reaction shown in Figure 1 was apparently due to the secondary reaction of H atoms.

Although we failed to detect the production of formaldehyde which should have been produced in amount equal to the H_2, nevertheless, we expect that the CH_2O would have been decomposed readily in the presence of CH_3 (or OH) radicals probably by the reactions

$$CH_3 + CH_2O \longrightarrow CH_4 + CHO \qquad (M12)$$

$$CH_3 + CHO \longrightarrow CH_4 + CO \qquad (M13)$$

The CO yield, shown in Figure 1, which was about equal to the quantity of H_2 when the irradiation time was short, may well be the result of reactions M12 and M13. Addi-

TABLE II: Effect of Addition of CH_2O on the Yields of N_2O–CH_4 Photolysis Products

CH_4 pressure, Torr	760	760	760
N_2O pressure, Torr	0	10	10
CH_2O pressure, Torr	4.5	4.5	None
Total pressure, Torr	765	775	770
	Yields Relative to N_2		
CO	0.290[a]	0.676	0.110
H_2	0.240[a]	0.347	0.120
C_2H_6		0.244	0.635

[a] N_2 yield taken as equal to that produced by irradiation with 10 Torr of N_2O present for same time period.

tional experiments were performed to determine the effect of added CH_2O on the yield of the products. These data, listed in Table II, clearly showed that the decrease in the yield of C_2H_6 was approximately offset by the increase of CO when CH_2O was added to the reaction mixtures, indicating the participation of reactions discussed above. It appears therefore that the nitrous oxide-photosensitized decomposition of methane proposed by Bradley, *et al.*,[4] as the additional source of H_2 is not required.

The yields of C_2H_6 shown in Figure 1 decrease with the extent of reaction. This decrease was largely compensated for by the increase in the yield of C_3H_8 which was the result of the recombination of CH_3 and C_2H_5. The latter species came from the secondary reaction between OH and C_2H_6 as was explained earlier. Thus for each C_3H_8 formed, two molecules of C_2H_6 disappeared.

The product yields in the foregoing discussion accounted for about 95% of the O(¹D) consumption based on the measurements of N_2 yield. These yields include 70% C_2H_6, 10% H_2, about 5% CH_3OH plus C_2H_5OH, and about 10% CO. We were unable to determine the extent of O(¹D) quenching by CH_4 to the ground state, O(³P). However, the work of Paraskevopoulos and Cvetanovic[7e] indicated that the quenching process is insignificant.

The lifetime of CH_3OH^* formed from reaction M2a can be estimated from an equation derived from the steady-state treatment of reactions M1, M2, M3, and M4.

$$\frac{[CH_3OH]}{[N_2]} = f\left(\frac{k_{M3}[M]}{k_{M4} + k_{M3}[M]}\right)$$

or

$$\frac{[N_2]}{[CH_3OH]} = \frac{1}{f}\left(1 + \frac{k_{M4}}{k_{M3}[M]}\right)$$

where $f = k_{M2a}/k_{M2}$, is the fraction of CH_3OH formed. A plot of $[CH_3OH]$ *vs.* $1/[M]$ is shown in Figure 3, where [M] represents $[CH_4]$. In this plot, the point corresponding to the yield of CH_3OH at the CH_4 pressure of 1 atm (not shown) is far off the smooth line drawn from other points obtained from high pressures, indicating that the CH_3OH yield at normal pressure does not come from the physical quenching of CH_3OH^*. This is in line with the argument presented earlier. The yield of CH_3OH at 1 atm of CH_4 was therefore subtracted from the actual yield measured at higher pressures and a straight line was drawn through these points. The slope to intercept ratio gives the lifetime of CH_3OH^* to be about 8×10^{-13} sec assuming $k_{M3} = 2 \times 10^{11}\ M^{-1}\ sec^{-1}$. The reciprocal of the intercept gives the extent of reaction M2a to be about 40%. Therefore abstraction reaction M2b should account for about 40% of the overall reaction because reactions M2b and M4, in the absence of CH_3OH^* stabilization, occurred to the extent of about 80% as was concluded earlier. This breakdown in

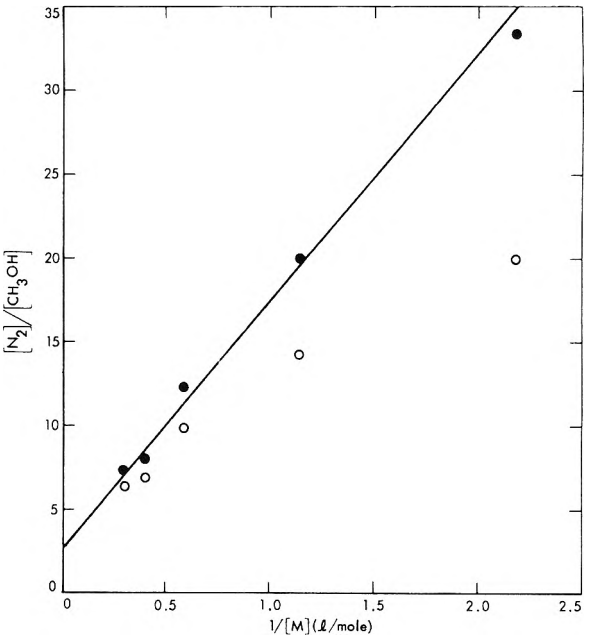

Figure 3. Stabilization plot for CH_3OH. Open circles are actual data; solid points are values after subtraction of the CH_3OH yield obtained at 1 atm. The later yield evidently does not arise through CH_3OH^* stabilization.

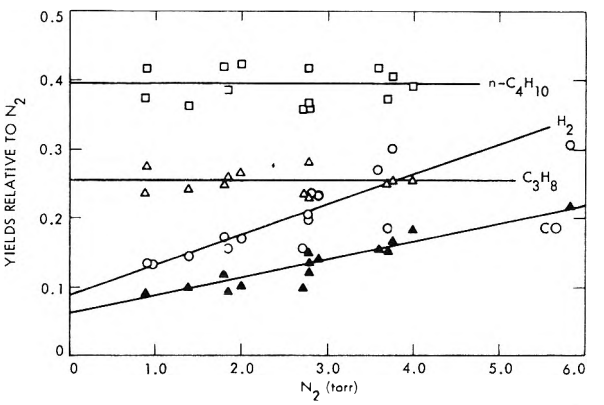

Figure 4. Dependence of major product yields on the extent of the O(¹D) + C_2H_6 reaction (10 Torr of N_2O–300 Torr of C_2H_6).

percentage between reaction M2a and M2b is uncertain because of the rough extrapolation of the few experimental points. An attempt to use He as the CH_3OH^* stabilizer failed, at a pressure of 103 atm, to produce a noticeable increase in the yield of CH_3OH over the 10 Torr of N_2O–760 Torr of CH_4 value, indicating a poor quenching efficiency of He gas.

Reaction between O(¹D) and C_2H_6. The major products except water for the 10 Torr of N_2O–300 Torr of C_2H_6 mixtures are shown in Figure 4. The radical recombination yields of C_3H_8 (~26%) and *n*-C_4H_{10} (~40%) were relatively constant with increasing photolysis time. On the contrary the yields of H_2 and CO increased with the extent of irradiation. Small quantities of CO_2 and C_2H_4 were also detected. A decision can not be made as to whether the latter came from the disproportionation reaction of radicals or from the direct reaction between O(¹D) and C_2H_6 because C_2H_4 is likely to undergo secondary reactions with radicals and is readily photolyzed by 1849-Å light. The direct reaction is known to occur, however, in the liquid Ar experiments.[3c] The yields of CH_3OH and

TABLE III: Effect of Additions of NO, CO, and Isobutane on the Yield of N_2O–C_2H_6 Photolysis Products

C_2H_6 pressure, Torr	600	600	600	600	300	300
N_2O pressure, Torr	20	20	20	20	10	10
Additive, Torr	None	NO, 3	He, 54.5[a]	He, 54.5[a] and NO, 3.6	CO, 67.5	Isobutane, 10
Total pressure, Torr	620	623	55.5[a]	55.5[a]	378	320
N_2 yield, Torr	1.2	1.8	1.8	1.8	3.88	3.78
			Yields Relative to N_2[b]			
C_3H_8	0.26	0	0.205	0	0.161	0.164
n-C_4H_{10}	0.40	0	0.268	0	0.236	0.145
CO	0.095	Present	Present	Present	Present	0.139
H_2	0.15	Present	Present	Present	Present	0.218
CH_3OH	0.034	0.063	0.047	0.102	Present	0.01
C_2H_5OH	0.052	0	0.147	0.110	Present	0.023
n-C_3H_7OH	~0.03	0	~0.025	0	Present	~0.01
Neopentane	0	0	0	0	0	Present
2,2-Dimethylbutane	0	0	0	0	0	Present

[a] Atmospheres. [b] Present indicates product was identified but not quantitatively determined.

C_2H_5OH, not shown in Figure 4, accounted for about 2 and 4%, respectively, relative to N_2 yield. n-C_3H_7OH was also detected in small quantities. The yields of C_3H_8, n-C_4H_{10}, and C_2H_5OH as a function of pressure using He as the stabilizing gas are shown in Figure 5. The C_2H_5OH yield increases with the increase in pressure while the yields of C_3H_8 and n-C_4H_{10} show the opposite effect. The latter results were badly scattered but the trend points to the fact that the decrease of C_3H_8 and n-C_4H_{10} yield is real as it has to be when more C_2H_5OH is stabilized. Again, the yield of N_2 in these high-pressure experiments was taken as the same value in the experiment without added He but under the same experimental conditions. These results indicated that the photolysis of N_2O–C_2H_6 mixtures by 1849-Å light mainly proceeds as follows

$$N_2O + h\nu \longrightarrow N_2 + O(^1D) \quad \text{(E1)}$$

$$O(^1D) + C_2H_6 \longrightarrow C_2H_5OH^* \quad \text{(E2a)}$$

$$\longrightarrow C_2H_5 + OH \quad \text{(E2b)}$$

$$\longrightarrow H_2 + CH_3CHO \quad \text{(E2c)}$$

$$\longrightarrow C_2H_4 + H_2O \text{ (probable)} \quad \text{(E2d)}$$

$$C_2H_5OH^* + M \longrightarrow C_2H_5OH + M \quad \text{(E3)}$$

$$C_2H_5OH^* \longrightarrow C_2H_5 + OH \quad \text{(E4a)}$$

$$\longrightarrow CH_3 + CH_2OH \quad \text{(E4b)}$$

$$OH + C_2H_6 \longrightarrow C_2H_5 + H_2O \quad \text{(E5)}$$

$$C_2H_5 + C_2H_5 + M \longrightarrow n\text{-}C_4H_{10} + M \quad \text{(E6a)}$$

$$\longrightarrow C_2H_4 + C_2H_5 \quad \text{(E6b)}$$

$$C_2H_5 + CH_3 + M \longrightarrow C_3H_8 + M \quad \text{(E7a)}$$

$$\longrightarrow C_2H_4 + CH_4 \quad \text{(E7b)}$$

$$CH_3 + CH_3 + M \longrightarrow C_2H_6 + M \quad \text{(E8)}$$

For reasons similar to the previous discussions in conjunction with the reaction between $O(^1D)$ and CH_4, we discounted the recombination of CH_3, C_2H_5, and C_3H_7 radicals with OH as sources of CH_3OH, C_2H_5OH, and n-C_3H_7OH. In addition to the very small contribution of

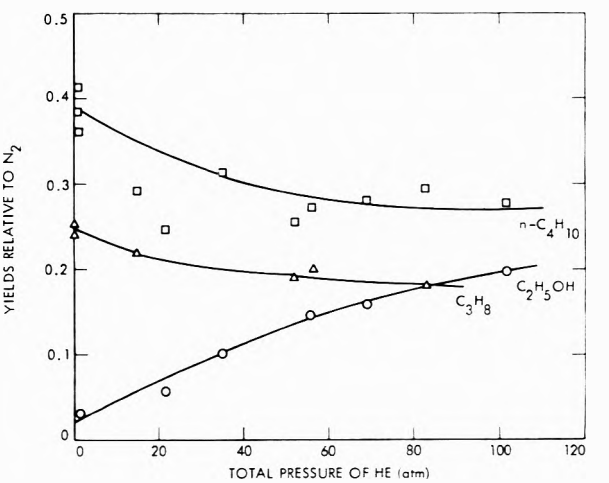

Figure 5. Pressure dependence of some product yields in the $O(^1D)$–C_2H_6 reaction.

CH_3O_2 and $C_2H_5O_2$ to the formation of CH_3OH and C_2H_5OH, the H atom abstraction from C_2H_6 by CH_2OH is probably the major source of CH_3OH. This reaction probably competes with the recombination reactions between C_2H_5 and CH_2OH, respectively. These conclusions on the role of CH_2OH were borne out in the NO addition experiments shown in Table III. Upon the addition of NO to the reaction mixtures, n-C_3H_7OH disappeared both at normal and high pressures, indicating the nature of radical recombination. The C_2H_5OH disappeared entirely at normal pressure but only reduced slightly at the total pressure of 55.5 atm, indicating the direct stabilization of $C_2H_5OH^*$ at high pressure. In all cases, CH_3OH increased in the presence of NO. The reason for this increase is not known with certainty, but it may be related to the fact that CH_3OH was not completely eliminated when NO was added in the CH_4 experiments. Table III also shows some data on the CO and isobutane addition experiments which, again, provide evidence for the existence of OH, C_2H_5, and CH_3 species.

If we assume that the fate of C_2H_5 and CH_3 radicals formed from the processes E2b, E4, and E5 is only the formation of n-C_4H_{10} (E6), C_3H_8 (E7), and C_2H_6 (E8)

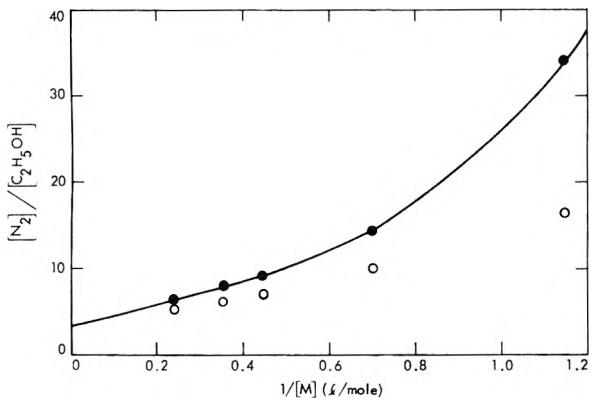

Figure 6. Stabilization plot for C_2H_5OH. Open circles are actual data; solid points are values after subtraction of the C_2H_5OH obtained at 1 atm. The latter yield evidently does not arise through $C_2H_5OH^*$ stabilization.

and adopt the rate ratio[14] of the disproportionation to recombination as 0.13 for $C_2H_5 + C_2H_5$ and as 0.045 for $CH_3 + C_2H_5$, then from the percentage yields of n-C_4H_{10} and C_3H_8 we can estimate that reactions E2b and E4a occur, in the absence of $C_2H_5OH^*$ stabilization, to the extent of about 59% and reaction E4b about 27%. It may be argued that part of the C_2H_5 radicals may come from the abstraction reaction between CH_3 and ethane. However, this process evidently is not important because only a trace of CH_4 was detected.

Reaction E2c occurred to the extent of about 3% since the H_2 yield dropped to this value when 30 Torr of radical scavenger, O_2, and 20.4 atm of molecular stabilizer, SF_6, were added to the N_2O-C_2H_6 photolysis mixture (the O_3 filter was again used to cut off the 2537-Å light). The excess yield of H_2, shown in Figure 4, may be due in part to the secondary reactions of H atoms produced from the $C_2H_5OH^*$ fragmentation and in part to the photolysis of C_2H_6 by 1849-Å light.

Following the same precedure used to obtain the lifetime of CH_3OH^*, we plotted $[N_2]/[C_2H_5OH]$ against the reciprocal of the total He concentration, [M], as shown in Figure 6. Again, the measured values of C_2H_5OH at high pressures were corrected by an amount equal to the value obtained from the 10 Torr of N_2O-300 Torr of C_2H_6 mixture experiment, which was not due to the direct stabilization of $C_2H_5OH^*$. However, the curve drawn through the "corrected" points showed some curvature. Because of limited data, a more detailed analysis is unwarranted. However, comparison with CH_3OH data indicates that the lifetime of $C_2H_5OH^*$ is at least five times greater than that of CH_3OH^*.

The curve, shown in Figure 6, when extrapolated to infinite pressure (*i.e.*, intercept), again gives a rough value of the extent of insertion reaction E2a to be ~40%. Since reaction E4b occurred to the extent of ~27% as was estimated earlier, reaction E4a should account for about 13%. This, in turn, implies that abstraction reaction E2b should have occurred to the extent of about 46% because the combined reactions E2b and E4a account for about 59%.

Conclusions

The reaction of O(¹D) with methane gives mainly CH_3 and OH radicals as initial products, along with about 9% of CH_2O and H_2. The $O(^1D) + C_2H_6$ reaction gives C_2H_5, OH, CH_3, and CH_2OH as major initial products, with only a few per cent of H_2.

It is clear that all of the reaction paths cannot be described in terms of the unimolecular decomposition of a "chemically activated" ROH* intermediate. For example, the contribution of the step

$$O(^1D) + CH_4 \longrightarrow CH_2O + H_2$$

is essentially the same both in the gas phase and in liquid argon,[3b] which is inconsistent with a CH_3OH^* intermediate of appreciable lifetime for this particular reaction step. In addition, the present results and the earlier work of Cvetanovic and coworkers have shown that the abstraction of H by O(¹D) does not proceed *via* the ROH* intermediate. The abstraction reaction is not suppressed at high pressures in the gas phase, but it does not occur in the liquid phase.[3c] The reason for this difference is not known.

Acknowledgment. The authors wish to thank A. Chutjian for the helpful discussion on the N_2O photolysis.

(14) S. W. Benson and W. B. DeMore, *Annu. Rev. Phys. Chem.*, **16**, 397 (1965).

Effect of Particle-Size Distribution on the Thermal Decomposition of α-Lead Azide

Richard W. Hutchinson, Sidney Kleinberg, and Fred P. Stein*

Chemical Engineering Department, Lehigh University, Bethlehem, Pennsylvania 18015 *(Received November 13, 1972)*

Publication costs assisted by the U. S. Army Research Office—Durham

Samples of α-lead azide powder having known, but different, particle-size distribution were thermally decomposed at temperatures between 210 and 270°. The finer powders (mean equivalent-spherical radius, 8 μ) began to decompose sooner and exhibited a maximum rate greater than twice that of the coarser powders (mean equivalent-spherical radius, 24 μ). A single-equation mathematical model, which contains two parameters and incorporates the independently measured particle-size distribution, gave an excellent fit of the sigmoid-shaped decomposition curves. One of the parameters extracted from the data *via* the model was shown to be the rate of penetration of the reaction front into a single crystal. Thermal decomposition data for α-lead azide powder of a given particle-size distribution can be transformed to another size and distribution and, thereby, permit study of other effects, such as purposely added impurities, in the absence of the significant particle-size effects.

Introduction

α-Lead azide is a metastable, white crystalline compound which decomposes at temperatures in the range of approximately 200 to 270°.

$$PbN_6 \longrightarrow Pb + 3N_2 \qquad (1)$$

At somewhat higher temperatures, or when subjected to shock or friction, it explodes.

Several of the previous studies[1-4] of the thermal decomposition or explosion of lead azide mentioned qualitative observations of the effect of particle size, but none seriously studied nor quantitatively reported on more than one size of material of the same type. Garner and Gomm,[1] and others,[4,5] also observed that thermal decomposition began at the surface of the particles as evidenced by the rapid darkening over the whole surface. It can, therefore, be expected that the rate of thermal decomposition would be significantly related to the surface area per unit mass of particles, and, furthermore, that the particle-size distribution as well as the total surface area would be important.

Because the state of the art does not permit the preparation of different batches of high-purity α-lead azide powder with well-controlled, identical particle-size distributions, quantitative comparison of thermal decomposition data cannot be accomplished in the absence of particle-size information. If one wants to study, for example, the effect of certain impurities on the thermal decomposition of α-lead azide, as we do, the effect of the impurity is compounded and, in some cases, completely masked by the effect of particle size.

The purpose of this work was to demonstrate, measure, and correlate the effect of particle size on the thermal decomposition of α-lead azide powders *in vacuo*. In this study powders of α-lead azide which had known, but different, particle-size distributions were thermally decomposed. The per cent of decomposition was monitored continuously throughout each run, and the per cent of total conversion was measured. These data were correlated with a new model which approximated the decomposition data very well and which produced descriptive parameters that were independent of particle size.

Most of the studies of the thermal decomposition of powders of α-lead azide either considered the reaction to be autocatalytic in nature[6-8] or fit the resulting sigmoid-shaped decomposition curves with various functions of reaction time.[4,9-11] However, measurement of the thermal decomposition of single crystals of α-lead azide[1,12] did not produce sigmoid-shaped decomposition curves, although there were various delays in the start of reactions of some of the single crystals. The model developed hereinafter, based on particle-size distribution, describes the sigmoid-shaped curves observed during decomposition of lead azide powders but does not require the autocatalytic kinetics which are apparently not observed in single crystals.

Experimental Section

Apparatus. The apparatus used in this work has been described in detail elsewhere.[13] The decomposition of α-lead azide was monitored by collecting the released nitrogen on activated charcoal which was maintained at the temperature of liquid nitrogen and by continuously recording the weight of the charcoal as given by a Cahn Instrument Co. electrobalance. The entire decomposition was performed *in vacuo* at a pressure of less than 5×10^{-4} Torr. The decomposition was carried out in a constant-temperature furnace which was controlled to within ±0.05° and which was designed such that the decomposing sample could "see" only surfaces that were at the con-

(1) W. E. Garner and A. S. Gomm, *J. Chem. Soc.*, 2123 (1931).
(2) A. S. Hawkes and C. A. Winkler, *Can. J. Res., Sect. B*, **25**, 548 (1947).
(3) F. P. Bowden and K. Singh, *Proc. Roy. Soc., Ser. A*, **227**, 22 (1954).
(4) P. J. F. Griffiths and J. M. Groocock, *J. Chem. Soc.*, 3380 (1957).
(5) O. H. Hill, Appendix B(DRL-A 126) to D. R. L. Accoustical Report No. 128, U. S. Army Contract DA-44-099-ENG-2566, University of Texas, 1957.
(6) W. E. Garner, "Chemistry of the Solid State," Butterworths, London, 1955, pp 184, 238.
(7) B. Reitzner, *J. Phys. Chem.*, **65**, 948 (1961).
(8) B. Reitzner, J. V. R. Kaufman, and E. F. Bartell, *J. Phys. Chem.*, **66**, 421 (1962).
(9) W. E. Garner, A. S. Gomm, and H. R. Hailes, *J. Chem. Soc.*, 1393 (1933).
(10) J. Jach, *Trans. Faraday Soc.*, **57**, 947 (1963).
(11) D. Young, *J. Chem. Soc.*, 3141 (1964).
(12) P. G. Fox, *J. Solid State Chem.*, **2**, 491 (1970).
(13) S. Kleinberg and F. P. Stein, *Ind. Eng. Chem., Fundam.*, 11, 134 (1972).

TABLE I: Parameters for Normal Size Distribution

Sample		$\bar{R}$, mean equivalent spherical radius, μ	S, standard deviation, μ
Pure α-Lead Azide			
Fine		8.3	2.6
Intermediate	80%	13.6	3.3
	20%	22.9	8.4
Coarse		23.8	6.3
Fe^{2+} Doped α-Lead Azide			
Fine		6.6	1.8
Intermediate		8.3	2.5
Coarse		20.5	7.1

trolled temperature. Approximately 10-mg samples were used for each run.

Materials. Two batches of α-lead azide were prepared by bubbling HN_3 through an aqueous solution of lead nitrite which had been prepared from Johnson, Matthey, & Co., Ltd. Specpure lead oxide (<10 ppm impurity), 99.995% pure NO–NO_2 gas mixture, and triple-distilled, deionized water. One batch was pure α-lead azide, and the other was α-lead azide which contained a known amount of Fe^{2+}. (This paper concerns the effect of particle size on the decomposition data of these two batches. Data and discussion of the effect of Fe^{2+} and other impurities will be offered in a subsequent paper.) X-Ray analysis showed that the lead azide was totally of the α form. Elemental analysis by spark-source mass spectograph showed overall undesired impurities to be approximately 270 ppm by weight.

The particles in both batches varied greatly in size from small needle-shaped particles approximately 60 μ long to the largest particles which appeared in the shapes of both needles and platlets with a length of 400 to 600 μ. Both batches were classified according to particle size by an hydraulic settling technique which is described in detail elsewhere.[14] Three particle-size fractions were obtained for each of the two batches. The volume particle-size distribution of each sample was measured with a Coulter counter. The distribution of each size fraction, with the exception of the intermediate sample of the pure material, was essentially normal. The exception was approximated as the sum of two normal distributions. The parameters for the normal size distributions are listed in Table I.

The samples of lead azide were stored *in vacuo* and in the dark. These precautions were taken to avoid buildup of surface contaminants and photodecomposition which could interfere with the experimental results. Photographic darkroom lights were used when handling the lead azide.

Results

The decomposition data, recorded as weight of released nitrogen adsorbed on the charcoal *vs.* time, were recast in the form of cumulative-weight-per cent-decomposed *vs.* time.

The isothermal decomposition data for the three size cuts of the pure α-lead azide are shown in Figures 1 and 2 for the temperatures of 240 and 230°, respectively. It is readily observed that the small particles decomposed at a faster rate than did the large ones.

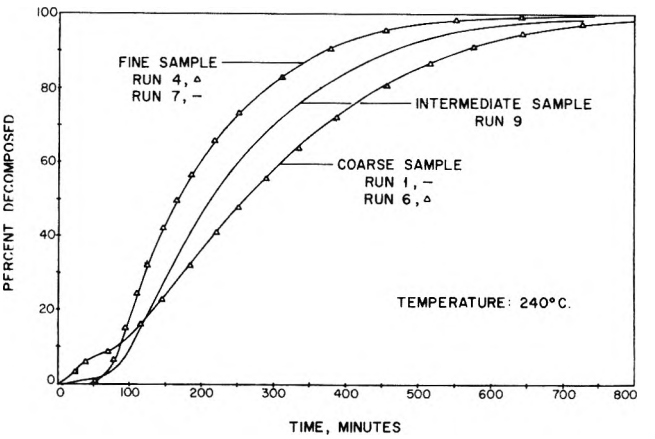

Figure 1. Effect of particle size on the isothermal decomposition of pure α-lead azide at 240°.

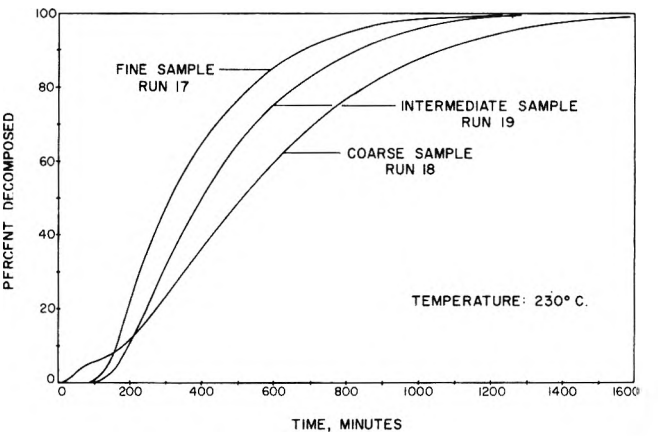

Figure 2. Effect of particle size on the isothermal decomposition of pure α-lead azide at 230°.

The hump and crossover of the initial portion of the decomposition curve for the coarse particles was an anomaly observed only with the coarse sample. The hump appeared, and was very reproducible, at all temperature levels studied. The temperature coefficient of the rate for this initial reaction period (E = 38 ± 3 kcal) was similar to the temperature coefficient of the maximum rate (E = 35.2 ± 0.5 kcal). Thus, it is believed that this initial hump and crossover were the result of decomposition of lead azide rather than of the decomposition or desorption of some other gross impurity. There was also an experimental safeguard against the measurement of a surface impurity provided by the liquid nitrogen cooled traps in the apparatus ahead of the cold charcoal. Higher boiling materials, such as carbon dioxide and water, would have been removed by the traps before they could have reached the cold charcoal and have been recorded as nitrogen weight gain. All of the pure α-lead azide was prepared in the same batch and all of it was treated identically subsequent to preparation, so that the only difference in the material decomposed to obtain the data in Figures 1 and 2 was particle size. It is suggested that the giant particles, which were present only in the coarse sample, cracked at the onset of decomposition and released nitrogen from the newly formed surfaces in quantities sufficient to cause the hump in the initial portion of the decomposition curve. Such a speculation is not totally unprecedented, for

(14) R. W. Hutchinson and F. P. Stein, *Ind. Eng. Chem., Fundam.*, **10**, 635 (1971).

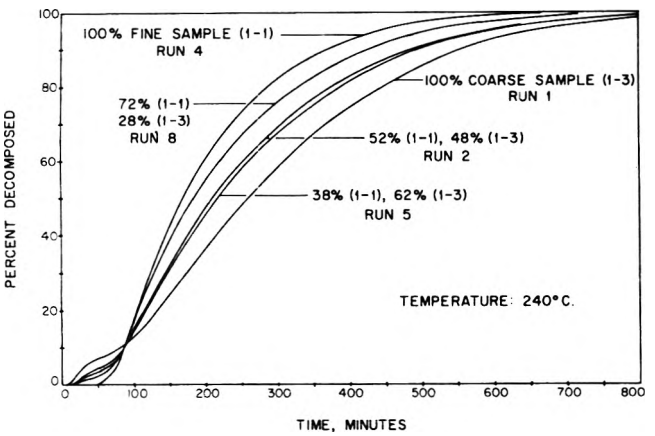

Figure 3. Isothermal decomposition of mixtures of fine and coarse particles of pure α-lead azide.

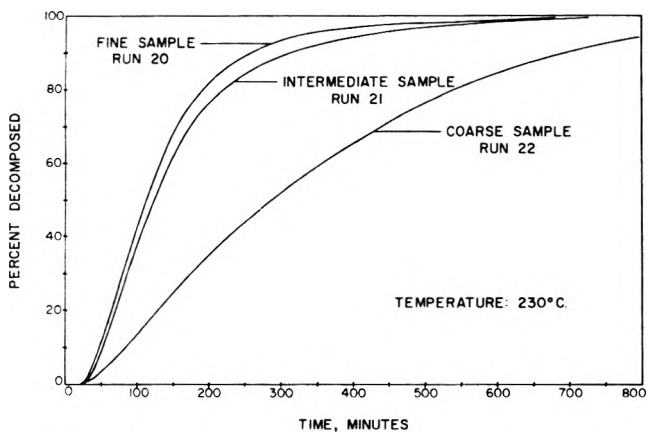

Figure 4. Effect of particle size on the isothermal decomposition of Fe^{2+} doped α-lead azide at 230°.

Hawkes and Winkler[2] observed that their largest crystals (length on the order of 0.8 mm) of lead azide broke up abruptly on heating to temperatures below an explosion temperature, whereas the smaller crystals did not. Hill[5] also observed that large particles do sometimes fly apart early in the reaction.

The reproducibility of the decomposition data can be assessed by comparing the triangles to the solid lines in Figure 1; the solid line is for one particular run, and the triangles are for a different run at identical conditions on another day. The average reproducibility between two runs was ±0.5% decomposed at any given time.

Samples consisting of a mixture of the fine and the coarse size cuts of pure α-lead azide were decomposed. The decomposition curves corresponding to different weight fractions of the fine and coarse size cuts are presented in Figure 3. The decomposition curves for the mixtures were, in all cases, bracketed by the curves for the separate fine and coarse samples, and there is quantitative agreement, as well, which is considered in a subsequent section.

The isothermal decomposition curves for the three samples of Fe^{2+} doped α-lead azide are presented in Figure 4 for the temperature of 230°. The effect of particle size is qualitatively the same as for the pure material.

The per cent of total conversion was obtained for each run by dividing the amount of lead azide decomposed, based on the weight of nitrogen collected, by the amount of lead azide introduced into the furnace. The per cents of total conversion are listed in Table II. The total conversions at 240° were between 94 and 98% for the different size fractions. At higher temperatures the per cent conversions increased and approached 100% when the samples exploded. The particle size did not significantly affect the percentages of total conversion.

TABLE II: Per Cent of Total Conversion[a]

Temp. °C	Sample	% conversion
	Pure α-Lead Azide	
240	Fine	97.9
240	Intermediate	96.4
240	Coarse	96.3
265	Fine	98.4
Exploded	Fine	99.3
	Fe^{2+} Doped α-Lead Azide	
240	Fine	95.5
235	Intermediate	94.1
240	Coarse	94.7
255	Fine	97.6
Exploded	Fine	100.0

[a] Reproducibility of data ±0.5%.

Model of Lead Azide Decomposition

The objectives of the model are twofold. First, to fit the experimental data of the complete decomposition curve with only one equation. Current models[4,10] used for the type of data shown in Figures 1 and 2, for example, models derived from nucleation theory, require two or more different equations to fit the several parts of the curve with the attendant disadvantages of several different constants for each equation and the difficulty of matching the solution at common points between two equations. Second, to account for the effect of particle size on the observed rate of thermal decomposition using independently measured size-distribution parameters. In addition to the objectives, the curve-fit parameters of the model should be useful and dependent only on temperature and the type of lead azide.

The following model met the objectives including an excellent fit of the data with one equation. Equation 2 gives the total fraction decomposed at any time of interest as the summation of the decomposition of each particle at that time. (Since all particles may not have started to react at the time of interest, the upper limit is not the largest particle but a variable which will be explained in more detail subsequently.)

$$\alpha(t) = \int_0^{R'} F'(r)\alpha_p(t,r)\,dr \qquad (2)$$

where t is the time of interest of the reaction (minutes), r is the initial characteristic dimension (radius) of a particle (μ), $\alpha(t)$ is the total weight-fraction decomposed at time t, $F'(r)$ is the weight fraction of particles that have radius r, and $\alpha_p(t,r)$ is the weight-fraction decomposed of an individual particle of radius r at time t.

The function $F'(r)$ was determined to be a normal distribution for the powder samples used in this work.

$$F'(r) = \frac{1}{s\sqrt{2\pi}} \exp\left[\frac{-(r-\bar{R})^2}{2s^2}\right] \qquad (3)$$

The distribution parameters, R and s, were independently measured quantities. These parameters were always of such a magnitude that for $r = 0$, $F'(r)$ was less than 10^{-3} which was insignificant, albeit not zero.

The individual particle was modeled as a sphere which, when it started to react, was immediately covered with a layer of lead that penetrated the particle at a constant rate of advance in a shrinking envelope mechanism.

$$\alpha_p(t,r) = 1 - \left[1 - \frac{t - t_b}{(\rho/k)r}\right]^3 \quad (4)$$

where ρ is the crystalline density (moles/micron^3), k is the penetration rate constant of the reaction (moles/μ^2 minute), k/ρ is the penetration rate of the reacting interface (μ/minute), and t_b is the time at which the particle of radius r started to decompose (minutes).

The selection of the shrinking-sphere model was made in the face of contradictory observations. On the positive side, the decomposition curves for single crystals of lead azide reported by Garner and Gomm[1] were very closely approximated by curves for shrinking spheres. Our own photographs of partially decomposed lead azide at several stages showed that certain areas of the crystals darkened very rapidly. A given dark area did not seem to spread much in area indicating that after the initial rapid coverage, decomposition must have proceeded primarily by penetration. Contrariwise, the particles were not spherical in shape; they have been described hereinbefore as needles and platelets. General model eq 2 could accept any geometry and function for $\alpha_p(t,r)$. In addition to spherical geometry, slab and cylindrical geometries were tried in place of eq 4. Of these, the shrinking-sphere model gave the best fit of the data and, hence, was adopted.

The time at which a particle of radius r started to react, t_b, was found to be related to r by the following relationship

$$t_b = Ar^{1/3} \quad (5)$$

A is the induction period constant. In the photographs mentioned in the previous paragraph the smaller particles in general appeared to begin to react earlier, thus, lending qualitative support to eq 5.

Equations 3, 4, and 5 were substituted into eq 2 to obtain the completed model.

$$\alpha(t) = \int_0^{R_1} \frac{1}{s\sqrt{2\pi}} \exp\left[\frac{-(r - \bar{R})^2}{2s^2}\right] dr + \int_{R_1}^{R_2} \left\{1 - \left[1 - \frac{t - Ar^{1/3}}{(\rho/k)r}\right]^3\right\} \frac{1}{s\sqrt{2\pi}} \exp\left[-\frac{(r - \bar{R})^2}{2s^2}\right] dr \quad (6)$$

The first integral accounts for the particles of radius R_1 and less which are completely decomposed at time t. R_1 is obtained from the following equation which is a combination of eq 4 and 5 for the special case of complete decomposition.

$$\frac{t - AR_1^{1/3}}{(\rho/k)R_1} = 1 \quad (7)$$

The second integral represents the particles larger than R_1 which are partially decomposed at time t. The upper bound limits t_b to time t.

$$t_b = AR_2^{1/3} = t \quad (8)$$

Because time (t) is a constant within the integrals and in the limits, eq 6 must be solved for each time of interest. The model was integrated numerically using a general integration program that utilized the Runge-Kutta-Merson integration algorithm.[15] Ten to fifteen integrations were required to construct an entire decomposition curve.

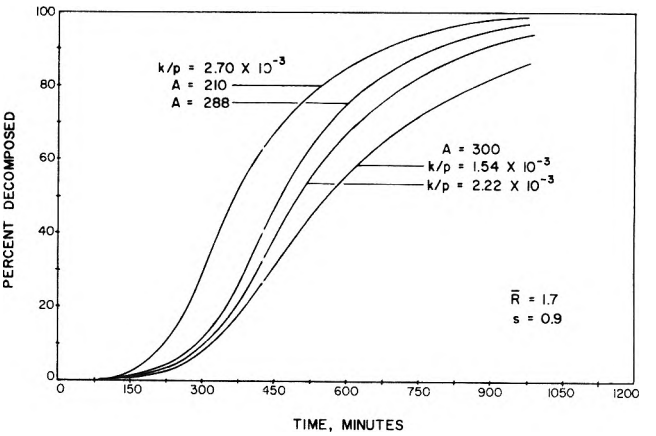

Figure 5. Effect of model parameters A and k/ρ on the predicted decomposition curves.

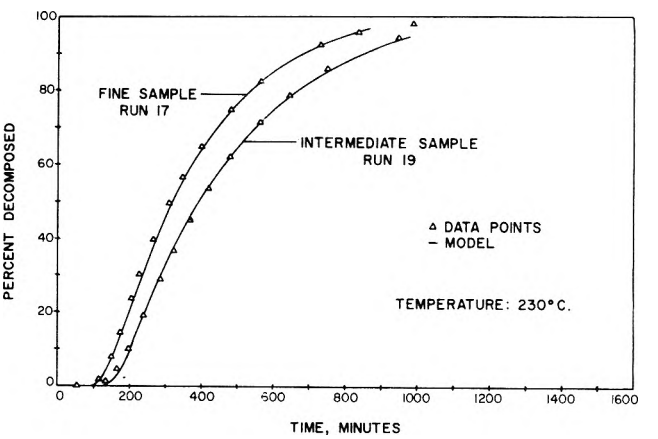

Figure 6. Comparison of decomposition data of pure α-lead azide to the calculated decomposition curves.

The complete model for the decomposition of lead azide, eq 6, contains two adjustable parameters, A and k/ρ, which are independent of particle size. The particle-size distribution is measured independently and is incorporated within the model.

Sample decomposition curves generated by the model are shown in Figure 5. It can be observed that the parameter k/ρ affects the slope of the curve; whereas, A tends to displace the entire curve to the right or to the left. The interaction between these two parameters is slight. The influences of the parameters are consistent with the derivation of the model: (1) k/ρ is the penetration rate and should, therefore, influence the slope of the decomposition curve (rate); and (2) A is the induction period constant which influences the time when the particles start to react.

Figures 6 and 7 show a sample of the fit between the model and the data for pure and Fe^{2+} doped lead azide, respectively. It was not possible to fit the model to the data of the coarse sample of the pure material because of the complication of the hump. The average agreement be-

(15) W. E. Schiesser, "LEANS III Programming System for Continuous Systems Simulation," Copyright assigned to Lehigh University, Bethlehem, Pa., 1970.

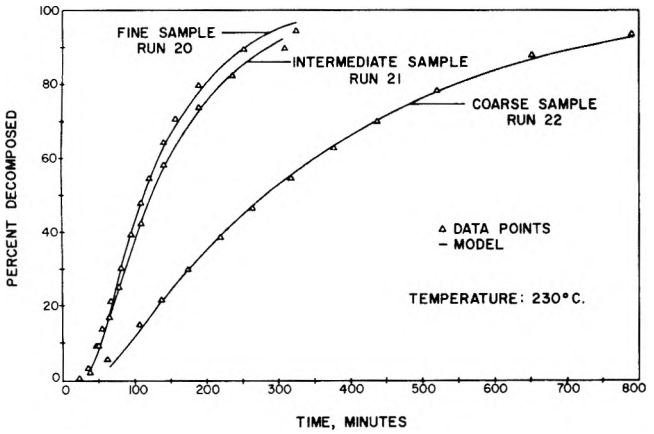

Figure 7. Comparison of decomposition data of Fe^{2+} doped α-lead azide to the calculated decomposition curves.

TABLE III: Model Parameters

Temp, °C	Sample	$k/\rho \times 1000$, μ/min	A, min/$\mu^{1/3}$
	Pure α-Lead Azide		
240	Fine	17.0 ± 0.4	38 ± 1
240	Intermediate	22.7 ± 0.6	35 ± 1
	Fe^{2+} Doped α-Lead Azide		
230	Fine	17.5 ± 0.4	22.5 ± 0.6
230	Intermediate	19.6 ± 0.5	21.0 ± 0.5
230	Coarse	17.5 ± 0.4	22.0 ± 0.5

tween the model and the data is ±1.0% decomposed at any given time. This number can be compared to the reproducibility of the original decomposition data of ±0.5% decomposed. Thus, the model gives a good approximation of the decomposition data.

In addition to fitting the data, it was required that the model parameters k/ρ and A be independent of particle size. The model parameters are listed in Table III. The induction period constants for the different size fractions agreed to within ±6% for the pure material and ±4% for the Fe^{2+} doped material, and the penetration rate constants varied by ±14 and ±8%, respectively. Thus, the model is capable of discerning the effects of particle size with an accuracy on the order of ±10%. Such a correlation of the effects of particle size is crucial when the effects of other variables, such as impurity levels, are to be considered.

Discussion

From the decomposition data it was possible to demonstrate that the individual particles decomposed independently of each other. Table IV shows the observed per cents decomposed for a 62–38% mixture of coarse and fine fractions of pure α-lead azide as well as the predicted per cents decomposed. The predicted per cents are based on a linear combination of the respective masses of coarse and fine samples within the mixture and the decomposition data of the coarse and fine samples. The excellent agreement between the observed and predicted per cents is a demonstration that the coarse and fine particles did not interact during the decomposition.

When the samples exploded, the measured total conversions were essentially 100%. Thus, it was demonstrated that the apparatus was capable of accounting for all of the

TABLE IV: Observed and Predicted Per Cent Decomposition for Mixtures of Coarse and Fine Particles of Pure α-Lead Azide[a]

	% decomposition	
Time, min	Observed	Predicted
50	4.5	4.6
150	31.0	31.0
300	67.5	67.9
450	86.5	86.2
600	95.5	95.3

[a] 61.9% coarse (by weight), 38.1% fine.

TABLE V: Temperature Coefficients for Pure α-Lead Azide

Sample	ΔE_{mr},[a] kcal/mol	$\Delta E_{k/\rho}$,[b] kcal/mol	ΔE_A,[c] kcal/mol
Fine	35.0 ± 0.5	34.9 ± 0.3	35.1 ± 1.8
Intermediate	34.6 ± 1.1	33.3 ± 1.3	36.7 ± 0.2
Coarse	35.2 ± 0.5		

[a] ΔE_{mr} is the temperature coefficient of the maximum rate of decomposition (from experimental data). [b] $\Delta E_{k/}$ is the temperature coefficient of the penetration rate constant (from the model). [c] ΔE_A is the temperature coefficient of the induction period constant (from the model).

nitrogen which was released, that the lead azide was stoichiometric PbN_6, and that the decomposition products were lead and nitrogen gas. The material balance obtained should virtually eliminate speculation that lead nitrides are significant decomposition products in a lead azide explosion. (It is recognized that there are more definitive tests for the residue of a thermal decomposition.) To the best of the authors' knowledge no material balance of this type and accuracy has been reported previously for lead azide explosions.

The experimental data for each individual decomposition were curve fit by arbitrarily adjusting the numerical values of the model parameters, k/ρ and A, such that a statistically best fit was obtained. Two tests of the physical significance ascribed to the model parameter k/ρ, the rate of penetration of the reaction front into the crystal, are available. One is its agreement with an independent experimental measurement, and the other is the agreement between the Arrhenius temperature coefficient for k/ρ and the temperature coefficient for the experimentally measured maximum rate. Fox[12] reported experimental rates in units of molecules m^{-2} sec^{-1} for thermal decomposition of single crystals of α-lead azide which had known dimensions and geometry. For 240° the rate was 2.2×10^{18}, which, transformed to units of μ per minute, is 1.4×10^{-2}. The agreement of the model parameter values for pure α-lead azide shown in Table III (1.7×10^{-2} and 2.3×10^{-2}) with Fox's experimental value is exceptionally good in view of the nature, origin, and independence of the values. The rather good comparison of Arrhenius temperature coefficient between k/ρ and the experimentally measured maximum rate is shown in Table V. The values are also in the 30–38-kcal range of activation energies reported by several authors[6,10,12,16] for lead azide, although reported values range widely from about 21[17] to

(16) F. P. Bowden and A. D. Yoffe, "Fast Reactions in Solids," Butterworths, London, 1958, p 150.
(17) H. Henkin and R. McGill, *Ind. Eng. Chem.*, **44**, 1391 (1952).

65 kcal.[2] Such a wide variation is due, as some of the authors themselves point out, to the nature of the original data which is sometimes in the form of explosion data or nonisothermal experiments or to widely varying purity levels of the lead azide. The Arrhenius temperature coefficient for the induction period parameter A of the model is not significantly different from that for k/ρ, which would indicate that the same mechanism is controlling both the initiation of decomposition and the progress of the decomposition reaction. There was no significant effect of particle size on the temperature coefficients, a result which would be expected for a model that was constructed correctly so as to separate and describe particle-size effects independently. The model could not be fit to the data for the coarse particles because of the hump in the early part of the curve, presumably caused by the splitting of the very largest particles.

One of the major objectives of this work was met by the ability of the model to discern the effects of particle size with an accuracy on the order of 10%. The thermal decomposition data for α-lead azide powder of a given particle-size distribution can be transformed rather reliably to a different particle-size distribution and, thus, permit comparison and study of other effects, such as those of added impurities, in the absence of particle-size effects of the same order of magnitude. Furthermore, the derived model parameter k/ρ was demonstrated to have the physical significance of the rate of penetration of the reaction front into the crystal.

Acknowledgment. This work was supported by the U. S. Army Research Office—Durham. The α-lead azide and guidance on its safe handling were provided by the personnel of the Explosives Division of Picatinny Arsenal.

Collisionally Induced Production of $Hg(^3P_1)$ from $Hg(^1P_1)$[1]

V. Madhavan, Norman N. Lichtin,* and Morton Z. Hoffman

Department of Chemistry, Boston University, Boston, Massachusetts 02215 *(Received August 4, 1972)*

Emission at 2537 Å is observed when mercury vapor is exposed to 1849-Å resonance radiation in the presence of each of the following gases: He, Ne, Ar, Kr, D_2, CO, N_2, CH_4, H_2O, D_2O, C_2H_6, C_2D_4, C_3H_8, c-C_6H_{12}, and CF_4. It was not detected with H_2, NH_3, ND_3, C_2H_4, and CO_2. The only plausible mechanism of scintillation in the case of the monatomic gases is one-step collisionally induced intersystem crossing from $Hg(^1P_1)$ to $Hg(^3P_1)$. This process may possibly occur to some degree with any of the di- and polyatomic gases, but is not obligatory. Analysis of the pressure dependence of the intensity of 2537-Å emission for eight of the gases provides values of relative cross sections for quenching of 1849-Å emission. Relative cross sections for collisionally induced intersystem crossing can be estimated from limiting values of the intensity of 2537-Å emission and relative quenching cross sections if a one-step mechanism for intersystem crossing is assumed.

Introduction

An earlier study[2] examined the dependence upon pressure of N_2 or CO of the intensity of 2537-Å scintillation produced by 1849-Å irradiation of mixtures of each of these gases with mercury vapor.[3] These data were shown to be equally consistent with induction of intersystem crossing from $Hg(^1P_1)$ to $Hg(^3P_1)$ by a single collision, *e.g.*, eq 3 or by a two-step process, *e.g.*, eq 6 and 8. Two-step processes involving triplet intermediates are energetically possible with both N_2 (triplet energy 6.16 eV) and CO (triplet energy 6.01 eV) since $Hg(^1P_1)$ lies 6.68 eV above $Hg(^1S_0)$. Induction of 2537-Å scintillation by Ne and He was also reported in our earlier paper[2] but the significance of this phenomenon was not recognized. Since $Hg(^1P_1)$ does not contain enough energy to excite either of these atoms, intersystem crossing to $Hg(^3P_1)$ must occur in a single step. This process is not only optically doubly forbidden (spin and orbital angular momentum) but involves a large loss of energy by mercury, 1.82 eV. There seems to be little if any precedent for such a transition in a collision of the second kind.

$$Hg(^1S_0) + h\nu\ (1849\ Å) \xrightarrow{I_{abs}^{1849}} Hg(^1P_1) \quad (1)$$

$$Hg(^1P_1) \xrightarrow{k_f^{1849}} Hg(^1S_0) + h\nu\ (1849\ Å) \quad (2)$$

$$Hg(^1P_1) + N_2(X^1\Sigma_g^+) \xrightarrow{k_{ISC}} Hg(^3P_1) + N_2(X^1\Sigma_g^+) \quad (3)$$

$$Hg(^3P_1) + N_2(X^1\Sigma_g^+) \xrightarrow{k^{2537,N_2}} Hg(^3P_0) + N_2(X^1\Sigma_g^+) \quad (4)$$

$$Hg(^3P_1) \xrightarrow{k_p^{2537}} Hg(^1S_0) + h\nu\ (2537\ Å) \quad (5)$$

$$Hg(^1P_1) + N_2(X^1\Sigma_g^+) \xrightarrow{k_{ET}^{Hg^*\rightarrow N_2}} Hg(^1S_0) + N_2(A^3\Sigma_u^+) \quad (6)$$

(1) Research supported by Air Force Office of Scientific Research Contract No. AFOSR-765-67
(2) A.Granzow, M. Z. Hoffman, N. N. Lichtin, and S. K. Wason, *J. Phys. Chem.*, **72**, 3741 (1968).
(3) T. A. Gover and H. G. Bryant, Jr., *J. Phys. Chem.*, **70**, 2070 (1966).

$$N_2(A^3\Sigma_u^+) \xrightarrow{k_p^{VK}} N_2(X^1\Sigma_g^+) + h\nu \text{ (Vegard-Kaplan)} \quad (7)$$

$$N_2(A^3\Sigma_u^+) + Hg(^1S_0) \xrightarrow{k_{ET}^{N_2 \rightarrow Hg}} N_2(X^1\Sigma_g^+) + Hg(^3P_1) \quad (8)$$

This paper is devoted to the induction of 2537-Å scintillation by 1849-Å irradiation of mixtures of mercury vapor with each of a wide variety of compounds.

Experimental Section

Equipment and procedures have been described previously.[2] Mercury was maintained at room temperature in all cases. Spectrographic measurements were not employed in the present work. Matheson Prepurified N_2 (99.98%) was further purified as described previously.[2] Airco CP H_2 (99.5%) and Matheson CP CO (99.5%) were freed of condensible gases by passage through a liquid nitrogen trap. Matheson Research Grade He, Ne, Ar, Kr, and CH_4, Phillips Petroleum Research Grade C_2H_4, C_2H_6, and C_3H_8, Stohler D_2 and ND_3 (both 99%), Merck C_2D_4, and Matheson CF_4 (99.7+%) were used as supplied. Distilled water, Stohler D_2O (more than 95% pure), Fisher Spectrograde c-C_6H_{12}, and Matheson CP NH_3 (99.99%) were each subjected to two freeze-pump-thaw degassing cycles. CO_2 was obtained by vacuum sublimation of Airco Dry Ice.

Data

No 2537-Å emission was detectable when mercury vapor was irradiated at 1849 Å in the absence of added gas. Thus leakage of 2537-Å radiation from the low-pressure mercury discharge through the irradiated LiF window was negligible. However, 2537-Å scintillation was observed with all the gases employed except H_2, NH_3, ND_3, C_2H_4, and CO_2. Scintillation intensities (peak heights) were measured as a function of pressure for 15 gases. For most of these gases intensities of 2537-Å emission produced by 2537-Å irradiation of their mixtures with mercury vapor were also measured over appropriate pressure ranges. These data were used to correct intensities of 2537-Å scintillation for quenching of $Hg(^3P_1)$.[2] In most cases, scintillation intensities corrected in this way, $(I_p^{2537})_{cor}$, increased with pressure of added gas to pressure-independent plateau values, as was observed previously[2] with N_2, CO, He, and Ne. In some cases maxima were observed.

Kinetics analysis[2] of the one- and two-step mechanisms leads, respectively, to eq 9 and 10, in which Q is the quencher and k_e^{Q*} is the specific rate of emission from excited quencher (*e.g.*, Vegard-Kaplan emission from $N_2(A^3\Sigma_u^+)$. Both equations are linear relationships between $1/(I_p^{2537})_{cor}$ and $1/(Q)$. A similar formalism emerges[2] from the two-step mechanism regardless of the form of energy storage in the quenching gas. The ratio of the slope to the intercept of eq 9 is k_f^{1849}/k_{ISC}^{Q}. For eq 10 it is $k_f^{1849}/k_{ET}^{Hg*-N2}$. In both cases the ratio of k_f^{1849} to the specific rate of quenching of $Hg(^1P_1)$ is obtained. If one-step quenching of $Hg(^1P_1)$ occurs by a set of parallel bimolecular processes, only one of which produces $Hg(^3P_1)$, an expression results which differs from eq 9 only in that the term $[1 + k_f\, k_{ISC}^{Q}]$ is replaced by $[1 + k_\Sigma^{Q}/k_{ISC} + k_f^{1849}/k_{ISC}(Q)]$, where k_Σ^{Q} is the sum of all bimolecular specific rates of quenching processes which do not produce $Hg(^3P_1)$. The ratio of the slope to the intercept of eq 9, modified in this fashion, is $k_f^{1849}/[k_{ISC}^{Q} + k_\Sigma^{Q}]$. $k_{ISC}^{Q} + k_\Sigma^{Q}$ is identical with the specific rate of quenching, k_Q^{1849}, of 1849-Å emission, relative values of which we have measured directly for a number of gases.[4] Incorporation into the two-step mechanism of quenching of $Hg(^1P_1)$ by a parallel set of bimolecular processes, only a fraction of which transfer energy to quencher equal to or greater than the energy of $Hg(^3P_1)$, and of analogously inefficient bimolecular transfer of energy to $Hg(^1S_0)$ from those quencher molecules which contain energy equal to or greater than that of $Hg(^3P_1)$, leads to a similar result. Again, the ratio of the slope to the intercept of the relationship between $1/I_p^{2537}$ and $1/(Q)$ equals the ratio of k_f^{1849} to the total bimolecular specific rate of quenching of $Hg(^1P_1)$.

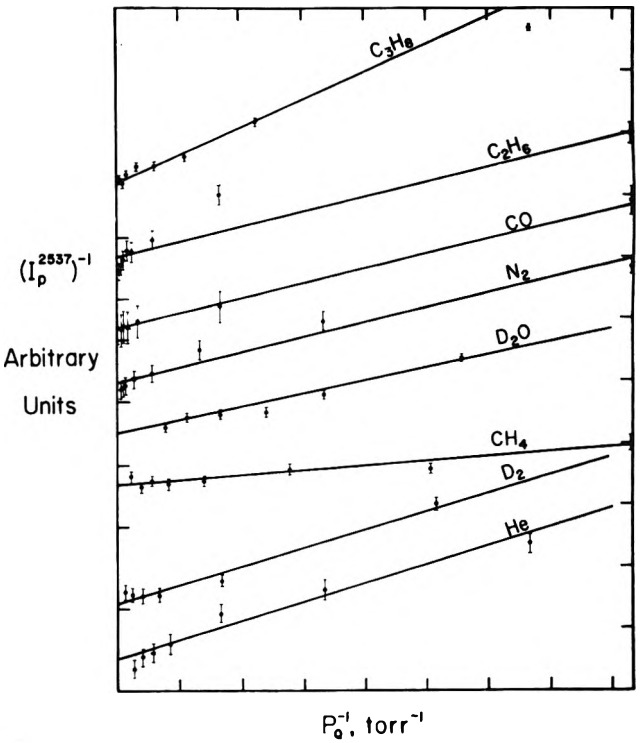

Figure 1. Double reciprocal plots of 2537-Å scintillation data. Ordinate scales (indicated at right-hand border): He, one division = 0.006; N_2, C_3H_8, one division = 0.03; D_2O, C_2H_6, one division = 0.06; CH_4, CO, one division = 0.12; D_2, one division = 0.15. Abscissa scales: CO, one division = 0.3; all others, one division = 0.6. Origin of each plot is indicated at left-hand border.

$$\frac{1}{(I_p^{2537})_{cor}} = \frac{1}{I_{abs}^{1849}}\left[1 + \frac{k_f^{1849}/k_{ISC}^{Q}}{(Q)}\right] \quad (9)$$

$$\frac{1}{(I_p^{2537})_{cor}} = \frac{k_e^{Q^*} + k_{ET}^{Q^* \rightarrow Hg}(Hg)}{k_{ET}^{Hg^* \rightarrow Q} k_{ET}^{Q^* \rightarrow Hg} I_{abs}^{1849}(Hg)}\left[k_{ET}^{Hg^* \rightarrow Q} + \frac{k_f^{1849}}{(Q)}\right] \quad (10)$$

Plots of $1/(I_p^{2537})$ *vs.* $1/P_Q$ for eight gases are presented in Figure 1. Imprisonment of 1849-Å radiation introduces uncertainty as to the value of k_f^{1849} which should be used in calculating rate constants from the data. However, since I_{abs}^{1849} was constant throughout these experiments, relative values of k_Q^{1849} are available from the data of Figure 1. Relative values of cross sections for quenching of

(4) A. Granzow, M. Z. Hoffman, and N. N. Lichtin, *J. Phys. Chem.*, **73**, 4289 (1969).

TABLE I: Relative Cross Sections[a] for Quenching of $Hg(^1P_1)$

Quencher	$\sigma_Q^2/\sigma_{N_2}^2$ From 2537-Å scintillation[b]	$\sigma_Q^2/\sigma_{N_2}^2$ From quenching of 1849-Å fluorescence[c]
He	0.11 ± 0.01	0
D_2	0.55 ± 0.15	
CH_4	2.3 ± 0.2	0.3
D_2O	2.5 ± 0.2	
N_2	(1.00 ± 0.05)	(1.00)
CO	2.3 ± 0.2	1.0
C_2H_6	4.8 ± 0.05	
C_3H_8	2.1 ± 0.06	

[a] Rate constants converted to cross sections by means of eq 2-50, ref 8, p 73. [b] Values of slopes and intercepts determined by least-squares analysis. Uncertainties are standard deviations. [c] Taken from ref 4.

$Hg(^1P_1)$ calculated from them, $\sigma_Q^2/\sigma_{N_2}^2$, are presented in Table I along with relative cross sections obtained[4] by Stern–Volmer treatment of quenching of 1849-Å fluorescence.

The single-step quenching mechanism, generalized by allowing for parallel quenching of $Hg(^1P_1)$ without formation of $Hg(^3P_1)$, leads to

$$(I_p^{2537})_{cor} = \frac{k_{ISC}^{Q}(Q)I_{abs}^{1498}}{k_f^{1849} + [k_{ISC}^{Q} + k_\Sigma^{Q}](Q)} \quad (11)$$

From this equation it follows that limiting values of $(I_p^{2537})_{cor}$ are given by

$$(I_p^{2537})_{cor,\,lim} = \frac{k_{ISC}^{Q}I_{abs}^{1498}}{k_{ISC}^{Q} + k_\Sigma^{Q}} \quad (12)$$

Since I_{abs}^{1849} was not measured, eq 12 allows only relative values of $k_{ISC}^{Q}/[k_{ISC}^{Q} + k_\Sigma^{Q}]$ to be determined. However, it can be easily demonstrated that

$$\frac{(\sigma_{ISC}^2)^Q}{(\sigma_{ISC}^2)^{N_2}} = \frac{(I_p^{2537})_{cor,\,lim}^{Q}}{(I_p^{2537})_{cor,\,lim}^{N_2}} \frac{\sigma_Q^2}{\sigma_{N_2}^2} \quad (13)$$

Values of $(\sigma_{ISC}^2)^Q/(\sigma_{ISC}^2)^{N2}$ calculated by eq 13 are given in Table II. Unless otherwise stated, the employed values of $\sigma_Q^2/\sigma_{N_2}^2$ were obtained by the 2537-Å scintillation method which has given values larger than those obtained more directly from quenching of 1849-Å emission (see Table I).

Equation 14 is the expression for the limiting value of I_p^{2537} according to the two-step mechanism including the possibility of collisions between $Hg(^1P_1)$ and quencher, *e.g.*, $N_2(X^1\Sigma_g^+)$ and between $Hg(^1S_0)$ and excited quencher, *e.g.*, $N_2(A^3\Sigma_u^+)$, which do not produce, respectively, $N_2(A^3\Sigma_u^+$ or $Hg(^3P_1)$.

$$(I_p^{2537})_{cor,\,lim} = \frac{k_{ET}^{Hg^*\to Q}k_{ET}^{Q^*\to Hg}(Hg)I_a^{1849}}{[k_{ET}^{Hg^*\to Q} + k_{15}^{Q}][k_e^{Q^*} + (k_{ET}^{Q^*\to Hg} + k_{16}^{Q})(Hg)]} \quad (14)$$

$$Hg(^1P_1) + Q \xrightarrow{k_{15}^{Q}} \text{products not involved in emission or energy transfer} \quad (15)$$

$$Q^* + Hg(^1S_0) \xrightarrow{k_{16}^{Q}} \text{products not involved in emission or energy transfer} \quad (16)$$

Although values of σ_Q^2 correspond to $[k_{ET}^{Hg^*\to Q} + k_{15}^{Q}]$ and are available from the double reciprocal plots, it is not possible to evaluate relative cross sections for excitation of quenchers to states capable of exciting $Hg(^3P_1)$, $k_{ET}^{Hg^*\to Q}/k_{ET}^{Hg^*\to N2}$ from eq 14 unless $k_{ET}^{Q^*\to Hg} \gg k_{16}^{Q}$ and $k_{ET}^{Q^*\to Hg}(Hg) \gg k_e^{Q^*}$. The meaning with respect to the two-step mechanism of values presented in Table II as $(\sigma_{ISC}^2)_Q/(\sigma_{ISC}^2)_{N_2}$ is therefor not defined.

TABLE II: Apparent Relative Cross Sections for Collisionally Induced Intersystem Crossing from $Hg(^1P_1)$ to $Hg(^3P_1)$[a]

Gas	$\frac{(I_p^{2537})_{corr,\,lim}^{Q}}{(I_p^{2537})_{corr,\,lim}^{N2}}$	$\frac{(\sigma_{ISC}^2)^Q}{(\sigma_{ISC}^2)^{N2}}$
He	0.06	0.007
Ne	0.025	[0.008][b]
Ar	0.06	[0.07][b]
Kr	0.05	
H_2	0[c]	0
D_2	0.1	0.06
CO	0.25	0.6
N_2	(1.00)	(1.00)
CH_4	0.3	0.7
C_2H_6	0.45	2.2
C_3H_8	0.25	0.5
$c\text{-}C_6H_{12}$	0.03	[0.09][b]
C_2H_4	0[c]	0
C_2D_4	0.1	
NH_3	0[c]	0
ND_3	0[c]	0
H_2O	0.02	
D_2O	0.035	0.09
CO_2	0[c]	0
CF_4	~0.2	[~0.6][b]

[a] Calculated on the basis of the one-step energy transfer mechanism by means of eq 13. See text for a discussion of the relationship of these numbers to the two-step mechanism. [b] Calculated using values of σ_Q^2/σ_{N2}^2 taken from ref 4. [c] Uncorrected $(I_p^{2537})_{lim}$ less than 1% of value for N_2.

Discussion

Whatever its mechanism may be, collisional production of $Hg(^3P_1)$ from $Hg(^1P_1)$ is a quite general phenomenon, occurring with monatomic, diatomic, and polyatomic quenchers. A consequence of this is that 1849-Å mercury photosensitization is likely to be admixed with 2537-Å mercury photosensitization, regardless of the monochromatic nature of the exciting light.

The data of this paper are incapable of distinguishing the one- and two-step mechanisms from each other. However, none of the four rare gases which were studied can be excited by the energy available in $Hg(^1P_1)$ and, with them, only a one-step mechanism is possible. The mode of dissipation of the 1.82-eV energy difference between $Hg(^1P_1)$ and $Hg(^3P_1)$ is not known. The common occurrence of satellite bands near the 1849-Å line of fluorescence from 1849-Å photoexcited mixtures of mercury vapor with a variety of gases,[5] including He, Ne, and Ar, indicates that $Hg(^1P_1)$ readily forms weakly bound exciplexes. Possibly a fraction of such associated species undergo intersystem crossing to triplet manifold and lose energy collisionally or emissively before dissociating. One-step collisional induction of intersystem crossing may also contribute to the action of diatomic and polyatomic quenchers although it is obligatory with few of them. Where it occurs, additional modes of dissipation of the 1.82-eV energy difference are available.

(5) A. Granzow, M. Z. Hoffman, and N. N. Lichtin, *J. Chem. Phys.*, **51**, 3621 (1969).

We have previously elaborated[2] possible two-step mechanisms for N_2 and CO in which these quenchers are represented as excited by energy transfer from $Hg(^1P_1)$ to electronic or vibrational states which can then collisionally excite Hg from $^1S_0$ to $^3P_1$. With N_2 and CO electronic states of appropriate energy, $A^3\Sigma_u^+$ and $a^3\pi$, are known spectroscopically. However, nonspectroscopic upper electronic states of diatomic and polyatomic quenchers cannot be ruled out as possible intermediates in two-step mechanisms. Both one- and two-step mechanisms may be significant for some diatomic and polyatomic quenchers and two-step mechanisms may, for some quenchers, involve more than one excited state of a given quencher.

The meaning of the relative cross sections for quenching of $Hg(^1P_1)$ assembled in Table I is independent of quenching mechanism. Although agreement between values determined from 2537-Å scintillation data and those determined directly from quenching of 1849-Å fluorescence[4] is only fair, both sets of data display the same striking feature; measured cross sections for quenching $Hg(^1P_1)$ vary with the nature of the quenching gas far less than do cross sections for quenching $Hg(^3P_1)$.[4]

The fact that 2537-Å scintillation was not detectable for H_2, NH_3, ND_3, C_2H_4, and CO_2 does not, of course, mean that no $Hg(^3P_1)$ is produced. NH_3, and presumably ND_3, absorb intensely at 1849 Å[6] ($\epsilon > 10^2$ atm^{-1} cm^{-1}) and may compete effectively for imprisoned 1849-Å radiation. C_2H_4 absorbs about one-tenth as intensely at 1849 Å[7] but is almost ten times as effective a quencher of $Hg(^3P_1)$[8] as NH_3 and more than 100 times as effective as N_2. Both factors may contribute to reducing the 2537-Å emission below the threshold of detection in our system. Neither CO_2 nor H_2 absorbs significantly at 1849 Å. Both are effective quenchers of $Hg(^3P_1)$[8] but the 2537-Å scintillation was observed in the presence of gases which are similarly effective (CO, D_2, C_3H_8) or even more so (c-C_6H_{12}). Apparently, CO_2 and H_2 are relatively inefficient in inducing conversion of $Hg(^1P_1)$ to $Hg(^3P_1)$.

The difference in behavior of C_2D_4 and C_2H_4 may possibly be due in part to the lower absorptivity of C_2D_4 at 1849 Å.[7] Since D_2 is a somewhat more effective quencher of $Hg(^3P_1)$ than is H_2 no such trivial contribution to the different behavior of these isotopic compounds is apparent. The data for H_2O and D_2O do not warrant analysis of an "isotope effect."

(6) K. Watanabe, *J. Chem. Phys.*, **22**, 1564 (1954).
(7) P. G. Wilkinson and R. S. Mulliken, *J. Chem. Phys.*, **23**, 1895 (1955).
(8) J. G. Calvert and J. N. Pitts, "Photochemistry," Wiley, New York, N.Y., 1966, p 74.

Isotopic Enrichment of Carbon-13 and Oxygen-18 in the Ultraviolet Photolysis of Carbon Monoxide

O. Dunn, P. Harteck, and S. Dondes*

Chemistry Department, Rensselaer Polytechnic Institute, Troy, New York 12181 *(Received November 5, 1971)*

Publication costs assisted by the National Science Foundation

Using the 2062.4-Å iodine line, the isotopic enrichment of ^{13}C and ^{18}O has been studied in the photolysis of CO. Using CO containing $^{13}C^{16}O$, $^{12}C^{18}O$, and $^{13}C^{18}O$, the isotope effect has been examined in the products of the photolysis, *i.e.*, CO_2 and C_3O_2. Isotope separation factors for ^{13}C enrichment in C_3O_2 of 4 and in CO_2 of 2.5 and ^{18}O enrichment in CO_2 of 5 for a single-step process have been obtained. Also included are extinction coefficient determinations at 2062.4 Å. The mechanism of the photolytic reaction is examined from the enrichment, which serves as a tracer, and from energy transfer considerations.

The photochemical isotopic enrichment of ^{13}C and ^{18}O in the ultraviolet photolysis of natural CO using the 2062.4-Å iodine line has been reported previously by Liuti, Dondes, and Harteck.[1,2] They have shown that by making use of the sharp 2062.4-Å line of monoisotopic atomic iodine emitting from a lamp developed by Harteck, Reeves, and Thompson[3] one can promote preferential excitation of $^{13}C^{16}O$ and $^{12}C^{18}O$ to the $a^3\Pi$ (v = 0) state of the intercombination ($a^3\Pi \leftarrow x^1\Sigma$) Cameron band system. Isotopic shifts of 4.7 cm^{-1} for $^{13}C^{16}O$ and 5.2 cm^{-1} for $^{12}C^{18}O$ in the $a^3\Pi \leftarrow x^1\Sigma^+$ (0,0) transition position the band head of a rotational branch for these isotopic species of CO at a wavelength which corresponds closely to the 2062.4-Å iodine line. Reaction of the relatively long-lived excited $a^3\Pi$ CO molecules with ground state CO molecules leads to a substantial isotopic enrichment of ^{13}C and ^{18}O in the reaction products, CO_2 and C_3O_2, by the following reaction mechanism

$$^{13}CO^* + CO \longrightarrow {}^{12}CO_2 + {}^{13}C \quad (1a)$$

$$^{13}CO^* + CO \longrightarrow {}^{13}CO_2 + {}^{12}C \quad (1b)$$

(1) G. Liuti, S. Dondes, and P. Harteck, *J. Chem. Phys.*, **44**, 4052 (1966).
(2) G. Liuti, S. Dondes, and P. Harteck, *Advan. Chem. Ser.*, **No. 89**, 1 (1969).
(3) P. Harteck, R. R. Reeves, Jr., and B. A. Thompson, *Z. Naturforsch. A*, **19**, 2 (1964).

$$^{12}C^{18}O^* + CO \longrightarrow {}^{18}O^{12}C^{16}O + {}^{12}C \quad (1c)$$

$$^{13}C + CO + M \longrightarrow {}^{13}C{=}{}^{12}C{=}O + M \quad (2)$$

$$^{13}C{=}{}^{12}C{=}O + CO + M \longrightarrow O{=}{}^{12}C{=}{}^{13}C{=}{}^{12}C{=}O + M \quad (3)$$

To further substantiate these findings and to provide some of the finer details of this isotope effect a series of photochemical experiments using the iodine lamp were performed with natural CO enriched with various concentrations of $^{13}C^{16}O$, $^{12}C^{18}O$, and $^{13}C^{18}O$.

Experimental Section

The experimental apparatus (Figure 1) employed in this work differs from the apparatus used previously. The temperature of the lamp which influences the isotopic enrichment of the products (CO_2 and C_3O_2) primarily through the temperature dependence of Doppler broadening of the excitation line was controlled by inserting a water cooling tube in the lamp. Although the results with lamp cooling tended to give a little better isotope separation, the main advantage to lamp cooling was seen in the consistency of results obtained from one experiment to the next. The Optosil quartz lamp which has about 80% transmission at 2000 Å was operated in a vertical position in a closed loop with a gas circulating device and product trap. The total volume of this system is 3 l. The gas circulating device, developed specially for use in this system for the rapid removal of C_3O_2 which is subject to photodecomposition, consists of a nylon fan wheel with ceramic magnets mounted on its base enclosed in a heavy walled glass container which is joined to the system by means of ball and socket glass joints at its entrance and exit ports. An aluminum shaft recessed at both ends and fixed to the base of the fan wheel forms the axis of rotation for the unit. Inward protruding glass pivot points fused to the top and bottom of the glass container are fitted to tapered Teflon inserts placed in the recesses at the top and bottom of the aluminum shaft. The glass to Teflon surfaces of the glass pivot points and Teflon inserts provide a good bearing for the rotational motion induced on the fan wheel by an external bar magnet mounted on the shaft of an electric motor. Under the usual operating conditions of 400 Torr of gas in the apparatus, a fan wheel speed of 2200 revolutions per minute produces a gas flow rate of approximately 200 cc/sec.

The natural CO used in these experiments was research grade carbon monoxide obtained from Matheson Co. Further purification consisted of adsorbing the CO on activated silica gel at 77°K and retaining only the middle portion of the desorbing gas on warming. The CO was also flowed through a U-tube immersed in a liquid nitrogen bath before entry to the reaction vessel. Emphasis is placed on the purity of the CO used since it is essential to the isotope effect that all inhibiting and side reactions caused by impurities be eliminated. The purity of the carbon monoxide used, as determined by mass spectrometric analysis, was better than 99.99%.

The enriched carbon monoxide isotopic species, $^{13}C^{16}O$, $^{12}C^{18}O$, and $^{13}C^{18}O$, were obtained from Isomet Corp, Palisades Park, N. J., and could be used without further purification. The isotopic mixtures of purified natural CO with either $^{13}C^{16}O$, $^{12}C^{18}O$, or $^{13}C^{18}O$ were prepared in the following manner. The purified natural CO from a storage vessel was adsorbed on silica gel at 77°K. The desired amount of enriched CO was then introduced into the

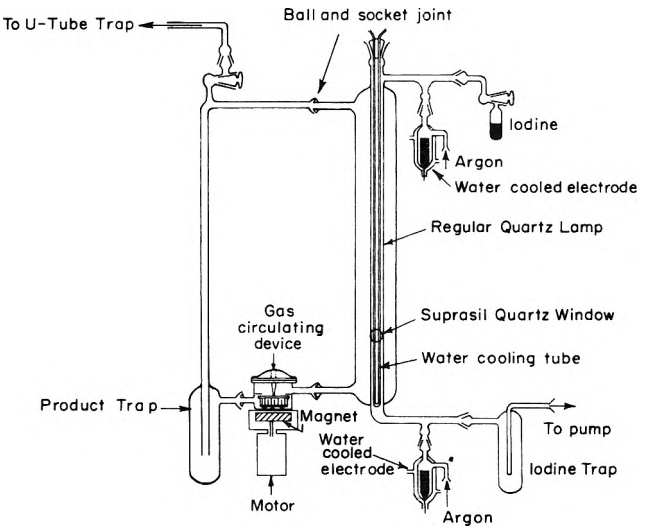

Figure 1. Iodine lamp modified to incorporate a gas circulating device and product trap.

evacuated reaction vessel through a sampling port. Next, the vessel containing the adsorbed CO was gradually warmed and as the CO desorbed from the silica gel it was conducted through a U-tube immersed in liquid nitrogen and introduced into the reaction vessel through a partially opened stopcock. The CO desorbing from the silica gel was always maintained at a higher pressure than the CO in the reaction vessel. This kept back-diffusion of the enriched CO from the reaction vessel to a minimum. Good mixing was obtained by use of the gas circulating device. Samples were taken of the isotope mixtures prior to each experiment for analysis on a CEC (21-130) mass spectrometer.

The photolysis experiment consisted of irradiating various isotopic mixtures of carbon monoxide for a period of 2.5 hr with an iodine lamp emitting 1.8×10^{18} quanta/sec at 2062.4 Å as determined by the decomposition of NH_3. Using liquid nitrogen as coolant for the product trap allows for a total CO pressure of 400 Torr in the reaction vessel. Following the irradiation, the isotopically enriched reaction products, CO_2 and C_3O_2, are separated from the carbon monoxide by slowly passing the unreacted CO together with the products through a U-tube immersed in liquid nitrogen. The flow rate for this procedure which takes about 3 hr is controlled by the rate of adsorption of CO on silica gel as it is cooled to 77°K. The distribution of the ^{13}C and ^{18}O isotopes was determined by mass spectrometric analysis.

With respect to the isotope separation found, it should be noted that procedures used in handling the isotopic mixtures of CO, such as adsorption on silica gel, had no noticeable effect on the relative abundances of the isotopes in CO.

Results

The results obtained from the irradiation of carbon monoxide in which the concentration of $^{13}C^{16}O$ and $^{12}C^{18}O$ are varied are shown in Tables I and II, respectively. The concentrations of the isotopes ^{12}C, ^{13}C, ^{16}O, and ^{18}O in the CO isotopic mixtures are expressed as a relative abundance with respect to the most abundant isotope. The isotope distribution of ^{13}C and ^{18}O in the products is also expressed in terms of relative abundance. The ^{13}C content in C_3O_2 as determined by the mass spectro-

TABLE I

Relative abundances of the isotopes in CO				Relative abundances[a] of ^{13}C in C_3O_2 at mass 69	Separation factor[b] of ^{13}C in C_3O_2	Separation factor of ^{13}C in C_2O^+ mass fragment	Relative abundances[a] of ^{13}C in CO_2 at mass 45	Separation factor of ^{13}C in CO_2	Relative abundances[a] of ^{18}O in CO_2 at mass 46	Separation factor of ^{18}O in CO_2
^{12}C	^{13}C	^{16}O	^{18}O							
98.71	1.52	100	0.231	9.58	4.3	4.27	3.58	2.36	1.18	4.13
98.64	1.57	100	0.227	9.52	4.06	4.16	3.50	2.23	1.17	4.15
98.34	1.89	100	0.24	12.36	4.54	4.51	4.30	2.28	1.16	3.83
97.67	2.55	100	0.225	17.14	4.72	4.69	7.34	2.87	1.36	5.04
96.63	3.60	100	0.23	21.5	3.97	3.98	9.72	2.76	1.45	5.30
96.44	3.80	100	0.237	23.78	4.06	4.10	11.61		1.56	4.58
94.62	5.66	100	0.272	29.74	3.25	3.28	15.28	2.70	1.6	4.88
94.42	5.84	100	0.271	29.85	3.11	3.10	15.3	2.62	1.55	4.72
94.09	6.18	100	0.265	32.13	3.2	3.15	15.15	2.45	1.3	3.91

[a] The relative abundance of C_3O_2 at mass 68 and of CO_2 at mass 44 equals 100. Separation factor for ^{13}C in C_3O_2 is for the enriched central carbon atom of this molecule. [b] A separation factor of unity would indicate a normal random distribution of the isotopic components.

TABLE II

Relative abundances of the isotopes in CO				Relative abundances[a] of ^{18}O in CO_2 at mass 46	Separation factor[b] of ^{18}O in CO_2	Relative abundances[a] of ^{18}O in C_3O_2 at mass 70	Separation factor of ^{18}O in C_3O_2	Relative abundances[a] of ^{13}C in CO_2 at mass 45	Separation factor of ^{13}C in CO_2
^{12}C	^{13}C	^{16}O	^{18}O						
100	1.33	99.97	1.35	9.22	5.83	2.65	0.963	4.30	3.23
100	1.33	99.93	1.39	9.42	5.76	2.84	1.04	4.55	3.42
100	1.33	99.86	1.47	9.59	5.52	2.98	1.03	4.15	3.12
100	1.34	99.8	1.54	10.40	5.75	3.36	1.10	4.26	3.18
100	1.34	99.67	1.69	11.53	5.94	3.73	1.05	4.14	3.09
100	1.34	99.59	1.75	12.91	6.38	3.55	1.03	4.57	3.41
100	1.35	99.55	1.80	12.54	5.97	3.79	1.10	4.32	3.20
100	1.33	99.47	1.86	12.2	5.55	3.86	1.08	4.27	3.21

[a,b] See corresponding footnotes to Table I.

metric peak height at m/e 69 (one ^{13}C atom) is expressed as a relative abundance with respect to the peak height of C_3O_2 at m/e 68 arbitrarily set at relative abundance 100. Similarly, the relative abundance of ^{13}C and ^{18}O in CO_2, as determined by their respective mass spectrometric peak heights at m/e 45 and 46, are expressed as relative abundances with respect ot CO_2 at m/e 44 arbitrarily set at relative abundance 100.

The isotopic enrichments of ^{13}C and ^{18}O in the products are presented as isotope sepraration factors. The calculation of the isotope separation factors is best explained in terms of an example. Preferential absorption of the 2062.4-Å iodine line by $^{13}C^{16}O$ leads to an enrichment of ^{13}C only in the center position of the C_3O_2 molecule as reported previously.[1,2] Therefore a separation factor for ^{13}C in C_3O_2 is calculated only for the center atom of this molecule. From Table I, a relative abundance for ^{13}C in C_3O_2 of 9.58 was obtained when the carbon monoxide used contained ^{13}C with a relative abundance of 1.52. The contribution, 2(1.52), made to the relative ^{13}C abundance in C_3O_2 at m/e 69 by the two end carbon atoms was substracted from the total abundance found. This leaves a relative abundance of 6.54 for ^{13}C in the center position of the C_3O_2 molecule. Dividing this value by the relative abundance of ^{13}C in the CO used gives an isotope separation factor of 4.3 for ^{13}C enrichment in C_3O_2 for this particular experiment. Since a separation factor of unity would indicate a normal random distribution of ^{13}C in C_3O_2, this value (4.3) means that C_3O_2 has been enriched 4.3 times normal in the center position of the C_3O_2 molecule, or, expressing this in another way, the relative abundance of ^{13}C in C_3O_2 has been increased by 330%. Similarly, separation factors for ^{13}C in CO_2 and ^{18}O in CO_2 and C_3O_2 have been determined and are shown in Tables I and II.[4] Also, using the mass spectrometric cracking pattern of C_3O_2, a separation factor for ^{13}C in the C_2O^+ mass fragment has been determined. As shown in Table I, the separation factor for ^{13}C in C_3O_2 and ^{13}C in C_2O are, within experimental error, the same. This could only result if ^{13}C enrichment is in the center carbon atom of the C_3O_2 molecule. Support for the presence of free carbon atoms in the system and the reaction mechanism as presented previously[1,2] is also provided by this result.

From the data presented in Table I, a graph of the relative abundance of ^{13}C found in the carbon suboxide *vs.* the relative abundance of ^{13}C in CO was plotted and is shown in Figure 2. The distinctive falling off from linearity at higher ^{13}C abundance in CO displayed in this graph is an interesting feature which will be discussed. A graph of the relative ^{18}O abundance in CO_2 *vs.* the relative ^{18}O abundance in CO was plotted from the data in Table II and is shown in Figure 3. A similar falling off from linearity to that observed for ^{13}C enrichment in C_3O_2 was anticipated for ^{18}O enrichment in CO_2 but was not found.

A series of experiments was also performed in which the concentration of $^{13}C^{18}O$ was varied. Because this molecule could be obtained with only 42% concentration, the remainder being primarily $^{12}C^{18}O$, the range of concentrations that could be used in admixture with natural CO

(4) The data in these tables have been treated in a slightly different manner than data reported previously.[1]

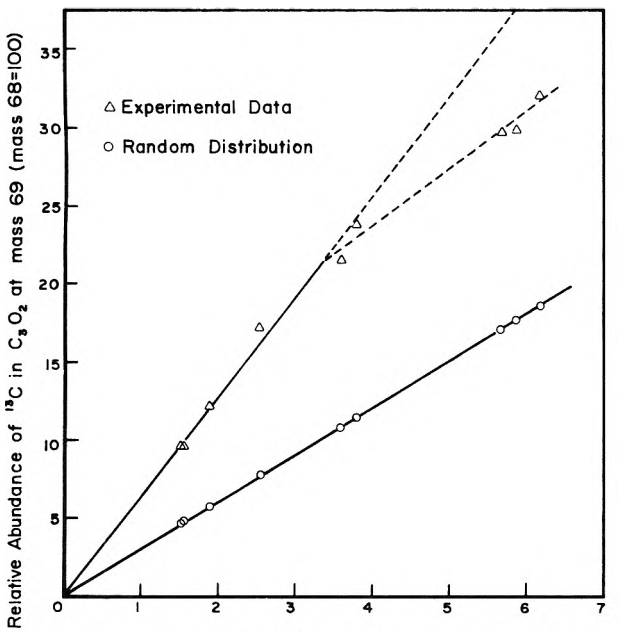

Figure 2.

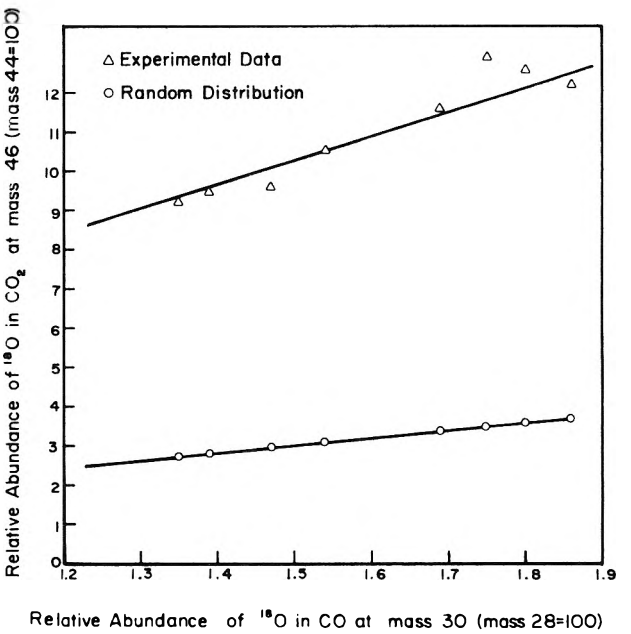

Figure 3.

was limited. The results from the photolysis experiments with $^{13}C^{18}O$ revealed that no isotope effect of similar magnitude to that for $^{13}C^{16}O$ and $^{12}C^{18}O$ is realized for this molecule. This result and the preferential absorption of the 2062.4-Å iodine line by $^{13}C^{16}O$ and $^{12}C^{18}O$ can be illustrated in terms of the fortrat parabolas for $^{12}C^{16}O$, $^{13}C^{16}O$, $^{12}C^{18}O$, and $^{13}C^{18}O$ which were plotted[5] from computer-generated data for the transition $a^3\Pi \leftarrow x^1\Sigma$ ($v' = 0, v'' = 0$).

The isotope sepration factors obtained for ^{13}C enrichment in C_3O_2 (≈ 4) and CO_2 (≈ 2.5) and ^{18}O enrichment in CO_2 (≈ 5) for a single-step process are substantially greater than isotope separation factors realized in most isotope separation techniques. Because of this advantage over other isotope separation methods, this photochemical system has been considered for use as a practical method for ^{13}C and ^{18}O separation. Since absorption of 2062.4-Å ultraviolet light is low, the important factor that enters into this consideration is the quantum yields of CO_2 and C_3O_2 product formation.

As a consequence of exploratory experiments with the iodine lamp performed by Harteck, Reeves, and Thompson[3] and the large isotope separation factor obtained for ^{13}C enrichment in C_3O_2 in the original investigation[1,2] of this isotope effect, the quantum yield for the production of CO_2 was prematurely estimated to approach unity before all of the details of this system were known. Because Donovan and Husain[6] later reported that a significant energy transfer occurred from the $a^3\Pi$ state of CO to a high vibrational level of $x^1\Sigma^+$ state followed by vibrational relaxation to the ground and because of the need to evaluate this system for use as a method to separate ^{13}C and ^{18}O, the efficiency of this system in producing isotopically enriched CO_2 and C_3O_2 was given closer examination.

In an experiment in which 400 Torr of natural CO was irradiated for 3 hr with the 2062.4-Å iodine line (1.9×10^{22} quanta emitted by the lamp at 2062.4 Å in this period of time) 0.09 mg of CO_2 were obtained. This gives a quantum yield of 0.016 for the production of CO_2. The absorption coefficient of natural CO used in this calculation was measured to be 2.4×10^{-1} cm^{-1} atm^{-1}. The measurement was made at a CO pressure of 400 Torr. Since the lifetime of $a^3\Pi$ CO from the latest reports in the literature[7] is on the order a millisecond, loss of $a^3\Pi$ CO by reaction and energy transfer is favored over fluorescence emission. In the flash photoexcitation work of Donovan and Husain[6] they indicate an estimated conversion efficiency of 20% for the transfer of energy from the $a^3\Pi$ state of CO and found no evidence for product formation. It should be noted that the experimental conditions used by Donovan and Husain differ radically from the conditions used in this work. To mention one point of difference, Donovan and Husain used at most 50 Torr of CO compared to the 400 Torr of CO used here. Energy transfer is no doubt strongly dependent on pressure and both energy transfer and the extent of reaction are expected to be greater at the higher pressures used in this work.

The reaction mechanism established[8] for the formation of CO_2 and C_3O_2 indicates that one molecule of each of these products should be obtained for each $a^3\Pi$ CO molecule that reacts, however, equivalent quantities of CO_2 and C_3O_2 were not found. The quantum yield for C_3O_2 production in these experiments is alway about one-sixth of that for CO_2 production. This can be explained in terms of the more labile nature of C_3O_2. There are a number of possibilities for the loss of C_3O_2 in this system. Since the absorption coefficient of C_3O_2 at 2052.4 Å is approximately 50 cm^{-1} atm^{-1},[9] photodecomposition of C_3O_2 by the same light that initiated its formation is possible. Because the concentration and residence time of C_3O_2 in the zone of illumination are minimized by efficient circulation of the gas through a product trap, photodecomposition at this wavelength is estimated not to exceed 5 or 10% of the total C_3O_2 formed. Although the quantity of

(5) O. Dunn, Ph.D. Thesis, Rensselaer Polytechnic Institute, 1971.
(6) R. J. Donovan and D. Husain, *Trans. Faraday Soc.*, **63**, 2879 (1967).
(7) V. Hasson and R. W. Nicholls, *J. Phys. B*, **4**, 481, (1971).
(8) G. Liuti, S. Dondes, and P. Harteck, *J. Chem. Phys.*, **44**, 4051 (1966).
(9) H. H. Kim and J. L. Roebber, *J. Chem. Phys.*, **44**, 1709 (1966).

C_3O_2 produced is small, polymerization[10] may occur when it is transferred to a small sample vessel for analysis. Also C_3O_2 is known[10] to attack hydrocarbon greases and readily combines with water to form malonic acid. The slower diffusion of C_3O_2 compared to CO_2 may likewise contribute to losses of this product in transferring procedures.

Discussion

From the results on the enrichment of ^{13}C presented in Tables I and II, a substantial enrichment is obtained for this isotope in carbon suboxide, and in carbon dioxide to a lesser extent. Considering the first step in the reaction mechanism following the absorption of light by $^{13}C^{16}O$ as

$$^{13}C^{16}O^* + {}^{12}C^{16}O \longrightarrow {}^{12}CO_2 + {}^{13}C \qquad (1a)$$

$$^{13}C^{16}O^* + {}^{12}C^{16}O \longrightarrow {}^{13}CO_2 + {}^{12}C \qquad (1b)$$

if (1a) is the preferred reaction, then the greater enrichment of ^{13}C will be obtained in carbon suboxide, as observed. Because the absorbed energy is located in the $^{13}C^{16}O$ molecule in the form of electronic excitation, the depth of the potential well for the electronically excited $a^3\Pi$ CO molecules, and hence the dissociation energy from this excited state, will be substantially less than the dissociation energy of the ground-state molecule with which it reacts.

The separation factor for ^{13}C in the carbon suboxide displays a decreasing trend with increasing ^{13}C abundance in the carbon monoxide isotopic mixtures (Table I). This trend manifests itself as the distinctive falling off from linearity shown in Figure 2. Because of the large isotope separation factors obtained it was originally thought that energy transfer, which is not an isotopically selective process, was not important since it would have the effect of reducing the isotope separation. From the results presented here, it is apparent that energy transfer is the predominant process for the loss of $a^3\Pi$ CO. This means that the initial absorption of the 2062.4-Å iodine line by $^{13}C^{16}O$ and $^{12}C^{18}O$ compared to $^{12}C^{16}O$ must be greater than is indicated by the isotope separation factors obtained. As part of this investigation, the absorption coefficients for some of the isotopic components of CO at 2062.4 Å were experimentally determined and are shown in Table III.[5] From the values obtained for the absorption coefficients of $^{12}C^{16}O$ and $^{13}C^{16}O$, equivalent concentrations of $^{12}C^{16}O$ ($a^3\Pi$) and $^{13}C^{16}O$ ($a^3\Pi$) are produced when about 4% $^{13}C^{16}O$ is present in the CO isotopic mixtures. Figure 2 indicates that it is at approximately this concentration that falling off from linearity begins to occur. If it is assumed that the rates for energy transfer from either $^{12}C^{16}O$ ($a^3\Pi$) or $^{13}C^{16}O$ ($a^3\Pi$) are the same, then in CO isotopic mixtures containing about 4% $^{13}C^{16}O$ with the remainder being $^{12}C^{16}O$, the probability for an excited $^{13}C^{16}O$ ($a^3\Pi$) molecule transferring its energy to a high vibrational level of a ground-state ($x'\Sigma$) $^{12}C^{16}O$ molecule is much greater than the probability for an excited $^{12}C^{16}O$ ($a^3\Pi$) molecule to transfer energy to a high vibrational level of a ground-state ($x^1\Sigma$) $^{13}C^{16}O$ molecule because of the much greater concentration of ground-state $^{12}C^{16}O$ molecules.

Since the first step in the reaction mechanism results in both oxygen atoms being left in the CO_2 molecule, ^{18}O from excited $^{12}C^{18}O$ molecules involved in this reaction step should appear only in the CO_2 molecule. This is in agreement with the experimental results in Table III,

TABLE III: Absorption Coefficients of the Carbon Monoxide Isotopic Species at 2062.4 Å

Gas mixtures[b]		Measured values,[a] cm^{-1} atm^{-1}
98.7%	$^{12}C^{16}O$	
1.1%	$^{13}C^{16}O$	
0.2%	$^{12}C^{18}O$	2.4×10^{-3}
6.96%	$^{12}C^{16}O$	
0.32%	$^{13}C^{16}O$	
92.64%	$^{12}C^{18}O$	5.9×10^{-2}
15.39%	$^{12}C^{16}O$	
83.99%	$^{13}C^{16}O$	
0.129%	$^{12}C^{18}O$	4.13×10^{-2}
100%	$^{12}C^{16}O$[d]	1.7×10^{-3}
100%	$^{13}C^{16}O$[d]	4.7×10^{-2}
100%	$^{12}C^{18}O$[d]	6.2×10^{-2}
100%	$^{13}C^{18}O$[c,d]	$\simeq 1 \times 10^{-4}$

[a] Absorption measurements were made at room temperature in an 8-cm cell at a total gas pressure of 400 mm. [b] Enriched carbon monoxide was obtained from Isomet Corp., N. J. [c] Obtained by difference from a fourth isotopic mixture containing 43% $^{13}C^{18}O$. [d] Absorption coefficients for the pure isotopic species are based on the above measurements.

which shows an ^{18}O enrichment in CO_2 but not in C_3O_2. It should be noted that the problem of accounting for the observed isotopic distribution of ^{13}C and ^{18}O in the products is made more complex by the possibility of side reactions with impurities as well as the possible presence of isotope exchange reactions. For example, with water present the reaction

$$CO + H_2O \longrightarrow CO + H + OH$$
$$CO + OH \longrightarrow CO_2 + H$$

is energetically possible especially if the CO molecules contain vibrational energy. The CO_2 resulting from this reaction would have a normal isotopic distribution of ^{13}C and ^{18}O and would therefore dilute the enrichment of the CO_2 molecule.

Because the CO_2 produced in this system is efficiently removed from the zone of illumination by the gas circulating device and product trap and is not decomposed to any significant extent, it was used to calculate the absolute rate constants for the reaction of ($a^3\Pi$) CO with ground-state ($x^1\Sigma$) CO compared to the rate constant for energy transfer from ($a^3\Pi$) CO. The absorption coefficient of CO_2 at 2062.4 Å is less than 10^{-4} cm^{-1} atm^{-1} [11] and is known[12] to be a poor quencher of ($a^3\Pi$) CO. The concentrations of CO_2 and ($a^3\Pi$) CO maintained in the gas phase during the experiment are very small, hence, loss of CO_2 by photodecomposition or by quenching of ($a^3\Pi$) CO will be negligible. Also, the small contributions to the production of CO_2 in this system from the reaction of CO with H_2O impurity should not be significant in this calculation. From the literature the absolute rate constant for the total quenching of ($a^3\Pi$) CO by ground state CO is known[12]

(10) G. Brauer, Ed., "Handbook of Preparative Inorganic Chemistry," Academic Press, New York, N. Y., 1963.
(11) B. A. Thompson, P. Harteck, and R. R. Reeves, *J. Geophys. Res.*, **68**, 6431 (1963).
(12) R. A. Young and G. Van Volkenburgh, *J. Chem. Phys.*, **55**, 2990 (1971).

$$CO\ (a^3\pi) + CO \xrightarrow{K_1} CO_2 + C$$
$$K_{1+2} = 1.2 \times 10^{-10}\ cm^3\ particles^{-1}\ sec^{-1}$$
$$\xrightarrow{K_2} CO^\dagger + CO^\dagger$$

(where $CO^\dagger$ denotes vibrationally excited CO). Knowing from the quantum yield calculation that only 1.6% of ($a^3\Pi$) CO react, K_1 and K_2 are determined to be respectively 1.9×10^{-12} and 1.2×10^{-10} cm^3 $particles^{-1}$ sec^{-1}. This calculation assumes that fluorescence emission from the long-lived $a^3\Pi$ state of CO to be negligible.

Conclusion

The isotope separation factors determined for ^{13}C in C_3O_2 and CO_2 and ^{18}O in CO_2 indicate a large isotope enrichment resulting from the preferential absorption of the 2062.4-Å iodine line by $^{13}C^{16}O$ and $^{12}C^{18}O$. The data obtained reveal some of the finer details of this isotope effect. One distinctive feature displayed in a plot of ^{13}C relative abundance in C_3O_2 *vs.* ^{13}C relative abundance in CO is explained in terms of energy transfer from ($a^3\Pi$) CO. Quantum yield determinations reveal that this energy transfer is probably the predominant process occurring for the disappearance of ($a^3\Pi$) CO and numerous photophysical and photochemical processes occur after excitation.

Acknowledgment. This research was sponsored by the National Science Foundation under Grant No. GP-14518.

Laser Driven Chemical Reactions of Dinitrogen Tetrafluoride with Hydrogen and Sulfur Hexafluoride with Hydrogen[1]

John L. Lyman* and Reed J. Jensen

Los Alamos Scientific Laboratory, University of California, Los Alamos, New Mexico 87544 *(Received August 30, 1972)*

Reactions of N_2F_4 or SF_6 with H_2 were initiated with a high-power pulsed CO_2 laser. Explosion threshold data free from wall effects were obtained for butene-stabilized mixtures of N_2F_4 and H_2. Ultraviolet, visible, and infrared chemiluminescence data were used to corroborate the occurrence of chemical explosions. HF laser gain was observed at early times after laser irradiation of SF_6-H_2 mixtures. In the case of N_2F_4-H_2 mixtures, lower HF laser gain was measured during the preexplosion induction time and was strongly quenched by the explosion. An energy-dependent, unexpectedly short induction time occurred between the laser irradiation and the onset of the explosion. This induction time and observation of early time HF laser gain are indicative of reaction acceleration due to vibrational excitation.

Introduction

In this study we employ vibrational excitation from a pulsed CO_2 laser to ignite the explosion of mixtures of N_2F_4 plus H_2 and to induce the chemical reaction of SF_6 with H_2. Infrared laser excitation has been shown to be useful in laser-induced fluorescence studies of energy transfer,[2a] and Odiorne, *et al.*,[2b] demonstrated a dramatic increase in the reaction rate of HCl with K atoms for HCl molecules that are vibrationally excited as a result of irradiation with an HCl laser. Karlov, *et al.*,[3] induced the explosion of mixtures of BCl_3 and H_2 with a continuous wave (cw) CO_2 laser, and Basov, *et al.*,[4] used a cw CO_2 laser to initiate reactions in several gas mixtures. These authors attributed the observed reactions to vibrationally excited molecules. However, Buchwald, *et al.*,[5] observed the laser-driven pyrolysis of NH_3, and concluded that his data and similar work with cw CO_2 laser radiation could be explained on the basis of thermal energy input.

The data reported here indicate that (1) pulsed infrared laser radiolysis is a viable method for obtaining a fast nonequilibrium increase in the energy of a system, and (2) that vibrational excitation results in chemical reaction more rapidly than if the same amount of energy were added thermally.

Experimental Section

The CO_2 TEA laser used in these experiments is described elsewhere.[6] However, in this work, the beam was reduced to give a spot size of 0.35 cm^2 at the reaction cell except where otherwise noted. The laser pulse was approximately 1 μsec full width at half maximum and lasing occurred for about 8 μsec (Figure 1b, ref 6).

(1) Work performed under the auspices of the U. S. Atomic Energy Commission.
(2) (a) C. B. Moore, *Annu. Rev. Phys. Chem.*, **22**, 387 (1972), and references therein, including C. B. Moore, *Advan. Chem. Phys.*, to be published; (b) T. J. Odiorne, P. R. Brooks, and J. V. V. Kasper, *J. Chem. Phys.*, **55**, 1980 (1971).
(3) N. V. Karlov, N. A. Karpov, Yu. N. Petrov, A. M. Prokhorov, and O. M. Stel'makh, *JETP Lett.*, **14**, 140 (1971).
(4) N. G. Basov, E. P. Markin, A. N. Oraevskii, and A. V. Pankratov, *Sov. Phys. Dokl.*, **16**, 445 (1971); N. G. Basov, E. P. Markin, A. N. Oraevskii, A. V. Pandratov, and A. N. Skachkov, *JETP Lett.*, **14**, 165 (1971).
(5) M. I. Buchwald, R. McFarlane, and S. H. Bauer, Third Conference on Chemical and Molecular Lasers, St. Louis, Mo., May 1-3, 1972.
(6) J. L. Lyman and R. J. Jensen, *Chem. Phys. Lett.*, **13**, 421 (1972).

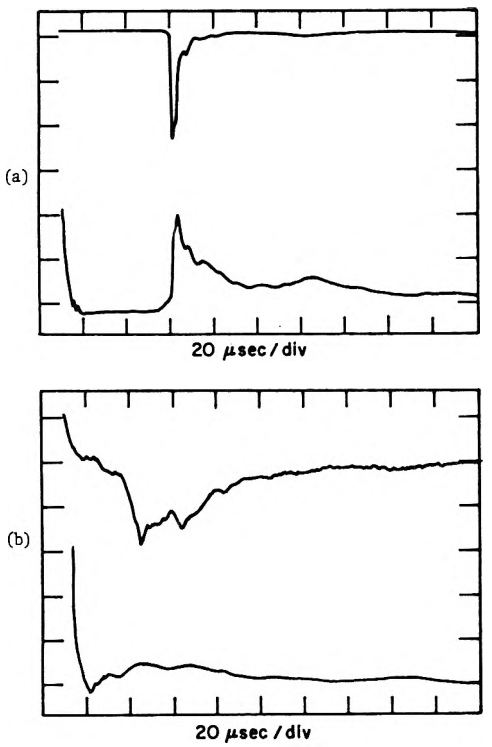

Figure 1. Emission from laser initiated reactions: (a) 26.8% N_2F_4, 72.5% H_2, 0.7% C_4H_8, pressure = 36.8 Torr, spot size = 0.35 cm^2, and laser energy = 0.20 J (upper trace is the photomultiplier response, 50 mV/division; lower trace is the infrared detector response, 2 mV/division); (b) 33.3% SF_6, 66.7% H_2, pressure = 27.9 Torr, spot size = 0.35 cm^2, and laser energy = 0.36 J (upper trace is the photomultiplier response, 1 mV/division; lower trace is the infrared detector response, 0.5 mV/division).

The reaction cell consisted of a 2.5 × 3.8 × 5.1 cm brass block with a 1.27-cm diameter hole centered in its small face and drilled through it lengthwise. A 0.556-cm diameter hole centered 0.793 cm from the front of the cell was drilled at right angles to the 1.27-cm hole and fitted with CaF_2 windows. The gas mixtures were introduced through the rear of the cell and the CO_2 laser pulse entered through a BaF_2 window on the front of the cell.

A 1P28 (S-5) photomultiplier was used to monitor the visible and ultraviolet emission through one of the CaF_2 side windows. A modified Czerny-Turner monochromator was used with the photomultiplier for spectral analysis of the light emission in the visible and ultraviolet regions of the spectrum.

The infrared emission in the region from 2 to 7 μ was monitored by a Philco GPC-216 infrared detector. The frequency range was determined by the response of the GeAu detector and the transmittance of the CaF_2 window.

The HF optical gain and absorption measurements were made by splitting the output from a small HF probe laser into two beams and passing one through CaF_2 side windows and routing the other (reference) outside the reaction cell. The reference beam was passed through a Jarrell-Ash 0.5-m monochromator. The two beams were directed by mirrors to a pair of infrared detectors. The detectors used were either InAs photovoltaic infrared detectors or GeAu infrared detectors from Santa Barbara Research Corp.

A Tektronix 556 dual-beam oscilloscope was used to display the response of the photomultiplier and infrared detectors used in these experiments.

The SF_6–H_2 probe laser consisted of a 30 cm long by 1 cm i.d. quartz discharge tube fitted with CaF_2 Brewster angle windows and with electrodes for longitudinal discharge. The optical cavity was defined by a totally reflecting mirror and a diffraction grating for wavelength selection. The laser radiation was coupled out of the cavity by a CaF_2 flat set at approximately 45° from the optical axis. The time between CO_2 laser pulse and the HF probe laser pulse was controlled electronically. The probe laser output consisted of a submicrosecond pulse at a single selectable HF vibrational-rotational transition frequency.

The N_2F_4 used was determined mass spectrometrically to be 97% pure. The major impurities were N_2 (1.4%), N_2O (0.5%), and N_2F_2 (0.4%). The purities of the H_2 and SF_6 used were 99.9 and 99.8%, respectively. Phillips Petroleum Co. 99.5% pure *cis*-2-butene was used to inhibit spontaneous explosions in N_2F_4–H_2 mixtures. The gases were premixed in a stainless steel vessel and gas pressures were measured with a Texas Instruments Model 145 precision pressure gauge.

The energy incident on the reaction cell was measured by splitting off a few per cent of the beam to a Hadron Model 100 thermopile. The estimated accuracy of the laser energy measurement was ±5% with a precision of ±2%.

N_2F_4–H_2–Butene Explosion Experiments

Explosive reactions of a range of mixtures of N_2F_4, H_2, and *cis*-2-butene were initiated with the pulsed CO_2 laser. The N_2F_4 absorbance of CO_2 laser radiation in two pressure ranges (Figure 2, ref 6) is given approximately by the expressions

$$\log I_0/I = 0.0039lP \quad (P < 18 \text{ Torr})$$

$$\log I_0/I = 0.0078lP - 0.07l \quad (P > 18 \text{ Torr})$$

where l is the path length and P is the N_2F_4 pressure. Both N_2F_4 and its dissociation product NF_2 have infrared absorption bands in the 10.6-μ region.[7,8] The ν_9-NF_2 symmetric stretch band of N_2F_4 is at 946 cm^{-1} and the ν_3 asymmetric stretch band of NF_2 is in the region from 930 to 940 cm^{-1}. Both species could contribute to observed absorption.

Mixtures consisting of 2% or less of butene and 20 to 73% H_2 were investigated. Figure 1a shows a typical oscillogram of the photomultiplier and infrared detector response to the laser-initiated explosion.

The intensity of the emitted radiation was strongly dependent on gas composition and pressure. The infrared emission intensity increased linearly with pressure for a given gas composition. The visible-ultraviolet emission was most intense for the stoichiometric ratio of H_2/N_2F_4 = 2. If H_2/N_2F_4 was decreased from 2 to ¼ while keeping the N_2F_4 and butene partial pressures constant, the visible-ultraviolet emission intensity was reduced by a factor of 100.

For near stoichiometric and hydrogen-rich mixtures, the intensity of the radiation emitted from the exploding gases was nearly independent of laser energy. It was also observed that the reaction propagated well out of the irradiated region. The laser served only to initiate an explosive reaction, and the observed properties of the reaction were independent of the method of initiation after ignition had occurred.

(7) J. R. Durig and R. C. Lord, *Spectrochim. Acta*, **19**, 1877 (1963).
(8) M. D. Harmony, R. J. Myers, L. J. Schoen, D. R. Lide, Jr., and D. E. Mann, *J. Chem. Phys.*, **35**, 1129 (1961).

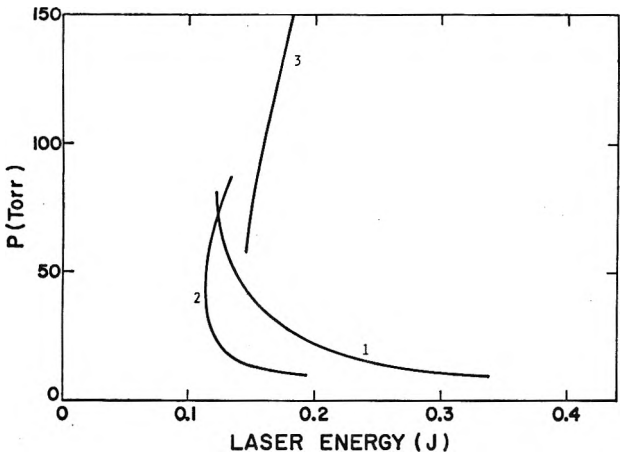

Figure 2. Explosion thresholds for three different gas compositions. P is the total initial pressure and the laser spot size is 0.35 cm^2: (mixture 1) 78.0% N_2F_4, 20.0% H_2, and 2.0% C_4H_8; (mixture 2) 26.8% N_2F_4, 72.5% H_2, and 0.7% C_4H_8; (mixture 3) 26.8% N_2F_4, 71.5% H_2, and 1.7% C_4H_8.

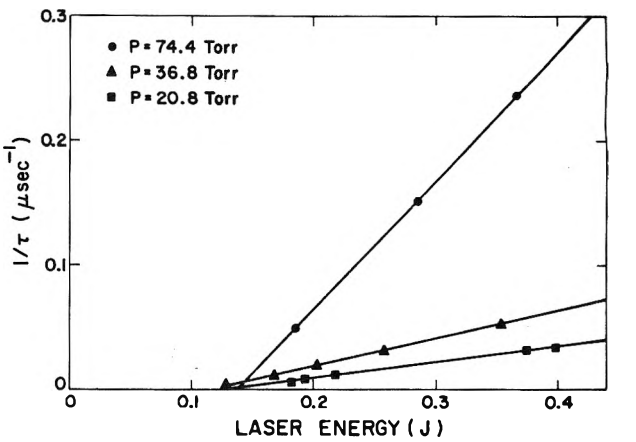

Figure 3. Reciprocal induction time *vs.* laser energy at three different pressures of mixture 2 in Figure 2; laser spot size = 0.35 cm^2.

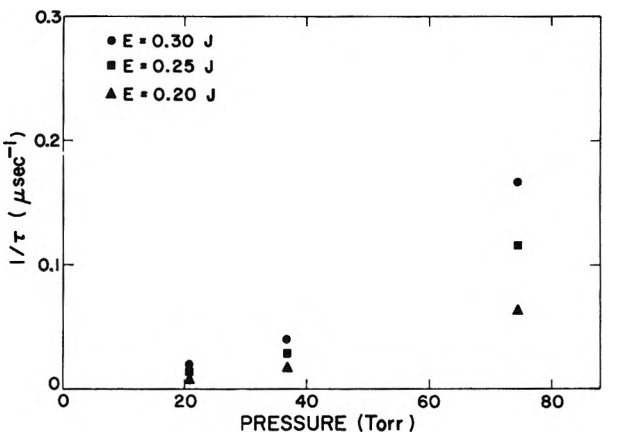

Figure 4. Reciprocal induction time *vs.* pressure for mixture 2 in Figure 2; laser spot size = 0.35 cm^2.

The spectral distribution of the radiation emitted during the explosive reaction of a gas mixture containing 21.5 Torr of N_2F_4, 57.4 Torr of H_2, and 1.34 Torr of *cis*-2-butene was determined by passing the emitted light through a monochromator. The region scanned was from 260 to 600 nm at 20-nm intervals with 20-nm slits. The regions of strong emission were then rescanned at 5-nm intervals with 5-nm slits. Four strong bands and one weak band were observed. The stronger bands were identified as (0,0) and (0,1) bands of the CN violet system at 388 and 422 nm and the (0,0) and (0,1) bands of the C_2 Swan bands at 517 and 564 nm. The weak band was attributed to the ($A^3\Pi \rightarrow X^3\Sigma^-$) transition of NH at 336 nm.

The infrared emission was not investigated spectroscopically; however, emission from vibrationally excited HF in the 2.6–3-μ region was likely a major portion of the observed infrared emission.

It was observed that for a given gas composition and pressure, there was a laser energy below which an explosive reaction would not occur. Figure 2 shows plots of that threshold for three different gas compositions. Explosions occur only to the right of the lines. Mixture 1 was hydrogen lean, mixture 2 was slightly hydrogen rich, and the butene–N_2F_4 ratio was constant for these two mixtures. Note that mixture 2 was more easily ignited than 1 below 75 Torr even though the concentration of the laser absorbing species (N_2F_4) was considerably less than in mixture 1. Mixture 3 differed from 2 only in mole fraction of *cis*-2-butene. The added butene increased the explosion threshold apparently by consuming reactive species such as H or F atoms. Kuhn and Wellman[9] have investigated and discussed the effect of this and other inhibitors on the thermal ignition of this reaction.

The induction time, τ, between the beginning of the CO_2 laser pulse and the first detectable visible–ultraviolet emission was strongly dependent on the laser pulse energy, as well as pressure and gas composition. Induction times in the range from 4 to 300 μsec were observed. The phenomena that determine the induction time appeared to be nearly independent of wall effects and diffusion out of the irradiated region on this short time scale. For example, the time for H atoms to diffuse out of the center of the irradiated region is on the order of 300 μsec for 50 Torr of gas mixture. These induction times are not closely related to the much longer thermal induction times such as those measured by Kuhn and Wellman[9] for this reaction. The latter are strongly dependent on diffusion, wall deactivation of active species, and wall temperature.

Figure 3 shows a typical plot of $1/\tau$ against laser energy for one gas composition at several pressures. The induction times for all gas mixtures investigated obeyed the following equation

$$1/\tau = k(E - E_0) \qquad (1)$$

k is a function of pressure and gas composition, E is the laser energy, and E_0 is the threshold energy for laser ignition of the reaction.

Figure 4 is a plot of $1/\tau$ against total gas pressure for several laser energies. The reciprocal of τ increases nearly as P^2.

Laser Initiated Reaction of SF_6 with H_2

The CO_2 laser radiation is strongly absorbed by the ν_3 band of SF_6 at 946 cm^{-1}. The absorption coefficient of SF_6 at 10.6 μ is several times that of N_2F_4 at the laser intensities used in these experiments and this effective coupling of the laser radiation to gas mixtures containing SF_6 made possible the laser initiation of its reaction with H_2.

This reaction was less thoroughly studied than the N_2F_4–H_2–butene reaction; however, the following observa-

(9) L. P. Kuhn and C. Wellman, *Inorg. Chem.*, 9, 602 (1970).

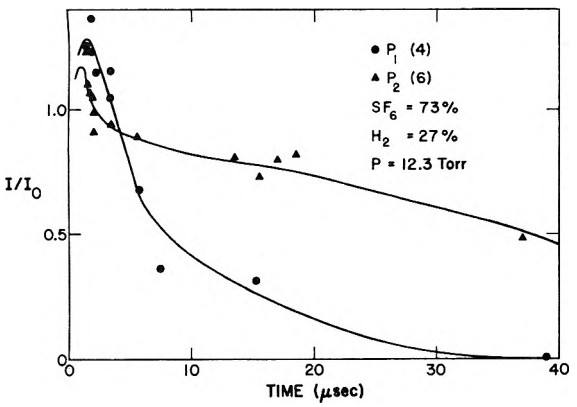

Figure 5. Transmitted to incident intensity ratio of an HF probe laser pulse in the laser driven reaction of N_2F_4 and H_2. The CO_2 laser energies range from 0.5 to 0.7 J, the spot size is 0.35 cm^2, and the path length of the probe laser is 1.0 cm.

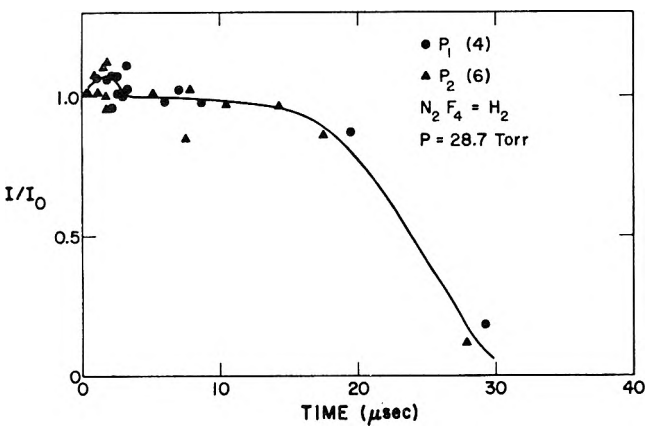

Figure 6. Transmitted to incident intensity ratio of an HF probe laser pulse in the laser driven reaction of SF_6 and H_2. The CO_2 laser energies range from 0.5 to 0.7 J, the spot size is 0.35 cm^2, and the path length of the probe laser is 1.0 cm.

tions were made. (1) The intensity of the light emitted from the reaction increased with increasing laser energy. (2) The amount of gas that reacted, as determined by the increase in pressure, was small and increased with increasing laser energy. (3) Although SF_6 is a stronger absorber of 10.6-μ radiation than is N_2F_4, the threshold for laser initiation of the reaction is greater for the SF_6–H_2 system. (4) As shown in Figure 1b, the time of reaction was less sharply defined than the explosive reaction of N_2F_4 and H_2. The intensity of the emitted radiation was also much less than in the N_2F_4–H_2 system. These observations indicate that the SF_6–H_2 reaction was not a laser ignition of an explosion, but was merely reaction of species activated by absorption of laser energy.

HF Laser Gain Developed by the Reacting Media

HF laser gain measurements were made on the CO_2 laser driven reactions of N_2F_4 with H_2 and SF_6 with H_2, by probing the reacting mixtures at various times after the beginning of the CO_2 laser pulse. The ratio of transmitted to incident intensity of the HF probe laser signal was plotted against time for reactions of the two systems in Figures 5 and 6. The accuracy of the determination of I/I_0 was approximately ±6%. The path length of the probe beam through the CO_2 laser irradiated gas was approximately 1 cm. There was evidence of laser gain in the N_2F_4–H_2 reaction during the first few microseconds of the CO_2 laser pulse, but the gain was greater for the SF_6–H_2 system. It is noticeable in the SF_6–H_2 system that the gain on the $P_1(4)$ transition lasted longer than on the $P_2(6)$ transition, and that the absorption of the $P_2(6)$ line did not become as intense as that of the $P_1(4)$ line.

In the N_2F_4–H_2 system, the gain occurred well before the explosion of the gas and no gain was observed during the explosion. The induction times for the N_2F_4–H_2 system of Figure 5 were from 20 to 10 μsec, as the laser energy varied from about 0.5 to 0.7 J.

Discussion

The observed short delays between the CO_2 laser irradiation of the reacting gas and the onset of laser gain and explosion indicate that rates of some dissociative reactions are increased by vibrational excitation. Figure 7 helps to illustrate some of the features of the absorption of laser radiation by N_2F_4. This figure shows the results of a calculation of the extent of N_2F_4 dissociation into the product NF_2 as well as the temperature as functions of deposited laser energy at 10 μsec after the beginning of the laser pulse. The measured laser absorption[6] was used in the calculation, and thermal equilibrium was assumed. The general features would be unchanged if an enhanced N_2F_4 dissociation rate due to vibrational excitation were used.

Note from Figure 7 that the dissociation of N_2F_4 tends to act as a heat sink. That is, the temperature is kept constant near 500 K if the laser energy absorbed is insufficient to dissociate all of the N_2F_4. High temperatures result if the laser energy is increased above that point.

Figure 7 also shows that above some threshold energy, the concentration of NF_2 increases linearly with energy. The linear dependence of NF_2 concentration on laser energy was experimentally observed. A mixture of 106 Torr of 20% N_2F_4 and 80% Ar was irradiated with laser energies ranging up to 0.5 J and with a laser spot size of 2.3 cm^2. The measured concentration of NF_2 10 μsec after the beginning of the laser pulse is given by $[NF_2] = 8.33 \times 10^{-7}(E - 0.1)$ mol/cc.

The rate of CO_2 laser-induced dissociation of N_2F_4, previously studied by Lyman and Jensen,[6] is much faster than the thermal dissociation rate that has been measured by shock tube methods.[10,11] This enhanced rate of the laser-induced reaction was attributed to nonequilibrium population of vibrationally excited states of N_2F_4.

A chain reaction mechanism is proposed for the laser-driven reaction of N_2F_4 with H_2 with the following as chain-initiating reactions

$$N_2F_4^* + M \longrightarrow 2NF_2 + M \quad \Delta H = +20 \text{ kcal} - E_{vib} \tag{2}$$

$$NF_2^* + M \longrightarrow NF + F + M \quad \Delta H = +66 \text{ kcal} - E_{vib} \tag{3}$$

where the rates of both of these endothermic reactions are greatly accelerated by laser excitation of vibrational modes of the reactants.

Reaction 2 is very rapid for the laser energies used in these experiments. Comparison of Figure 2 with Figure 7 shows that the concentration of NF_2 is very high at laser energies near the explosion threshold. This NF_2 evidently reacts very rapidly by reaction 3 when the NF_2 is vibrationally excited as from laser absorption or as a result of

(10) A. P. Modica and D. F. Hornig, *J. Chem. Phys.*, **49**, 629 (1968).
(11) L. M. Brown and B. deB. Darwent, *J. Chem. Phys.*, **42**, 2158 (1965).

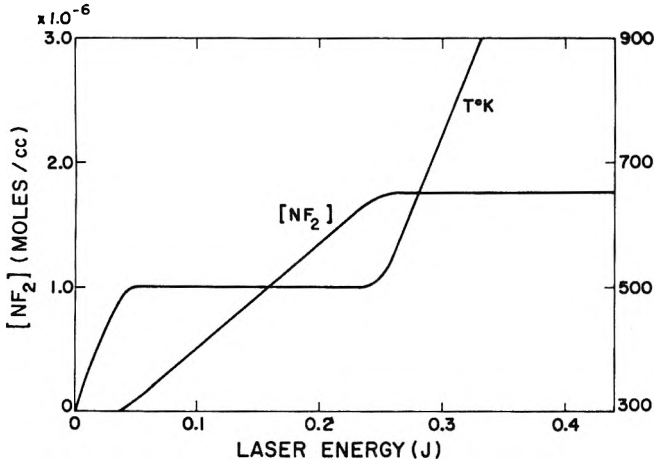

Figure 7. Calculation of NF_2 concentration and temperature as functions of laser energy at 10 μsec after the CO_2 laser pulse begins for a laser spot size of 0.35 cm^2 and N_2F_4 concentration of 8.8×10^{-7} mol/cc (~16.5 Torr).

vibrational-vibrational energy transfer from N_2F_4. By analogy with the laser-induced dissociation of N_2F_4, the amount of F produced during the laser pulse by reaction 3 should increase linearly with laser energy above some threshold.

The observation of HF laser gain only during the CO_2 laser pulse indicates that reaction 3 does indeed occur at that time and is followed by the very fast reaction

$$F + H_2 \longrightarrow HF^* + H \qquad (4)$$

A third possible chain-initiating reaction proposed by Kuhn and Wellman[9] as the chain-initiating reaction for thermal explosions of N_2F_4 and H_2 is

$$NF_2 + H_2 \longrightarrow HNF_2 + H \quad \Delta H = +25 \text{ kcal} \qquad (5)$$

This reaction is slow,[12] and is believed to play only a minor role in the present experiment. Figures 2 and 7 show that even high concentrations of both reactants do not ensure that an explosion will occur.

Since the laser-induced dissociation of N_2F_4 is very fast, the NF_2 concentration will be high during most of the induction period. The propagating reactions likely to be important, therefore, are those involving NF_2, such as

$$NF_2 + H \longrightarrow HF + NF \qquad (6)$$

$$NF + NF_2 \longrightarrow N_2F_2 + F \qquad (7)$$

as well as reaction 4.

A simple model is proposed to explain the observed explosion thresholds and induction times. The model includes the chain reaction mechanism suggested above with acceleration of dissociation of both N_2F_4 and NF_2 by vibrational excitation.

The model assumes, for a given gas composition and pressure, that (1) the number of chain-propagating species (F and possibly H) produced during the CO_2 laser pulse increases linearly with laser energy above some threshold E_0; (2) the temperature and the concentrations of major species remain essentially constant during the induction period (since the concentration of initial chain propagators is small compared with the concentration of H_2, NF_2, and N_2F_4); and (3) the induction time is the time taken for the heat release from the propagating exothermic reactions to heat the medium to the ignition temperature. Reaction 4 is so fast the F atoms produced during the laser pulse by reaction 3 react immediately with H_2 to give H atoms. Thus, the H atom concentration during the induction period will be given approximately by $[H] = C_1(E - E_0)$. The rate of heat release is limited by the slowest of the propagating reactions. If reaction 6 is the slowest

$$d[HF]/dt = 2k_6[NF_2][H] = 2k_6[NF_2]C_1(E - E_0)$$

The factor 2 arises because every chain cycle releases two HF molecules. Assumption 2 of the model allows easy integration

$$\Delta[HF] = 2k_6[NF_2]C_1(E - E_0)\ \Delta t$$

which can be rearranged to

$$\Delta(HF)/C_1 2k_6[NF_2] = (E - E_0)\ \Delta t$$

The left-hand side of the above equation is proportional to the temperature rise of the medium, and the temperature rise necessary for ignition for a given gas composition is constant. Therefore

$$1/\tau = 1/\Delta t = k(E - E_0)$$

The same result is obtained if reaction 7 is the slowest.

This simple model does give the proper dependence of the induction time on laser energy, and requires that vibrational excitation does indeed accelerate the dissociation rate of NF_2. However, in order to acquire further insight into the processes involved, a more comprehensive model was employed. The model included (1) reaction of F with H_2 (reaction 4) and the subsequent deactivation of the vibrationally excited HF by V-T and V-V energy transfer processes (the Appendix of the paper by Kerber, *et al.*,[13] lists these reactions and their rate constants); (2) dissociation[10,14] of N_2F_4 and NF_2; (3) reaction[15] of H with nitrogen fluorides; and (4) vibrational relaxation of the nitrogen fluorides. In order to simulate the effect of vibrational excitation on the dissociation rate of N_2F_4 and NF_2, a vibrational temperature was defined that included all of the vibrational modes of both N_2F_4 and NF_2. This vibrational temperature was used in the rate coefficients of these two dissociation reactions. The vibrational relaxation time was assumed to be 10^{-7} sec atm. The rate equations of the reactions involved were solved numerically by computer and laser gain was calculated for several HF vibrational-rotational transitions.

As expected, the calculations showed that there was a high degree of vibrational excitation during the laser pulse as is shown in Figure 8. The calculated vibrational and translational temperatures are plotted out to 40 μsec where the explosion is just beginning to occur as indicated by the temperature rise.

Computer simulations with 20 Torr of N_2F_4, 40 Torr of H_2, and relaxation time of 10^{-7} sec atm gave the following for induction time

$$1/\tau = 0.79(E - 0.925)$$

where τ is in microseconds and energy is in joules. This

(12) G. L. Schott, L. S. Blair, and J. D. Morgan, of this laboratory, demonstrated in a shock tube study of the N_2F_4-H_2 reaction in an argon diluent that the reaction between NF_2 radical and H_2 does not take place on the time scale of the experiment except at temperatures above approximately 1700°K (to be published).
(13) R. L. Kerber, G. Emanuel, and J. S. Whittier, *Appl. Opt.*, **11**, 1112 (1972).
(14) A. P. Modica and D. F. Hornig, *J. Chem. Phys.*, **43**, 2739 (1965).
(15) S. W. Rabideau (the rate coefficients for reaction of H with all nitrogen fluorides were taken to be the same as the measured rate coefficient for reaction of H with NF_3), *J. Magn. Resonance*, to be published.

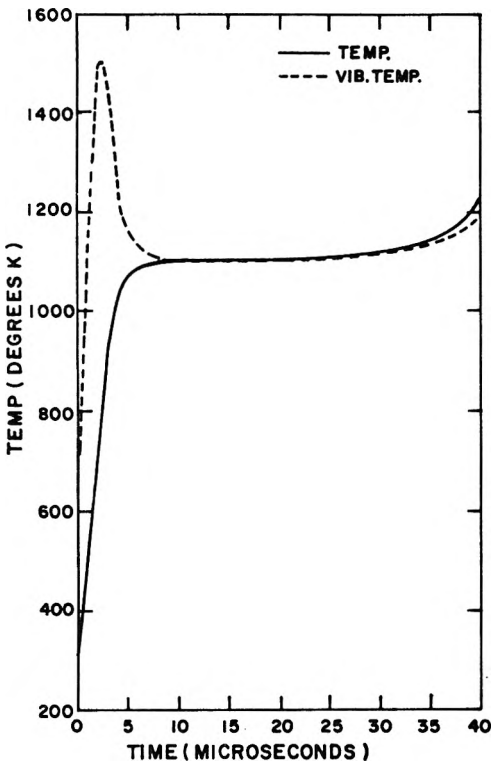

Figure 8. Computer-generated plot of translational and vibrational temperature during the induction time of a laser-driven reaction of 15 Torr of N_2F_4 with 30 Torr of H_2. The relaxation time is 0.1 μsec atm and the laser energy is 1.0 J.

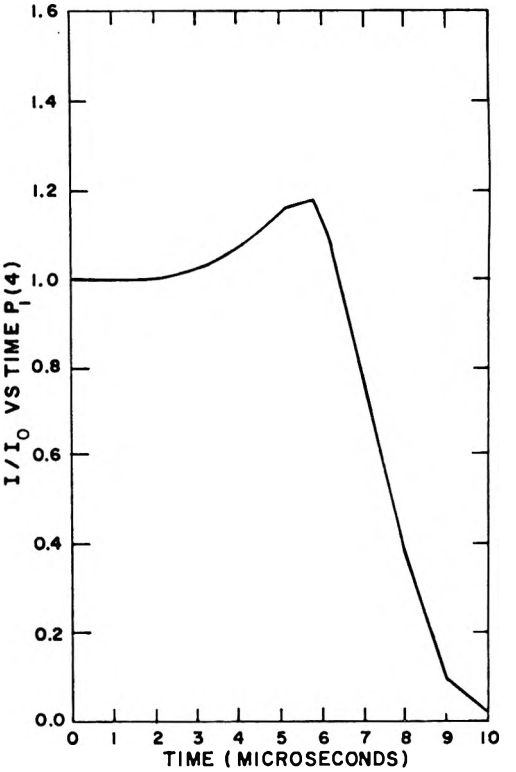

Figure 9. Computer-generated plot of transmitted to incident intensity ratio of a $P_1(4)$ HF laser transition. The reactants are 14.35 Torr each of N_2F_4 and H_2, laser energy is 1.0 J, and the relaxation time is 0.5 μsec atm.

compares with an experimental result of

$$1/\tau = 0.80(E - 0.107)$$

Note that the computer-generated equation has the proper form, but the computer threshold energy is much larger than the experimental value. Inclusion of reaction 7 in the code gave some improvement, as follows

$$1/\tau = 0.77(E - 0.700)$$

The threshold energy in this expression is still large by about a factor of 7. Altering the vibrational relaxation time did not improve the agreement with the experimental expression. However, close agreement with the experiment was achieved by increasing the rate coefficient for reaction 3 during the laser pulse well above that given by including the calculated vibrational temperature in the rate coefficient.

Attempts to simulate the experimentally measured HF laser gain (and absorption) met with the same difficulties. Gain was indeed predicted as shown in Figure 9, but it occurred later than the experimentally observed gain (Figure 5). Here again the experimental results could be duplicated by assuming a very rapid rate of reaction 3 during the laser pulse. We must therefore conclude that the rate of formation of F atoms during the CO_2 laser irradiation of N_2F_4 is greatly enhanced by vibrational excitation of the reactant molecules when the laser pulse intensity is on the order of 1 MW/cm^2.

The initial reactions operative in the laser-driven reaction of SF_6 with H_2 are probably

$$SF_6^* + M \longrightarrow SF_5 + F + M \qquad (8)$$

$$F + H_2 \longrightarrow HF^* + H \qquad (4)$$

where the rate of (8) is accelerated by vibrational excitation. Since reaction 4 is fast on the time scale of this experiment, the HF laser gain will reflect the rate of F atom production. If F atoms were produced thermally, the gain would occur near the end of the laser pulse. However, gain was actually observed during the first few microseconds (Figure 6) which indicates that reaction 8 is operative.

This conclusion was further justified by a computer model of the laser-initiated reaction. The computer program discussed above was modified to include the dissociation[16] of SF_6 and measured vibrational relaxation rates[17] of SF_6. The peak calculated gain (using an SF_6 dissociation rate based on the vibrational temperature of SF_6) on both $P_1(4)$ and $P_2(6)$ HF transitions occurred about 4 μsec later than the peaks of the experimental gain curves. Much better agreement was obtained when an even faster rate of dissociation was assumed during the CO_2 laser pulse. We conclude then that vibrational excitation accelerated the rate of dissociation of SF_6 when it was irradiated with intense CO_2 laser pulses.

Acknowledgment. We wish to acknowledge the support from the NDEA Fellowship for John L. Lyman through Brigham Young University.

(16) J. F. Bott and T. A. Jacobs, *J. Chem. Phys.*, **50**, 3850 (1969).
(17) T. B. Hodkinson and A. M. North, *J. Chem. Soc. A*, 885 (1968), J.

Photoisomerization Pathways in the Visually Important Polyenes. I. The Retinals[1a]

R. A. Raubach[1b] and A. V. Guzzo*

Chemistry Department, The University of Wyoming, Laramie, Wyoming 82070 *(Received August 10, 1972)*

Publication costs assisted by The U. S. Atomic Energy Commission

The photoisomerization of *all-trans*, 13-*cis*-, and 11-*cis*-retinal was carried out using energy transfer techniques. In this way the isomerization was initiated in the retinal triplet state. From the triplet the quantum efficiencies found were 0.17 and 0.35 for the all-trans and 13-cis isomer, values comparable to the efficiencies measured by direct singlet irradiations; however, 11-*cis*-retinal had a measured triplet isomerization efficiency of 0.75, a value much higher than that measured by direct photoisomerization. These findings are in qualitative agreement with recent theoretical predictions providing that the higher steric factors in 11-*cis*-retinal are considered.

Introduction

When the visual pigment rhodopsin absorbs light, a bleaching process is initiated and the pigment passes through a number of spectrally unique intermediates, ultimately yielding a colorless protein and a highly colored polyene aldehyde, retinal. This sequence of reactions has been adequately summarized in various reviews.[2] The primary light event involves the isomerization of the polyene chromophore from a sterically hindered 11-cis form to the all-trans configuration. For this process the quantum yield is near 0.6 and thus it is clear that very little of the excitation energy is dissipated in nonisomerization pathways.[3]

Several studies using the isomeric forms of the retinals as models have touched on this point. For instance Inuzuka and Becker[4] have argued, on the basis of calculated barriers to isomerization in 11-*cis*-retinal[5] and *all-trans*-retinal, that the lowest barrier to this process should be from the triplet state and they predicted a high yield for the 11-cis to all-trans process. On the other hand, the barrier for this same conversion occurring in the singlet state was not so high as to eliminate this pathway.

Kropf and Hubbard's[6] study of the quantum efficiency of photoisomerization of several isomers of the retinals provided further key information on this point. It was shown that the 11-*cis*- to *all-trans*-retinal quantum efficiency was near 0.2 at room temperature. Of course, such a small value produced a discrepancy with the *in vivo* measured efficiency. In other words, how could the model system have a much lower quantum efficiency for the process which in the visual pigment is relatively high. It was further noted in their work that the oxime of *all-trans*-retinal, which in some respects is a better model for the visual pigment, has a lower photoisomerization efficiency.

These studies raised the point that perhaps in the visual pigment the chromophore, upon excitation, is quickly brought ot its triplet state and then efficient isomerization takes place from that state. There is some reason to doubt this, however, since the studies of Dawson and Abrahamson[7] have shown that in *all-trans*-retinal, at least, the quantum efficiency of intersystem crossing is only 0.11 (and lower in polar solvents). Further these workers could find no evidence of triplet state population in either the retinols or in the protonated Schiff base of retinal. Thus it would appear that in the isolated chromophore the triplet state is populated to only a minor extent. However, it is not possible to rule out protein participation in the initial visual process possibly providing some mechanism for an increased yield of intersystem crossing and thus producing a higher triplet yield.

In the present study we set out to measure various features of the isomerization directly out of the triplet state. Such an experiment is possible since the triplet state of the retinals may be quantitatively populated by energy transfer techniques.[8] The rate constant for the triplet energy transfer from biacetyl to *all-trans*-retinal was measured and from this the population of the retinal triplet could be calculated. Since the extinction coefficients of the various isomers are known it is also possible to measure the amount of isomerization produced for a given radiation time. With this information we then could calculate the quantum yield of isomerization from the triplet state with no participation from the singlet.[9]

Materials and Methods

Only highest purity commercially available isomers of retinal were used. Sigma Chemical Co., St. Louis, Mo., furnished the all-trans- and 13-cis isomers of retinal. These were recrystallized two times in the dark from *n*-hexane. The 11-*cis*-retinal was a gift from the Hoffman-LaRoche Institute, Nutley, N. J., and was used as received.

(1) (a) This work was supported in part by the United States Atomic Energy Commission through Contract No. AT-(11-1)-1627. (b) Division of Natural Sciences, University of California, Santa Cruz, California 95060.
(2) (a) E. W. Abrahamson and S. Ostroy, *Progr. Biophys. Mol. Biol.*, **17**, 179 (1967); (b) S. Bonting, *Bioenergetics*, **2**, 351 (1970).
(3) E. E. Schneider, C. F. Goodeve, and R. J. Lythgoe, *Proc. Roy. Soc., Ser. A*, **170**, 102 (1939); C. F. Goodeve, R. H. Lythgoe, and E. E. Schneider, *Proc. Roy. Soc., Ser. B*, **130**, 380 (1942.
(4) K. Inuzuka, and R. S. Becker, *Nature (London)*, **219**, 383 (1968).
(5) Becker's model for these calculations was the polyene 2,4,6,8,10-dodecapentaenal which closely resembles the retinal π electron system. No steric interactions, however, were included.
(6) A. Kropf and R. Hubbard, *Photochem. Photobiol.*, **12**, 249 (1970).
(7) W. Dawson and E. W. Abrahamson, *J. Phys. Chem.*, **66**, 2542 (1962).
(8) A. V. Guzzo, and G. L. Pool, *J. Phys. Chem.*, **73**, 2512 (1969); A. Knowles, *Nature (London), New Biol.*, **236**, 202 (1972).
(9) A blank photoirradiation was carried out on a retinal solution with no biacetyl present. It was found that irradiation at 445 nm (the biacetyl maximum) was absorbed and caused about 20% of the isomerization, for a given time period, that would have been observed with the sensitizer present. However, in the actual runs, the biacetyl will filter most of the 445-nm light from reaching the retinal. At 445 nm the ratio of absorbance of retinal to that of biacetyl is $\sim$0.02. Thus no significant correction need be applied to our results due to direct photoisomerization.

The solvent used in this study, Analytical Reagent grade, low sulfur content CCl_4 (Mallinckrodt Chemicals, St. Louis, Mo., was further purified by passage through a short column of activity grade I chromatographic alumina. This treatment removed all detectable fluorescent impurities. The purified solvent was stored over molecular sieves in amber bottles until used.

The triplet state donor, 2,3-butanedione (biacetyl) (Eastman Organic Chemicals, Rochester, N. Y.), was purified two times by distillation in a nitrogen atmosphere. The purified material was stored in a freezer and protected from light until used.

Stock solutions of the isomers of retinal were prepared in CCl^4 and found to be very stable if stored at $-20°$ and protected from light. Sample solutions were prepared by dilution of a stock solution with enough biacetyl (also dissolved in CCl_4) to make a final solution approximately 2×10^{-5} M in retinal and 0.05 M in biacetyl. Before irradiation the samples were degassed in a cell having an optical cuvet (Helma) connected to a small degassing bulb. Three freeze–pump–thaw cycles were used on each sample which was then sealed under vacuum ($\sim 10^{-6}$ Torr).

Irradiations were carried out at the wavelengths chosen using the Bausch and Lomb High Intensity xenon light source and monochromator.

Spectroscopic data were recorded using various systems. The Cary 14R spectrophotometer was used to obtain visible spectra and the retinal–biacetyl samples were run *vs.* a biacetyl blank in the same solvent (CCl_4). Phosphorescence lifetimes and spectra were obtained using the Aminco-Bowman spectrophotofluorometer with the Aminco-Kiers phosphoroscope. A cooled RCA4517 photomultiplier was used, and for lifetime measurements, its output was fed directly into a Hewlett-Packard Model 140A oscilloscope.

The light flux was measured using the ferrioxalate actinometer discussed in detail by Hatchard and Parker.[10]

Results and Discussion

In order to begin experiments utilizing the quantitative transfer of triplet energy it was necessary to measure the rate constant for the transfer process between the donor chosen, biacetyl, and one of the retinal isomers. Biacetyl was selected as a donor because its phosphorescence lifetime could easily be measured at room temperature;[10] in addition its triplet level is known to be at 56 kcal/mol[11] which is above the retinal (0–0) level of 35 kcal/mol.[12]

Transfer indeed occurred since the lifetime of the biacetyl emission markedly decreased with increasing retinal concentration. This, of course, is evidence of an acceptor mediated depopulation of the excited triplet. Since the singlet of *all-trans*-retinal is at 70 kcal/mol only triplet-triplet transfer may occur. All experiments were carried out on degassed samples to be free of the complicating effects of oxygen quenching.

A Stern-Volmer plot of the quenching of the biacetyl emission is given in Figure 1. Note that in the solvent chosen for this study, carbon tetrachloride, the lifetime measured in the absence of acceptor -0.77 ± 4, msec, is in good agreement with the literature value of 0.78 msec[11] and at the highest retinal concentration chosen (1×10^{-6} M) the value was found to be 0.27 msec. From the slope of the line found we obtain a value of 2.3×10^9 M^{-1} sec^{-1}. for the energy transfer rate constant. This value is in the range expected at room temperature for a suitably positioned donor–acceptor pair using biacetyl as the donor.[11]

If we consider the efficiency of triplet transfer from biacetyl to retinal, we have

$$\phi_{ET} = \frac{k_{ET}[\text{retinal}]}{k_p + k_r + k_{ET}[\text{retinal}]}$$

where the sum $k_p + k_r$ is the reciprocal of the measured lifetime of the biacetyl emission in the absence of any acceptor, *i.e.*

$$k_p + k_r = \frac{1}{\tau_0} = \frac{1}{0.77 \times 10^{-3}\ \text{sec}} = 1.3 \times 10^3/\text{sec}$$

Thus if the concentration of retinal is maintianed near or greater than 10^{-5} M, ϕ_{ET} will be near unity.

The energy transfer rate constant measured above was for *all-trans*-retinal as an acceptor. It is possible that the constant for the other isomers may be somewhat different. However, with a concentration of acceptor of 4×10^{-5} M as actually used, ϕ_{ET} still is near unity even if the various k_{ET} values differ by an order of magnitude.

The efficiency of acceptor triplet population through a sensitization process is given by the expression

$$\phi_A{}^T = \phi_{IC}\phi_{ET}$$

Here ϕ_{IC} is the quantum efficiency of donor intersystem crossing to its triplet state. In biacetyl this quantity was estimated by Lamola[13] to be 0.9 and by Almgren[14] to be 1.0. We have used the former value since this will give an upper limit to the triplet-state isomerization efficiency, as we measure it, and thus give an upper limit to triplet participation in the direct photoisomerization process.

The quantum efficiency of sensitized isomerization may be written as

$$\phi_I = \frac{[\text{number of molecules isomerized}]}{[\text{number of retinal triplets formed}]}$$

which in terms of basic quantities is

$$\frac{NRV}{\Phi_{IC}\Phi_{ET}I_{abs}}$$

In this equation R is the rate of photoisomerization of whichever retinal isomer is chosen (M sec^{-1}), V is the volume of solution irradiated, N is Avogadro's number, and I_{abs} is the number of photons absorbed by biacetyl per second.

Aside from the quantities ϕ_{IC} and ϕ_{ET} discussed above the determination of ϕ_I amounts to determining R and I_{abs}. The number of photons absorbed by the sensitizer per second (I_{abs}) can be found knowing the absorbance of the solution at the wavelength of irradiation and from actinometry.

The rate of the isomerization reaction, R, was obtained primarily through absorbance measurements made on the various donor–acceptor solutions for various times of actinic irradiation. We assumed that the measured absorbance at 380 mm, the *all-trans*-retinal maximum, was due to the presence of only two chromophores: the original material and *one* isomerized product. By recourse to Beer's law for the absorbance of a two component mixture, we have

(10) C. G. Hatchard and C. A. Parker, *Proc. Roy. Soc., Ser. A*, **235**, 518 (1956).
(11) H. J. L. Backstrom and K. Sandros, *Acta Chem. Scand.*, **12**, 832 (1958).
(12) N. J. Turro in "Molecular Photochemistry," W. A. Benjamin, New York, N. Y., 1967, p 132.
(13) A. Lamola, private communication sited by P. S. Engel and B. M. Monroe, *Advan. Photochem.*, **8**, 29 (1971).
(14) M. Almgren, *Photochem. Photobiol.*, **6**, 829 (1967).

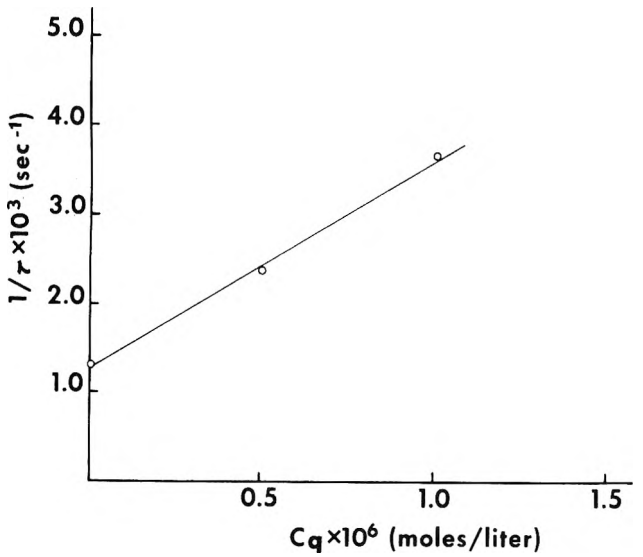

Figure 1. Stern–Volmer plot of the quenching of the biacetyl lifetime *vs.* *all-trans*-retinal concentration.

TABLE I: Spectral Characteristics for the Isomeric Retinals[a]

Isomer	λ_{max}	ϵ_{376}	ϵ_{380}
All-trans	380	4.55×10^4	4.65×10^4
13-cis	376	3.78×10^4	3.72×10^4
11-cis	376	2.62×10^4	2.58×10^4

[a] In carbon tetrachloride solution at 25°.

$$A_{380} = e_1^{380} C_1 + e_2^{380} C_2$$

that is, at fixed wavelength the absorbance of the solution may be regarded as the sum of the absorbancies of the components of the mixture. For this analysis the extinction coefficients of the various retinal isomers were measured in carbon tetrachloride. The values obtained are given in Table I.

The concentration of each component of the mixture may easily be found since our assumption of only two components in the mixture requires that the total retinal concentration be a constant, *i.e.*, that

$$C_0 = C_1 + C_2$$

where C_0 is the initial concentration of whatever retinal isomer is to be isomerized.

The assumption of only one cis isomer formed upon irradiation of *all-trans*-retinal was justified on the basis of thin layer chromatography. After 500 sec of irradiation of an *all-trans*-retinal solution, only two components were revealed corresponding to the original starting material and to 13-*cis*-retinal. Only after much longer irradiation times do we begin to see the formation of other components.

In order to determine the quantum yield of the isomerization it is necessary to examine only the initial rate of reaction. As the tlc experiments showed, long irradiation times will cause reisomerization of the photo products and thus possibly result in the formation of di-cis isomers. It should be emphasized then that we did not seek the cis yield at the photostationary state, but rather we required the initial photoisomerization rate.

During the course of our early experiments, we observed that the initial isomerization rate was complicated by the fact that a photostationary state for long irradiation time

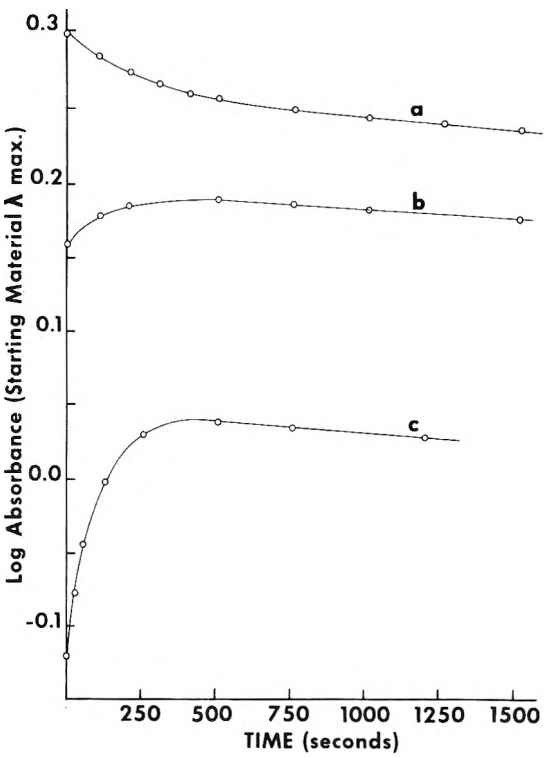

Figure 2. The change in the total absorbance as a function of time of irradiation of a solution in CCl_4 of (a) *all-trans*-retinal, (b) 13-*cis*-retinal, and (c) 11-*cis*-retinal. The photostationary state reached after 600 sec presents a different log (absorbance) for each of the three isomers because of initial concentration differences.

was never achieved. Rather we observed a continuous decrease in the total retinal concentration indicative of a chromophore destruction process. A typical plot of log A_{380} *vs.* time is given in Figure 2, curve a, for the isomerization of *all-trans*-retinal. It can be seen, nevertheless, that this linear process is slow enough to be subtracted from the isomerization data to give a fairly accurate net isomerization plot such as given in Figure 3. In Figures 3 and 4 we have plotted the concentration of isomerized photoproduct formed as discussed above *vs.* integrated light intensity. (Integrated light intensity is the product of time of irradiation and the radiative flux. Its introduction is valuable in that it allows a direct comparison of all the irradiation studies.) For the irradiation of *all-trans*-retinal the photoproduct is 13-*cis*-retinal.

Isomerization data were obtained for a number of conversions, *i.e.*, (a) all-trans → 13-cis, (b) 13-cis → all-trans, and (c) 11-cis → all-trans. The basic data for reactions a, b, and c are given in Figure 2, and from these the corrected isomerization data were plotted in Figures 3 and 4. In these figures only the initial, corrected points were recorded since these provide the initial rate data we seek. For each run the light flux was measured, usually immediately after the full irradiation.

Using the data gathered above we were able to calculate quantum yields for these sensitized isomerizations. These values are given in Table II. Since our tlc data indicated that only 13-cis was formed by the irradiation of *all-trans*-retinal, only this species was considered in calculating the yield for reaction a above. We also give in the table the direct photoisomerization data for these reactions obtained by Kropf and Hubbard. Note that the sensitized yields agree roughly with the direct yields for reactions a

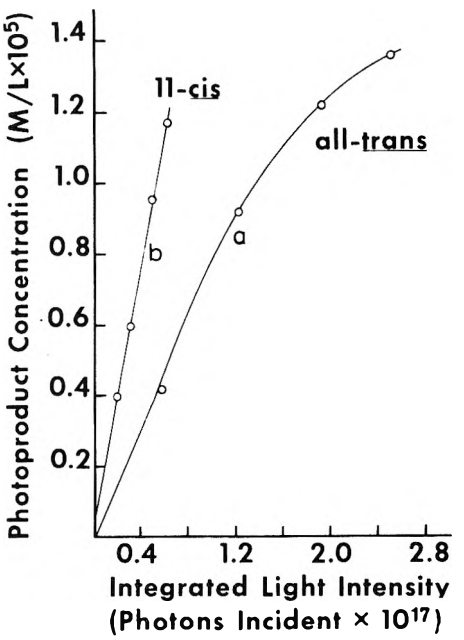

Figure 3. Photoproduct yield as a function of the total number of photons incident to the sample. Data for the conversion of (a) *all-trans*-retinal and (b) 11-*cis*-retinal.

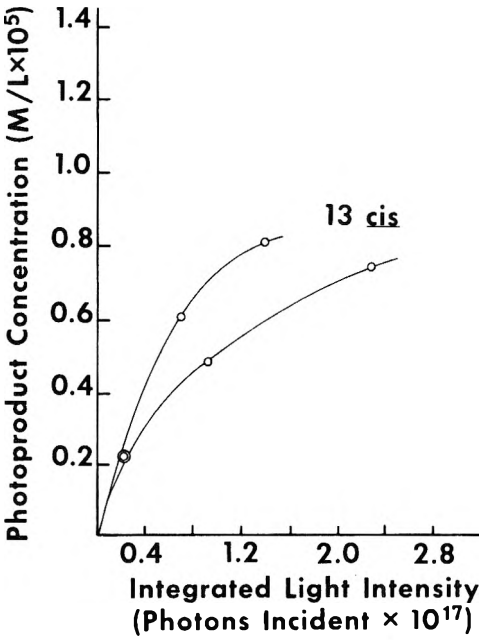

Figure 4. Data for the conversion of two samples of 13-*cis*-retinal differing in their total oxygen content and therefore in the amount of chromophore photodestruction present at any time. It can be seen that the earliest points coincide for the two samples indicating that both initial slopes are identical.

TABLE II: Quantum Yields of Photoisomerization of the Isomeric Retinals and Comparison of Triplet Sensitization and Singlet Irradiation

Reaction	Triplet sensitized Φ^a	Singlet irradiated Φ^b	Calculated triplet contribution Φ^c
All-trans to 13-cis	0.17	0.2[d]	0.02
11-cis to all-trans	0.75	0.2	0.08
13-cis to all-trans	0.35	0.4	0.04

[a] 2,3-Butanedione sensitized in CCl_4 solution at 25°. [b] Data of Kropf and Hubbard in *n*-hexane at 25°. [c] Calculated extent of triplet state involvement in the direct singlet irradiation experiments of Kropf and Hubbard using $\Phi_{ic} = 0.11$. [d] As discussed in the text, our tlc findings indicate that only 13-*cis*-retinal is formed upon irradiation of *all-trans*-retinal. We, therefore, have chosen the value of Φ that applied to this conversion only.

and c but differ widely for the visually important process b. In this latter case it is clear that isomerization from the triplet state is highly efficient. Since both *n*-hexane (the solvent for the Kropf and Hubbard study) and carbon tetrachloride are nonpolar and aprotic solvents, this difference for reaction b is probably not due to solvent differences. The high quantum efficiency of isomerization from the 11-*cis*-retinal triplet state is in complete agreement with the theoretical analysis of Inuzuka and Becker.[4] Their study of the barriers to isomerization in the various states of these isomers predicted a much larger barrier for the 11-cis to all-trans process in the singlet state than in the triplet. They thus predicted a major role for the triplet in this process. However, for this to occur, a highly efficient intersystem crossing pathway must exist. Apparently, at least according to Dawson and Abrahamson,[7] such a pathway does not exist. These authors contended that ϕ_{IC} for the cis isomers of retinal was approximately the same as in *all-trans*-retinal with perhaps a variation of 15%. Since they found ϕ_{IC} in this latter case to be 0.11 it appears that the triplet does not dominate the direct photoisomerization process.

Using the quantum efficiences for the sensitized process and Abrahamson and Dawson values for ϕ_{IC} we are able to calculate its extent of triplet participation in the direct photoisomerization process. These values are given in column c of Table I.

It is clear that the triplet state plays only a minor role in reactions a and b above, but appears to be responsible for ~50% of the direct photoisomerization of the 11-cis isomer. A similar finding, of a mixed mechanism for the isomerization of 11-*cis*-retinal, was also encountered by Hubbard[15] in her study of the thermal parameters of the 11-*cis*-retinal isomerization. She found that the activation energy of the process was characteristic of a triplet mechanism, but the frequency factor more resembled that encountered in singlet processes.

It would be tempting at this point to claim that in the visual pigment also, singlet and triplet states play equally important roles in the initial isomerization process. However, this extrapolation is certainly not justified since there is good evidence to show that in rhodopsin the polyene chromophore does not exist as an aldehyde but rather is bound to the protein through a Schiff base linkage.[16] The examination of the photoisomerization properties of the retinylic Schiff bases will be the subject of a future report.

In summary then, our findings show that the triplet state is not significantly involved in the direct photoisomerization of either *all-trans*- or 13-*cis*-retinal. However, the triplet appears to be involved to a considerable extent in the 11-*cis*-retinal isomerization and may be responsible for half of the observed isomerization with the other half arising from the singlet state. Clearly a further test of these conclusions must come from direct excitation experiments of retinal solutions with and without various triplet quencher.

(15) R. Hubbard, *Biol. Chem.*, **241**, 1814 (1966).
(16) R. A. Raubach and A. V. Guzzo, *J. Phys. Chem.*, **75**, 983 (1971).

On the Scavenging of e_{aq}^- and on the Possible Breakdown of Smoluchowski's Equation at High Concentrations of Solutes

Gideon Czapski* and Emanuel Peled

Department of Physical Chemistry, The Hebrew University, Jerusalem, Israel *(Received July 7, 1972)*

It is shown that in very concentrated aqueous solutions of electron scavengers, the initial decay of e_{aq}^- with scavengers by diffusion-controlled reactions may break down due to different reasons. In addition to the known time dependence of these rate constants, it is argued that other effects have to be taken into consideration: (a) the finite lifetime of encounter pairs; (b) the initial formation (not through diffusion) of encounter pairs in concentrated solutions; and (c) possible effects prior to thermal equilibration. These effects may explain some of the anomalies in kinetic behavior and in $G(e_{aq}^-)$ in the radiation chemistry of such concentrated solutions without necessarily having to postulate any chemical reactivity with dry electrons.

Several attempts have been made in recent years to study early processes in the radiation chemistry of aqueous solutions in the time range of 10 psec. Very concentrated solutions of electron scavengers had to be used for these studies, in order to reach half-lives of e_{aq}^- of the order of 10^{-10}–10^{-11} sec.

In some of these studies the decay of e_{aq}^- in the 10-psec range was followed by direct observation[1-4] while in others product analysis and competition kinetics were the in concern.[5-8] Results were compared to those in dilute solution (where lifetimes are microseconds or longer) and a few anomalies were discerned which led to the suggestion that dry electrons (e_{dry}^-) may react with scavengers in times shorter than 10 psec (reaction 1), in competition with the solvation process (2). Hunt was able to show that the overall solvation process is complete in less than 10 psec[9] and recently a lower limit of 4 psec has been given for this process.[10]

$$e_{dry}^- + S \longrightarrow S^- \qquad (1)$$

$$e_{dry}^- + H_2O \longrightarrow e_{aq}^- \qquad (2)$$

The principal deviations in the behavior of concentrated solutions when compared to dilute ones can be summarized as follows. (a) When two solvated electron scavengers are in competition, it has been shown that the relative rate constants depend, sometimes strongly, on the concentrations.[2,5] (b) The extrapolated initial yield of e_{aq}^- in concentrated solutions gave, for Cd^{2+}, NO_3^-, etc., values which were much lower than expected.[3] The indirect determination of $k(e_{aq}^- + S)$ at $t < 10$ psec from the extrapolated yields gave different values than at longer times, and for several scavengers, rate constants as high as 2.5×10^{11} M^{-1} sec^{-1} were indicated. These high values were attributed by Hunt to reactions of e_{dry}^-[2,3] by assuming that S and H_2O compete for e_{dry}^- through reactions 1 and 2.

The purpose of this communication is to show that the above-described phenomena may be interpreted without necessarily taking into consideration the reaction of e_{dry}^-, and also to show that extrapolation of initial yields of e_{aq}^- in concentrated solutions is questionable.

The time dependence and the concentration dependence of rate constants and their ratios of the reactions of e_{aq}^- with electron scavengers has been discussed by Schwarz.[11] His theoretical treatment accounted only for part of the anomalies found in rate constants of shorter times, both for diffusion-controlled reactions of e_{aq}^- (with acetone, for example) and for somewhat slower reactions, such as $H^+ + e_{aq}^-$. This reaction is about five times slower than diffusion controlled. Schwarz considered both the time dependency of diffusion-controlled reactions of neutral scavengers, and those with opposite charged ions, the latter being somewhat slower. The results of Aldrich, *et al.*,[3] show that there is such a time dependence for various reactions rate constants of e_{aq}^- with H_2O_2, acetone, as well as with some cations and anions. With the ions, the time dependence is complicated by the effect of the ionic strength which increases with increased concentration. Correcting for this effect[12] the time dependence observed in 1 M solutions shows an increase of 50–100%, which is of the right order of magnitude as predicted.[11,13]

The reactions of e_{aq}^- with scavengers S (generally with S in a big excess over e_{aq}^-) obey second-order kinetics. The process can be visualized to occur in two steps. The first one is the transport of S toward e_{aq}^- yielding a reactive configuration (an encounter pair (e_{aq}^-:S)). The second step involves the transformation of this configuration (encounter pair) into the product S^-. In addition, the encounter pair may separate through diffusion without reacting.

For fast reactions the overall rate is limited by the transport process by which e_{aq}^- and S meet, *i.e.*, it is controlled by diffusion. The typical diffusion-controlled reactions are those where practically every encounter

(1) M. J. Bronskill, R. K. Wolf, and J. W. Hunt, *J. Chem. Phys.*, **53**, 4201 (1970).
(2) R. W. Wolff, M. J. Bronskill, and J. W. Hunt, *J. Chem. Phys.*, **53**, 4211 (1970).
(3) J. E. Aldrich, M. J. Bronskill, R. K. Wolf, and J. W. Hunt, **55**, 530 (1971).
(4) M. J. Bronskill, R. K. Wolf, J. E. Aldwich, and J. W. Hunt, *J. Phys. Chem.*, in press.
(5) E. Peled and G. Czapski, *J. Phys. Chem.*, **75**, 3626 (1971).
(6) T. Sawai and W. H. Hamill, *J. Phys. Chem.*, **74**, 3914 (1970).
(7) P. L. T. Bevan and W. H. Hamill, *Trans. Faraday Soc.*, **66**, 2533 (1970).
(8) S. Khorana and W. H. Hamill, *J. Phys. Chem.*, **75**, 3081 (1971).
(9) M. J. Bronskill, R. K. Wolf, and J. W. Hunt, *J. Phys. Chem.*, **73**, 1175 (1969).
(10) P. M. Rentzepis, R. P. Jonas, and J. Jortner, to be published.
(11) H. A. Schwarz, *J. Chem. Phys.*, **55**, 3647 (1971).
(12) E. Peled and G. Czapski, *J. Phys. Chem.*, **74**, 2903 (1970).
(13) R. M. Noyes, *Progr. React. Kinet.*, **1**, 129 (1961).

yields a product.

$$e_{aq}^- + S \underset{k_{-1}}{\overset{k_1}{\rightleftharpoons}} (e_{aq}^-:S) \xrightarrow{k_2} S^- \qquad (3)$$

For these reactions $k_{-1} < k_2$ (otherwise not every encounter would yield S^-), while for $e_{aq}^- + H^+$, $k_{-1}/k_2 = 5$.[11] (Since for H^+, k_{obsd} is about five times smaller than the diffusion-controlled value would be.) For reactions which are diffusion controlled, τ_{en} (the encounter pair lifetime) is $1/k_2 + 1/k_{-1}$ which is at most 10 psec. ($1/k_{-1} \leq 10$ psec for such reactions at room temperature.[14])

Theories of diffusion-controlled reactions were developed by Smoluchowski.[15] The model assumes that S (uncharged) has to diffuse toward e_{aq}^- and, when the distance between their centers reaches a value R, they react.

The solution of the diffusion equation with the boundary conditions

$$S(r, 0) = S_0 \quad \text{for } r > R$$

$$S(r,t) = 0 \quad \text{for } r < R \qquad (4)$$

yields

$$k = \frac{4\pi DRN}{1000}\left[1 + \frac{R}{(\pi Dt)^{1/2}}\right]$$

the time dependent form of k_{obsd} which reduces at longer times to the stationary form

$$k_{obsd} = 4\pi NDR/1000 \qquad (5)$$

For charged particles Debye[16] extended the theory taking the interaction into account. The solution of the diffusion equations in this case yields an equation similar to (5) but R is replaced by r_{eff} given by

$$r_{eff} = \left[\int_R^\infty \exp(U/KT)\left(\frac{dr}{r^2}\right)\right]^{-1} \qquad (6)$$

where U is the coulombic interaction energy.

For dilute solutions this integration yields

$$r_{eff} = R\frac{Q}{\exp[Q] - 1} \qquad (7)$$

where $Q = Z_S e^2/\epsilon kTR$ (Z_S is the charge number of S, e is the electron charge, ϵ is the dielectric constant, and k is Boltzmann's constant).

R in eq 4-7 is the distance between e_{aq}^- and S at which they react. R is often taken as the sum of the crystallographic radii, ($r_S + r(e_{aq}^-) = R$) although there is no proper foundation for this. For example, R may exceed $r_S + r(e_{aq}^-)$ if the reaction occurs *via* tunneling as suggested by Anbar and Hart[17] for these reactions. Furthermore, for several reactions it was found experimentally that R exceeds $r_S + r(e_{aq}^-)$ by a factor of up to 3, both for anions and neutral molecules[17] (assuming $r(e_{aq}^-) \sim 2.8$ Å[17] and R is calculated from k_{obsd} and eq 5). For cations reacting with e_{aq}^- it is difficult to estimate R, as the value of k_{obsd} is very insensitive to the value of R.

Let us examine whether the assumptions for the diffusion-controlled reactions are valid in very concentrated solutions.

The boundary condition in Smoluchowski's equation, $S(r,0) = 0$ for $r \leq R$, assumes that no e_{aq}^- is present at $t = 0$ in the spheres of radius R around S. In concentrated solutions of S, the volume occupied by S molecules may be very appreciable.

We can calculate the probability P that n molecules of S, each of an "encounter volume" $v = \frac{4}{3}\pi R^3$, do not cover a random spot in the solution of volume V.

If we assume that $R^3 > r_S^3$, P will be given by

$$P = \left(1 - \frac{v}{V}\right)^n \simeq e^{-[S]\bar{v}} \qquad (8)$$

where [S] is the concentration in moles/liter and $\bar{v}$ is the partial molar volume of S in liters/mole. Table I gives the concentrations of S for various values of R with the respective values of P.

Since for diffusion-controlled reactions the average value of R can be taken as ~6 Å, it follows that in ~1 M solution of S, $P \sim 0$, 5, or 0.5 of e_{aq}^- which would be introduced randomly into this solution would be formed initially as encounter pairs (e_{aq}^-:S). Thus, if $S(r,0) = 0$ for $r < R$, this means that half of e_{aq}^- will disappear instantaneously as soon as they are incorporated into encounter pairs. Therefore, any yield of e_{aq}^- as extrapolated to $t = 0$ will account only for the fraction of e_{aq}^- which is not initially formed as encounter pairs. This analysis assumes a zero lifetime of the encounter pairs (e_{aq}^-:S).

The relative yield of e_{aq}^-, as given by P in eq 8, has the identical functional form as derived by Wolff, *et al.*,[2] for a model where dry electrons compete in reactions 1 and 2. Their experimental results[2] show that for acetone, H_2O_2, NO_3^-, and Cd^{2+} eq 8 holds.

If we attribute the linear decrease of log [$G(e_{aq}^-)$] with [S], found experimentally[2] as due to eq 8, the following values of R are found: R = 6, 6.5, 9, and 9.5 Å for H_2O_2, acetone, NO_3^-, and Cd^{2+}, respectively. Values of $R \sim 6$ Å are within the average value of R for diffusion-controlled reactions of e_{aq}^-.[17] A value of R of 9 or 9.5 Å is high, although such values are suggested for several solutes in their reactions with e_{aq}^-.[17] If, with these values of R, we calculate the rate constants of the reactions of e_{aq}^- with these solutes from eq 5-7, the computed values are only about twice the value of the measured one. (For a positive ion such as Cd^{2+}, at low ionic strength the computed value of R is changed only by 25% should R be either 3 or 10 Å). Thus, the results of Wolff, *et al.*,[2] seem to be interpreted reasonably well without having to assume any reaction of e_{dry}^- with these solutes.

We will try to visualize the possible meaning of the encounter pair and its lifetime.

R as defined in eq 4-7 is the distance between the centers of S and e_{aq}^- at which they react and, as argued earlier, R can exceed $r_S + r(e_{aq}^-)$.

Obviously, R is some average value as the reaction in all probability will not be a step function with distance. If we assume that the probability function is rather steep, namely, the reaction will occur only if the distance between e_{aq}^- and S is not changed by more than an average diffusional jump of 1 Å, this would take $\sim 10^{-12}$ sec. With this model, when e_{aq}^- and S reach the reactive configuration (e_{aq}^-:S) the lifetime τ of the process (e_{aq}^-:S) → product cannot exceed 10^{-12} sec, but may be faster. τ may be different for various solutes but their diffusion-controlled rate constants will not differ, at least in dilute solutions, as long as for these solutes, $\tau \leq 10^{-12}$ sec, and R and D are independent of the solutes. The effect of such a behavior in concentrated solutions will be discussed later.

(14) S. W. Benson, "The Foundations of Chemical Kinetics," McGraw-Hill, New York, N. Y., 1960, p 496.
(15) M. V. Smoluchowski, *Z. Phys. Chem.*, **92**, 129 (1917).
(16) P. Debye, *Trans. Electrochem. Soc.*, **82**, 265 (1942).
(17) E. J. Hart and M. Anbar, "The Hydrated Electron," Willey-Interscience, New York, N. Y., 1970, p 187.

TABLE I: Concentration Dependence of the Probabilities of Initial Formation of Encounter Pairs on the Reaction Cross Section (*R*)[a]

	P[b]								
R, Å	0.9	0.8	0.7	0.6	0.5	0.4	0.3	0.2	0.1
3	1.45	3.2	5.07	7.25	10	13	17.4	28.3	33
4	0.41	0.9	1.44	2.07	2.85	3.72	4.95	6.64	9.5
5	0.32	0.7	1.12	1.59	2.2	2.87	3.83	5.12	7.36
6	0.18	0.4	0.64	0.92	1.27	1.66	2.21	2.96	4.24
7	0.11	0.25	0.41	0.58	0.8	1.04	1.39	1.86	2.66
8	0.08	0.17	0.27	0.39	0.54	0.71	0.94	1.26	1.79
9	0.055	0.12	0.19	0.28	0.38	0.44	0.66	0.88	1.27
10	0.04	0.09	0.146	0.20	0.276	0.36	0.48	0.64	0.92

[a] All concentrations are in moles/liter. [b] *P* is defined in eq 8.

It seems to us also possible that τ can last as long as 10 psec which implies that for diffusion-controlled reactions the reaction probability would vary slowly from 0 to 1 (possibly the reaction probability can vary over this range form 0 to a fraction of 1) over a distance of about 3 Å. In this case, however, the diffusion theory would find itself in error, but it would seem that the error would not be a large one and the theory giving an average value of R would still be giving a good approximation.

If the (e_{aq}^-:S) has a finite lifetime ($\tau < 10^{-11}$ or 10^{-12} sec) the following questions arise. (1) What is the dependence of concentration of the (e_{aq}^-:S) on time and on [S]? Obviously, at sufficient low [S], the concentration of (e_{aq}^-:S) rapidly reaches a very low stationary state. (2) What are the properties of (e_{aq}^-:S)? The two extreme cases would be that either it resembles S^- or it will be very similar to e_{aq}^- + S as long as it did not react. This last possibility seems more plausible at least concerning the absorption spectrum, as it was found that in 5 *M* solutions of $NaClO_4$, NaOH, and KF, the spectrum of e_{aq}^- is hardly affected, although all the e_{aq}^- is present in encounter pairs.[2,18]

The implications of the above-mentioned points concerning some of the anomalies observed in concentrated solutions of S are as follows.

(I) In Hunt's experiments[12] e_{aq}^- is observed at $t \sim 10$ psec, and the yield of e_{aq}^- is integrated from $t = 0$. In our opinion this integration is invalid, even if the time dependence of k_{obsd} is taken into account, as was done by Schwarz,[11] since this integration takes into account only the decay which is due to encounter pairs formed through diffusion and neglects those which were formed initially. Such a mathematical treatment necessarily gives too low values of $G(e_{aq}^-)$ depending on the fraction of encounter pairs formed initially. Hence, in concentrated solutions the error may be very large (Table I).

To demonstrate the extent of this effect, the results obtained by Wolff, *et al.*,[2] concerning the decay of e_{aq}^- in 0.25 *N* acid with acetone of 0.1, 1.0, and 3 *M*, will be analyzed.

Figure 1 shows the measured[2] dependence of e_{aq}^- with time, and the lines computed by Schwarz,[11] taking into account the time dependence of the rate constants. In all these computed lines, e_{aq}^- exceeds the measured values and this may suggest that e_{dry}^- must have some sort of role to play in these systems. We added a third line which is the line computed by Schwarz[11] but corrected also for those e_{aq}^- initially formed as (e_{aq}^-:S) and assumed to decay away within less than 10 psec. It can be seen that

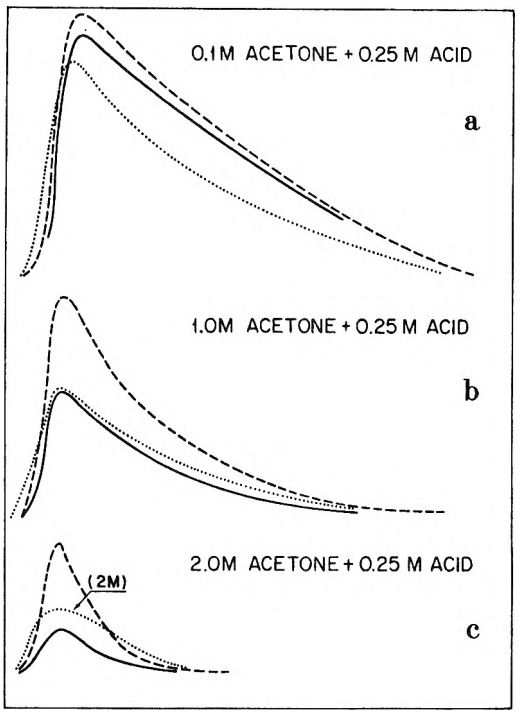

Figure 1. Optical density (arbitrary units) as a function of time during linac cycle: (.....) observed lines;[2] (- - - -) calculated cooperating time dependence;[11] (——) correcting the above line according to eq 8. (Note that [acetone] = 2 *M* in the experimental curve c where the correction[11] is made for 3 *M*).

this correction is even larger than the one due to time dependence in concentrated solutions. With this additional correction taken into consideration, the computed concentration of e_{aq}^- in solution of 2 *M* acetone is less than the observed one. (This is partially due to the fact that Schwarz's correction is too high as his was done for 3 *M* acetone.) For 1 *M* acetone, the agreement is excellent, far better than the accuracy of both corrections. In principle these corrections could give yields at $t \sim 10$ psec which would be too low, if (e_{aq}^-:S) would have a lifetime τ which would be in the range $10^{-12} < \tau < 10^{-11}$ sec. In such a case part of (e_{aq}^-:S) would still be present at t = 10 psec, and should its absorption be similar to that of e_{aq}^- the observed yield would stand for the sum of e_{aq}^- and (e_{aq}^-:S), whereas the computed one was only for e_{aq}^-. The high values of the decay rate constants as derived by Hunt[3] from the fraction of e_{aq}^- which decayed during his pulse ($t < 10$ psec) and attributed by him to reactions of dry electrons with S, could be, in fact, solely due to the decay of encounter pairs initially formed.

Figure 2 shows the relative yield of e_{aq}^- as a function of τ, the lifetime of e_{aq}^- in the presence of S, as computed by Aldrich, *et al.*[3] The observed yields of e_{aq}^- in concentrated solutions of various solutes were much lower than predicted from Figure 2, and the known values of τ for the reactions of e_{aq}^- with these solutes (Table II, ref 3).

Values of τ which could have been consistent with the observed yields were up to 20 times shorter than the known values of τ for the reaction of e_{aq}^- with these same solutes. The line computed by Aldrich, *et al.*,[3] did not incorporate a time dependence of $k(e_{aq}^- + S)$; a correction to this effect would have shortened $\tau(e_{aq}^- + S)$ in concentrated solutions of S by a factor of up to about 2. We

(18) M. Anbar and E. J. Hart, *J. Phys. Chem.*, **69**, 1244 (1965).

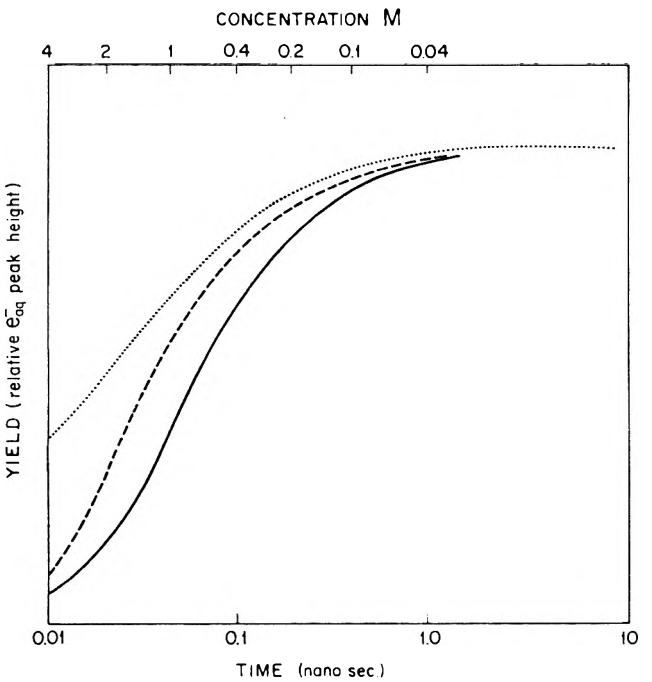

Figure 2. Relative yields of e_{aq}^- as a function of τ or [S]. τ is the lifetime of e_{aq}^- + S. [S] is for a reaction with $D = 6 \times 10^{-5}$ cm^2 sec^{-1}, $R = 6$ Å, and $k(e_{aq}^- + S) = 2.5 \times 10^{10}$ M^{-1} sec^{-1}: (. . . . . .) predicted by Wolff, *et al.*;[2] (- - -) predicted by eq 8; (——) correction of Wolff's[2] line with eq 8.

added to Figure 2 the yields of e_{aq}^- as predicted by eq 8 and then corrected Aldrich's[3] curve accordingly. The corrected curve predicts much lower yields of e_{aq}^- for a given value of $\tau(e_{aq}^- + S)$ than did the original[3] correction. The time dependency would even lower further the yield of e_{aq}^-. For example, if $k(e_{aq}^- + S) \sim 2.5 \times 10^{10}$ M^{-1} sec^{-1}, $D = 6 \times 10^{-5} \sim$ cm^2 sec^{-1}, $R = 6$ Å, and [S] = 4 M, the relative yield of e_{aq}^- predicted by Aldrich, *et al.*,[3] is 0.45, while with our correction, it is less than 0.05.

When Aldrich's correction is included as well as ours, the yield is expected to drop, and this drop is accounted for without necessarily assuming that dry electrons react with S and compete through reactions 1 and 2.

If, on the other hand, (e_{aq}^-:S) has a finite lifetime, a similar though somewhat smaller error in extrapolating $G(e_{aq}^-)$ will occur. If τ, the lifetime of (e_{aq}^-:S), is between 10^{-12} and 10^{-11} sec, the decay rate of e_{aq}^- as observed in very concentrated solutions may approach the decay rate of (e_{aq}^-:S) and not that of e_{aq}^-. This will occur in solutions where the bulk of e_{aq}^- is formed initially as encounter pairs with S, provided that the lifetime of these encounter pairs is long enough. These conditions may be fulfilled for reactions which are a little slower than diffusion controlled, where only one out of every few encounters will lead to reaction. The reaction of e_{aq}^- with H^+ could be such a case, and this may explain the relatively low reactivity of H^+ in concentrated solutions. The low relative reactivity of H^+ in such solutions was partially accounted for earlier by Schwarz[11] as due to the time dependence of this reaction.

If R for the reaction of H^+ with e_{aq}^- is about 5 Å, in 5 N $HClO_4$ $\sim$ 80% of e_{aq}^- are formed as (e_{aq}^-:H^+). If ⅕ of these encounter pairs will yield H in $\sim 10^{-12}$ sec, the ⅘ escaping their originally formed encounter pairs have a very high probability of forming within one diffusional displacement new encounter pairs, and therefore the expected yield of e_{aq}^- in this solution at $t = 10$ psec is expected to be much lower than observed.[2] (In 5 N acid, the yield drops only by ~40%.) This suggest either a lifetime for (e_{aq}^-:H^+) of several psec, or that R is much smaller.

Clearly, τ and R are averaged values, since as long as $R > (r_S + r(e_{aq}^-))$, several configurations of (e_{aq}^-:S) with various values of R may be formed, and they will have different reaction probabilities or lifetimes.

As it was found[17] experimentally for diffusion-controlled reactions of e_{aq}^- with S, values of R may be much larger than $(r(e_{aq}^-) + r_S)$. Therefore, it is not possible to decide whether any "normal" reaction of e_{aq}^- (for which $R \sim (r(e_{aq}^-) + r_S)$) actually occurs on every encounter. If for the normal reactions, the real value of R is larger than $(r(e_{aq}^-) + r_S)$ and only a part of the encounter pairs reacts, the value of k_{obsd} in dilute solutions will be unaffected. In principle one would be able to distinguish between these cases in concentrated solutions, by studying the time dependence of the reaction, which should be different for the two cases.

This uncertainty makes it even more difficult to estimate the values of R, and therefore the fraction of initially formed encounter pairs in concentrated solutions cannot be well estimated.

(II) Another implication of the direct formation of encounter pairs in concentrated solutions is that the competition kinetics may be affected.

Should two scavengers S_1 and S_2, yielding products P_1 and P_2, in their reactions with e_{aq}^- have the same charges, diffusion coefficients, and values of R, they will have identical values of k_{obsd} in dilute solutions, as calculated from eq 5. In competition studies of e_{aq}^- with S_1 and S_2 at low concentrations of the solutes, normal competition kinetics will be observed, with

$$\frac{[P_1]}{[P_2]} = \frac{k_{1(S_1)}[S_1]}{k_{1(S_2)}[S_2]} \tag{9}$$

and

$$\frac{-d[e_{aq}^-]}{dt} = k_{1(S_1)}[S_1][e_{aq}^-] + k_{1(S_2)}[S_2][e_{aq}^-] \tag{10}$$

If one would keep $[S_1]/[S_2] = 1$, in dilute solutions one-half of e_{aq}^- will react with each S_1 and S_2.

In concentrated solutions of two solutes, e_{aq}^- may initially participate simultaneously in an encounter pair with both S_1 and S_2. If the reactions of e_{aq}^- with both of these solutes are diffusion controlled, both will react with e_{aq}^- on every encounter, or within less than the encounter lifetime. If S_1 reacts faster than S_2 with e_{aq}^- within the encounter lifetime, one will expect that in their simultaneous encounter pairs with e_{aq}^- the relative reactivity, or the product ratio $[P_1]/[P_2]$, will exceed that predicted by eq 9. Therefore, $[P_1]/[P_2]$, as measured, will depend on and grow with the concentration. This is in addition to the time dependence predicted by Schwarz.[11] At very high concentrations, $[P_1]/[P_2]$ will approach the ratio of the lifetimes of S_1 and S_2 in their respective encounter pairs.

The last point which we shall consider in processes occurring at times as short as 10^{-11}–10^{-12} sec after the deposition of radiation is that of the effects concerning the temperature in the reaction zone. Mozumder[19] calculated that on the average, in the spur, in a volume with a radius of 20 Å, 30 eV are converted into heat in less than 1 psec. This could correspond to a "temperature increase" of 30° in this region. (If a larger fraction of the energy is deposit-

(19) A. Mozumder, *Advan. Radiat. Chem.*, **1**, (1969).

ed initiatly in the central core of the spur ($r \sim 15$ Å), the temperature increase may be as high as 70°).

Mozumder[19] calculated that the thermal equilibration times in H_2O are about 18, 5.85, and 2.95 psec respectively at 273, 313, and 353°K.[20] Any process occurring at times shorter than 10 psec may be influenced by conditions occurring prior to thermal equilibrium. This effect could account for solvation of electrons faster than expected at room temperature. The solvation time of electrons in various alcohols at room temperature was found to be less than 20 psec,[1] although the expected value for some of these alcohols is much larger.[1,19] If we assume that the solvation occurs in this time range and at the higher temperature existing at that time, the solvation process is expected to be much faster.[20]

In very concentrated solutions, where chemical reactions take place in times as short as 10 psec, the rate of these reactions maybe somewhat faster due to the lack of thermal equilibrium during part of these processes, although this effect will most probably be small it could lower to a small extent the yield of e_{aq}^- at $t \sim 10$ psec.

The effects which should be considered in concentrated solutions and studies in the picosecond range may be summarized as follows. (1) At very short reaction times, the initial temperature is higher than after thermal equilibration and may accelerate solvation and also to some extent chemical reaction rates. (2) In concentrated solutions the rate constants of e_{aq}^- with scavengers will depend on the concentration, due to (a) the time dependence of rate constants as discussed by Schwarz,[11] (b) the temperature effect, (c) the breakdown of Smulochowski's equation in the time range where the encounter's lifetime becomes comparable to the half-life of e_{aq}^-, and (d) the direct formation of encounter pairs.

The last effect may be the most serious one in concentrated solutions and the extent of it the most difficult to estimate since it is very sensitive to R, the value of which is hard to evaluate. A similar effect could occur where photochemical cages are studied in concentrated scavenger solutions.

These effects may explain most of the anomalies in competition studies of concentrated solutions of e_{aq}^- scavengers and of the kinetic studies in the picosecond range. They may explain the low $G(e_{aq}^-)$ observed in some of the concentrated solutions, and seem to be able to explain the results without having to have recourse to novel chemical species such as dry electrons. This, however, does not rule out the possibility of reactions of dry electrons prior to solvation, but indicates this assumption is not yet a necessity.

Acknowledgment. We would like to acknowledge many helpful discussions with Professor I. Z. Steinberg and with Dr. M. S. Matheson during the latter's stay in this laboratory and we are especially grateful to one of the referees (H. A. Schwarz), whose repeated critical refereeing was extremely helpful to us.

(20) A. Mozumder, *J. Chem. Phys.*, **50**, 3153 (1969).

Mass Spectrometric Studies of Some Gaseous Sulfur Fluorides

D. L. Hildenbrand[1]

McDonnell Douglas Astronautics Company, Huntington Beach, California 92647 *(Received November 6, 1972)*

The reaction of gaseous SF_6 with carbon in a heated Knudsen cell was studied by mass spectrometry, and several new molecular species including SF, SF_2, and SCF_2 were identified and characterized. From electron impact threshold measurements, ionization potentials with an estimated accuracy of 0.10 eV were obtained for these species, while similar measurements on SF_4 and SF_6 were used to derive ΔH_0° = 146.7 ± 3.2 kcal for the process $SF_6 = SF_4 + 2F$ and $\Delta H_f^\circ{}_{298} = -180.0 \pm 5.0$ for SF_4. Gaseous equilibration was observed for several isomolecular reactions, and the resulting equilibrium data were used to derive the standard heats of formation, $\Delta H_f^\circ{}_{298}$, of 3.2 ± 1.2, −71.4 ± 2.5, and −75.0 ± 3 kcal/mol for SF, SF_2, and SCF_2, respectively. For SF, this is equivalent to the dissociation energy $D_0^\circ(SF)$ = 81.0 ± 1.2 kcal or 3.51 ± 0.05 eV. The results can be combined with available literature data to evaluate the six individual bond dissociation energies in the SF_6 molecule, yielding values which are in qualitative agreement with the valence state concept of covalent bonding.

Introduction

Although gaseous SF_6 is now being used in several high-temperature applications (*e.g.*, as an electron scavenger in plasmas and as a fluorine atom source in chemical lasers), very little is known about the thermochemistry of the lower sulfur fluorides. Since these lower fluorides may play a significant role in the overall chemistry, a thermochemical study was undertaken using the familiar technique of high-temperature mass spectrometry.

SF_6 itself has been rather thoroughly studied, and the thermochemical properties and the spectroscopic con-

(1) Present address: Stanford Research Institute, Menlo Park, Calif. 94025.

stants are known with relatively high accuracy.[2] A similar situation holds for SF_4, although the heat of formation is known with only moderate accuracy.[2] The electron resonance spectrum of molecular SF has been observed and the rotational constant derived,[3a] but no direct thermochemical data are available. Some additional molecular data for SF have been obtained from Hartree–Fock molecular orbital calculations.[3b] SF_2 has been identified through its microwave spectrum and the structural parameters determined,[4] while SF_3 and SF_5 have not been characterized experimentally; some estimated spectroscopic and thermochemical data have been reported.[5] In the research described here, SF, SF_2, and SF_4 have been studied by equilibrium and electron impact methods, and these results have been coupled with various literature data to give a rather complete picture of the S–F thermochemistry. Thermochemical data have also been obtained for the molecular species (SCF_2) thiocarbonyl fluoride.

Experimental Section

Basically, the experimental approach is as follows. The molecular species to be studied are generated by chemical reaction in a heated Knudsen cell and leave the cell orifice in the form of a collision-free molecular beam. Atomic and molecular species in the beam enter the ionization chamber where they are ionized by electron impact, and the resulting ions are extracted, focused, accelerated, mass analyzed, and collected. The neutral beam composition, which mirrors the oven gas composition, can be inferred from the ion abundances and can be used to derive equilibrium thermodynamic data. It must be demonstrated, of course, that chemical equilibrium is attained in the beam oven for the processes to be studied.

After several unsuccessful attempts with condensed-phase reactions, it was found that some of the desired S–F molecular species could be generated through the reaction of SF_6 with carbon when the gas was admitted to the base of a graphite effusion cell heated to about 1500°K. A number of cell configurations were explored in order to find the optimum conditions for studying the reaction. In the series I measurements, a graphite liner packed with graphite cloth was contained in a molybdenum cell; this was satisfactory in some respects, but there were indications that surface reactions in the vicinity of the orifice did not yield an equilibrium distribution of all products, particularly not for SF_2, SF_4, and SCF_2. For series II, a graphite cell containing a loosely wound plug of platinum wire was used. Generally satisfactory results were obtained with this arrangement, where the platinum baffling apparently increased the residence time of, and the number of collisions between, gaseous products in the oven. In one further configuration, that of series III, a thin platinum partition containing two 0.3-mm diameter holes was placed between the upper and lower sections of the graphite cell. The lower section of the cell was then packed with graphite cloth, while the upper section containing the beam exit orifice held the plug of platinum wire. Results obtained with this third configuration were essentially identical with those of series II. Even so, it was still not possible to establish equilibrium with respect to SF_4 and SF_6, but this did not affect the other reactions discussed.

SF_6 entered the cell through a graphite tube, and the flow rate was controlled externally with a variable leak valve. Because of the large number of permanent or semipermanent gases involved as reactants or products, it was necessary to enlarge both the pyrometer viewing aperture and the beam exit aperture in the radiation shields surrounding the cell, so as to achieve better pumping and better discrimination between beam and background signals. This discrimination was made *via* neutral beam profiles measured with the aid of the movable beam defining slit. Temperatures were measured by optical pyrometry, utilizing a black-body cavity in the cell lid. All other aspects of the magnetic deflection mass spectrometer and the experimental technique have been amply described.[6,7]

Gaseous SF_6 and SF_4 were obtained from the Matheson Co. Room temperature mass spectra showed the SF_4 to contain an appreciable SOF_2 impurity, which is apparently common. These spectra also indicated a small SF_2 impurity in the SF_4, which was rather surprising. The microwave studies[4] indicate SF_2 to be moderately stable at room temperature.

Results

In order to clarify the nature of the various ionization processes, threshold measurements were first made for the major ions in the mass spectra of SF_6 and SF_4 at room temperature. The more accurate threshold values were obtained by the extrapolated voltage difference method using xenon or argon as standard,[7] while the others resulted from the vanishing current method. For SF_6, the observed appearance potentials (AP) are as follows: SF_5^+, 15.50 eV; SF_4^+, 18.44 eV; SF_3^+, 20.0 eV; SF_2^+, 27.5 eV; and SF^+, 30.5 eV. Values given to two decimal places are believed accurate to within 0.10 eV, with all others 0.5 eV. The threshold for SF_5^+ is somewhat higher than those from photoionization[8] (15.29 eV) and photoelectron spectroscopy[9] (15.35 eV), but not excessively so. There are no accurate values with which to compare the others. No parent ion was observed for SF_6. For SF_4, the measured AP's were SF_4^+, 12.08 eV; SF_3^+, 12.63 eV; and SF_2^+, 10.25 and 17.4 eV. The first threshold for SF_2^+ must be due to an SF_2 impurity; an almost identical value was obtained for SF_2^+ resulting from the products of the high-temperature SF_6–C reaction. Glemser and colleagues[10] report threshold values of 12.28 and 12.70 eV, both ±0.03 eV, for SF_4^+ and SF_3^+ in the mass spectrum of SF_4, obtained with an RPD source. The reason for the 0.20-eV discrepancy on AP(SF_4^+/SF_4) is not apparent; as with all the others, our value is the result of three or more determinations with a reproducibility on the order of 0.02 eV. Numerous comparisons on well-known substances have shown such threshold measurements to be accurate to within 0.10 eV.[7] A threshold AP of 12.58 eV was found for SOF_2^+, the parent ion associated with the thionyl fluoride

(2) D. R. Stull, Ed., "JANAF Thermochemical Tables," Dow Chemical Co., Midland, Mich., 1965, and supplements.
(3) (a) A. Carrington, G. N. Currie, T. A. Miller, and D. H. Levy, *J. Chem. Phys.*, **50**, 2726 (1969); (b) P. A. G. O'Hare and A. C. Wahl, *ibid.*, **53**, 2834 (1970).
(4) D. R. Johnson and F. X. Powell, *Science*, **164**, 950 (1969).
(5) R. L. Wilkins, *J. Chem. Phys.*, **51**, 853 (1969); see also Aerospace Corporation Report No. TR-0158(3240-20)-19 (1968).
(6) D. L. Hildenbrand, *J. Chem. Phys.*, **48**, 3657 (1968).
(7) D. L. Hildenbrand, *Int. J. Mass Spectrom. Ion Phys.*, **4**, 75 (1970); **7**, 255 (1971).
(8) V. H. Dibeler and J. A. Walker, *J. Chem. Phys.*, **44**, 4405 (1966).
(9) D. C. Frost, C. A. McDowell, J. S. Sandhu, and D. A. Vroom, *Advan. Mass Spectrom.*, **4**, 781 (1968).
(10) O. Glemser, A. Muller, D. Bohler, and B. Krebs, *Z. Anorg. Allg. Chem.*, **357**, 184 (1968).

TABLE I: Threshold Appearance Potentials of Species Resulting from the SF_6 + C Reaction at ~1500°K

Ion	AP, eV	Neutral	Lit., eV
S^+	10.5 ± 0.3	S	10.36[a]
S_2^+	9.42 ± 0.10	S_2	9.36[b]
SF^+	10.09	SF	10.0[c]
SF_2^+	10.29	SF_2	
SF_3^+	12.8	SF_4	12.70[d]
SF_4^+	12.1	SF_4	12.28[d]
SF_5^+	15.6	SF_6	15.29,[e] 15.35[f]
CF_2^+	11.54	CF_2	11.7,[g] 11.86[h]
CS^+	11.39	CS	11.33[i,j]
CS_2^+	10.07	CS_2	10.06[a]
SCF_2^+	10.53	SCF_2	

[a] Reference 11. [b] Reference 12. [c] Reference 3b. [d] Reference 10. [e] Reference 8. [f] Reference 9. [g] Reference 13. [h] Reference 14. [i] Reference 15. [j] Reference 16.

impurity; the ionization potential of SOF_2 has not been reported previously.

When SF_6 was admitted to the graphite cell at about 1500°K, a number of new and interesting ion species were observed; these ion signals were totally dependent on the SF_6 flow, and they dropped to zero when the flow was terminated. The observed ions, their threshold appearance potentials, and the inferred neutral precursors are listed in Table I.[11-16] As can be seen, the measured AP's are generally in close agreement with the literature values, where the latter are accurately known from photoionization or photoelectron spectroscopy. Thus the assignment of the neutral precursors is relatively straightforward. For SF, SF_2, and SCF_2, it is expected that the highest ionizing orbitals would be derived largely from the sulfur 3p atomic orbital, and the close proximity of their AP's to that of atomic sulfur bears this out.

With the large number of neutral beam species, there are many possibilities for equilibrium thermochemical measurements. The following isomolecular gaseous reactions were chosen for study

$$CS + SF_2 = CF_2 + S_2 \quad (1)$$

$$CS_2 + 2SF = CF_2 + 2S_2 \quad (2)$$

$$S + SCF_2 = CF_2 + S_2 \quad (3)$$

since they are reasonably symmetrical and each contains just one species whose heat of formation is unknown or uncertain. Ion intensities, measured at ionizing energies 2.0 ± 0.2 eV above the various thresholds in order to eliminate fragmentation effects, were obtained at a number of temperatures in the range 1400–1600°K, and the data are summarized in Table II. As in previous studies, the ion current analogs of the equilibrium constants for these reactions were calculated directly from the ion abundance ratios, and it is assumed that these analogs are within a factor of 2 of the true equilibrium constants. The rationale for using the uncorrected ion abundance ratios to represent the equilibrium constant has been discussed previously;[6] in one of the very few instances in which this approach can be checked directly, it was recently found that the ion current analogs for the reaction

$$S + SO_2 = 2SO \quad (4)$$

were within about 15% of the accurately known equilibrium constants over a wide range of temperatures.[17]

TABLE II: Ion Abundances[a] in Mass Spectra of Products of the SF_6 + C Reaction

T, °K	S^+	S_2^+	SF^+	SF_2^+	CF_2^+	CS^+	CS_2^+	SCF_2^+
				Series I				
1529		0.66	0.035		0.75		1.10	
1611		3.40	0.195		4.00		6.30	
				Series II				
1436	0.09	1.75	0.21	1.00	2.24	0.07	0.60	
1500	0.27	4.30	0.465	1.45	4.83	0.33	1.95	
1505	0.19	2.80		0.54	2.45	0.25	0.95	
1530	0.465	5.70	0.51	1.15	6.51	0.735	3.15	
1564	0.60	4.40	0.355	0.385	3.78	1.29	1.95	
				Series III				
1478	0.245	3.50	0.255	0.60	8.25	0.945	3.90	2.75
1510	0.44	5.00	0.39	0.57	11.7	2.30	7.50	2.70
1510	0.20	1.44	0.10	0.115	3.90	1.32	3.30	0.60
1556	0.69	6.00	0.51	0.585	18.5	4.35	11.0	3.30
1556	0.30	0.93	0.075	0.035	3.60	2.15	3.30	0.30
1556	0.295	0.96	0.075	0.04	3.00	1.90	3.15	0.27
1588	1.04	5.85	0.525	0.51	18.0	6.00	15.0	2.55

[a] In arbitrary units, measured at AP + 2 eV.

The derived equilibrium constants are given in Table III. These constants were found to be essentially independent of changes in the partial pressures of the various species when the latter were varied over a wide range by changing the SF_6 flow rate, thereby demonstrating that gaseous equilibration was achieved. In the same way, it was found that equilibration of SF_4 and SF_6 could not be attained with the present configuration, since equilibria involving these species varied widely with the SF_6 flow. As expected, increasing the SF_6 flow and raising the total pressure forced the reactions involving SF_4 and SF_6 toward the equilibrium position, but it was not practical to use this approach to force equilibration. The stripping of fluorine atoms from SF_6 and SF_4 to yield SF and SF_2 is no doubt a complex kinetic process, and it seems unlikely that equilibration of these larger polyatomic molecules can be achieved under Knudsen flow conditions.

For use in thermodynamic calculations, the free-energy functions of CS, CS_2, S, S_2, and CF_2 were taken from the JANAF Tables.[2] Functions for SF were calculated from the spectroscopic constants of Carrington and coworkers,[3a] along with an estimated vibrational frequency of 900 cm^{-1}. The estimated spectroscopic constants of Wilkins[5] and the microwave structure data[4] were used for SF_2, since they are in good accord with those of the structurally similar molecule SiF_2. It was assumed that the free-energy functions for SCF_2 could be closely approximated by those of the isoelectronic and probably isostructural molecule ($ClBF_2$) chlorodifluoroboron. The changes in free-energy function of reactions 1, 2, and 3 are listed in Table IV.

(11) J. L. Franklin, J. G. Dillard, H. M. Rosenstock, J. T. Herron, K. Draxl, and F. H. Field, National Bureau of Standards Report No. NSRDS-NBS 26 (1969).
(12) J. Berkowitz and C. Lifshitz, *J. Chem. Phys.*, **48**, 4346 (1968).
(13) I. P. Fisher, J. B. Homer, and F. P. Lossing, *J. Amer. Chem. Soc.*, **87**, 957 (1965).
(14) R. F. Pottie, *J. Chem. Phys.*, **42**, 2607 (1965).
(15) N. Jonathan, A. Morris, M. Okuda, and D. A. Smith, *Chem. Phys. Lett.*, **13**, 334 (1972).
(16) G. H. King, H. W. Kroto, and R. J. Suffolk, *Chem. Phys. Lett.* **13**, 457 (1972).
(17) D. L. Hildenbrand, unpublished data.

TABLE III: Derived Equilibrium Constants and Third-Law Heats[a] of Gaseous Reactions

T, °K	K_1	$\Delta H_{298}(1)^b$	K_2	$\Delta H_{298}(2)^c$	K_3	$\Delta H_{298}(3)^d$
			Series I			
1529			242	−16.3		
1611			193	−16.5		
			Series II			
1436	56.0	−11.3	259	−15.4		
1500	43.4	−11.1	212	−15.6		
1505	52.6	−11.7				
1530	43.9	−11.3	258	−16.5		
1564	45.2	−11.7	298	−17.3		
			Series III			
1478	50.9	−11.4	398	−17.2	42.8	−3.8
1510	44.6	−11.2	256	−16.2	49.2	−4.4
1510	37.0	−10.7	245	−16.1	46.8	−4.2
1556	43.7	−11.5	233	−16.5	48.8	−4.5
1556	44.5	−11.6	168	−15.5	37.2	−3.7
1556	37.9	−11.1	156	−15.2	36.1	−3.6
1588	34.5	−11.0	158	−15.6	39.8	−4.0
Third law av.		−11.3		−16.1		−4.0
Second law av.		−10.6 ± 3.1		−13.9 ± 5.9		−4.9 ± 5.3

[a] In kcal. [b] Reaction 1. [c] Reaction 2. [d] Reaction 3.

TABLE IV: Free-Energy Functions for Gaseous Reactions

Reaction	$-\Delta(F - H_{298})/T$, cal mol^{-1} deg^{-1} 1400°K	1600°K
1	0.12	0.10
2	0.32	0.23
3	4.97	4.77

These functions were used to calculate the third-law enthalpies, also listed in Table III, with the average values $\Delta H_{298}(1) = -11.3$ kcal, $\Delta H_{298}(2) = -16.1$ kcal, and $\Delta H_{298}(3) = -4.0$ kcal. An uncertainty of 2 kcal is assigned to each of these values. The corresponding second-law heats, although more uncertain, are in good agreement, as seen in Table III.

Even though no equilibrium data were obtained for SF_4, it is possible to derive thermochemical data from the electron-impact threshold measurements on SF_4 and SF_6. The appearance potential $AP(SF_4^+/SF_6)$ is taken to be $\Delta H_0°$ for the process

$$SF_6 + e \rightarrow SF_4^+ + 2F + 2e \qquad (5)$$

with F atoms believed to be a much more likely product than the F_2 molecule based on energetic considerations and on similar data for other fluorides. This can be combined with $IP(SF_4)$ to yield $\Delta H_0° = 18.44 - 12.08 = 6.36$ eV = 146.7 kcal for the reaction

$$SF_6 = SF_4 + 2F \qquad (6)$$

on the assumption of negligible excess energy in the products of reaction 5 and no overriding thermal effects which would obscure the true threshold for the process. Conversion to standard conditions gives $\Delta H_{298}(6) = 149.5$ kcal, with an estimated uncertainty of 5 kcal.

The third-law enthalpies of reactions 1, 2, and 3 and the electron impact value for reaction 6 can now be used to derive the heats of formation of SF, SF_2, SCF_2, and SF_4.

TABLE V: Derived Heats of Formation of S–F Species

	$\Delta H_f°_{298}$, kcal/mol This work	Lit.
SF	3.2 ± 1.2	−13.4[a]
SF_2	−71.4 ± 2.5	
SF_4	−180.0 ± 5.0	−186.6,[b] −161.8[c]
SCF_2	−75.0 ± 3.0	
SF_3	−115 ± 5[d]	
SF_5	−232 ± 5[d]	

[a] Reference 3b. [b] Reference 2. [c] Reference 19. [d] See text.

For this purpose, the heats of formation of all species but CS were taken from the JANAF Tables, while the CS data were taken from some recent equilibrium measurements[18] which gave $\Delta H_f°_{298}(CS) = 70.0 \pm 2$ kcal/mol. In Table V the derived heats of formation are listed and compared with various literature results.

It is also possible to derive the heat of formation of SF_2 without recourse to the thermochemistry of CS. By treating the gaseous equilibrium

$$S + SF_2 = 2SF \qquad (7)$$

one obtains $\Delta H_{298}(7) = 11.5$ kcal and $\Delta H_f°_{298}(SF_2) = -71.4$ kcal/mol, utilizing the data on SF resulting from the study of reaction 2. This alternate value for SF_2 is identical with that obtained from reaction 1, and says only that the data are consistent with $\Delta H_f°_{298}(CS) = 70.0$ kcal/mol, determined earlier from similar studies[18] of the reaction

$$CS_2 + S = CS + S_2 \qquad (8)$$

Discussion

The heat of formation of SF can be coupled with the atomization energies of the elements to give the dissocia-

(18) D. L. Hildenbrand, *Chem. Phys. Lett.*, **15**, 379 (1972).

tion energy $D_0°(SF) = 81.0 \pm 1.2$ kcal (3.51 ± 0.05 eV). By adding an estimated electron correlation energy correction to their Hartree-Fock binding energy, O'Hare and Wahl[3b] obtained $D_0°(SF) = 4.2 \pm 0.2$ eV = 97 ± 5 kcal, but it seems that the correlation correction is about 25% too large. The S-F bond is rather weak in comparison to other fluorides, and this is no doubt why more detailed spectroscopic data on SF have not been reported. In fact, the results of this work have shown that SF_6 is a very satisfactory high-temperature fluorinating agent. The SF_4 heat of formation reported here essentially confirms the relatively inaccurate result obtained from solution thermochemistry (−186.6 ± 6 kcal/mol),[2] but at the same time indicates the indirect result of O'Hare, *et al.*,[19] based on electron impact measurements to be significantly in error (−161.8 ± 1.1 kcal/mol). There are no previous measurements on SCF_2 or SF_2, but the thermochemical data are in approximate agreement with what one would estimate from bond energy considerations.

There are several bits of information available which allow one to fix the bond dissociation energies $D(F_5S-F)$ and $D(F_3S-F)$ within fairly narrow limits, and this in turn can be used with the present results to evaluate all six of the bond dissociation energies (BDE) in the SF_6 molecule. The thresholds for F^- formation by dissociative attachment in SF_4 and SF_6 have been determined,[20] and these can be used together with the electron affinity of fluorine to give $D(F_5S-F) = 78$ kcal and $D(F_3S-F) = 83$ kcal. Further, the fragment ion appearance potentials $AP(SF_5^+/SF_6)$ and $AP(SF_3^+/SF_4)$ may be combined with upper limit values[21] for $IP(SF_5)$ and $IP(SF_3)$ so as to yield $D(F_5S-F) > 76$ kcal and $D(F_3S-F) > 78$ kcal. Similarly, shock tube kinetic studies[22,23] on SF_4 and SF_6 have been interpreted to give ~76 and ~79 kcal as the energies for removal of the first fluorine atom from SF_6 and SF_4, respectively. There is reasonably good accord among these different values, leading one to select the dissociative attachment results as the best values. The step-wise bond dissociation energies in SF_6 are then as follows: $D(F_5S-F) = 78$ kcal; $D(F_4S-F) = 72$ kcal; $D(F_3S-F) = 83$ kcal; $D(F_2S-F) = 63$ kcal; $D(FS-F) = 94$ kcal; and $D(S-F) = 82$ kcal.

These BDE's follow the expected pattern among the even- and odd-electron molecules, with the formation of even-electron molecules leading to the alternately stronger bonds. Qualitatively, this even-odd variation can be rationalized in terms of the excited valence state concept of covalent bonding. The sulfur atom, with its $3s^23p^4(^3P)$ divalent ground state, could form two p bonds directly without valence excitation. However, in view of the 98° apex angle in SF_2 and in line with what is known[24] about the geometry and bonding in SF_4, it seems very likely that the bonds in SF and SF_2 are not pure p bonds, but rather partial s-p hybrids of the isovalent type. The amount of s character should be relatively small since the F-S-F valence angle in SF_2 is near the 90° associated with p^2 bonding, but nevertheless, some valence excitation would be required prior to formation of the bond in SF. This excitation would come at the expense of the first S-F bond, making $D(FS-F) > D(S-F)$, as observed. Before any further bonds can be formed, however, a major excitation from the divalent to the tetravalent state is required. Tolles and Gwinn[24] have shown the S-F bonds in SF_4 are of two distinct types, an equatorial pair with 101° valence angle and $r(S-F) = 1.545$ Å, and a nearly linear polar pair with $r(S-F) = 1.646$ Å. It is envisioned[24] that the equatorial bonds are rather "normal" S-F bonds made up of s-p hybrids (probably not very different from those in free SF_2) while the polar pair are p-d hybrids, the whole being a sort of sp^2d hybrid. The promotional energy associated with this tetravalent configuration must be supplied as the third fluorine is added, making $D(FS-F) \gg D(F_2S-F) < D(F_3S-F)$. A further unpairing of spins is required upon addition of the fifth fluorine as the hexavalent sp^3d^2 hybrid configuration is achieved, with the energetic implications such that $D(F_3S-F) > D(F_4S-F) < D(F_5S-F)$. All of these conjectures are in accord with the observed BDE's, although we are not yet in a position to account for the differences on a quantitative basis.

The BDE's $D(F_5S-F)$ and $D(F_3S-F)$ can be used to calculate the heats of formation of SF_5 and SF_3, and these values are included in Table V. These heats of formation are entirely consistent with the nonobservation of SF_5 and SF_3 in the present experiments. For example, the derived heat of formation of SF_3 would have to be in error by more than 18 kcal/mol (more negative) if SF_3 were to be just barely detectable, a very unlikely situation. The same holds true for SF_5. Furthermore, the observed AP's of SF_3^+ and SF_5^+ are quite conclusive on this point, since the charge exchange studies of Fehsenfeld[21] indicate that $IP(SF_3) < 9.25$ eV and $IP(SF_5) < 12.07$ eV.

The measured appearance potentials of SF, SF_2, SF_4, SCF_2, and CF_2 are believed to be close to the true ionization potentials, perhaps within 0.10 eV. Normally these would be the vertical IP's, but it is possible that strong autoionization near threshold could influence the ion yield such that the observed onset would be closer to the adiabatic IP; a clear differentiation between the two could be obtained from the photoelectron spectra. In any event, the present electron-impact values for S_2, CS, and CS_2 lie well within 0.10 eV of the accurate photoionization and photoelectron spectroscopic values, giving some indication of the accuracy of the other results. Vibrational hot bands could influence the high-temperature beam measurements so that some of the AP's of Table I might be below the 0°K thresholds, but on the other hand there may be certain mitigating factors. The close agreement with the photoelectron data on CS and CS_2 can probably be ascribed to the fact that the PE spectra show the vertical and adiabatic IP's to be practically coincident, thereby indicating a large Franck-Condon factor for the $0 \rightarrow 0$ transition to the ground state of the ion, which would override any thermal tailing effects. Since the magnitudes of the observed AP's of SF, SF_2, SCF_2, and CF_2 suggest that the ionizing orbitals are essentially nonbonding, one would expect only minimal geometry changes in the ionization process and, therefore, highly favorable Franck-Condon factors for the $0 \rightarrow 0$ transition. Clearly, however, it would be valuable to have both photoelectron and photoionization data on these molecules, not only to check the interpretation of the electron impact measurements, but also because of the useful information that could be obtained about ionic states. The calculated vertical IP of SF, 10.0 ± 0.4 eV, obtained from the difference between Hartree-

(19) P. A. G. O'Hare, W. N. Hubbard, O. Glemser, and J. Wegener, *J. Chem. Thermodyn.*, **2**, 71 (1970).
(20) P. Harland and J. C. J. Thynne, *J. Phys. Chem.*, **73**, 4031 (1969); 75, 3517 (1971).
(21) F. C. Fehsenfeld, *J. Chem. Phys.*, **54**, 438 (1971).
(22) J. F. Bott and T. A. Jacobs, *J. Chem. Phys.*, **50**, 3850 (1969).
(23) J. F. Bott, *J. Chem. Phys.*, **54**, 181 (1971).
(24) W. M. Tolles and W. D. Gwinn, *J. Chem. Phys.*, **36**, 1119 (1962).

Fock energies of the molecule and molecule-ion plus a correlation correction,[3b] agrees well with the experimental value, suggesting that the procedure for estimating the correlation correction is reliable. Moreover, the IP(SF) derived from Koopmans' theorem, 11.4 eV, is higher than the experimental value, and the uncorrelated difference between H-F energies of neutral and ion, 9.6 eV, is lower, the two values bracketing the true IP as pointed out by Richards.[25]

Information about the electron affinities of all the S-F molecular species but SF_2 is available, although the data are of rather mixed accuracy. These values are EA(SF) = 2.5 ± 0.5 eV;[3a] EA(SF_3) = 2.9 ± 0.1 eV;[20] EA(SF_4) = 1.3 ± 0.2 eV;[20] EA(SF_5) = 3.3 ± 0.2 eV;[20] and EA(SF_6) = 1.4 ± 0.2 eV.[21,26] Here again the even-odd electron variation manifests itself, with the odd-electron molecules naturally having the higher EA's. Because of this regularity, one can estimate with some confidence EA(SF_2) = 1.2 ± 0.5 eV. It is then possible to use the electron affinities and the ionization potentials together to obtain a rather complete set of thermochemical data for the positive and negative ions in the S-F system.[27]

(25) W. G. Richards, *Int. J. Mass. Spectrom. Ion Phys.*, **2**, 419 (1969).
(26) J. Kay and F. M. Page, *Trans. Faraday Soc.*, **60**, 1042 (1964).
(27) Note Added in Proof. After this manuscript was submitted, a value of 10.45 ± 0.01 eV was reported for the adiabatic ionization potential of SCF_2 from photoelectron spectroscopy [H. W. Kroto and R. J. Suffolk, *Chem. Phys. Lett.*, **17**, 213 (1972)], as compared to the near-vertical IP of 10.53 ± 0.10 eV reported here.

Triplet-State Phosphorescence of Adsorbed Ionic Organic Molecules at Room Temperature[1]

Edward M. Schulman and Cheves Walling*

Department of Chemistry, University of Utah, Salt Lake City, Utah 84112 *(Received June 2, 1972)*

Strong phosphorescence (triplet-state emission) is observed at room temperature from salts of a wide variety of polynuclear carboxylic or sulfonic acids, phenols, and amines adsorbed on paper, silica, alumina, and other supports. This phosphorescence is O_2 insensitive but requires thorough drying and is not observed with nonionic materials. Emission and excitation spectra are very similar to those observed from frozen solutions at −196°, and the technique provides a convenient means of demonstrating phosphorescence phenomena, measuring triplet-state and delayed fluorescence spectra, and identifying a variety of organic molecules including many of biological interest.

Introduction

Although very weak phosphorescence has been observed from rigorously deoxygenated solutions of dyestuffs, and in the classic studies of E-type delayed fluorescence,[2] and recently a few examples of stronger emission involving particularly rigid molecules have been reported in solution at room temperature,[3] strong phosphorescence (efficient triplet-state emission) from organic molecules is normally observed only in the gas phase, in rigid media, or at very low temperatures.[4] Accordingly, in the course of working up a reaction mixture from the decomposition of benzoyl peroxide in tetrachloroethylene[5] by thin layer chromatography on silica developed with isopropyl alcohol-ammonia, we were surprised to observe strong blue-green phosphorescence of dried spots corresponding to biphenylcarboxylic acids, present as their ammonium salts. We decided to pursue the matter further and this paper describes our results.

Results

Although we have been unable to find any comparable observation in the literature,[6] further study showed that similar phosphorescence is a general property of a wide variety of ionic organic molecules. Essentially every salt of a carboxylic acid, phenol, amine, or sulfonic acid investigated which might be expected to show visible phosphorescence did so, but none was observed with any nonionic species. Phosphorescence is observed from materials adsorbed on a variety of supports, silica, alumina, paper, asbestos, and (more weakly) glass fibers, although filter

(1) Reported in part at the 13th Annual Rocky Mountain Spectroscopy Conference, Society for Applied Spectroscopy, Denver, August, 1971. A preliminary account has also been published: E. M. Schulman and C. Walling, *Science*, **178**, 53 (1972).
(2) C. A. Parker, "Photoluminescence of Solutions," Elsevier, New York, N. Y., 1968, pp 45–46.
(3) R. B. Bonner, M. K. DeArmond, and G. H. Wahl, Jr., *J. Amer. Chem. Soc.*, **94**, 988 (1972).
(4) M. Zander, "Phosphorimetry," Academic Press, New York, N. Y., 1968, p 117.
(5) E. M. Schulman, R. D. Bertrand, D. M. Grant, A. R. Lepley, and C. Walling, *J. Amer. Chem. Soc.*, **94**, 5972 (1972).
(6) (a) Polynuclear aromatics have been observed to phosphoresce at 77°K on paper chromatograms: A. Szent-Gyorgyi, *Science*, **126**, 751 (1957). (b) Phosphorescence spectra of solutions frozen at 77°K on glass fiber paper, paper, and silica gel have been measured: M. Zander, *Erdoel Kohle*, **15**, 362 (1962); E. Sawicki and J. D. Pfuff, *Anal. Chim. Acta*, **32**, 521 (1965); E. Sawicki and P. Johnson, *Microchem. J.*, **8**, 85 (1964).

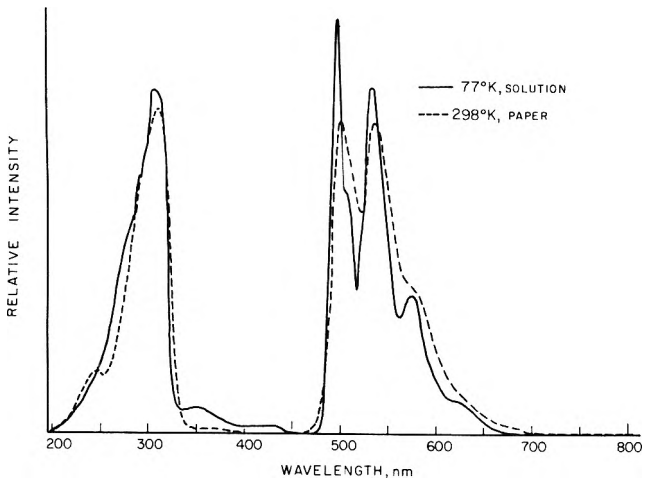

Figure 1. Comparison of emission (450–700 nm) and excitation (200–400 nm) spectra of Na naphthalate adsorbed on paper and in frozen solution.

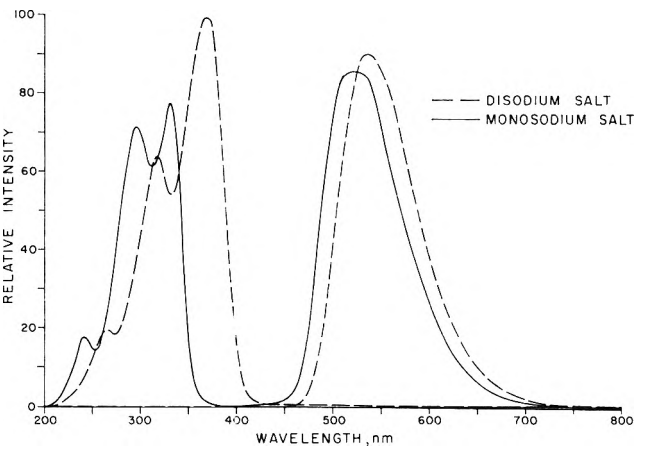

Figure 2. Comparison of emission and excitation spectra for Na 2-naphthol-6-sulfonate adsorbed on paper from water solution with that adsorbed from 1 *M* sodium hydroxide solution (singly and doubly ionized species).

paper seems to give the best results. Phosphorescence appears to involve surface adsorbed molecules, since none could be detected from finely ground samples of pure salts, or from crystals grown from solutions of the organic acid in just sufficient NaOH to neutralize, whereas the same solutions gave excellent phosphorescence samples when impregnated onto paper and dried. 2-Naphthoic acid dissolved in *excess* aqueous NaOH and rigorously evaporated to dryness (giving material adsorbed on $NaOH$–Na_2CO_3) phosphoresced strongly. Dryness is also essential; samples adsorbed on paper lose the ability to phosphoresce when exposed to a humid atmosphere, but regain it on heating or drying in a desiccator. The phosphorescence is completely oxygen insensitive. No difference is observed in phosphorescence intensity of samples stored for weeks under pure atmospheres of *dry* oxygen, nitrogen, or air.[7] Finally, the intensity of emission is sometimes most striking. Phosphorescence of sodium, potassium, or ammonium salts of 2-naphthoic acid adsorbed on Whatman No. 1 paper, irradiated intermittently by a 15-W Mineralight short-wave uv source, is detectable under ordinary room lighting and may be observed for over 5 sec in the dark.

Quantitative Measurements. For more detailed study, materials adsorbed on paper were examined in an Aminco-Keirs spectrophotophosphorimeter, and emission and excitation spectra compared with those from frozen solutions at −196°. Figure 1 shows an example and, in general, peak positions under the two conditions were almost identical although the adsorbed species exhibited some line broadening and loss of spectral detail. Our measurements are summarized in Table I which gives the location of maxima for both excitation and emission, together with relative intensities. In some cases (*e.g.*, the naphthol sulfonates) it was possible to obtain spectra from both singly and doubly ionized species, Figure 2. Although ionization of the naphthol group shifts the excitation spectrum (*i.e.*, singlet absorption) to longer wavelengths, emission is hardly changed, consistent with Jackson and Porter's results on 2-naphthol and its anion in rigid media at low temperatures.[8]

Phosphorescence lifetimes of several molecules were also examined by flash photolysis with results listed in Table II. Characteristic decay times ($t = 1/k$) lie for the most part in the 100–700-msec range. These were usually somewhat shorter than those observed at liquid nitrogen temperatures, although some lifetimes appeared longer on paper at ambient temperatures.

Finally, it seemed possible that the technique might permit observation of esr spectra of the triplets involved. However, irradiation of the sodium salt of 2-naphthoic acid adsorbed on paper produced only a broad, ill-resolved esr peak which increased in intensity with irradiation time and failed to decay in the dark, a result similar to that observed on irradiation of many solid organic compounds in bulk.

Discussion

Evidently surface adsorption of the triplet states of organic molecules holds them rigidly so as to retard their usual nonradiative decay, and also somehow inhibits oxygen quenching. Why this should be the case is not at all clear,[7b] but nevertheless we believe that the technique should have a number of applications. Qualitatively it provides a simple means of demonstrating phosphorescence phenomena and identifying substances in chromatographic separations without resorting to oxygen exclusion or cryoscopic techniques. Combined with quantitative spectrophosphorimetry it yields quite well-resolved phosphorescent spectra, suitable for further product identification or the study of triplet states. Thus, for a number of the molecules we have investigated we have been able to approximate 0,0 peaks and thus determine separation of singlet and triplet energy levels, Table III. As might be anticipated, species showing small separations such as Eosin Y exhibit E-type delayed fluorescence as well as phosphorescence,[9] Figure 3, so our technique may be used as well to examine this phenomenon which is not accessi-

(7) Similar insensitivity of phosphorescence to oxygen in solid solutions at normal temperatures have been observed. (a) P. Pringsheim and H. Vogels, *J. Chim. Phys.*, **33**, 345 (1936), noted O_2 insensitive delayed fluorescences in dyes dissolved in gelatine, sugar glasses, and cellophane but found color differences indicative of phosphorescence quenching by O_2. (b) G. Oster and G. K. Oster in "Luminescence of Organic and Inorganic Materials," H. P. Kallmann and G. M. Spruch, Ed., Wiley, New York, N. Y., p 186, report that polymer molecules are effective in protecting included dyes from oxygen quenching. Our thanks to a referee for pointing out these references.

(8) G. Jackson and G. Porter, *Proc. Roy. Soc., Ser. A*, **260**, 13 (1961).

(9) C. A. Parker and C. G. Hatchard, *Trans. Faraday Soc.*, **57**, 1894 (1961).

TABLE I: Ambient Temperature Phosphorescence Spectra on Paper Support[a]

Compound	λ excitation, nm[b]	λ emission, nm[b]	Relative intensity
	Carboxylic Acids		
2-Biphenylcarboxylic acid	(280)	485	20
2-Biphenylcarboxylic acid[c]	(300)	445	65
		475	80
		490–515	50
	280	(475)	95
4-Biphenylcarboxylic acid	(290)	450	75
		482	84
		500–515	56–53
	285	(480)	84
4-Biphenylcarboxylic acid[c]	(300)	350	08
		412	15
		488	79
		523	70
		535–575	50–25
	295	(520)	69
Diphenic acid	(275)	490	80
	278	(490)	75
	320–375		30–10
Naphthalic acid	(310)	497	80
		535	80
		570–585	39–34
	245	(535)	15
	309		84
Naphthalic acid[c]	(300)	490	100
		530	89
		575	35
		610–640	9–5
	310	(530)	87
1-Naphthoic acid	(300)	500	68
		530	74
		560–575	40–37
	230–250	(530)	10
	300		69
2-Naphthoic acid	(290)	490	69
		525	75
		550–570	38–34
	290	(525)	69
	325		48
	(325)	490	42
		523	45
	Sulfonic Acids		
1-Aminonaphthalene-4-sulfonic acid	(345)	505–555	90
	260	(535)	19
	350		86
Naphthalene-β-sulfonic acid	(310)	495–510	69
		525	78
	235	(525)	23
	290		70
	~320		37
1-Naphthol-5-sulfonate sodium salt	(385)	450–750	100
	255	(575)	19
	372		96
2-Naphthol-6-sulfonate sodium salt[d]	(350)	533	92
	260	(535)	19
	315		64
	367		99
2-Naphthol-6-sulfonate sodium salt[e]	(300)	525	87
	240	(520)	18
	295		72
	330		78
2-Naphthol-7-sulfonate sodium salt[d]	(360)	555	97
	298	555	39
	368		97
2-Naphthol-7-sulfonate sodium salt[e]	(335)	530	88
	235	(530)	19
	277		37
	335		80
	Miscellaneous		
Auramine 0[f]	(460)	520	85
	375	(520)	24
	460		89
Coproporphyrin III[g,h]	(410)	582	20
		625	54
		682	16
	410	(625)	55
	510		10
	545		8
Eosin Y[h]	(530)	555	89
		680	66
	495	(680)	40
	530		67
Eosin Y[c,i]	(520)	695	75
	305	(695)	15
	345		17
	500		65
Ethyl violet[j]	(590)	655	27
	300	(655)	5
	590		25

[a] All samples prepared 3–5 m*M* in 1 *M* NaOH and dried on Whatman No. 1 paper unless otherwise noted. [b] Numbers in parentheses indicate fixed wavelengths for scanning of spectrum presented in other column. [c] Frozen solution, 77°K. [d] Sodium sulfonate in 1 *M* NaOH to yield disodium salt. [e] Sodium sulfonate in water to yield monosodium salt. [f] 0.4 m*M* hydrochloride in water. [g] ~0.3 m*M* in pH 8 buffer. [h] 0.5 m*M* in pH 8 phosphate buffer. [i] 0.1 m*M* in pH 9 borate buffer. [j] 0.4 m*M* chloride in water. [k] The emissions at 625 and 682 nm correspond to fluorescences reported in pH 7.4 aqueous buffer at 611 and ~672 nm (P. Sayer, private communication).

TABLE II: Phosphorescence Lifetimes for Sodium Salts of Organic Acids on Paper Supports at 298°

Compound	*T*, msec
2-Naphthoic acid	740
4-Biphenylcarbcxylic acid	710
2-Naphthalenesulfonic acid	655
1-Naphthoic acid	469
Naphthalic acid	356
2-Naphthol-6-sulfonic acid	177
Diphenic acid	80

ble at low temperatures. Delayed fluorescences are also noted in Auramine 0 and Ethyl Violet.[10]

Finally, the variety of compounds listed in Table I, including porphyrins, suggests that the technique should have application for the qualitative analysis and identification of numerous types of ionic organic molecules including many of biological interest.

(10) The S_1 0,0 of Auramine 0, for example, lies at approximately 505 nm, thus a 9–12-kcal activation energy would load us to expect the T_1 0,0 band somewhere between 600 and 650 nm; no such band is observed. The failure to observe these bands, however, does not rule out E-type delayed fluorescence.

TABLE III: Singlet–Triplet Energy Splittings from Extrapolated (0,0) Bands of Sodium Salts

Compound	λ_2, nm	λ_1, nm	ΔE, kcal/mol	Conditions
4-Biphenylcarboxylic acid	336	466	23.7	77°K, frozen solution
	315	433	24.7	298°K, paper
2-Biphenylcarboxylic acid	331	431	20.0	77°K, frozen solution
	323	415	19.6	298°K, paper
Eosin Y	521	630	9.5	298°K, paper
2-Naphthol-7-sulfonate	408	489	11.6	298°K, paper, disodium salt
	356	472	19.7	monosodium salt
2-Naphthol-6-sulfonate	404	480	11.2	298°K, paper, disodium salt
	355	464	18.9	monosodium salt

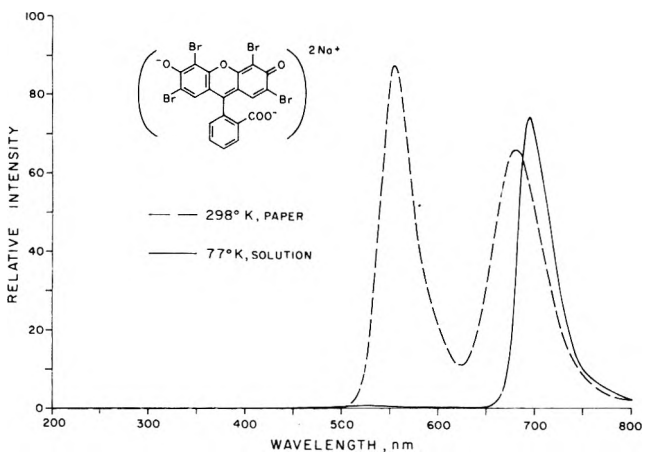

Figure 3. Emission spectra of 0.5 m*M* Eosin Y in phosphate buffer, adsorbed on paper at room temperature, and in frozen solution at 77°K. The band at 555 nm is the classic E-type delayed fluorescence.

Experimental Section

Qualitative. Solutions of compounds to be tested in any convenient solvent (usually tetrachloroethylene) were spotted onto circles of Whatman No. 1 filter paper. The papers were then rigorously dried either by means of a heat gun or more gently with an infrared lamp (I^2R Hotspot). The spots were then examined with both the short- and long-wave tubes of a 15-W Mineralight for fluorescence and phosphorescence. In general, nonionic compounds showed only fluorescence. The papers were then spotted with 1 *M* NaOH, redried, and reexamined under uv irradiation. Those samples which phosphoresced were examined quantitatively.

Quantitative. Reagent grade chemicals were in the general used as received. Solutions of the compounds were made up to be approximately 4×10^{-3} *M* in 1 *M* aqueous sodium hydroxide. Whatman No. 1 filter paper, cut in 5.3 × 0.5 cm strips, was then saturated with the solution and slowly dried under an infrared lamp. Solutions of commercially available sodium naphthol sulfonates were made both in water and in 1 *M* NaOH to observe singly and doubly ionized species.

Excitation and emission spectra were obtained on an Aminco-Bowman spectrophotofluorometer equipped with accessory phosphoroscope, ellipsoidal condensing assembly, Hanovia 901-C-11 xenon lamp, and an R 446 S flat response photomultiplier. Paper strips were placed in the standard quartz dewar used for low-temperature phosphorescence measurements. The dewar was rotated to the optimum angle for maximum response, slits were chosen for maximum sensitivity and both emission and excitation spectra recorded. Frozen aqueous solutions were measured in the same instrument with the dewar filled with liquid nitrogen and dry air being passed over the window. The phosphorescence blank from paper treated only with NaOH and dried was negligible at 298°K, although substantial at 77°K.

Phosphorescence lifetimes were measured by flash photolysis using the apparatus described by Hadley.[11] Rate constants and lifetimes were determined from first-order rectified least-squares plots.

Acknowledgments. This work was supported by a grant from the National Science Foundation. We wish to express our thanks to Professor Art Lepley of the Department of Chemistry, Marshall University, for many helpful discussions and assistance in the spectral experiments. Our thanks also go to Professor John D. Spikes of our biology department for the kind use of his spectrophotofluorometer and the donation of several biological samples and to Mr. Vernon Alvarez and Professor Stephen G. Hadley of this department for the flash photolysis measurements.

(11) S. G. Hadley, *J. Phys. Chem.*, **74**, 3551 (1970).

Crystal Structure of an Acetylene Sorption Complex of Zeolite 4A

Allen A. Amaro and Karl Seff*

Chemistry Department, University of Hawaii, Honolulu, Hawaii 96822 *(Received August 24, 1972)*

The crystal structure of an acetylene sorption complex of zeolite A has been determined by single-crystal X-ray techniques. Fully vacuum-dehydrated zeolite A of approximate composition $Na_{12}Al_{12}Si_{12}O_{48}$ per unit cell was exposed to dry acetylene for 24 hr at a pressure of 650 Torr. The cubic space group $Pm3m$ was used with $a = 12.260(5)$ Å. Approximately six C_2H_2 molecules are absorbed per unit cell and occupy two or perhaps three kinds of sites in the large cavity. Three C_2H_2 molecules participate in a symmetric approach to threefold axis sodium ions; each carbon atom in each of these three molecules is 2.8(1) Å from a sodium ion. Two other carbon positions have been determined and refined, but the assignment of molecular positions to these is uncertain. One C_2H_2 appears to be symmetrically associated with the twofold axis sodium ion at distances of 2.6(1) Å and simultaneously asymmetrically associated with a sodium ion in the eight-oxygen window with distances of 2.6(1) and 3.0(1) Å. Crystallographically refined occupancy parameters indicate that the remaining two C_2H_2 molecules are (nearly) equivalent to this one except that each associates with only one ion, one of the remaining two sodium ions in the eight-oxygen windows. However, a chemically more reasonable distribution of occupancy parameters for these two carbon positions would allow each of these latter two C_2H_2 molecules to be symmetrically associated (2.6(1) Å) with an eight-window sodium ion. In each case, the sorption mechanism involves an ion to induced dipole interaction between Na^+ and the laterally polarizable π system of acetylene.

Introduction

Zeolites find extensive commercial application as catalysts for hydrocarbon cracking or for specific high yield rearrangement reactions involving hydrocarbons and other organic molecules.[1] In order to determine the sorption sites (these may be catalytic sites as well in some cases) selected by a hydrocarbon in a zeolite, this structure was studied. Because unsaturated hydrocarbons are sorbed more tenaciously than saturated ones, and because the carbon atoms in acetylene were likely to be equivalent in the complex, C_2H_2 was selected as the sorbate material. Previous sorption measurements[2,3] indicated that approximately six C_2H_2 molecules are sorbed per unit cell in zeolite 4A; the effect of less absorbent binder materials contained in the commercial pellets was taken into account.

The mechanism for sorption could involve a direct ion to induced dipole interaction[4] between the cations and the polarizable π systems in these hydrocarbons as spectroscopic[5-7] and nuclear magnetic resonance[8] evidence indicates, and/or weak hydrogen bonding between the very weakly acidic protons, whose acidity might be enhanced by the former interaction, and the negatively charged zeolite framework oxygen atoms. Specific results[9] for acetylene on variously exchanged zeolite A samples support the former mechanism for zeolite 4A. Ethylene sorbed onto variously exchanged samples[10] was found to be freely rotating except in the case of Ag(I)-exchanged zeolite.[11] Further work on alkene sorption[12,13] and subsequent catalytic oxidation[14] has been reported. In partially Co(II)- and Ni(II)-exchanged zeolite A, olefins and cyclopropane have been found[15-19] to change the symmetry of these transition metal ions to C_{3v} upon sorption.

In all of these studies, involving a wide range of systems, problems, and physical methods, specific structural information has not been available; accordingly this work was undertaken.

Experimental Section

Single crystals of zeolite A were prepared by a modification of Charnell's[20] method, to include a second crystallization using seed crystals from the first preparation, and have the approximate stoichiometry of $Na_{12}Al_{12}Si_{12}O_{48}$ per unit cell in the dehydrated form.[21] A relatively large single crystal, a cube approximately 75 μ on an edge, was dehydrated for 48 hr at 350° and a pressure of 3×10^{-6} Torr. The crystal was then exposed to 650 Torr of zeolitically dried 99.6% pure acetylene (from Matheson Co.) for 20 hr. Concurrent measurements of C_2H_2 uptake by 0.25-inch spherical pellets of Linde 4A indicated that the sorption was essentially complete in 15 hr. The sample in its fine Pyrex capillary tube was then sealed off from the vacuum system at 650 Torr by torch and mounted onto a goniometer head for X-ray investigation.

(1) R. F. Gould, *Advan. Chem. Ser.*, **No. 102**, 1 (1971).
(2) C. K. Hersh, "Molecular Sieves," Reinhold, New York, N. Y., 1961.
(3) "Isotherm Data Sheet No. 43," Linde Division, Union Carbide Corp., New York, N. Y.
(4) J. W. Ward, *Advan. Chem. Ser.*, **No. 101**, 399 (1971).
(5) M. R. Basila, *Appl. Spectrosc. Rev.*, **1**, 289 (1968).
(6) D. J. C. Yates, *Catal. Rev.*, **2**, 113 (1968).
(7) D. J. C. Yates, "Molecular Sieves," Society of Chemical Industry, London, 1968, p 334.
(8) G. M. Muha and D. J. C. Yates, *J. Chem. Phys.*, **49**, 5073 (1968).
(9) G. V. Tsitsishvili, G. D. Bagratishvili, and N. I. Oniashvili, *Zh. Fiz. Khim.*, **43**, 950 (1969).
(10) J. L. Carter, D. J. C. Yates, P. J. Lucchesi, J. J. Elliott, and V. Kevorkian, *J. Phys. Chem.*, **70**, 1126 (1966).
(11) D. J. C. Yates, *J. Phys. Chem.*, **70**, 3693 (1966).
(12) P. L. Corio and S. Shih, *J. Phys. Chem.*, **75**, 3475 (1971).
(13) J. F. Tempere, J. Kermarec, and B. Imelik, *C. R. Acad. Sci.*, **77**, 269 (1969).
(14) I. Mochida, S. Hayata, A. Kato, and T. Seiyama, *J. Catal.*, **23**, 31 (1971).
(15) K. Klier, *Advan. Chem. Ser.*, **No. 101**, 480 (1971).
(16) K. Klier, *J. Amer. Chem. Soc.*, **91**, 5392 (1969).
(17) K. Klier and M. Ralek, *J. Phys. Chem. Solids*, **29**, 951 (1968).
(18) R. Polak and V. Cerny, *J. Phys. Chem. Solids*, **29**, 945 (1968).
(19) R. Polak and K. Klier, *J. Phys. Chem. Solids*, **30**, 2231 (1969).
(20) J. F. Charnell, *J. Cryst. Growth*, **8**, 291 (1971).
(21) R. Y. Yanagida, A. A. Amaro, and K. Seff, *J. Phys. Chem.*, **77**, 805 (1973).

A Syntex four-circle computer-controlled diffractometer with graphite-monochromatized Mo $K\alpha$ radiation ($K\alpha_1$, λ 0.70926 Å; $K\alpha_2$, λ 0.71354 Å) and a pulse-height analyzer was used throughout for preliminary experiments and for the collection of diffraction intensities. The cubic cell constant (12.260(5) Å at 20°) was determined by a least-squares refinement of 11 intense reflections with 2θ values up to 23.6°. The space group $Pm3m$ (no systematic absences) was used instead of $Fm3c$ because Gramlich and Meier[22] have shown that deviations from the former space group are small, and because previous checks of Gramlich and Meier's most intense b reflections in related materials from the same crystallizations[21,23,24] indicated that they would be absent here. The θ-2θ scan technique was employed at a constant scan rate of 0.5°/min (in 2θ). The scan range varied from 2.0° at 2θ = 3° to 2.5° at 2θ = 70°. All 881 unique reciprocal lattice points for which $2\theta < 70°$ were examined. A time equal to half of the scan time for each reflection was spent counting background at each end of the scan range. Two check reflections which were measured periodically during data collection showed no significant trend in intensity.

Standard deviations were assigned according to the formula

$$\sigma(I) = [CT + 0.25(t_c/t_b)^2(B_1 + B_2) + (pI)^2]^{1/2}$$

where CT is the total integrated count obtained in a scan time of t_c, B_1 and B_2 are the background counts each obtained in time t_b, and $I = CT - 0.5(t_c/t_b)(B_1 + B_2)$. A value of 0.02 was assigned to the empirical parameter p to account for instrument instability. The net counts were then corrected for Lorentz and polarization effects. An absorption correction (μR = 0.02) was unnecessary. All 171 reflections for which the net count exceeded three times its standard deviation were used in the final cycles of least-squares refinement.

Structure Determination

Initial full-matrix least-squares refinement using the framework and the cation positions near the centers of the six- and eight-oxygen windows found for the 32 ammonia complex[23] of zeolite 4A converged quickly to an R_1 index ($R_1 = (\Sigma||F_o| - |F_c||)/\Sigma F_o$) of 0.078, using anisotropic thermal parameters for Na(1) only. The corresponding generalized weighted R_2 index ($R_2 = (\Sigma w(F_o - |F_c|)^2/\Sigma w F_o^2)^{1/2}$) was 0.080. Introducing six carbon atoms at position C(1), as suggested by a difference Fourier function, allowed R_1 and R_2 to decrease to 0.072 and 0.078, respectively. Increasing the occupancy of C(1) (although not suggested by the difference Fourier) to 12 carbon atoms caused the error indices to rise to 0.073 and 0.080 and caused its isotropic thermal parameter to diverge upward, confirming the incorrectness of this higher occupancy. Because concurrent results[21] on dehydrated zeolite 4A indicated that a third Na^+ position was present in our samples, Na(3) was introduced with an occupancy parameter of one ion per unit cell. This position behaved well in least-squares refinement, and caused R_1 to increase by 0.001 and R_2 to decrease by the same amount. Introducing three carbon atoms at C(2) caused R_1 and R_2 to decrease further to 0.064 and 0.073. Allowing Na(2) to refine anisotropically and introducing three more carbon atoms at C(3) yielded the final error indices of 0.062 and 0.071 at convergence. Calculated and observed structure factors are presented in Table I, and the final structural parameters are presented in Table II. The goodness-of-fit ($(\Sigma w(F_o - |F_c|)^2/(m - s))^{1/2}$) is 0.97; m is the number of observations (171), and s (28) is the total number of independent parameters. As was the case for dehydrated zeolite 4A,[21] structural models involving only 11 sodium ions always demonstrated R values greater than or equal to that of the 12 Na^+ structure.

TABLE I: Observed and Calculated Structure Factors[a]

H= 0, K= 0			11 719 726	16 492 433	5 262 193	7 443 -429	8 272 283	9 298 -298	6 570 523	8 373 355	10 347 363	11 633 656	16 355 329	6 514 -507	10 295 -271	16 348 328	1 1127 -1140	3 1263 1119	4 452 -423	5 277 -281	7 486 -487	8 303 293	10 476 -475	2 926 881	3 787 750	4 316 357	5 231 164	7 257 253	8 313 335	9 280 315	3 384 -314	7 739 723	8 302 320	9 249 254	10 346 309	6 313 -278	5 611 -595	6 623 -615	8 436 401	11 331 -346	12 254 -275
1 1284 1312	2 155 -223	3 654 645	5 1415 1335	6 1671 1695	8 834 834	9 540 648	10 1186 1223	11 1121 1164	16 580 596	H= 0, K= 1	1 1043 -1044	2 763 -787	4 516 -536	6 310 225	7 765 -759	9 242 -251	H= 0, K= 2	2 540 -546	3 345 -413	4 455 -505	5 260 -178	7 206 -208	8 266 -340	9 443 -459	10 330 -375	H= 0, K= 3	3 255 -192	5 452 -375	7 340 394	8 289 -301	9 523 -506	10 283 284	11 241 289	H= 0, K= 4	4 542 553	5 536 502	6 224 -155	7 487 -483	9 609 -606	12 352 -357	15 320 -244	H= 0, K= 5	5 1743 1735	6 609 607	7 458 -481	9 400 -382	10 472 494
H= 1, K= 0			16 492 433	H= 1, K= 1	1 1127 -1140	3 1263 1119	4 452 -423	5 277 -281	7 486 -487	8 303 293	10 476 -475	H= 1, K= 2	2 926 881	3 787 750	4 316 357	5 231 164	7 257 253	8 313 335	9 280 315	H= 1, K= 3	3 384 -314	7 739 723	8 302 320	9 249 254	10 346 309	H= 1, K= 4	5 611 -595	6 623 -615	8 436 401	11 331 -346	12 254 -275										
H= 1, K= 5			5 262 193	7 443 -429	8 272 283	9 298 -298	H= 1, K= 6	6 258 -252	7 237 -257	8 358 414	12 385 -333	H= 1, K= 7	10 312 -243	H= 1, K= 8	12 355 331	H= 2, K= 2	4 436 -472	3 663 -799	4 448 369	5 833 839	6 270 -275	8 516 -486	9 578 578	11 328 -321	H= 2, K= 3	3 1268 -1230	6 249 -266	8 679 -871	13 261 -327	14 323 -293	H= 2, K= 4	4 315 290	5 337 -308	6 247 -294	7 452 395	8 233 262	9 361 404	11 258 -251	H= 2, K= 6	6 313 -278	H= 2, K= 7	5 358 365	H= 2, K= 8	8 677 -655										
H= 2, K= 5			12 351 326	H= 3, K= 3	3 640 -873	4 580 550	6 276 305	8 1561 -1516	9 405 -413	13 397 -427	14 351 -413	H= 3, K= 4	4 680 661	5 243 -191	6 300 286	7 567 521	12 299 334	H= 3, K= 5	6 348 347	8 337 -331	9 293 -325	H= 3, K= 6	6 336 336	H= 3, K= 7	7 511 555	9 299 353	10 368 367	H= 3, K= 8	8 582 -1001	9 276 -292	13 475 -520	14 312 -430	H= 4, K= 4	4 249 321	5 711 -736	8 675 692	9 575 615	11 428 -385	H= 4, K= 5	5 417 -417	7 652 -635	H= 4, K= 6	7 440 -385	H= 4, K= 7	7 410 412										
8 333 323	H= 4, K= 10	12 251 -186	H= 4, K= 11	12 294 -206	H= 5, K= 5	5 1040 1042	6 757 778	7 541 -536	8 320 342	10 322 267	11 582 594	16 387 330	H= 5, K= 6	6 558 595	7 315 -300	11 438 482	H= 5, K= 11	11 523 494	H= 6, K= 6	6 257 174	7 339 -363	11 266 288	H= 6, K= 7	12 273 -255	H= 6, K= 11	11 358 341	H= 7, K= 7	9 308 303	H= 7, K= 8	8 477 -286	H= 8, K= 8	8 608 -605	13 366 -371	14 339 -306	H= 9, K= 9	9 340 353	H= 11, K= 11	11 368 368										

[a] The running index is l; values of h and k for each group immediately precede that group. The central column is $10F_o$; the right-hand column is $10F_c$.

Least-squares refinement of the occupancy parameters of the three carbon positions caused R_1 and R_2 to become 0.061 and 0.070, respectively, and indicated that approximately five molecules were present per unit cell, insignificantly different from the assumed value of six. In fact, a full occupancy parameter refinement for all atoms in the structure lowered R_1 and R_2 to 0.060 and 0.069, presumably an effect caused by the aluminum–silicon disorder or alternation which was not taken into account by the assumed space group; all framework atoms refined unrealistically to occupancies of 0.90. The thermal parameters of C(2) and C(3), which tended to become slightly negative, were fixed at 0.1 Å^2 in the final cycles of least-squares refinement. The inclusion of 12 hydrogen atoms in the structure factor calculation at positions (Table II) calculated assuming that the acetylene molecule is 3.32 Å in length (1.06 + 1.20 + 1.06 Å) had no effect on the final error indices.

The C(2) and C(3) positions are each 24-fold equipoints which contain three and three, or two and four atoms, respectively, to give the final error indices (R_1 = 0.062 and R_2 = 0.071). The apportioning of so few atoms among so many equipoints cannot be done unambiguously in this case. In addition, a consideration of possible chemically

(22) V. Gramlich and W. M. Meier, *Z. Kristallogr.*, **133**, 134 (1971).
(23) R. Y. Yanagida and K. Seff, *J. Phys. Chem.*, **76**, 2597 (1972).
(24) K. Seff, *J. Phys. Chem.*, **76**, 2601 (1972).

TABLE II: Positional, Thermal, and Occupancy Parameters[a]

Atom	Position	x	y	z	B, Å² or appropriate b's	Occupancy factor
(Si,Al)	24(*k*)	0	0.1829(4)	0.3704(3)	1.46(5)	1
O(1)	12(*h*)	0	0.222(1)	1/2	2.5(3)	1
O(2)	12(*i*)	0	0.291(1)	0.291(1)	2.6(3)	1
O(3)	24(*m*)	0.1129(7)	0.1129(7)	0.339(1)	3.1(2)	1
Na(1)	8(*g*)	0.2037(7)	0.2037(7)	0.2037(7)	0.0060(6)[b] 0.0056(12)	1
Na(2)	12(*i*)	0	0.430(5)	0.430(5)	0.026(12)[c] 0.013(4)	1/4
Na(3)	12(*j*)	0.270(7)	0.270(7)	1/2	3(2)	1/12
C(1)	24(*m*)	0.312(6)	0.312(6)	0.371(8)	6(3)	1/4
C(2)	24(*m*)	0.225(7)	0.476(3)	0.476(3)	0(3)	1/8
C(3)	24(*l*)	0.160(5)	0.448(6)	1/2	0(3)	1/8
H(1)[d]	48(*n*)	0.2455	0.3119	0.4375	6	1/8
H(2)[d]	48(*n*)	0.3098	0.4449	0.4870	6	1/16
H(3)[d]	48(*n*)	0.0749	0.4113	0.4686	6	1/16

[a] Standard deviations are in the units of the least significant digit given for the corresponding parameter. See Figures 1 and 2 for the identities of the atoms. [b] For Na(1), the anisotropic temperature factor = $\exp[-b_{11}(h^2 + k^2 + l^2) - b_{12}(hk + hl + kl)]$. [c] For Na(2), the anisotropic temperature factor = $\exp[-b_{11}h^2 - b_{22}(k^2 + l^2)]$. [d] Calculated positions and assigned thermal and occupancy factors are given.

reasonable solutions, especially in view of the two nonequivalent sodium ions, suggests strongly that more than these two equipoints must exist. The positions C(2) and C(3) might be averages of more general closely clumped positions; another very low occupancy equipoint might remain unlocated. Fortunately, of the several chemically plausible arrangements, all indicate the same general type of lateral approach as was indicated for the C(1)-C(1) molecule, namely, an ion to induced dipole interaction between Na^+ and the laterally polarizable π system of acetylene.

The solution most consistent with the crystallographic results involves three carbon atoms at C(2) and three at C(3). They form three equivalent molecules with a bond length of 0.92(10) Å; each of these would asymmetrically approach one of the three Na(2) ions near the center of the eight-oxygen window with carbon to Na^+ distances of 2.6(1) and 3.0(1) Å. This solution is demonstrated in Figures 1 and 2. One (or possibly two) of these three molecules probably also makes a symmetric approach to the lone Na(3) ion with distances of 2.57(8) and 2.61(8) Å.

If C(2) is discarded altogether, six carbon atoms may be placed at C(3) to form three C_2H_2 molecules, each with a bond length of 0.90 Å and each approaching a Na(2) ion symmetrically with a C(3) to Na(2) distance of 2.6 Å. For this solution, R_1 = 0.062 and R_2 = 0.073, and the x coordinate for C(3) has shifted to 0.193, the average of those for C(2) and C(3). The isotropic temperature factor for this position becomes 25 Å². Na(3), whose position indicates that it is associated with a sorbed molecule, is unaccommodated by this model.

With five atoms at C(3) and one at C(2), one C(2)-C(3) acetylene molecule can associate with Na(3) symmetrically and Na(2) asymmetrically. Two C(3)-C(3) molecules can then associate symmetrically with Na(2). The distances are as given in the above two paragraphs; this solution is a plausible composite of those two. The values of R_1 and R_2 for this model are 0.065 and 0.072, respectively.

With four atoms at C(3) and two at C(2), two solutions can be envisioned. For the first one, a C(2)-C(2) molecule must exist. Na(3) cannot be associated with an acetylene molecule, and the C_2H_2 molecules would associate in nonequivalent ways with Na(2). R_1 and R_2 are 0.062 and 0.071 for this least reasonable of these solutions.

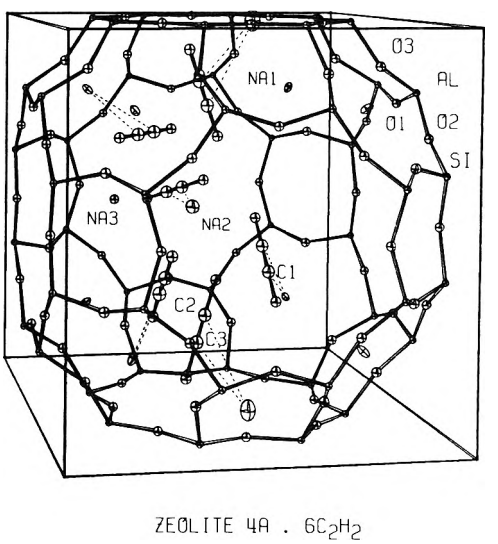

Figure 1. The unit cell (large cavity) of zeolite 4A·6C_2H_2. Sodium ions and acetylene molecules are statistically placed within their positions of partial occupancy so as to avoid unreasonably close approaches. Carbon to sodium ion approaches are shown with dashed lines. Thermal parameters of 6 Å² have been assigned to C(2) and C(3), and of 4 Å² to hydrogen atoms, for the preparation of these drawings only. Ellipsoids of 10% probability are used.

If a model with two C_2H_2 molecules symmetrically associated with Na(3) and each further associated with Na(2) is considered, in the sequence Na(2), C(2)-C(3), Na(3), C(2)-C(3), Na(2), the third C_2H_2 molecule, C(3)-C(3), could symmetrically associate with the remaining Na(2). This solution does offer the lowest R indices, as does the first, and offers an explanation for the asymmetric C(2)-C(3) approach to Na(2).

An exhausive search of the final difference Fourier function by least-squares methods failed to reveal any other positions or structural alternatives.

The standard deviation of the electron density on Fourier functions was approximately 0.1 $e^-/Å^3$, and the largest unassigned peak on the difference Fourier synthesis was 0.3 $e^-/Å^3$ in height. (No phase changes had occurred

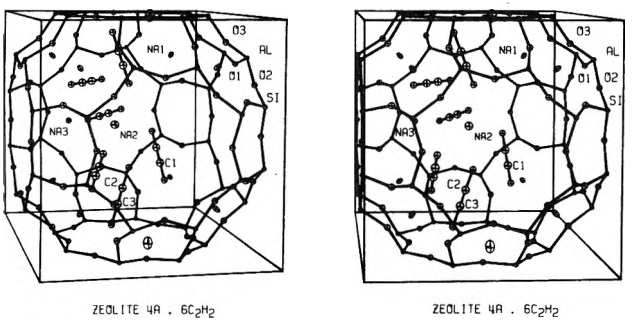

Figure 2. A stereoview[27] of the unit cell of zeolite $4A \cdot 6C_2H_2$. The comments with Figure 1 apply, except that carbon to sodium ion approaches are not shown.

since the preparation of the first difference Fourier function.) The full-matrix least-squares program used[25] minimizes $\Sigma w(\Delta|F|)^2$; the weights were the reciprocal squares of σ, the standard deviation for each observation. Atomic scattering factors[26] for Si^{2+}, $Al^{1.5+}$, Na^+, O^-, and C^0 (valence) were used. In the last cycle of least-squares refinement, all shifts were less than 0.6% of their corresponding esd's, except those involving the positional coordinates of Na(3) which were 1.4% of their esd's. The structure is shown[27] in Figures 1 and 2.

Discussion

Six acetylene molecules occupy two or more nonequivalent sorption sites in the zeolite 4A structure. Three molecules are symmetrically associated with Na(1) ions, and the remaining three are associated with the Na(3) and Na(2) ions. In each case the cation approaches an acetylene molecule equatorially, indicating that the principal interaction is between the cationic charge and the laterally polarizable π electron system of the unsaturated hydrocarbon. Significant contacts between acetylenic hydrogen atoms and framework oxygen atoms are entirely absent. Each Na(2) ion is associated with an acetylene molecule, indicating that this site is energetically more favorable than the site involving Na(1), which is partially filled since, from packing considerations, it might ideally hold eight instead of three C_2H_2 molecules. The sorption isotherm is, in fact, nonrectangular and still has a positive slope at 650 Torr, suggesting that the sorption sites are not filled by the six C_2H_2 molecules sorbed per unit cell of zeolite 4A.

It is expected that the single Na^+ ion at Na(3) has disrupted the structure to some extent. A single molecule of C_2H_2 might well be associated with Na(3) because that ion is the least stable[21] one in the structure and would accordingly tend to achieve more symmetric coordination more readily than the other sodium ions. The location of that single molecule is beyond the resolution of this investigation; however, one or two of the C_2H_2 molecules associated with Na(2) might also be associated with Na(3) as well, approaching it with distances of 2.61(8) Å to C(2) and 2.57(8) Å to C(3). Such a situation would cause the C(2) and C(3) positions reported to be averages for two nonequivalent C_2H_2 molecules.

A C_2H_2 molecule associated with Na(1) lies off the three-fold axis and occupies two of three equivalent atomic sites available near each Na(1) position. Once this is done, that Na^+ ion does not have a molecular site available for further complexation. Actually, the three atomic sorption sites associated with each Na(1) imply three molecular sites (involving six atoms) as well, so that each

TABLE III: Interatomic Distances (Å) and Angles (degrees)[a]

(Si,Al)-O(1)	1.659	(6)
(Si,Al)-O(2)	1.645	(5)
(Si,Al)-O(3)	1.674	(5)
Na(1)-O(3)	2.28	(1)
Na(1)-O(2)	2.92	(1)
Na(2)-O(2)	2.40	(9)
Na(2)-O(1)	2.69	(4)
Na(3)-O(1)	3.36	(11)
Na(3)-O(3)	3.36	(11)
O(1)-(Si,Al)-O(2)	109.3	(7)
O(1)-(Si,Al)-O(3)	111.6	(4)
O(2)-(Si,Al)-O(3)	106.2	(8)
O(3)-(Si,Al)-O(3)	111.5	(8)
(Si,Al)-O(1)-(Si,Al)	146.6	(5)
(Si,Al)-O(2)-(Si,Al)	162.0	(13)
(Si,Al)-O(3)-(Si,Al)	142.6	(8)
C(1)-C(1)	1.03	(15)
C(2)-C(3)	0.92	(10)
C(1)-Na(1)	2.78	(10)
C(2)-Na(2)	3.04	(8)
C(3)-Na(2)	2.61	(7)
C(2)-Na(3)	2.61	(8)
C(3)-Na(3)	2.57	(8)
C(2)-C(3)-Na(2)	109	(4)

[a] Standard deviations are in the units of the least significant digit given for the corresponding parameter.

atomic position reported should be the average of two close positions. This expected effect does not manifest itself strongly and would affect only the acetylenic bond length and neither the sorption site symmetry nor the sodium approach distance of this C_2H_2.

A C_2H_2 molecule associated with Na(2) is presented with a less symmetrical sorption site than one associated with Na(1) because Na(2) occupies a position of only *mm* symmetry and lies away from the center of the eight-oxygen window. While the first C_2H_2 molecule lies parallel to the window to which Na(1) is coordinated, this second C_2H_2 may not and appears to occupy a position of no molecular symmetry, even though each of its carbon atoms has been placed on a symmetry element in refinement.

The triple bond lengths found (Table III) are about 1.0 Å in length and are not to be considered significantly shorter than that usually accepted[28] (1.20 Å) for such a bond, for reasons involving already discussed approximations. The average C-Na^+ approach distances, 2.6(1) to 2.8(1) Å, are approximately the sum, 2.65 Å, of the ionic radius of Na^+ and the van der Waals radius of carbon as found in graphite (0.95 + 1.70 Å).[28] In complexes between Na^+ ions and neutral sulfur atoms, a distance equal to the corresponding sum is observed,[24] and in cyclic polyether (crown ether) complexes involving O^0 and Na^+ approaches, a distance 0.35 Å greater than such a sum is found.[29] Accordingly, the acetylene to Na^+ ap-

(25) P. K. Gantzel, R. A. Sparks, and K. N. Trueblood, UCLALS4, American Crystallographic Association Program Library (old) No. 317, modified.
(26) "International Tables for X-Ray Crystallography," Vol. III, Kynoch Press, Birmingham, England, 1962, p 202.
(27) C. K. Johnson, ORTEP, Report No. ORNL-3794, Oak Ridge National Laboratory, Oak Ridge, Tenn., 1965.
(28) L. Pauling, "The Nature of the Chemical Bond," 3rd ed, Cornell University Press, Ithaca, N. Y., 1960.
(29) M. A. Bush and M. R. Truter, *J. Chem. Soc. B*, 1440 (1971).

TABLE IV: Deviations[a] of Atoms from Planes in Å

	111	100		111	100
O(1)		0.0	Na(2)		0.0
O(2)	0.13	0.0	C(1)	3.05	
O(3)	0.0		C(2)		2.76
Na(1)	0.33		C(3)		1.96

[a] A negative deviation indicates that the atom lies on the same side of the plane as the origin.

proach distance observed here is indicative of a moderately energetic interaction.

The zeolite framework has undergone small framework distortions upon acetylene sorption, with respect to the dehydrated state,[21] which are qualitatively the same as those found for the 32 NH_3 complex[23] of zeolite 4A. The largest angular changes have been of only −4° at O(2) and O(3), and the average Si or Al to O bond has increased by 0.01 Å even though no hydrogen bonding occurs. This latter increase has been considered to be an effect[30] of hydrogen bonding in other structures. The Na(1) position has moved further into the large cavity by 0.13 Å upon partial coordination by acetylene while the Na(1)-O(3) distance has decreased slightly by 0.04 Å. Actually the Na(1) position must be the average of two positions corresponding to associated and unassociated Na^+ ions. The Na(2) to oxygen approach distances have not changed significantly. The Na(3) to O(1) and to O(3) distances have increased dramatically to 3.4 Å, 0.9 Å more than the distances found in the dehydrated structure,[21] indicating strongly that this ion participates in the complexation of an acetylene molecule. Increases in these Na(3)-O distances of 0.5 Å have been observed in the eight NH_3 and the two or three trimethylamine complexes[31] of zeolite 4A.

In a study of the adsorption of acetylene and methylated acetylenes on dried γ-alumina,[32] a sorption mechanism similar to that found in this work was suggested which involved Al^{3+} ions and dimethylacetylene. In general, however, chemisorption with the elimination of a hydrogen atom was the principal sorption process when acetylene or methylacetylene were used.

Acknowledgment. This work was supported by the U. S. Army Research Office—Durham. We are also indebted to the NSF for their assistance (Grant No. GP-18213) in the purchase of the diffractometer, and to the University of Hawaii Computing Center.

(30) G. Donnay and R. Allmann, *Amer. Mineral.*, **55**, 1003 (1970).
(31) R. Y. Yanagida, M.S. Thesis, University of Hawaii, 1973.
(32) M. M. Bhasin, C. Curran, and G. S. John, *J. Phys. Chem.*, **74**, 3973 (1970).

Ultraviolet Absorption Spectrum of Pentaerythritol Tetranitrate

P. A. Mullen* and M. K. Orloff

Chemical Research Division, American Cyanamid Company, Stamford, Connecticut 06904 *(Received November 27, 1972)*

Publication costs assisted by The American Cyanamid Company

The absorption spectrum of pentaerythritol tetranitrate (PETN) has been measured in acetonitrile from 3900 to 1825 Å. Absorption bands were observed at *ca.* 1935, 2600, and 2900 Å. Molecular orbital calculations were performed to facilitate assignment of these absorption bands. The following assignments were made: 1935 ($\pi \rightarrow \pi^*$ localized on the $-NO_2$ groups), 2600, and 2900 Å ($n \rightarrow \pi^*$ transitions of the $-NO_2$ groups).

The physical and chemical properties of the secondary explosive pentaerythritol tetranitrate (PETN), $C(CH_2O-NO_2)_4$, have been studied previously.[1] However, only limited spectral data are available based on work using a single crystal of PETN which did not transmit below 2800 Å.[2] In this paper an experimental and theoretical investigation of the electronic absorption spectrum of PETN is reported. Similar work on the secondary explosive hexahydro-1,3,5-trinitro-*s*-triazine has been published.[3]

A sample of PETN, available in this Laboratory as a slurry with 10% ethanol, was dried *in vacuo*. The absorption spectrum in Eastman spectrograde acetonitrile was obtained from 3900 to 2000 Å using a Cary 14R spectrophotometer and from 2250 to 1825 Å using a Jarrell-Ash vacuum scanning spectrometer. The vacuum ultraviolet instrumentation and solution cell have been described previously.[2,3] The concentrations of PETN solutions were between 10^{-2} and 10^{-4} *M*. The melting characteristics of the PETN sample were obtained using a microscope hot stage (Mettler FP-2). The sample was heated at 10°/min up to 135.0°, 1.0°/min from 135.0 to 139.5°, and at 0.2°/min from 139.5° until melt was completed. We observed three distinct particle shapes and a melting range from 139.5 to 140.4°. PETN has been reported to melt at 140–141° with the pure compound melting at 141.3°.[4]

(1) T. Urbanski, Ed., "Chemistry and Technology of Explosives," Vol. II, Pergamon Press, New York, N. Y., 1965, pp 175–185.
(2) Reference 1, p 177.
(3) M. K. Orloff, P. A. Mullen, and F. C. Rauch, *J. Phys. Chem.*, **74**, 2189 (1970).
(4) P. A. Mullen and M. K. Orloff, *J. Mol. Spectrosc.*, **30**, 140 (1969).

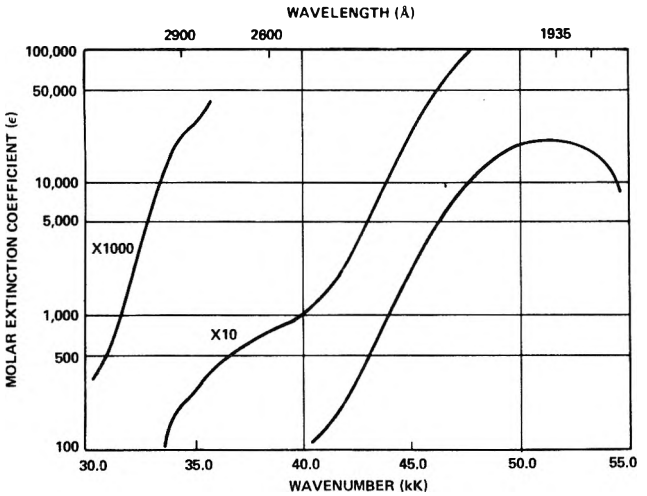

Figure 1. Absorption spectrum of PETN in acetonitrile.

The experimental solution spectrum of PETN is presented in Figure 1 as molar extinction coefficient (ϵ) in units of liters mole^{-1} cm^{-1} *vs.* wave number (kK). We observed broad bands at *ca.* 34.48 (2900 Å, ϵ 21.8), *ca.* 38.46 (2600 Å, ϵ 75.3), and *ca.* 51.68 kK (1935 Å, ϵ 20,400). Molecular orbital (MO) calculations were carried out to facilitate assignments of these bands.

MO calculations were performed on an individual ethyl nitrate moiety. This approximate approach of performing an MO calculation on part of a molecule in which the chromophoric groups are connected by a saturated linkage has been shown to be valid; *e.g.*, in the study of polynitramines.[5] The MO method employed was the CNDO/2 method of Del Bene and Jaffe[6] as developed for excited states. The input geometry used in the MO calculation to specify the location of the atoms in the $C_2H_5ONO_2$ molecule was taken from the crystal structure measurements of PETN.[7] All the valence electrons in the molecule and the 25 lowest singly excited states were included in the configuration interaction calculation of the absorption spectrum.

The MO calculation predicts two strong electronic transitions at 48.00 (2080 Å, f = 0.67) and 53.50 kK (1870 Å, f = 0.16). On the basis of the calculation the 48.00-kK transition is associated with electrons localized on the $-NO_2$ group in $C_2H_5ONO_2$. The transition at 53.50 kK is calculated to be due to a $\pi \rightarrow \pi^*$ transition of the $-NO_2$ group with a large contribution from an intramolecular charge transfer excitation involving the promotion of electrons from the C_2H_5O atoms to the $-NO_2$ group. The calculation also predicts the existence of essentially forbidden ($f = 5 \times 10^{-5}$) delocalized transitions at 23.00 (4350 Å) and 28.60 kK (3500 Å).

On the basis of the MO calculation we may consider that the broad prominent band in the spectrum of PETN at 1935 Å represents two electronic transitions. These transitions are calculated to be a $\pi \rightarrow \pi^*$ transition localized on the $-NO_2$ group (at 2080 Å) and a transition of mixed character at 1870 Å (64% $\pi \rightarrow \pi^*$ localized on the $-NO_2$ group plus 36% intramolecular charge transfer). The calculated oscillator strength for the 2080-Å transition is significantly larger than that of the 1870-Å transition. Therefore, the observed band at 1935 Å may be seen to arise primarily from $\pi \rightarrow \pi^*$ transitions localized on the $-NO_2$ groups. The position, intensity, and character of this band are in agreement with experimental and theoretical results for ethyl nitrate.[8] The weak bands observed in the spectrum of PETN at *ca.* 2900 and *ca.* 2600 Å are assigned as the $n \rightarrow \pi^*$ transitions of the $-NO_2$ groups.[9]

Acknowledgment. The authors acknowledge the encouragement and technical aid kindly provided by Dr. S. K. Deb.

(5) J. Stals, *Trans. Faraday Soc.*, **67**, 1739 (1971).
(6) J. Del Bene and H. H. Jaffe, *J. Chem. Phys.*, **48**, 4050 (1968).
(7) A. D. Booth and F. J. Llewellyn, *J. Chem. Soc.*, 837 (1947).
(8) K. Kaya, K. Kuwata, and S. Nagakura, *Bull. Chem. Soc. Jap.*, **37**, 1055 (1964).
(9) H. H. Jaffe and M. Orchin, "Theory and Applications of Ultraviolet Spectroscopy," Wiley, New York, N. Y., 1962, pp 182–184.

Ultrasonic Absorption and Rotational Phenomena in Tetraalkylammonium Ions. The Search for Appropriate Models

John Stuehr,* Terrence Noveske, and D. Fennell Evans

Department of Chemistry, Case Western Reserve University, Cleveland, Ohio 44106 *(Received July 31, 1972)*

Ultrasonic absorption data over the frequency range 15–200 MHz by the pulse method are reported for the following systems: 3,3-diethylpentane, tributylamine, and tetraalkyltin in 2-propanol, and tetrabutylammonium chloride and bromide in methanol. Based on the different behavior of the nonelectrolytes as compared to the tetraalkylammonium ions, we concluded that none of the former are appropriate models for relaxational processes observed in R_4N^+ salts in solvents such as 2-propanol and acetone.

Introduction

We have previously reported a series of ultrasonic measurements in tetraalkylammonium salts in 2-propanol.[1] The results were interpreted on the basis of a single concentration-dependent relaxation frequency which we attributed to ion association phenomena. Analogous studies in acetone[2] and nitrobenzene[3] have been carried out by Petrucci and coworkers. A series of articles by Blandamer and coworkers[4,5] however have raised the interesting possibility that other processes may account for, or contribute to, the ultrasonic relaxation spectrum of the tetraalkylammonium salts. In particular, they suggested that the rotation of the hydrocarbon side chains might be responsible for some of the absorption. One of the bases for this statement was the observation that pure 3,3-diethylpentane and solutions in hexane showed a relaxation process in the same vicinity as the tetraalkylammonium salts in other solvents.

We wish to raise the following questions: (1) is the 3,3-diethylpentane system a proper model for relaxation involving tetraalkylammonium salts, and (2) are there other ways of differentiating between the various relaxation effects? It is with these questions that this paper is concerned.

Experimental Section

Ultrasonic absorption measurements at 25° were carried out over the frequency range 15–250 MHz by a pulse send-receive apparatus described elsewhere.[1,6] Data are estimated to be accurate to ±3%. Compounds and solvents were purified by procedures described previously.[1,6]

Results

Ultrasonic absorption results are reported here for the following systems: 3,3-diethylpentane in 2-propanol; tributylamine in 2-propanol; tetrabutyl- and tetraethyltin in 2-propanol; tetrabutylammonium halides in methanol and propanol.

In virtually all instances ultrasonic absorption measurements were consistent with a single relaxation process according to the equation

$$\frac{\alpha}{f^2} = \frac{A}{1 + (f/f_r)^2} + B \qquad (1)$$

where f_r is the relaxation frequency ($= 1/(2\pi\tau)$, B is the "background" absorption at high frequencies, and A is the relaxation amplitude given by

$$A = \frac{2\pi^2 v}{RT}\Gamma\left(\Delta V^\circ - \frac{\alpha_{th}}{\rho c_p}\Delta H^\circ\right)^2 \qquad (2)$$

where ΔV° and ΔH° are the indicated volume and enthalpy changes and ρ, c_P, and α_{th} are the density, specific heat, and thermal coefficient of expansion, respectively. The quantity Γ is a concentration-dependent function, and τ is the relaxation time.

Since we are trying to distinguish between relaxation phenomena due to internal effects (internal rotation, configurational change, etc.) and due to association phenomena (*e.g.*, association), it may be desirable to reiterate the predicted behavior of the relaxation frequency and the ultrasonic amplitude A. For any *intramolecular* process, the relaxation frequency, in a given solvent, will be independent of concentration, and the relaxation amplitude will increase linearly with total solute concentration C^0. For an *intermolecular* process, on the other hand, the relaxation time will increase with total concentration, and the amplitude will increase less than linearly with C^0.

Figure 1 shows the absorption in 0.5 and 1 M 3,3-diethylpentane in 2-propanol. The relaxation frequency is 25 MHz for both solutions and the amplitudes are 60 and 120 $\times 10^{-17}$ sec^2 cm^{-1} for the two concentrations. That is, within experimental error the relaxation frequency is constant and the excess amplitude (with respect to the solvent absorption) is proportional to concentration. As a consequence, it is very likely that the relaxation process in this solute is due to some type of isomerism as suggested by Blandamer, *et al.*[4] They reported at 25° f_r = 43 MHz for pure diethylpentane, and f_r = 53 MHz for a 1 M solution in hexane. The true relaxation frequency however may be considerably lower since their lowest point was at 25 MHz and the absorption was changing rapidly at that frequency. Another feature of this system is that the high-frequency absorption (B), even at concentrations as high as 1 M, approaches the pure solvent value. We conclude that if diethylpentane is an appropriate model for tetraalkylammonium ions, then we must indeed worry about

(1) T. Noveske, J. Stuehr, and D. F. Evans, *J. Solution Chem.*, **1**, 93 (1972).
(2) G. S. Darbari and S. Petrucci, *J. Phys. Chem.*, **74**, 268 (1970).
(3) S. Petrucci and M. Battistini, *J. Phys. Chem.*, **71**, 1181 (1967).
(4) M. J. Blandamer, M. J. Foster, N. J. Hidden, and M. C. R. Symons, *J. Phys. Chem.*, **72**, 2268 (1968).
(5) M. J. Blandamer, M. J. Foster, N. J. Hidden, and M. C. R. Symons, *Trans. Faraday Soc.*, **64**, 3247 (1968).
(6) For further details see T. Noveske, Ph.D. Thesis, Case Western Reserve University, 1971.

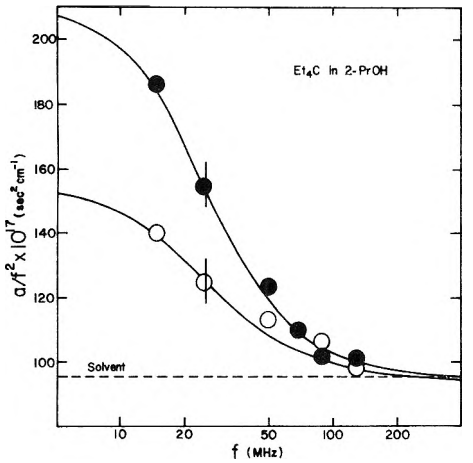

Figure 1. α/f^2 *vs.* frequency for 0.5 and 1 *M* 3,3-diethylpentane in 2-propanol. The location of the relaxation frequency is indicated by the vertical line.

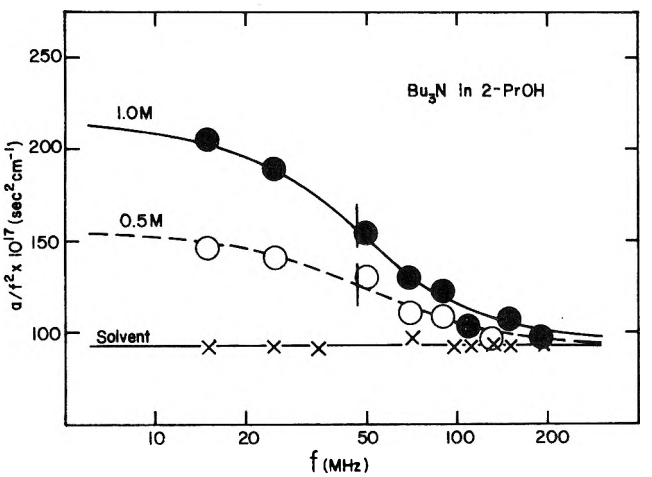

Figure 2. α/f^2 *vs.* frequency for 0.5 and 1 *M* tributylamine in 2-propanol.

rotational phenomena in alcohol and aqueous solutions of the latter.

Figure 2 shows the results of absorption measurements in 0.5 and 1.0 *M* tributylamine in 2-propanol. Once more the relaxation frequency is constant (47 MHz) and the excess amplitude proportional to C^0 (60 and 120 $\times$ 10^{-17} sec^2 cm^{-1}, respectively). In fact, the absorption profile in this system is remarkably similar to that of diethylpentane, except that the relaxation frequency is shifted to a slightly higher frequency. In this system, however, there are two intramolecular processes which could in principle generate a relaxation process: rotation of the butyl groups, or inversion of structure analogous to that in ammonia. Since the two inversion structures are isoenergetic and isochoric, there will be no way for an ultrasonic wave to couple to it eq 2, and so the ultrasonic amplitude would be zero. To test the possibility that an acid–base reaction involving traces of water in the solvent might account for the relaxation, we added several per cent of water incrementally to the Bu_3N–2-propanol system. No changes in the absorption were found. It would seem therefore that in this system as well as in diethylpentane the cause of the relaxation is associated with the butyl groups.

We next present data for tetrabutyl- and tetraethyltin in 2-propanol (Figure 3). These compounds would presumably be analogous to the corresponding tetraalkyl cations. For both concentrations of Bu_4Sn the total measured absorption is indistinguishable from that of the solvent alone over the entire frequency range investigated. There are only two explanations for this result: (1) any possible rotational process has a very low amplitude, presumably because the relaxation time is much shorter (see eq 2), or (2) the relaxation frequency has shifted in this system to much lower frequencies, *i.e.*, it is slower in this system than in diethylpentane. For no observable absorption to be present it would be necessary for the relaxation frequency to *decrease* by a factor of at least 5, or to *increase* by at least tenfold, all other factors remaining the same. The same frequency-independent absorption is observed in Et_4Sn, except that the absorption is discernibly less than that of the solvent. It is more likely that the relaxation frequency *increases* in these compounds, due to the fact that the alkyl groups interfere with each other less as a result of the larger size of the tin atom.

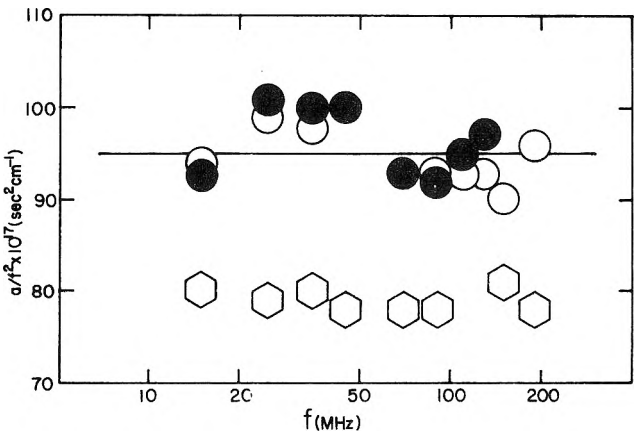

Figure 3. α/f^2 *vs.* frequency for tetrabutyltin (○ = 0.3 *M*, ● = 1.0 *M*) and 1 *M* tetraethyltin (⬡) in 2-propanol. The horizontal line is that for the pure solvent.

In summary, a variety of behavior is observed for these hydrocarbons, amines, and alkyltin compounds. Any of these compounds can be viewed, in one way or another, as appropriate models for the tetraalkylammonium ions. The fact however that the "similar compounds" behave quite differently challenges the whole concept of analogs or models for the tetraalkylammonium salts. The reason is that any process present in the models might have shifted out of the ultrasonic range investigated in the corresponding tetraalkylammonium salt, and *vice versa*. This requires that any mechanism proposed for solutions of the Alk_4N^+ salts must be deduced from data in the system itself.

We now turn our attention to the tetraalkylammonium salts themselves, first in solvents in which the absorption profile bears a strong resemblance to the hydrocarbon systems discussed earlier. Figure 4 shows the ultrasonic absorption spectrum in Bu_4NBr in 2-propanol. The data are consistent with a relaxation frequency in the vicinity of 40 MHz. The relaxational amplitude (A in eq 2) increases with total concentration, but not linearly. In addition the relaxation frequency is clearly concentration dependent. This is what would be predicted for an association mechanism; these compounds are in fact significantly associated[7] in 2-propanol.

(7) M. A. Matesich, J. A. Nadas, and D. F. Evans, *J. Phys. Chem.*, **74**, 4368 (1970).

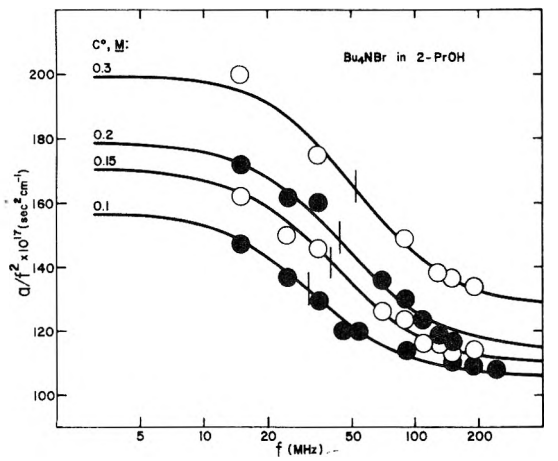

Figure 4. α/f^2 *vs.* frequency for various concentrations of Bu_4NBr in 2-propanol. The relaxation frequencies are indicated by vertical lines.

Let us examine now the frequency profile of Bu_4NCl and Bu_4NBr in *methanol,* in which the association is quite small ($K \cong 5$)[8] (Figure 5). In both systems at the relatively high total concentration of 0.3 M (C^0), the absorption is only about 8 units above the solvent value, and is constant.[9]

The excess absorption observed in methanol solutions is probably due to an association mechanism, but with a relaxation frequency above 200 MHz. From the known diffusion coefficients and equilibrium constants,[8] one can compute from equations in ref 1 that the relaxation frequency will be on the order of 5000 MHz,accompanied by a small amplitude. If the absorption were due to a rotational process, it is difficult to understand why it should be so much more rapid in methanol as compared to the propanols.[10] The lack of any evidence for rotational phenomena involving the tetraalkylammonium ions in methyl alcohol, coupled with the concentration-dependent frequency in the propyl alcohols, plus the behavior observed

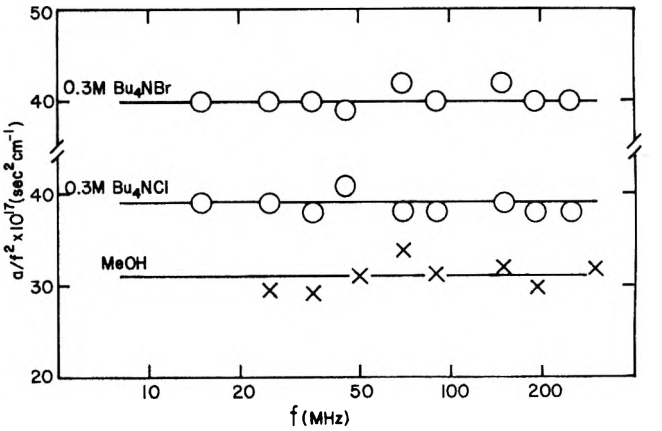

Figure 5. α/f^2 *vs.* frequency for 0.3 M Bu_4NCl and Bu_4NBr in methyl alcohol.

in the neutral compounds, leads us to the following conclusions: (1) the primary mechanism responsible for the relaxations in the tetraalkylammonium salts is ion association, and (2) the use of compounds analogous to the R_4N^+ ions as models for rotational processes is misleading.

Acknowledgments. We thank Professor E. B. Yeager for making available the ultrasonic instrumentation used in this study. This work was supported by the Department of the Interior, Office of Saline Water, in the form of research grants to D. F. E. (No. 14-1281) and J. E. S. (No. 14-1273) and by the National Institutes of Health in the form of a research grant to J. E. S. (No. GM 13116).

(8) R. L. Kay, C. Zawoyski, and D. F. Evans, *J. Phys. Chem.*, **69**, 4208 (1965).
(9) When the concentration of Bu_4NBr is increased to 1 M, evidence for a relaxation process is apparent. This is similar to the behavior of these salts in a wide variety of solvents, including water, and may be attributed to association phenomena.
(10) A possible explanation might be that the energy barrier to rotation is diffusional. Since the viscosity of methanol is less than that of propanol, a higher relaxation frequency would then be expected.

A Study of the Validity of the Ilkovic and Other Standard Direct and Alternating Current Polarographic Equations at Short Drop Time

A. M. Bond* and R. J. O'Halloran

Department of Inorganic Chemistry, University of Melbourne, Parkville 3052, Victoria, Australia *(Received September 18, 1972)*

Both short drop time ac and dc polarography, which permit fast scan rates and increase the polarographic time scale several orders of magnitude, are potentially extremely valuable techniques in many kinetic, analytical, and electrochemical investigations. Early work utilizing short drop times indicated that standard polarographic equations were inapplicable to such measurements, and the use of drop times below 2 sec has been generally discouraged in the literature. Recently, however, data have been obtained in the millisecond drop time region which indicated that much of the standard theory can in fact apply in this drop time range. The present study reports an investigation of short drop time polarography in an endeavor to resolve apparent anomalies currently existing in the literature, and to overcome possible unjustified discrimination preventing the much wider use of a valuable technique of polarography. Results demonstrate conclusively that the presence of the short drop time itself does not lead to a breakdown of conditions for which standard ac and dc theories were derived. If short controlled drop times are obtained by mechanically knocking the capillary then the short drop time experiment is found to be critically dependent on the theory applicable to the natural drop, from which the short controlled drop is derived. In obtaining the short controlled drop time, the flow rate of mercury is essentially unaltered. On the other hand, if short drop times are obtained by gravity control, it is confirmed that the standard theory no longer applies, because the flow rate of mercury becomes too large, and it would appear that it is variations in this parameter, rather than the drop time which has caused many of the difficulties encountered in the past.

Polarography, the measurement, interpretation, and use of current-voltage curves at a dropping mercury electrode, DME, has been widely used in many branches of chemistry for over 50 years. Workers interested in fundamental electrochemistry, analytical chemistry, kinetics, and a wide spectrum of physical, inorganic, and organic areas frequently have occasion to use the techniques.

The fundamental theories and equations in dc polarography have been well established now for several decades.[1-3] The theory for diffusion-controlled limiting currents was first solved successfully in 1934 by Ilkovic,[1-5] and the mathematical formulation describing a reversible polarographic wave in 1935 by Heyrovsky and Ilkovic.[1-3,6] The validity of these equations, particularly the Ilkovic equation, and modifications to this theory have come under scrutiny in many publications as summarized in ref 2 and 3.

Of particular relevance to this paper is the work of Maas[7] and others.[8,9] The Ilkovic equation predicts a linear dependence of the limiting or diffusion current on concentration. These authors have reported that the limiting current relationships do not hold exactly with short drop times. This work has led many authors of reviews and textbooks to recommend with reasons why polarographic techniques should only be undertaken at long drop times. Heyrovsky and Kuta, for example, report,[10] "the drop time should not be less than 2 sec, because under these conditions whirling occurs and destroys the diffusion layer; the currents are increased. The most suitable drop time is from 3 to 5 sec." Meites in his textbook[11] also reports in the same vein as do Kolthoff and Lingane[12] in their standard reference book.

Recently, however, Cover and Connery,[13] using drop times down to the millisecond region, obtained with a vibrating DME, have found close correlations to much of the existing theory and they specifically comment that their data do not show the sharp increase in diffusion current constant found by other workers with drop times below 2 sec. They suggest that this may result in part from their lack of data in the 0.01-1.0-sec drop time range, although they note that other data[14] in this range also conform to existing theory, as has now been verified elsewhere.[15] They alternatively propose "perhaps the convection due to electrode vibration at the vibrating DME is sufficient to render negligible the stirring effect due to rapid drop fall."

At present, therefore, an apparent anomaly exists, and the widespread use of very short drop time polarography has undoubtedly been hindered by the uncertainty of the correct theoretical expressions to be used. Importantly doubts persist as to whether linear limiting current *vs.*

(1) I. M. Kolthoff and J. J. Lingane, "Polarography," Vols. I and II, 2nd ed, Interscience, New York, N. Y., 1952.
(2) J. Heyrovsky and J. Kuta, "Principles of Polarography," Academic Press, New York, N. Y., 1966.
(3) L. Meites, "Polarographic Techniques," 1st ed, Interscience, New York, N. Y., 1955; 2nd ed, 1965.
(4) D. Ilkovic, *Collect. Czech. Chem. Commun.*, **6**, 498 (1934).
(5) D. Ilkovic, *J. Chem. Phys.*, **35**, 129 (1938).
(6) J. Heyrovsky and D. Ilkovic, *Collect. Czech. Chem. Commun.*, **7**, 198 (1935).
(7) J. Maas, *Collect. Czech. Chem. Commun.*, **10**, 42 (1938).
(8) J. J. Lingane and B. A. Leveridge, *J. Amer. Chem. Soc.*, **66**, 1425 (1944).
(9) F. Buckley and J. K. Taylor, *J. Res. Nat. Bur. Stand. U. S.*, **34**, 97 (1945).
(10) Reference 2, p 85.
(11) Reference 3, pp 111-125 (2nd ed); p 47 (1st ed).
(12) Reference 1, Vol. I, pp 63-98.
(13) R. E. Cover and J. G. Connery, *Anal. Chem.*, **41**, 1797 (1969).
(14) D. Wolf, *J. Electroanal. Chem.*, **5**, 186 (1963).
(15) A. M. Bond, *J. Electrochem. Soc.*, **118**, 1588 (1971), and references cited therein.

concentration relationships exist. The use of short drop times permit very rapid data acquisition in analytical applications and from the kinetic point of view is invaluable in that the usual time scale of polarography is restricted to the 2–8-sec region. However, if Cover and Connery's data are valid, this time scale could be extended to three or four orders of magnitude which would be an invaluable aid in kinetic studies. Indeed, if it can be established conclusively under what conditions the relatively simple theory is valid at short drop times, and the apparent anomaly in the literature can be satisfactorily resolved so as to remove any uncertainty in the minds of users of polarographic techniques, then short drop time polarography could advantageously replace the conventionally recommended 2–5-sec drop time polarography, in many situations.[15-20]

In addition to using short drop times with dc polarography, other polarographic techniques can gain substantially from using this modification. Derivative dc polarography[20] and ac polarography[15] are two examples which have been discussed. In particular, with ac polarography, every aspect of the experiment seems to be improved the shorter the drop time.[18,21,22] Zatka[23] has commented that the widespread use of short drop time ac polarography became possible in the early 1960's when a commercially available unit was made available. However, as he states, the first publication was not forthcoming until 1969. These authors believe that a significant reason for this is the doubts held about short drop time techniques arising from the early dc work being extended to ac polarography. Now that the theory for ac polarography has been satisfactorily solved,[24-27] it is possible to test the validity of ac polarographic equations as well as the dc ones over a wide range of drop times and conditions.

The purpose of this paper is therefore to report a study of short drop time dc and ac polarography obtained under all possible conditions, in an endeavor to resolve apparent literature anomalies with respect to the validity of the well-established equations. In this manner it is hoped to prevent any possible unjustified discrimination against the use of potentially extremely valuable techniques.

Experimental Section

Reagents. All chemicals used were of reagent grade purity. Bismuth(III) was added as the nitrate salt and cadmium(II) as its carbonate. The supporting electrolyte used was 1 *M* hydrochloric acid and unless otherwise stated the concentration of cadmium used was 1.8×10^{-4} *M* and that of bismuth 8.1×10^{-4} *M*.

All solutions were thermostated at 25.0 ± 0.1° and degassed with argon.

Instrumentation. All polarograms were recorded with PAR electrochemistry system, Model 170 (Princeton Applied Research Corporation, N. J.). A three-electrode system was used for both ac and dc polarography, with Ag|Ag (5 *M* NaCl) used as the reference electrode and tungsten wire as the third or auxiliary electrode.

The flow rate of mercury was evaluated by weighing the mercury deposited in the cell after 20 min. The drop time was calculated from measurement of current-time curves.

Phase sensitive detection was used in all ac work. Maximum currents were recorded with both ac and dc polarography, and all currents reported therefore refer to currents obtained at the end of the drop life. Further details of experimental arrangements are given at appropriate places in the text.

Results and Discussion

Rapidly Dropping Mercury Electrodes and Theory. Previous work has utilized many different approaches to achieving short drop times. Much of the early work varied the drop time by altering the mercury column height or constructing capillaries of varying geometry. More recently, however, the favored approach to obtaining short drop times has been through mechanically knocking the DME at selected time intervals, to give a controlled drop time shorter than that which would occur if the mercury drop were allowed to fall naturally. Thus the apparent anomalies could well arise from the different approaches to obtaining short drop times and from the fact that the experiments being conducted are not identical. Indeed Fisher, *et al.*,[20] have already commented that "The convention has somehow become established that DME's should be operated at a drop time between 2 and 6 sec; this is a misleading oversimplification. It is not the drop time alone but rather the combination of drop time and mercury flow rate that is important in the case of DME's operated with freely forming and falling drop, and in the case of DME's where drop time is properly controlled by mechanical hammering the magnitude of the flow rate is more important than the fact that the controlled drop time is <2 sec."

The approaches used to obtain short drop times, keeping the above information in mind, were as follows. (a) Increasing the mercury column height. (b) Cutting the capillary successively shorter and shorter, while maintaining a constant mercury column height. (c) Using a mechanical drop knocker consisting of a solenoid placed on top of the capillary to which a regularly pulsed voltage was applied. In this manner the capillary was periodically displaced vertically. Controlled drop times of close to 0.16, 0.20, 0.24, 0.28, and 0.32 sec were achieved in this manner using Metrohm Polarographie Stand E354. Metrohm capillaries were used with this system. (d) Using a mechanical drop knocker having a side arm attached in a horizontal fashion to the DME. This device was a PAR Model 172 drop knocker and functioned by periodically displacing the capillary sideways away from the mercury drop. The motion of the capillary on being knocked was therefore horizontal, in contrast to the Metrohm drop knocker. Controlled drop times of 5, 2, 1, and 0.5 sec were obtained in this manner. The capillary for this work was constructed from Marine Barometer tubing. (e) Combinations of methods a, b, c, and d.

Methods a and b shall be referred to as gravity-controlled short drop times and c and d as controlled short

(16) R. E. Cover and J. G. Connery, *Anal. Chem.*, **41**, 918 (1969).
(17) J. G. Connery and R. E. Cover, *Anal. Chem.*, **41**, 1191 (1969).
(18) A. M. Bond and D. R. Canterford, *Anal. Chem.*, **44**, 721 (1972).
(19) D. R. Canterford, A. S. Buchanan, and A. M. Bond, *Anal. Chem.*, in press.
(20) D. J. Fisher, W. L. Belew, and M. T. Kelley, *Proc. Int. Congr. Polarography, 3rd, 1964*, **1**, 89 (1964).
(21) A. M. Bond and D. R. Canterford, *Anal. Chem.*, **44**, 1803 (1972).
(22) A. M. Bond, submitted for publication.
(23) A. Zatka, *J. Electroanal. Chem.*, **27**, 164 (1970).
(24) D. E. Smith, "Electroanalytical Chemistry," Vol. I, A. J. Bard, Ed., Marcel Dekker, New York, N. Y., 1966, Chapter 1.
(25) D. E. Smith, *Anal. Chem.*, **43**, 247 (1971).
(26) D. E. Smith, "Application of Computers to Analytical Chemistry," Vol. 2, J. S. Mattson, H. B. Mark, Jr., and H. C. MacDonald, Ed., Marcel Dekker, New York, N. Y., 1972, Chapter 12.
(27) A. M. Bond, *Anal. Chem.*, **44**, 315 (1972).

drop times for the purpose of this paper. The methods used to obtain short drop times are believed to encompass most of the approaches documented in the literature, and a comparison of all five approaches should resolve any apparent anomalies.

The Ilkovic equation describing the limiting or diffusion-controlled current can be expressed as

$$i_d = kncD^{1/2}m^{2/3}t^{1/6} \quad (1)$$

where i_d is the limiting or diffusion-controlled current; n, the number of electrons ($n = 2$ for cadmium, $n = 3$ for bismuth); m, the flow rate of mercury (mg sec^{-1}); t, the drop time (sec); D, the diffusion coefficient; c, the concentration; and k, a constant. The Heyrovsky–Ilkovic equation describing the shape of a reversible dc current–voltage curve can be expressed as

$$E_{DME} = E_{1/2}{}^r + \frac{2.303RT}{nF} \log\left(\frac{i_d - i}{i}\right) \quad (2)$$

where $E_{1/2}{}^r$ is the reversible half-wave potential relative to a particular electrode and is closely related to the standard redox potential E^0.

E_{DME} is the potential of the DME, relative to a particular reference electrode and i is the current at potential E_{DME}. Other symbols are those defined above or those used conventionally.

In ac polarography, a reversible, diffusion-controlled electrode process is defined[24] by the analogous equations given below.

$$I = \frac{n^2F^2AC(\omega D)^{1/2}\Delta E}{4RT\cosh^2(j/2)} \sin\left(\omega t' + \frac{\pi}{4}\right) \quad (3)$$

where A is the electrode area; ω, the frequency; I, alternating current; ΔE, the amplitude of applied alternating potential; t', time; and $j = (nF/RT)(E_{dc} - E_{1/2}{}^r)$. Also, $A = 0.85m^{2/3}t^{2/3}$ at the end of the drop life,[2] the peak potential, E_p, is coincident with $E_{1/2}{}^r$, and the maximum value of I, the peak current, I_p, occurs when $E_{dc} = E_p = E_{1/2}{}^r$. Thus

$$I_p = \frac{k'n^2F^2m^{2/3}t^{2/3}(\omega D)^{1/2}\Delta E}{4RT} \sin\left(\omega t' + \frac{\pi}{4}\right) \quad (4)$$

where k' is a constant. The shape of the reversible diffusion-controlled ac electrode process[24] is given by eq 5 or 6, which are equivalent but rearranged forms of each other[28]

$$E_{dc} = E_{1/2}{}^r + \frac{2RT}{nF} \ln\left\{\left(\frac{I_p}{I}\right)^{1/2} \pm \left(\frac{I_p - I}{I}\right)^{1/2}\right\} \quad (5)$$

$$I = 4I_p\left[\frac{e^j}{(1 + e^j)^2}\right] \quad (6)$$

The above equations can be used conveniently to test the validity of the ac and dc theory over all drop times, using standard electrode processes that are known to comply with the theory at least in the normally recommended drop time range.

A. Short Drop Time dc Polarography

(i) Variation of Mercury Column Height. The most fundamental relationship in the Ilkovic equation reflecting diffusion control is the dependence of i_d on the capillary characteristics. That is the dependence of i_d upon the flow rate of mercury, m, the drop time, t, and the product $m^{2/3}t^{1/6}$ needs to be understood with each of the different approaches to obtaining short drop times.

Figure 1[29] shows a plot of i_d *vs.* $m^{2/3}t^{1/6}$ for an 8.1 × 10^{-4} M bismuth(III) solution in 1 M HCl. The electrode process being studied is

$$Bi(III) + 3e \rightleftharpoons Bi(amalgam) \quad (7)$$

and the $E_{1/2}$ value is −0 07 V *vs.* Ag|AgCl.

In this experiment both m and t were varied simultaneously by simply altering the mercury column height. These parameters were measured at the half-wave potential and the mercury column height was varied over the range of 40 to 57.6 cm. At 40 cm, t was 3.08 sec and m 2.34 mg sec^{-1} while the corresponding values at 57.6 cm were 2.10 sec and 3.4 mg sec^{-1}. Thus in the above experiments, both m and t were varied simultaneously, and the straight line plot, obtained over a small range of $m^{2/3}t^{1/6}$ values, shows that for this electrode process and under these conditions, the Ilkovic equation is obeyed in part at least. However, the value $i_d/m^{2/3}t^{1/6}$ is not strictly constant, as would be predicted by the Ilkovic equation. This was a general characteristic of the relatively high flow rate Metrohm capillaries used in this work and further comment on this point will be made later.

Figure 1[29] also shows the same plot for the cadmium(II) electrode process in 1 M HCl

$$Cd(II) + 2e \rightleftharpoons Cd(amalgam) \quad (8)$$

using mercury column heights from 30 ($t = 4.51$, $m = 1.64$ mg sec^{-1}) to 57.6 cm ($t = 2.18$ sec, $m = 3.49$ mg sec^{-1}). The same capillary was used as for the bismuth(III) case but m and t were measured at a different potential, corresponding to the cadmium electrode process's $E_{1/2}$ value of −0.62 V *vs.* Ag|AgCl. Again the fit to a straight line is satisfactory over a limited range of $m^{2/3}t^{1/6}$.

Figure 2[29] shows the variation of i_d *vs.* $m^{2/3}t^{1/6}$ for both electrode processes when a mechanically controlled drop time of 0.158 sec obtained with the Metrohm system is used, but with variable mercury column height. In this experiment t is kept constant at a short drop time and only m varies. For both the bismuth and cadmium systems a straight line plot is again obtained and it is readily apparent that the use of a short drop time alone is insufficient to invalidate the Ilkovic equation, or more strictly the theory to which the natural drop time polarography conforms.

The above experiments with Metrohm capillaries and the Metrohm controlled drop time system were all performed with the natural drop time in the 2–3-sec drop time region, *i.e.*, just above the minimum value usually recommended in polarography, although the flow rate of mercury is rather large. The above experiments were repeated with a wide range of different capillaries constructed from marine barometer tubing, but with much lower flow rates of mercury and longer drop times. With these capillaries $i_d/m^{2/3}t^{2/3}$ was both close to a constant and always lower than the nonconstant value of this ratio obtained with the Metrohm capillaries. The Metrohm

(28) A. M. Bond, *J. Electroanal. Chem.*, **35**, 343 (1972).

(29) Data presented in Tables II, IV, V, and VII and Figures 1, 2, 6, 7, and 12 will appear following these pages in the microfilm edition of this volume of the journal. Single copies may be obtained from the Business Operations Office, Books and Journals Division, American Chemical Society, 1155 Sixteenth St., N.W., Washington, D. C. 20036. Remit check or money order for $3.00 for photocopy or $2.00 for microfiche, referring to code number JPC-73-915.

TABLE I: Variation of dc Polarographic Parameters as the Capillary Length is Decreased[a]

Drop time, sec	Flow rate of mercury, mg sec^{-1}	$-E_{1/2}$, V vs. Ag|AgCl	Slope of log plot[b]
2.24	4.48	0.620	28
2.00	4.74	0.621	29
1.87	5.33	0.621	28
1.70	5.51	0.618	29
1.44	6.57	0.619	30
1.25	7.77	0.620	29
0.630	14.7	0.620	30
0.417	17.8	0.621	27
0.355	23.2	0.622	27
0.206	32.0	0.622	28
0.159	36.2	0.622	29
~0.03	51.7	0.622	28

[a] Mercury column height kept approximately constant at 65 cm. Concentration of cadmium = 1.8 × 10^{-4} *M*. [b] Slope of E_{DME} *vs.* log $[(i_d - i)/i]$ plot.

capillaries, under the conditions used, therefore do not rigorously comply with the Ilkovic equation but, as will be seen from data given throughout this paper, it is for this reason that they are extremely useful in enabling several important and definitive conclusions to be reached and/or verified.

For example, in this context it was found that when the mercury column height was increased to 95.9 cm, t decreased to 1.37 sec and m increased to 5.75 mg sec^{-1}. The value of i_d at the mercury column height departed substantially from the value calculated assuming the linear relationship obtained at 2-3-sec drop time in Figure 1[29] could be extended to these conditions. However, with the short drop time experiment in Figure 2[29] the equivalent phenomena were also observed. From this it was verified that the Ilkovic equation does not apply in all cases.

It was also most evident from these studies with a variety of Metrohm capillaries that $i_d/m^{2/3}t^{1/6}$ was only approximately independent of the capillary being used. The data obtained, however, strongly suggest that if the natural drop time conditions do not allow the usual polarographic theory to be obeyed, then the short controlled drop time data will not fit the theory either. That is, it is the natural drop time behavior, from which the short controlled drop time is derived, which governs the observed behavior of the controlled drop time experiment, and the actual value of the controlled drop time is not of fundamental importance. Such an explanation is consistent with all the published literature and can be used to rationalize apparent anomalies relating to the use of short drop time polarography. This point will be returned to after considerations of additional experiments.

(ii) Variation of Capillary Length. Table I and Figure 3 show some dc data obtained at very short naturally occurring drop times. These were achieved by progressively cutting lengths off the capillary and it can be noted that in these experiments extremely high flow rates of mercury simultaneously result with the short drop time.

It is interesting to observe that despite the high flow rate of mercury and extremely short drop times $E_{1/2}$ and the wave shape are essentially independent of m, t, and capillary length. However a plot of i_d *vs.* $m^{2/3}t^{1/6}$ broke down

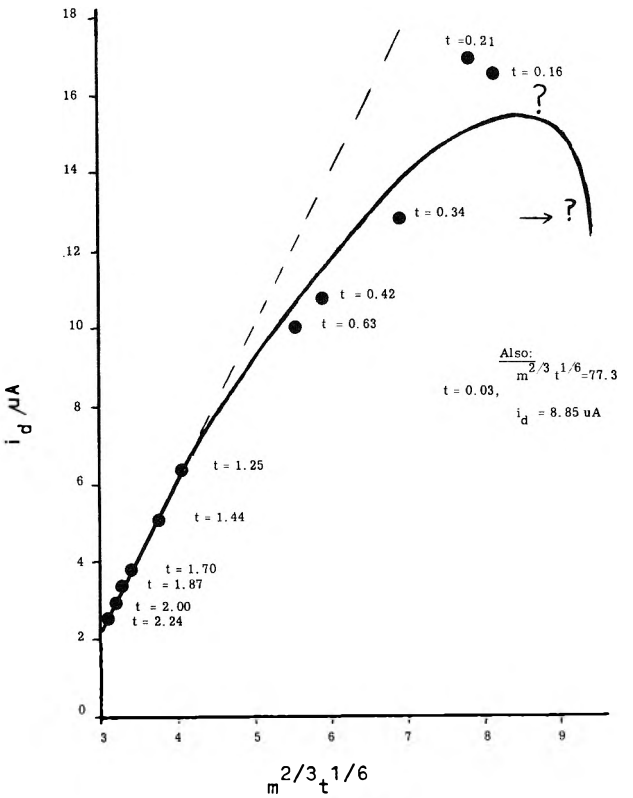

Figure 3. Dependence of i_d and $i_d/m^{2/3}t^{1/6}$ on $m^{2/3}t^{1/6}$ for the cadmium dc electrode process as the flow rate of mercury is increased by shortening the capillary length: [Cd] = 1.8 × 10^{-4} *M*, Metrohm capillary.

severely from linearity at the data point where t = 1.25 sec and m = 7.77 mg sec^{-1}. The same experiments using a controlled drop time of 0.158 sec, but varying the natural drop time down to 0.417 sec, again showed the $m^{2/3}t^{1/6}$ dependence breaking down severely at exactly the same data point and the short controlled drop time experiment again seems to be controlled by the natural drop time conditions.

(iii) Influence of Controlled Drop Time on m. Intuitively one would speculate that the application of a drop knocker to the DME would essentially not alter the flow rate of mercury and in treating a set of data of constant natural drop time conditions that this assumption could be invoked. Data in Table II[29] reveal, however, that the application of the drop knocker, whether applied either vertically or horizontally to the capillary, slightly decreases the value of m.

(iv) Variation of Controlled Drop Time at Constant Mercury Column Height. If the drop time is varied by altering the frequency of the drop knocker, all measurements being made at constant mercury column height, then the results presented in Figures 4 and 5 and Table II are obtained. Essentially these data were obtained under variable drop time–constant mercury flow rate conditions. Figures 4 and 5 show clearly that under these conditions the linear i_d *vs.* $m^{2/3}t^{1/6}$ relationship holds for both capillaries. Furthermore, the data at controlled drop time and the naturally occurring drop from which the short drop time emanates are, within the limit of experimental error, part of the same family of data. This is evidenced by the observation that the latter data point also fits onto the

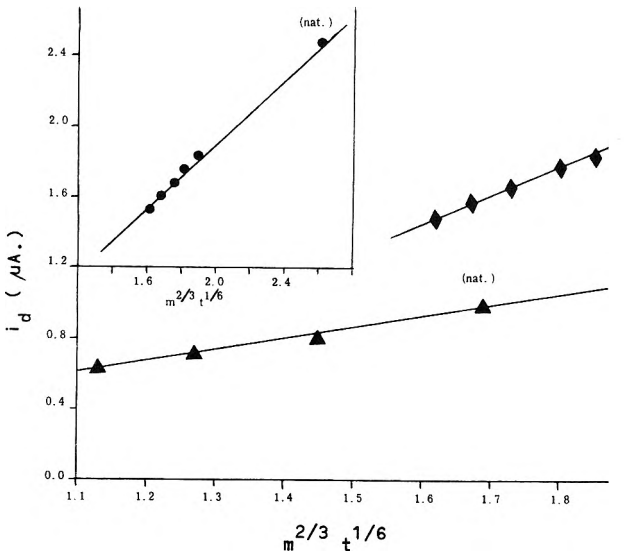

Figure 4. Dependence of i_d on $m^{2/3}t^{1/6}$ for cadmium dc electrode process at constant mercury column height but with variable controlled drop time: [Cd] = 1.8 × 10^{-4} *M*; (▲) PAR system, mercury column height = 59.3 cm; (●, ♦) Metrohm system, mercury column height = 57.6 cm.

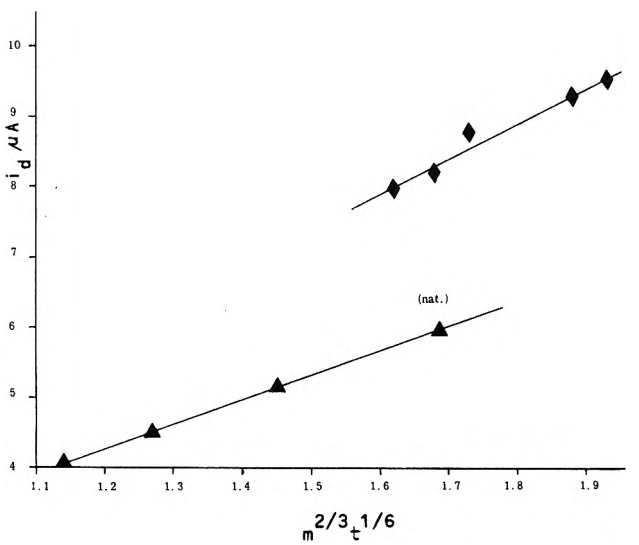

Figure 5. Dependence of i_d on $m^{2/3}t^{1/6}$ for the bismuth dc electrode process at constant mercury column height, but with variable controlled drop time: [Bi] = 8.1 × 10^{-4} *M*; (▲) PAR system, mercury column height = 59.3 cm; (♦) Metrohm system, mercury column height = 57.6

same linear relationship as do the controlled drop time experiments. Table III, as well as this feature, again confirms that it is the natural drop time behavior which governs that observed with short controlled drop times and that the absolute value of the drop time is relatively unimportant.

Dependence of i_d on Concentration. With all the above systems, i_d was found to be linearly dependent on concentration over the range 5 × 10^{-4}–10^{-3} *M*.

B. Short Drop Time ac Polarography

Considerably fewer studies on short drop time ac polarography have been undertaken. Indeed, with respect to short gravity controlled drop time no studies are apparently

TABLE III: Some dc Data Obtained when the Controlled Drop Time is Varied at Constant Mercury Column Height

Drop knocking system	Drop time, sec	$-E_{1/2}$, *V vs.* Ag|AgCl		Slope of log plot[f]	
		Cd[a]	Bi[b]	Cd[a]	Bi[b]
Metrohm[c]	2.38[e]	0.622		29	
	2.16[e]		0.068		20
	0.32	0.621	0.067	28	21
	0.28	0.622	0.068	29	20
	0.24	0.621	0.069	28	20
	0.20	0.622	0.066	29	20
	0.16	0.622	0.068	28	20
PAR[d]	4.00[e]	0.618		29	
	4.52[e]		0.065		20
	2.0	0.618	0.065	28	19
	1.0	0.621	0.066	28	19
	0.5	0.619	0.066	27	19

[a] Concentration of cadmium(II) = 1.8 × 10^{-4} *M*. [b] Concentration of bismuth(III) = 8.1 × 10^{-4} *M*. [c] Mercury column height = 57.6 cm. [d] Mercury column height = 59.3 cm. [e] Natural drop time. [f] See Table I, footnote *b*.

available, so this section of the work is reported in considerable detail. These detailed studies can be used to verify conclusively the above findings in the dc experiments as considerably more complexity is introduced into the theory.

The equation tested was that based on a diffusion-controlled reversible ac electrode process, in which the peak current, I_p, is related to other fundamental parameters.

$$I_p = k''Cm^{2/3}t^{2/3}\omega^{1/2}\Delta E \sin\left(\omega t' + \frac{\pi}{4}\right) \qquad (9)$$

In this equation k'' incorporates all the terms in eq 4 which can be considered constants for any given series of measurements.

Strictly speaking, no electrode process will be reversible and diffusion controlled in the ac sense, but the cadmium and bismuth electrode processes, at reasonably low frequencies, approximate this behavior satisfactorily.

Dependence of I_p on ΔE. Figures 6[29] and 7[29] show the dependence of I_p on the alternating potential at both short controlled and natural drop times. Table II[29] shows some appropriate data. The completely linear dependence of I_p on ΔE and the data in Table IV completely confirm this proportionality at the use of short controlled drop times does not invalidate the theory with respect to the ΔE term.

Dependence of I_p on $\omega^{1/2}$. Figure 8 shows some representative data for cadmium. For the bismuth(III) system at high concentrations a nonlinear relationship for I_p *vs.* $\omega^{1/2}$ was obtained with both controlled and natural drop times. However, parallel curvature was observed in all cases and identical data were evident at all drop times. At a concentration of 8.1 × 10^{-5} *M*, the normal linear relationship was found. Apparently this system exhibits some complexity at high concentrations such as incomplete diffusion control or adsorption. The cadmium system gives the expected dependence, independent of drop time, and it is concluded that the short controlled drop time has no influence on the dependence of I_p with respect to frequency. Table V[29] shows the variation of some ac parameters with drop time and frequency to reinforce this conclusion.

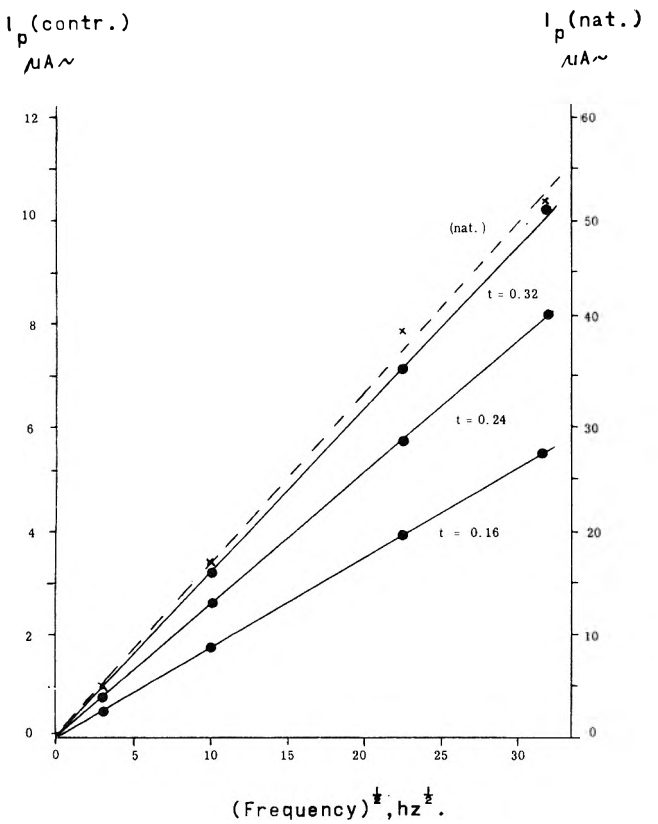

Figure 8. Dependence of I_p on the square root of frequency for the ac cadmium electrode process: ΔE = 10 mV peak-to-peak, [Cd] = 1.8 × 10^{-4} *M*, Metrohm system, natural drop time = 2.38 sec. Controlled drop times of 0.16, 0.24, and 0.32 sec as indicated on graph. Mercury column height = 59.3 cm: (—, •) controlled drop time; (– – –, ×) natural drop time.

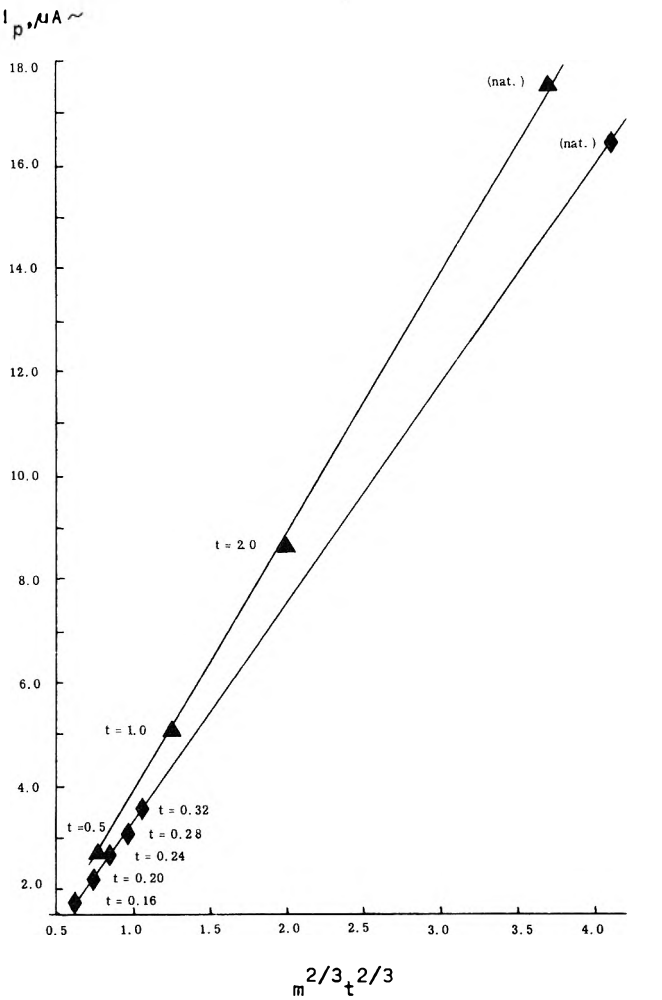

Figure 9. Dependence of I_p on $m^{2/3}t^{2/3}$ for the ac cadmium electrode process at constant mercury column height but with variable controlled drop time: frequency = 400 Hz; ΔE = 5 mV peak-to-peak; [Cd] = 1.8 × 10^{-4} *M*; (▲) PAR system, mercury column height = 59.3 cm; (♦) Metrohm system, mercury column height = 57.6 cm.

Dependence of I_p on Capillary Characteristics. The theory predicts a dependence of I_p on area of $m^{2/3}t^{2/3}$. Figures 9, 10, and 11 show the dependence of I_p upon this variable for a constant mercury column height. As with the dc experiments, the natural drop time point is representative of the same set of data in every instance. The linear dependence of I_p upon $m^{2/3}t^{2/3}$ is excellent. However, the difference between the two capillaries can be noted. The difference between the Metrohm system (Metrohm capillary) and the PAR system (marine barometer tubing capillary) is entirely analogous to that found in the dc polarography. Table VI shows some representative data obtained under these conditions.

Figure 12[29] shows some data with variable mercury column height, but with constant drop time. A linear $m^{2/3}t^{2/3}$ dependence is observed in accordance with theory.

Table VII[29] and Figure 13 show some data obtained when the capillary characteristics are altered by decreasing the length of the capillary. It can be seen that the dependence of I_p on $m^{2/3}t^{1/6}$ is not the same at the high flow rate short drop time data region as is the normally used low flow rate long drop time data. This experiment proves conclusively that the normal theory is certainly not valid if the short drop times are achieved naturally. However, if they are obtained as short controlled drop times, then the theory pertaining to the natural drop time from which the short drop times are obtained is the valid one. For the first four data points I_p was linearly dependent if the

TABLE VI: Some ac Data Obtained when the Controlled Drop Time is Varied at Constant Mercury Column Height

Drop knocking system	Drop time, sec	$-E_p$, V vs. Ag|AgCl		Half-width, mV	
		Cd[a]	Bi[b]	Cd[a]	Bi[b]
Metrohm[c]	2.38[e]	0.622		45	
	2.16[e]		0.072		32
	0.32	0.622	0.071	44	31
	0.28	0.622	0.073	45	32
	0.24	0.623	0.072	43	31
	0.20	0.623	0.073	44	32
	0.16	0.623	0.072	45	31
PAR[d]	4.90[e]	0.618		44	
	4.52[e]		0.071		31
	2.0	0.617	0.071	44	32
	1.0	0.621	0.073	43	32
	0.5	0.619	0.070	44	32

[a] Concentration of cadmium(II) = 1.8 × 10^{-4} *M*, ΔE = 5 mV, peak-to-peak, ω = 400 Hz. [b] Concentration of bismuth(III) = 8.1 × 10^{-4} *M*, ΔE = 5 mV, peak-to-peak, ω = 400 Hz. [c] Mercury column height = 57.6 cm. [d] Mercury column height = 59.3 cm. [e] Natural drop time.

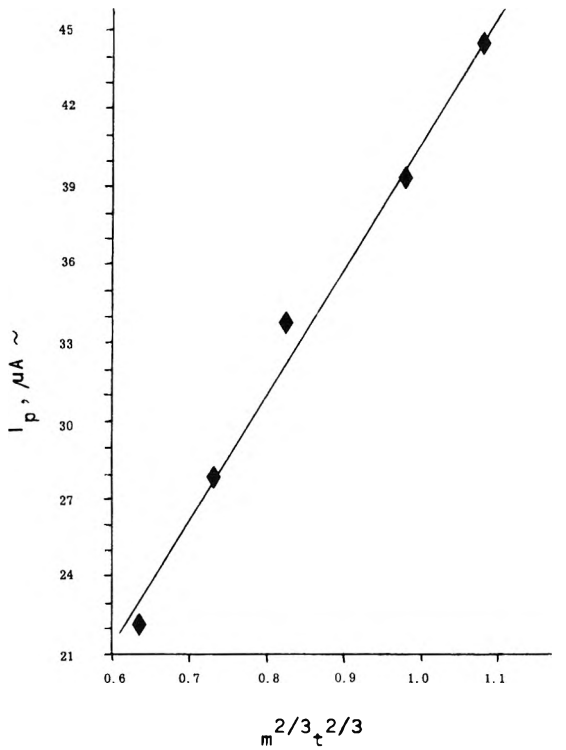

Figure 10. Dependence of I_p on $m^{2/3}t^{2/3}$ for the ac bismuth electrode process at constant mercury column height, but with variable controlled drop time: frequency = 400 Hz; ΔE = 5 mV peak-to-peak; [Bi] = 8.1 × 10^{-4} *M*; Metrohm system, mercury column height = 57.6 cm.

value of $m^{2/3}t^{2/3}$ is in accordance with theory. Over this range of data points values of $(mt)^{2/3}$ or area are in the more normally used range in polarography. However, at higher flow rates of mercury and shorter drop times $(mt)^{2/3}$ decreases as does I_p but no longer does a linear relationship exist and the graph takes on the appearance shown in Figure 13. The short drop times themselves do not account for this departure so the high flow rate of mercury must be the fundamental parameter contributing to the violation of the normally applicable theory.

Phase Angle Measurements. Equation 9 predicts I_p will be a function of the phase angle, ϕ, and that the maximum value occurs at 45°.

Figure 14 shows that exactly the same phase angle dependence is found with both natural drop time and short controlled drop time experiments. From these measurements the phase angle is calculated to be 43 ± 2°, in excellent agreement with theory.

Shape of the ac Wave. The shape of the ac wave fitted eq 5 and 6 irrespective of the capillary or drop time used. This is also reflected in the half-widths given in all tables. Similarly, the E_p value was independent of all variables within ±3 mV as can be seen from data in the tables. The same observation was made with the dc polarography and the two techniques appear to be entirely analogous with respect to the use of short drop times.

Dependence of I_p on Concentration. Both the cadmium and bismuth systems were studied over the concentration range 10^{-6}–10^{-4} *M* using in-phase measurements. With both natural and controlled drop time experiments, I_p was always a linear function of concentration. Similarly the half-width, E_p, and other characteristics were independent of concentration.

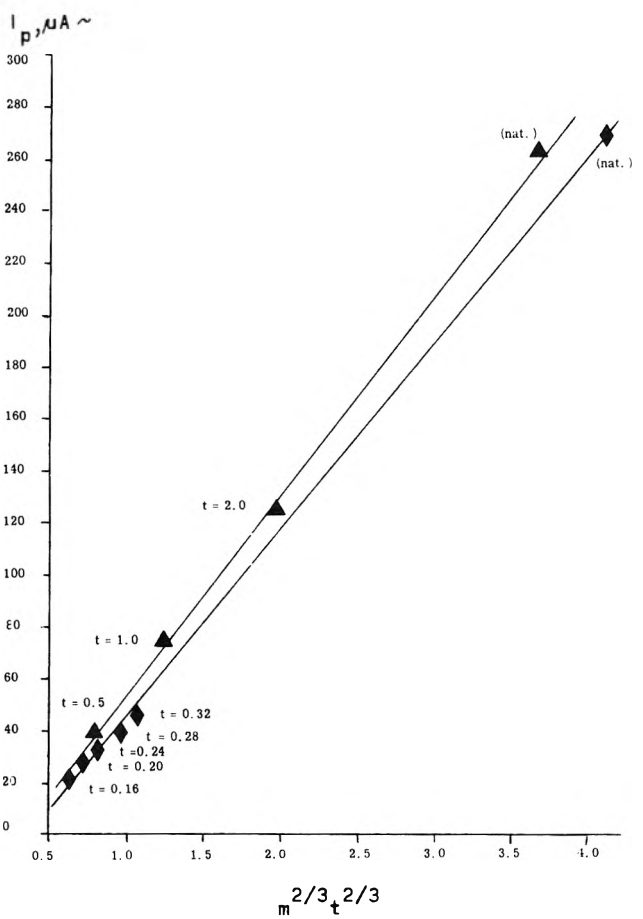

Figure 11. Dependence of I_p on $m^{2/3}t^{2/3}$ for the ac bismuth electrode process at constant mercury column height, but with variable controlled drop time: frequency = 400 Hz; ΔE = 5 mV peak-to-peak; [Bi] = 8.1 × 10^{-4} *M*; (▲) PAR system, mercury column height = 59.3 cm; (♦) Metrohm system, mercury column height = 57.6 cm.

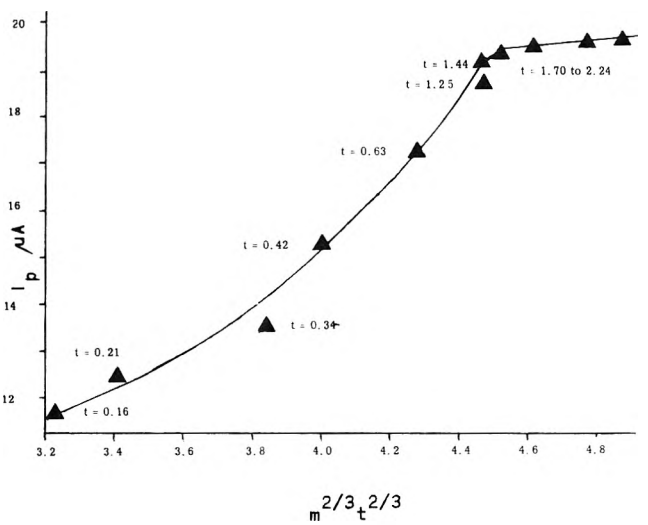

Figure 13. Dependence of I_p on $m^{2/3}t^{2/3}$ for the ac cadmium electrode process as the flow rate of mercury is increased by shortening the capillary length: [Cd] = 1.8 × 10^{-4} *M*; Metrohm capillary, ΔE = 10 mV peak-to-peak; frequency = 100 Hz.

Conclusions

From this work it is concluded that short controlled drop time ac and dc polarography can indeed be used with considerable advantage. The presence of the short

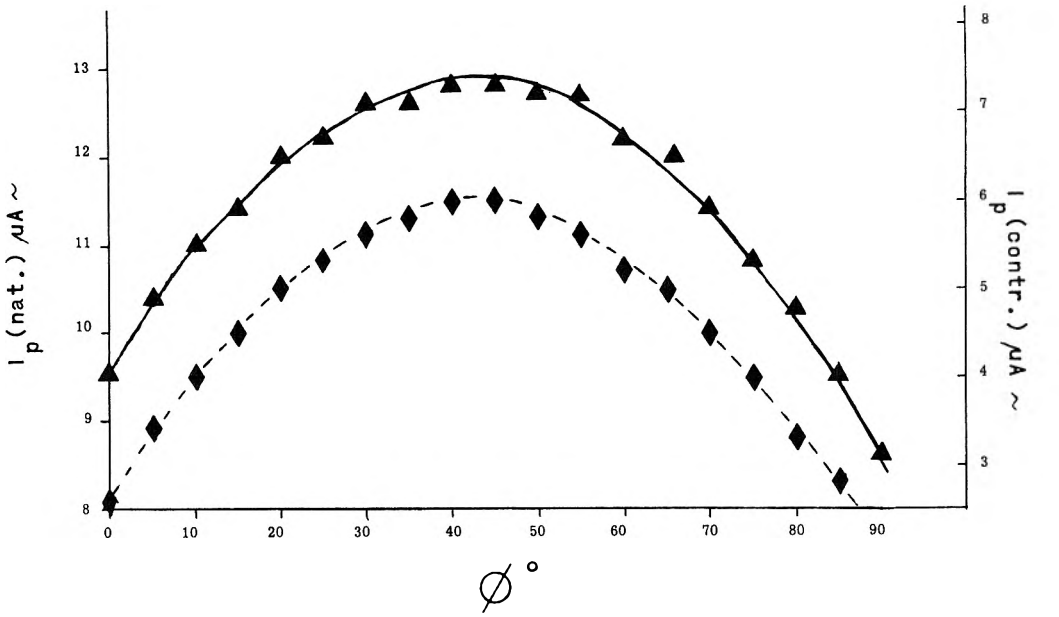

Figure 14. Dependence of I_p on phase angle of measurement, ϕ, for the ac cadmium electrode process at natural and short controlled drop times: [Cd] = 1.8×10^{-4} *M*; ΔE = 10 mV peak-to-peak; frequency = 100 Hz, mercury column height = 57.6 cm, Metrohm system; (▲) natural drop time = 2.16 sec; (♦) controlled drop time = 0.16 sec.

drop time in itself does not violate conditions under which the theory has been derived. Rather the behavior of the short controlled drop time experiment is critically dependent upon the theory applicable to the natural drop from which the short controlled drop is derived.

On the other hand, if short drop times are obtained by gravity controlled methods, it is confirmed that the standard theory no longer applies. With such methods, it is not the short drop time itself which induces nonideality, but the increase in flow rate of mercury. In the short controlled drop time experiment, the short drop time is achieved without significant alteration of the flow rate of mercury. Examination of current–time curves reveals that the short controlled drop time experiment in fact approximates very closely to that of current sampling of the first stage of a naturally falling drop. It is not surprising therefore that the normal theory is still applicable.

It is also concluded that any possible anomalies in the literature pertaining to the use of short drop times are now explained. Different results have referred to different approaches to obtaining the shortened drop times and, in fact, provided the short drop times are obtained by controlled knocking of the DME, short drop time, rapid scan rate polarography is a most valuable technique.

Dipole Moments of Some Neutral Organic Phosphates

Dj. M. Petković,* B. A. Kezele, and D. R. Rajič

The Boris Kidrič Institute, Beograd, Yugoslavia *(Received August 21, 1972)*

The dipole moments of a number of neutral esters of phosphoric acid were determined in *n*-hexane and correlated by the Hammett equation. The dipole moment of tributyl phosphate was determined in several diluents and used to study the solvent effect by the classical Müller equation. The value of the tributyl phosphate dipole moment in the gaseous state was approximated and the same value was obtained from the Onsager equation using the data for pure tributyl phosphate.

Introduction

Electric dipole moments of neutral esters of phosphoric acid, cited in the literature[1-10] (Table I), show considerable discrepancies. The differences are due to different diluents used, the method of dipole moment calculation, the evaluation of atomic polarization, etc. The diluent

(1) W. J. Svirbely and J. J. Lander, *J. Amer. Chem. Soc.*, **70**, 4121 (1948).

TABLE I: Dipole Moments of Trialkyl Phosphates

Phosphate	Solvent	T, °C	Dipole moment,	Ref
TMP	Carbon tetrachloride	20	3.02	2
	Carbon tetrachloride	20	3.02	8
	Carbon tetrachloride	20	3.02	This work
	Hexane	20	2.78	This work
	Benzene	25	1.18	5
TEP	Carbon tetrachloride	20	3.07	2
	Carbon tetrachloride	20	3.07	8
	Carbon tetrachloride	20	3.02	This work
	Benzene	25	3.12	5
	Benzene	25	3.08	3
	Benzene	25	3.00	4
	Benzene	24	3.07	1
	Hexane	20	2.86	This work
	Cyclohexane	20	2.84	2
	Dioxane	25	3.21	9
TPP	Carbon tetrachloride	20	3.09	9
	Carbon tetrachloride	20	3.03	This work
	Benzene	25	3.18	5
	Hexane	20	2.93	This work
	Dioxane	25	3.21	9
TBP	Carbon tetrachloride	20	3.05	2
	Carbon tetrachloride	20	3.10	This work
	Carbon tetrachloride	20	3.01	6
	Hexane	20	2.92	This work
	n-Octane	25	2.60	7
	Cyclohexane	20	2.76	This work
	Decalin	20	2.61	This work
	Benzene	25	3.07	3
	Benzene	20	3.08	10
	Benzene	20	3.05	6
	Benzene	20	3.09	This work
	Dioxane	25	3.21	9
	Pure TBP	20	3.28	6
	Pure TBP	25	3.35	3
	Pure TBP	20	3.32	This work

chosen is often nonpolar but not inactive. For example, benzene and carbon tetrachloride, which are used very often, are nonpolar but they are not inactive in relation to the phosphoryl group.[11-13] Therefore, to correlate the dipole moments of neutral organophosphates they must be determined under the same conditions and in the same diluent.

This paper is concerned with the determination of dipole moments of neutral esters of phosphoric acid in *n*-hexane as the inert diluent.

Since some phosphoryl compounds are not soluble in hexane, carbon tetrachloride was used as an alternative. Some other diluents were also used to study the solvent effect on the tributyl phosphate dipole moment.

Experimental and Results

The apparatus for measurement of dielectric constants was a dipolemeter WTW, Weilheim Oberbayern, West Germany, Model DM 01, with the measuring frequency of 2.0 MHz. The refractive index was measured with an Abbe refractometer, Carl Zeiss, Jena, East Germany, with sodium light. The densities were determined by a 50-ml pycnometer. All experiments were carried out at 20.0 ± 0.1°.

The phosphate esters were purified by fractional distillation at reduced pressure, except for triphenyl phosphate (TPhP), a British Drug House (BDH) product. Trimethyl phosphate (TMP), triethyl phosphate (TEP), tripropyl phosphate (TPP), tributyl phosphate (TBP), and trioctyl phosphate (TOP) were all BDH products, while tritoluol phosphate (TTP) was a Albright and Wilson product, and triallyl phosphate (TAIP) a Koch and Light products. Hexane, cyclohexane, decalin, carbon tetrachloride, all BDH products, were purified by distillation. All chemicals were dried with molecular sieve, type 4A, and TPhP was dried over P_2O_5 under reduced pressure for 1 week.

The dielectric constants, specific volumes, and squares of the refractive indexes were linear functions of their weight fractions over the concentration range investigated. From the slopes of the lines the electric dipole moment was calculated by the Halverstadt and Kumler[14] modification of the Debye equation. Atomic polarization was omitted on the grounds that it is small and partially compensated for by the refractive index estimation of electronic polarization. Electronic polarization was evaluated by the Le Fèvre and Vine[14] equation.

The concentration range of organic phosphates was 1–50 $\times 10^{-4}$ weight fraction.

The slopes of the linear graphs of dielectric constants (α), specific volumes (β), densities (γ), and squares of refractive index (Δ) of organic phosphates solutions against weight fractions of the organic phosphates, polarizations at infinite dilution ($P_{2\infty}$), and dipole moments (μ) of the organic phosphates are given in Table II. Dielectric constants (ϵ_1), densities (d_1), and the squares of refractive indices (n_1^2) of pure diluents as the intercepts of linear functions, mentioned above, are also given.

Correlation of Dipole Moments of Organic Phosphates

The relation between the substitution constant in the Hammett equation and the observed dipole moment of a compound was suggested by van Beek.[15] He has shown that available experimental data support an equation of the form

$$\log(\mu/\mu_0) = \kappa\sigma \quad (1)$$

Here, μ and μ_0 are dipole moments of substituted and unsubstituted compounds, respectively, κ is a constant, and σ is a substitution constant. Literature data appear to confirm[15] the proposed relationship.

In this paper eq 1 was applied to correlate the dipole

(2) A. E. Arbuzov and P. I. Rakov, *Izv. Akad. Nauk SSSR, Ser. Khim.*, **3**, 237 (1950).
(3) G. K. Estok and W. W. Wendland, *J. Amer. Chem. Soc.*, **77**, 4767 (1955).
(4) J. A. A. Ketelaar, H. R. Gersman, and F. Hartog, *Recl. Trav. Chim. Pays-Bas*, **77**, 982 (1958).
(5) M. J. Aroney, L. H. L. Chia, R. J. W. Le Fèvre, and J. D. Sahby, *J. Chem. Soc.*, 2948 (1964).
(6) J. Hurwic and J. Michalczyk, *Nukleonika, Suppl.*, **10**, 221 (1965).
(7) W. J. McDowell and C. F. Coleman, *J. Tenn. Acad. Sci.*, **41**, 78 (1966).
(8) W. Waclawek and W. Guzovski, *Rocz. Chem.*, **42**, 2183 (1968).
(9) P. Mauret, J. P. Fayet, D. Voigt, M. C. Labarre, and J. F. Labarre, *J. Chim. Phys.*, **65**, 549 (1968).
(10) V. A. Lanin, Yu. A. Dyadin, N. I. Yakovleva, Z. N. Mironova, and I. I. Yakovlev, *Izv. Sib. Otd. Akad. Nauk SSSR, Ser. Khim. Nauk*, **3**, 159 (1970).
(11) A. M. Rozen, L. P. Khokhorina, V. G. Yurkin, and N. M. Novikova, *Dokl. Akad. Nauk SSSR*, **153**, 1387 (1963).
(12) D. Dyrssen and Dj. M. Petkovič, *J. Inorg. Nucl. Chem.*, **27**, 1381 (1965).
(13) Dj. M. Petkovič and B. A. Kezele, *Solvent Extr., Proc. Int. Solvent Extr. Conf., 1971*, **2**, 1137 (1971).
(14) C. P. Smith, "Dielectric Behavior and Structure," McGraw-Hill, New York, N. Y., 1955.
(15) L. K. H. van Beek, *Recl. Trav. Chim. Pays-Bas*, **76**, 729 (1957).

TABLE II: Measured Physical Properties of Organic Phosphate Solutions and Calculated Dipole Moments at 20.0 ± 0.1°

Solution	α	β	γ	Δ	ϵ_1	d_1	n_1^2	$P_{2\infty}$	μ
TMP–hexane	3.880	−0.612	0.254	0.022	1.8885	0.6619	1.8934	191.70	2.78
TEP–hexane	3.125	−0.558	0.253	0.051	1.8820	0.6578	1.8937	212.07	2.86
TPP–hexane	2.700	−0.522	0.242	0.088	1.8857	0.6574	1.8931	233.87	2.93
TBP–hexane	2.302	−0.497	0.232	0.088	1.8833	0.6572	1.8929	247.46	2.92
TBP–cyclohexane	2.631	−0.250	0.155	0.224	2.0318	0.7761	1.8945	237.29	2.76
TBP–decalin	2.577	−0.100	0.079	−0.163	2.1741	0.8831	2.1793	211.17	2.61
TMP–carbon tetrachloride	12.426	0.257	−0.597	−0.212	2.2337	1.5939	2.1338	218.85	3.02
TBP–carbon tetrachloride	9.476	0.311	−0.773	−0.236	2.2441	1.5896	2.1340	231.01	3.02
TPP–carbon tetrachloride	7.639	0.391	−0.935	−0.197	2.2367	1.5937	2.1339	247.55	3.03
TBP–carbon tetrachloride	6.770	0.393	−0.974	−0.176	2.2478	1.5900	2.1345	268.42	3.10
TAlP–carbon tetrachloride	7.493	0.327	−0.868	−0.088	2.2344	1.5933	2.1333	232.50	2.92
TOP–carbon tetrachloride	4.022	0.420	−1.050	0.062	2.2360	1.5930	2.1337	316.33	3.02
TTP–carbon tetrachloride	4.935	0.199	−0.509	0.439	2.2362	1.5931	2.1343	279.30	2.92
TPhP–carbon tetrachloride	5.320	0.163	−0.415	0.494	2.2357	1.5934	2.1339	257.47	2.85
TBP–benzene	3.633	−0.111	0.083	−0.330	2.2906	0.8788	2.2545	261.71	3.09
Pure TBP					8.143	0.9744	2.0286		3.32

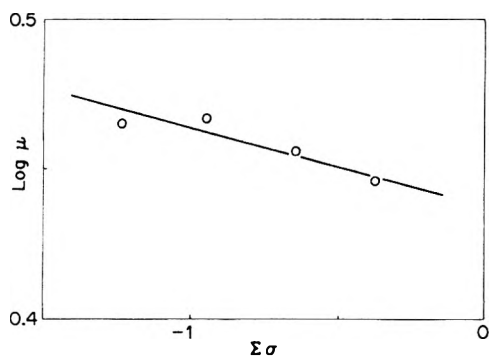

Figure 1. Presentation of trialkyl phosphate dipole moments determined in *n*-hexane by means of eq 1.

moments of trialkyl phosphates. The σ values of alkyl radicals bonded to the phosphoryl group were taken from the literature.[16] In Figure 1 the log μ_{TAP} values are plotted against the summation of σ values for the corresponding phosphates.

The points follow the straight line well and the negative slope of the line suggests that the dipole moments increase with electron-releasing substituents. This is in agreement with earlier observations[17] that the dimerization constants of trialkyl phosphates increase with increasing number of carbon atoms in aliphatic radicals.

The straight line from Figure 1 can be used for the dipole moment of phosphoric acid. Since the σ value for the hydroxyl group is 0.393,[16] one can say that the dipole moment of the phosphoric acid is very close to that of TBP.

Solvent Effect

The dipole moment of a substance measured in a solution is different from that measured in the vapor state and varies[14] from one diluent to another. Among a number of empirical equations which represent the relation of the apparent dipole moment in solution to that of the gas we applied the classical Müller empirical equation

$$\mu_S = \mu_0[1 - C(\epsilon_1 - 1)^2] \quad (2)$$

Here μ_S and μ_0 are the apparent dipole moments in the solution and in the gas state, respectively, C is an empirical constant, and ϵ_1 is the dielectric constant of a diluent. Accordingly, the dipole moments of TBP in different solvents (Table II) are presented in Figure 2. TBP dipole moments determined in hexane, cyclohexane, and decalin fit a straight line, whereas those determined in carbon tetrachloride and benzene are off the line. This phenomenon can be explained by the fact that these diluents are not inert. They form TBP·C_6H_6 and TBP·CCl_4 complexes.[12,13] The intercept of the straight line at $\epsilon_1 = 1$ approximates the dipole moment of TBP in the gaseous state. It is interesting that the value from the intercept, $\mu = 3.32$ D, is similar to that calculated from the dielectic constant of the pure TBP (data from Table II) by means of the Onsager equation.[14]

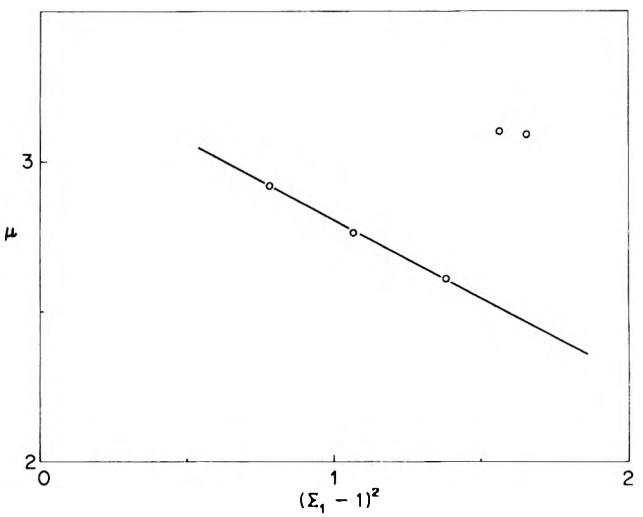

Figure 2. Tributyl phosphate dipole moments determined in different solvents correlated by eq 2.

Acknowledgment. The authors are indebted to Professor A. S. Kertes, The Hebrew University, Jerusalem, Israel, for valuable remarks.

(16) M. I. Kabachnik, *Dokl. Akad. Nauk SSSR.* **110**, 393 (1956).
(17) Dj. M. Petkovič, *J. Inorg. Nucl. Chem.*, **30**, 603 (1968).

Thermal Formation of Oxygen Radicals on Y-Type Zeolites

Tamotsu Imai and H. W. Habgood*

Research Council of Alberta,[1] Edmonton, Alberta, Canada *(Received June 12, 1972)*

Publication costs assisted by the Research Council of Alberta

Esr spectra showed that two different oxygen radicals were thermally formed on the sodium and the lithium forms of Y-type zeolite, but not on the potassium form. The radicals were formed only on the zeolites with high ratios of the alkali metal ions to aluminum ions. The spin concentration of the radicals was in the order of 10^{15} spin/g. The first radical is superoxide ion O_2^- adsorbed on the alkali metal ions and similar to that already known to be formed by γ irradiation. The second radical was favored at higher temperatures and distinctly increased upon adding copper or iron ions together with NaOH or LiOH to the samples. This latter radical reacted with hydrogen sulfide at room temperature and a sulfur radical was produced as a product.

Introduction

It has been known that the superoxide ion O_2^- can be produced on various cation forms of Y-type zeolites by X, γ, and uv irradiations.[2-5] Kasai[2] first reported the formation of superoxide ions on NaY and BaY and concluded that the principal g values of the radicals depended on the charge of the cations. Wang and Lunsford[4] studied the superoxide ions produced on alkaline earth Y-type zeolites and found no significant trend in the change of g_z values with the alkaline earth cations. However, the hyperfine interaction[3,5] between the cation and an unpaired electron of superoxide ion occurred on HY, AlY, ScY, and LaY indicating that the cation was part of the adsorption site.

Rabo and coworkers[6] reported that the superoxide ion O_2^- was thermally produced on unusual valent cation forms (Ni(I) and Na_4^{3+} ions) of Y-type zeolites which were respectively prepared by the reactions of Ni(II)Y and NaY with alkali metal vapors.

In the present paper, the thermal formation of oxygen radicals on Linde Y-type zeolites is reported.

Experimental Methods

Various Y-type zeolites were derived from a sample of sodium Y-type zeolite (Linde Lot No. 11007-73) having the composition $Na_{0.99}AlO_2(SiO_2)_{2.2}$. This parent sample was designated as NaHY(I). NaHY(O) and NaHY(II) were made by washing NaHY(I) respectively with a sodium hydroxide aqueous solution (pH 10.1) and with distilled water. NaHY(III) and NaHY(IV) were obtained by calcining the ammonium form samples, which were made by ion-exchanging NaHY(I) in ammonium chloride aqueous solutions followed by washing with distilled water, in flowing oxygen at 400 to 500°.

NaHY(I) contained impurities such as iron (0.07 wt %) and copper (7 ppm) ions. An impurity-free sodium Y-type zeolite was prepared by repeatedly exchanging NaHY(I) with 2 N NaCl aqueous solution. After the ion exchange, the sample was washed with a dilute NaOH aqueous solution (pH 10.1) and dried. The final impurity levels of copper and iron ions were lower than 0.3 ppm.

LiY was obtained by exchanging 1.5 g of NaHY(I) three times in 500 ml of 2 N LiCl aqueous solution at 95° and washing with a dilute LiOH solution (pH 10.1). KY was prepared, in the same way as LiY, by ion exchanging NaHY(I) with KCl aqueous solution followed by washing with KOH solution (pH 10.1). Other cation form Y-type zeolites were prepared by ion exchanging NaHY(I) with appropriate salt solutions followed by washing with distilled water.

Samples CuNaHY(I) and FeNaHY(I), containing small amounts of copper (II) and iron (II) ions, were prepared by treating NaHY(I) with dilute $CuCl_2$ and $FeCl_2$ solutions followed by washing with distilled water. CuLiY, CuKY, FeKY, and FeCuKY were prepared in the same way. The samples CuNaHY(I)-Na(n), where n varied from I to IV, were respectively prepared by soaking CuNaHY(I) in 0.001, 0.01, 0.22, and 0.54 N NaOH solutions overnight, followed by filtering and drying in air at 100°. FeNaHY(I)-Na(III) was made by soaking FeNaHY(I) in a 0.22 N NaOH aqueous solution. CuLiY-Li, CuKY-K, FeKY-K, and FeCuKY-K were prepared in the same way, using 0.1 N LiOH and KOH solutions.

The extent of exchange was determined on the basis of analyses of the cations in the exchanging solution or in the solution of dissolved zeolite (using hot HF solution) by atomic absorption spectrometry. The values are summarized in Table I. The other cation forms of Y-type zeolites are not listed individually in the table but all had ion-exchanged levels higher than 65%. All zeolite samples contained no binder and were pelleted, crushed, and sieved to 20-60 mesh. X-Ray powder diffraction analyses revealed that all zeolite samples preserved their crystalline structures.

Each esr sample was about 0.03 g of zeolite particles loaded in one side of a 4-mm o.d. quartz U-tube having a glass stopcock and a ground glass joint at the sample side. The sample was dried in flowing oxygen at 500° for at least 4 hr after the temperature had been raised from room temperature over a 2-hr period. After drying, the

(1) Contribution No. 600 from the Research Council of Alberta, Edmonton, Canada.
(2) P. H. Kasai, *J. Chem. Phys.*, **43**, 3322 (1965).
(3) K. M. Wang and J. H. Lunsford, *J. Phys. Chem.*, **73**, 2069 (1969).
(4) K. M. Wang and J. H. Lunsford, *J. Phys. Chem.*, **74**, 1512 (1970).
(5) K. M. Wang and J. H. Lunsford, *J. Phys. Chem.*, **75**, 1165 (1971).
(6) J. A. Rabo, C. L. Angel, P. H. Kasai, and V. Schomaker, *Disc. Faraday Soc.*, **41**, 328 (1966).

TABLE I: Compositions of Zeolites

Sample	Na/Al molar ratio	Remarks
NaHY(O)	0.997	Fe ≈ 0.07 wt %, Cu ≈ 7 ppm
NaHY(I)	0.99	Fe ≈ 0.07 wt %, Cu ≈ 7 ppm
NaHY(II)	0.95	Fe ≈ 0.07 wt %, Cu ≈ 7 ppm
NaHY(III)	0.79	Fe ≈ 0.07 wt %, Cu ≈ 7 ppm
NaHY(IV)	0.15	Fe ≈ 0.07 wt %, Cu ≈ 7 ppm
Impurity-free NaHY	>0.99	Fe and Cu < 0.3 ppm
LiY	<0.01	Li/Al > 0.99 Fe < 0.07 wt %, Cu < 7 ppm
KY	<0.01	K/Al > 0.99 Fe < 0.07 wt %, Cu < 7 ppm
CuNaHY(I)	≈0.95	Cu, 0.2/uc[a]
CuNaHY(III)	≈0.79	Cu, 0.2/uc[a]
CuNaHY(IV)	≈0.15	Cu, 0.2/uc[a]
CuLiY	<0.01	Cu, 0.2/uc,[a] Li/Al = 0.87
CuKY	<0.01	Cu, 0.2/uc,[a] K/Al = 0.90
FeNaHY(I)	0.85	Fe, 0.3/uc[b]
FeKY	<0.01	Fe, 0.3/uc,[b] K/Al = 0.90
CuNaHY(I)–Na(I)	>0.99	Cu, 0.2/uc[a]
CuNaHY(I)–Na(II)	≫0.99	Cu, 0.2/uc[a]
CuNaHY(I)–Na(III)	≫0.99	Cu, 0.2/uc[a]
CuNaHY(I)–Na(IV)	≫0.99	Cu, 0.2/uc[a]
CuLiY–Li	<0.01	Cu, 0.2/uc[a]
CuKY–K	<0.01	Cu, 0.2/uc[a]
FeNaHY(I)–Na(III)	≫0.99	Fe, 0.3/uc[b]
FeKY–K	<0.01	Fe, 0.3/uc[b]
FeCuKY–K	<0.01	Fe, 0.3/uc,[b] Cu, 0.2/uc[a]

[a] 1 Cu per 5 unit cell. [b] 1 Fe per 3 unit cell.

stopcock was closed, the sample side was sealed by a flame, and the other side of the U-tube was taken off. The sample was attached to a vacuum system by means of the ground joint and evacuated at 500° for more than 1 hr. The sample was then oxidized or reduced. Oxidation involved treating with 1 atm of oxygen at 500° overnight and evacuation at this temperature for 1 hr. Reduction involved treating with 1 atm of hydrogen at 500° for 1 hr followed by evacuation at the temperature for 1 hr, repeating twice, leaving the sample overnight at 500° with 1 atm of hydrogen, and then evacuating for 1 hr at this temperature. Some of the reduced samples were treated with oxygen under various conditions as described under Results. Oxygen was also added at room temperature to some samples of all types to test for line broadening.

Irradiation was carried out only on the reduced samples with or without added oxygen. The irradiation was made at room temperature using ^{60}Co γ-rays with a dose rate of 5.9×10^3 rads/min based on hydrocarbon samples. After irradiation, the sample was cooled in liquid nitrogen and one end of the quartz tubing was heated by a flame for 5–10 min in order to remove color centers.

The esr measurements were made at liquid nitrogen temperature using a Varian Model 4500 with a $T.E._{102}$ mode cavity operated using X-band microwave (9.0 GHz/sec). The uncertainty of g values (based on DPPH) was ±0.002 and of hyperfine constants ±1 G. Varian standard pitches were used to determine the spin concentration. The uncertainty of spin concentration was ±30%.

Results

The reduced NaHY(I) showed no esr signal. When it was treated with oxygen (1 atm for 1 hr) at various temperatures between 25 and 500° two radical species were produced. Figure 1 shows spectra for 25, 200, and 500° and for the two cases where the oxygen pressure (at room temperature) was adjusted to 10 and 760 Torr prior to the esr measurement. The first radical (Figure 1a) was characterized by g values at 2.003 and 2.011, and the second (Figure 1d) at 2.008. The split of the adsorption line at g = 2.074 in Figure 1d was caused by the overlap of the signal of impurity copper(II) ion (see below). The first radical was produced at room temperature, but not higher temperatures than 300°; it disappeared if the sample was evacuated at 500° for 1 hr. The same radical species was produced at a more than one hundred times greater concentration by γ irradiating the reduced NaHY(I) for 1 hr in the presence of 10 Torr of oxygen. Thus, and on the basis of the g values, this radical appears to be the superoxide ion reported by other workers.[2-5]

The second radical was formed at high temperatures and only 10 to 20% of its esr intensity decreased after the sample was evacuated at 500° overnight. This spectrum was then the same as that given by the oxidized sample. It disappeared if the sample was reduced with hydrogen at temperatures higher than 300°.

The reaction of hydrogen sulfide with this second radical showed interesting features and strongly points to its being an oxygen species. Figure 2a shows the spectrum observed when hydrogen sulfide was adsorbed on the reduced NaHY(I) at room temperature and 50 Torr. The radical readily disappeared when the sample was evacuated at room temperature showing that the species was only weakly adsorbed. Stiles and coworkers[7] irradiated

(7) D. A. Stiles, W. J. R. Tyeman, O. P. Strausz, and H. E. Gunning, *Can. J. Chem.*, **44**, 2149 (1966).

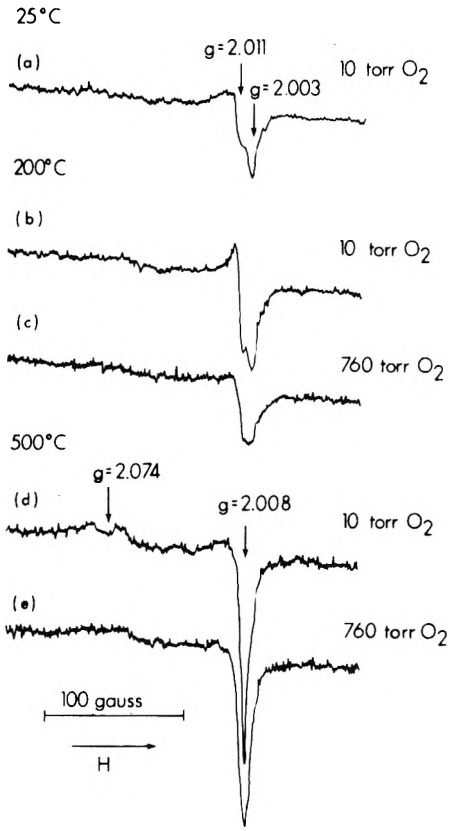

Figure 1. Esr spectra of oxygen radicals on NaHY(I). The samples were placed in contact with 1 atm of oxygen for 1 hr at temperatures indicated above and oxygen pressure in the sample tube was then adjusted at either 10 or 760 Torr at room temperature.

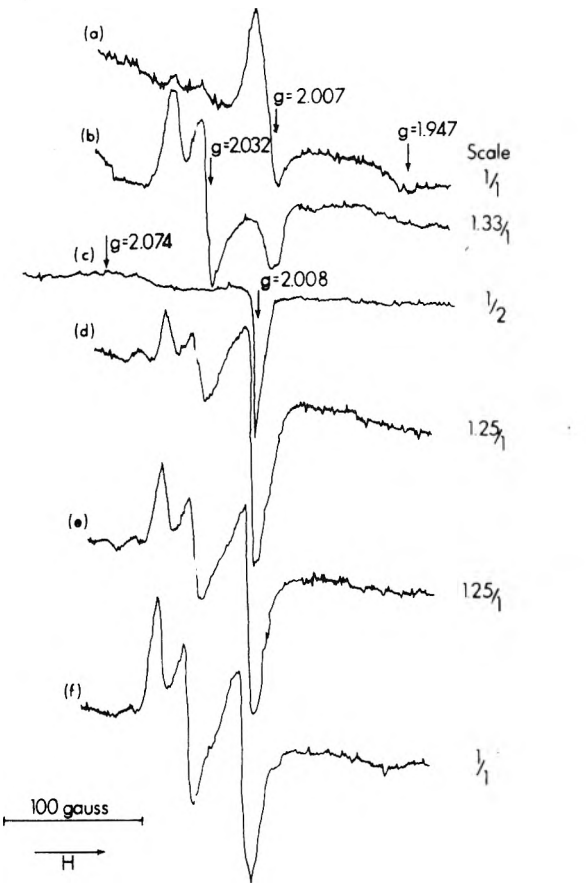

Figure 2. Reaction of H_2S with the second (high-temperature) oxygen radical. Esr spectra of radicals on NaHY(I): (a) H_2S radical, (b) sulfur radical (c) oxygen radical, (d) the state of the reaction at 3 min, (e) 6 min, and (f) 60 min.

solid hydrogen sulfide at 77°K using uv rays and assigned the esr spectrum obtained from the sample to HS radical. The spectrum showed orthorhombic g tensors having hyperfine splitting due to proton. The spectrum was greatly different from the axially symmetric signal of the hydrogen sulfide radical shown in Figure 2a. Figure 2b is the spectrum of sulfur radical which was obtained by evacuating the sample shown in 2f (see below) at room temperature, and is identical with the spectrum reported by Dudzik and Preston[8] for sulfur radical. Figure 2c is the spectrum of the second oxygen species and spectra 2d, 2e, and 2f show the effects of adding 50 Torr of H_2S to this sample at room temperature. The signal for the oxygen radical gradually decreases while that for the sulfur radical increases over the time period up to 60 min.

It was notable that none of the oxygen, the hydrogen sulfide, or the sulfur radicals were produced on the decationated zeolite, NaHY(IV).

The dipolar interaction between spins caused the line broadening of the esr signal of the oxygen radicals upon introducing oxygen over the sample at room temperature. Since the diffusion of oxygen into the β cage must be slow and into the hexagonal prism is probably negligible, the line broadening should occur mainly for the radicals existing in the supercage.[4] The esr spectrum of the superoxide ion formed at room temperature (Figure 1a) disappeared upon introducing 1 atm of oxygen. The sample treated with 1 atm of oxygen at 200° and then exposed to 10 Torr of oxygen at room temperature showed lines from both oxygen species in its esr spectrum (Figure 1b) and the introduction of 1 atm of oxygen only reduced but did not eliminate these peaks (Figure 1c). Consequently, a portion of the oxygen must be able to penetrate the β cages at 200° and both species can be formed in the β cage at this temperature. The spectrum of the second oxygen radical (that formed at higher temperature) was partly reduced in intensity as exemplified by Figure 1d and 1e. The spectra were regenerated if the oxygen pressure was reduced to 10 Torr. The relative intensities of the oxygen radicals measured at 10 and 760 Torr are shown in Figure 3 as a function of the temperature. Consequently, we conclude that most of the second oxygen radical was formed in the β cage.

A simple experiment was carried out to investigate the extent of diffusion of oxygen into the β cage of NaHY(I). A reduced NaHY(I) sample was placed in contact with 1 atm of oxygen at room temperature for 5 min. Another sample was heated at 500° in the presence of 1 atm of oxygen for 1 hr and quickly cooled to room temperature. Both samples were evacuated at room temperature overnight and then heated to 500° in a closed vacuum system. The first sample showed no increase of pressure but the second gave a decided increase in the pressure (from 3 to 5 × 10^{-3} mm). The result shows qualitatively that oxygen could enter the β cage at 500° and that it was then trapped when the sample was cooled to room tempera-

(8) Z. Dudzik and K. F. Preston, *J. Colloid Interface Sci.*, **26**, 374 (1968).

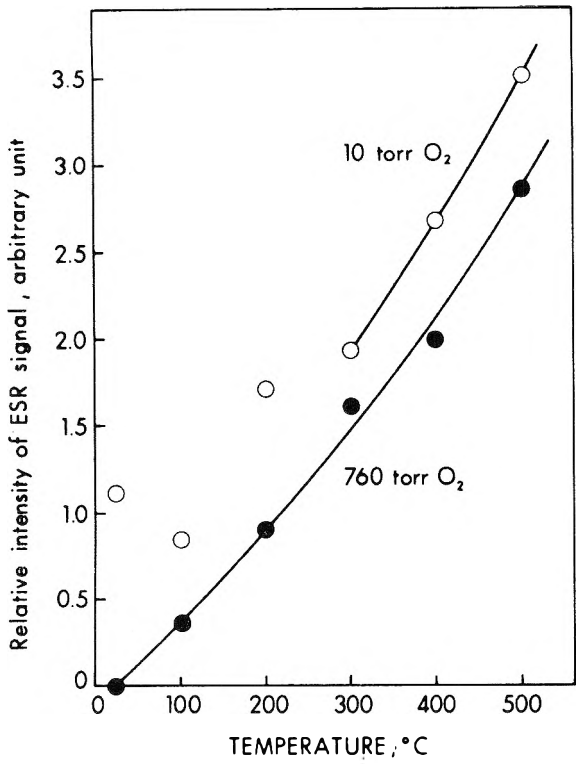

Figure 3. Relative concentration of oxygen radicals on NaHY(I).

ture. Oxygen could not enter into the β cage at room temperature.

The oxygen radicals corresponding to those produced on NaHY(I) were also found on LiY. The radical produced on the reduced LiY at 25° showed orthorhombic g tensors and had the values of g_x = 2.002, g_y = 2.010, and g_z = 2.054 (Figure 4a). The radical formed on CuLiY–Li at 500° had the values of g = 2.002 and 2.008 (Figure 4b). The signal in the low magnetic field is due to Cu(II) ion. The oxygen radicals were not produced on any of potassium form Y-type zeolites.

Oxidized samples of some other cation forms were also examined. No significant amount of oxygen radical was formed on titanium, thallium, uranium, lead, and lanthanum Y-type zeolites. A small amount of the second oxygen radical ($\sim 10^{15}$ spin/g) was formed on barium, magnesium, tin, yttrium, and zinc Y-type zeolites. The absorption lines appeared between g = 2.002 and 2.008. Two oxygen radicals were found on a cerium Y-type zeolite. The radical characterized by g = 2.010 and 2.031 was similar to that found on cerium oxide supported on alumina by previous workers.[9] This radical was produced if the oxidized sample was left at room temperature overnight. The other radical characterized by g = 2.010 and 2.023 appeared upon introducing 10 Torr of oxygen over the reduced or the oxidized samples at room temperature. The spin concentration of these radicals was 10^{16} to 10^{17} spin/g.

The effect of sodium decationation on the formation of the second oxygen radical was studied for oxidized NaHY samples. The radical was formed only at very low levels of decationation and as the samples were decationated to higher extents, the signal from the second oxygen species decreased strongly as shown in Figure 5 along with the increase of a new group of esr signals at low magnetic field which, as discussed below, are assigned to impurity Cu(II)

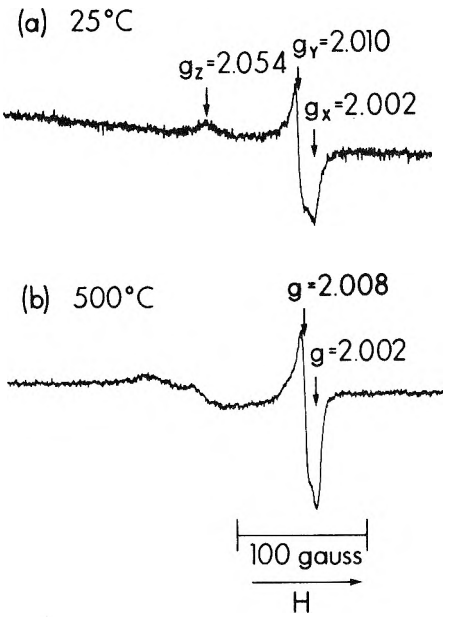

Figure 4. Esr spectra of oxygen radicals produced on: (a) the reduced LiY after contacted with 10 Torr of oxygen at 25°, and (b) the radical produced on the oxidized CuLiY–Li. The signal in the low magnetic field is due to Cu(II) ion.

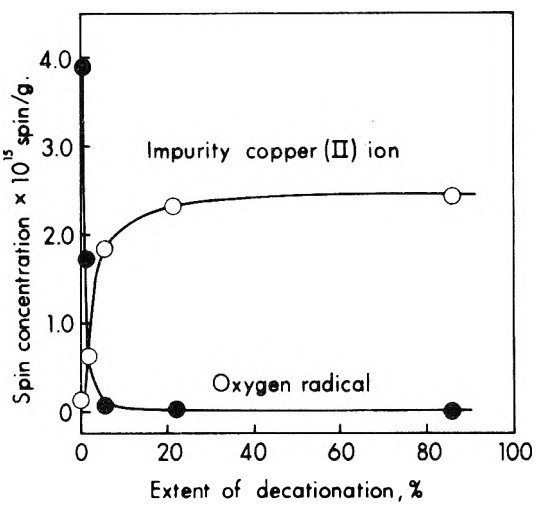

Figure 5. Spin concentration of the second oxygen radical and impurity copper(II) ion on oxidized sodium Y-type zeolites.

ions. The spin concentration of the second oxygen radical was nearly zero at levels of decationation higher than 5%.

The new esr signals that appear on decationation of NaHY are illustrated in Figure 6. It is reasonable, particularly in view of the inverse relationship of Figure 5 between these and the second oxygen radical signal, to attempt to assign them to an electron donor impurity. Furthermore, no oxygen radicals were found on oxidized impurity-free sodium zeolite. The most probable electron donor impurity was iron and the iron content of NaHY(I) was 0.07% (dry basis). The spectrum of iron-doped zeolite FeNaHY(I) was, however, quite different from those shown in Figure 6.

After some trial and error it was concluded that the new esr signals of Figure 6 were due to Cu(II) impurity. There was good agreement with the $g_\perp$ lines of copper-exchanged zeolites containing the same degree of sodium decationa-

(9) M. Setaka and T. Kwan, *Bull. Chem. Soc. Jap.*, 43, 2727 (1970).

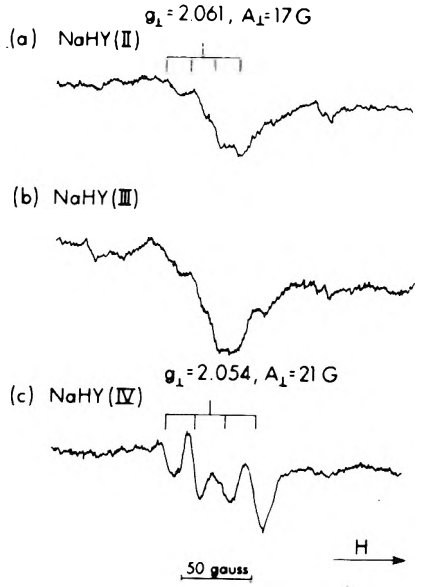

Figure 6. Esr spectra of the oxidized samples: (a) NaHY(II), (b) NaHY(III), and (c) NaHY(IV). g values and splitting constants assigned to spectra are based on spectra obtained with CuNaHY(I), CuNaHY(III), and CuNaHY(IV), respectively.

tion (Figure 7). The $g_{\parallel}$ lines of Cu(II) (see Figure 8) were not observed in the NaHY zeolites because of the low concentration of copper impurity. The zeolites of which the spectra are shown in Figures 5 and 6 must all have had nearly the same concentration of impurity copper since tests on the solution showed that no significant copper ion was removed during the preparation of the samples from NaHY(I).

Figure 7 shows the $g_\perp$ region of esr spectra for copper(II) ion contained in sodium Y-type zeolites. The absorption line at g = 2.008 indicates the second oxygen radical. The radical was not produced on CuNaHY(I) samples with sodium decationation levels of 5% or greater. The radical was formed and increased as more sodium cations were added to the sample as shown in Figure 7b, 7c, and 7d, although it decreased for sample CuNaHY(I)-Na(IV) having the most intensive NaOH treatment (Figure 7e). The treatment of NaHY(I) with 0.2 N NaOH solution did not increase the formation of the oxygen radical significantly. The intensity of signal from copper(II) ion decreased with the increase of sodium cation content. The same observation was made on the lithium and the potassium forms of Y-type zeolites where no oxygen radical was produced on the potassium forms. A further illustration of the decrease in the copper signal is shown by the $g_{\parallel}$ absorption lines illustrated in Figure 8 for the same sequence of samples as for Figure 7. If the data of Figures 7 and 8 were plotted in the form of Figure 5 the variation in oxygen and Cu(II) signals with Na^+ content would be qualitatively similar to the curves of Figure 5 but restricted to the decationation range below 5%, and with the exception that the oxygen curve would show a maximum and then a decrease toward the left-hand ordinate (corresponding to samples CuNaHY(I)-Na(III) and CuNaHY(I)-Na(IV)). The method of preparation of the samples for Figure 7 did not permit a quantitative determination of the exact extent of decationation. The highest spin concentration of the oxygen radical on the copper-exchanged zeolite (on CuNaHY(I)-Na(III)) was about eight times greater than that produced

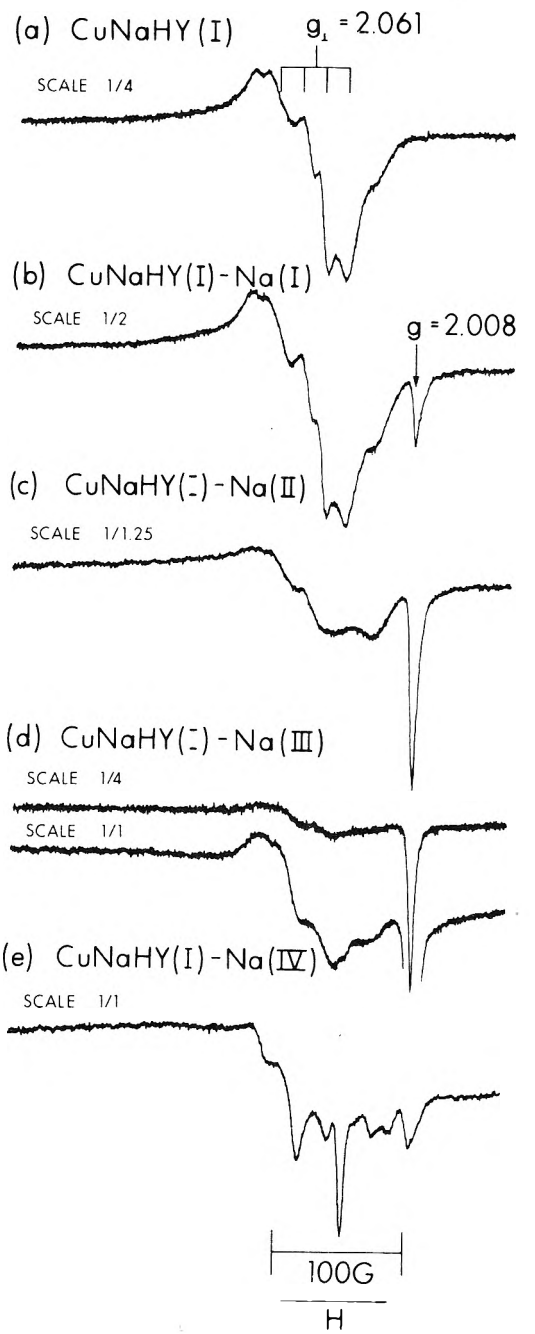

Figure 7. Esr spectra of $g_\perp$ absorption line region. Effects of sodium ion content on the $g_\perp$ signal of Cu(II) ion and the formation of the second oxygen radical (g = 2.008).

on NaHY(I), whereas the amount of copper ion in this sample was about 70 times more than the impurity copper in NaHY(I).

The results of esr studies of copper-exchanged zeolites by several workers[10-14] show that the spectra are influenced by the degree of dehydration and the temperature of heat treatment and by the nature and amount of the other cations in the zeolite. All of the previous authors found at least two distinct Cu(II) species. At least two

(10) A. Nicula, D. Stamires, and J. Turkevich, *J. Chem. Phys.*, **42**, 3684 (1965).
(11) I. D. Mikheikin, V. A. Shvets, and V. B. Kazanskii, *Kinet. Katal.*, **11**, 747 (1970).
(12) C. Naccache and Y. B. Taarit, *Chem. Phys. Lett.*, **11**, 11 (1971).
(13) H. B. Slot and J. L. Verbeck, *J. Catal.*, **12**, 216 (1968).
(14) J. Turkevich, Y. Ono, and J. Soria, *J. Catal.*, **25**, 44 (1972).

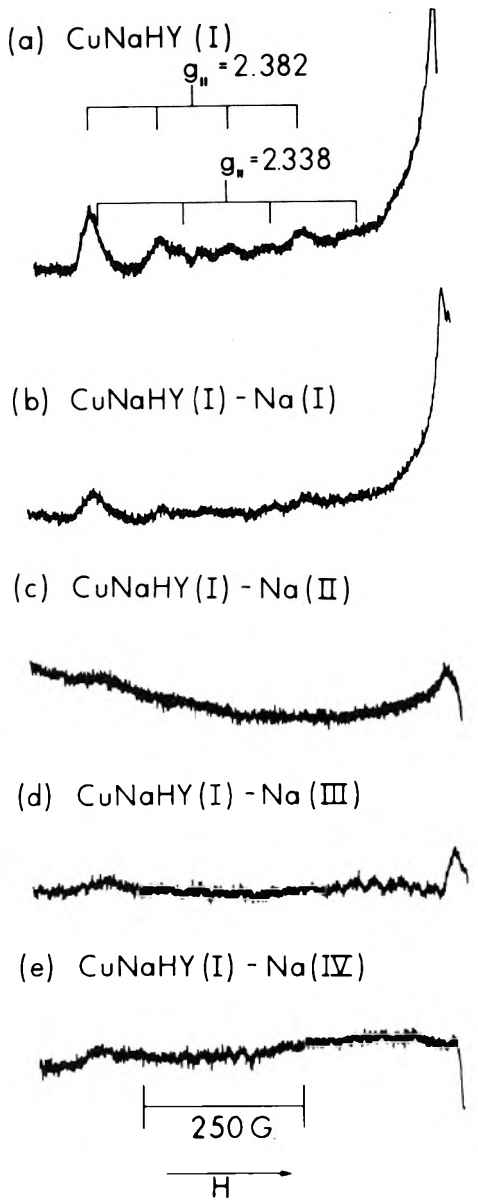

Figure 8. Esr spectra of $g_{\parallel}$ signal of Cu(II) ion. Effect of sodium ion content on $g_{\parallel}$ signal of Cu(II) ion.

species was also observed in this study (see Figure 8, $g_{\parallel}$ = 2.382 (major) and $g_{\parallel}$ = 2.338 (minor)), and the selectivity in the formation of these two species was affected by the sodium decationation as shown in Figure 6. The detailed presentation of our observation on copper-exchanged zeolites will be published separately.

An attempt was then made to observe some electron-donating properties associated with iron by doping NaHY(I) with higher quantities of Fe ion than the 0.07% present as an impurity. All oxidized samples showed the same broad signal due to Fe(III) ion as that previously found on dehydrated Y-type zeolite and mordenite.[15] The signal of Fe(III) ion was, however, not further studied since its intensity was two to three orders higher than the second oxygen radical and the change of the intensity was insignificant relative to the amount of the oxygen radical. The sample FeNaHY(I) had a higher degree of decationation than the copper-doped sample (15% *vs.* about 5%; see Table I) but still gave, after oxidation, the signal of the second oxygen radical at 65% of the intensity of that for NaHY(I) whereas CuNaHY(I) was decationated to an extent that no oxygen radical was observed. A higher concentration of the oxygen radical (three times that on NaHY(I)) was found on oxidized FeNaY(I)-Na(III) showing the enhancement by sodium ion.

Discussion

Previous workers have concluded that the superoxide ion O_2^- is produced when the Y-type zeolite is irradiated in an atmosphere of oxygen.[2-5] In the present study, the first oxygen radical (Figure 1a) which was thermally produced was identical with that produced by γ-ray irradiation indicating that this species could be the superoxide ion. The difference in the esr spectra between the sodium and the lithium Y-type zeolites is possibly due to the adsorption of this species on the cation. Kasai[2] found that the superoxide ion produced on NaY had the values of g_x = 2.0016, g_y = 2.0066, and g_z = 2.113. Wang and Lunsford[4] did not observe the esr absorption line at g_z = 2.113 for the same system but found three g_z lines at 2.098, 2.074, and 2.040. Their other values, g_x = 2.002 and g_y = 2.007, agreed with those of Kasai. The g_z absorption line, in this study, was not observed on NaHY(I) but appeared on LiY. The other values on NaHY(I), g_x = 2.003 and g_y = 2.011, were slightly higher than those found by the previous workers. This species was completely destroyed at 300°. Kasai also found that the O_2^- species was rapidly destroyed if the sample was heated higher than 150°.

The second oxygen radical (Figure 1d) was stable under evacuation at 500°. This species must have had a strong bonding with the surface of the zeolite. The result of esr line-broadening experiments indicates that most of this species was located in the β cage. The differences of the spectra of this species within the series NaHY(I) and the LiY- and KY-zeolites show the participation of the cation. The second oxygen radical was not produced on the potassium forms of Y-type zeolites. The oxygen radical might be stable on Li^+ and Na^+ because of their higher electrostatic field properties (ionic radii: Li^+ 0.68 Å, Na^+ 0.97 Å, and K^+ 1.33 Å).

In view of the various observations, we believe that only two possible oxygen species are worthy of serious consideration, either O^- or O_2^-, each tightly associated with the cation, that is a metal-deficient oxide or peroxide radical such as Na-O· or Na-O-O·. Wang and Lunsford[4] considered that a V-type center was formed in the β cage of CaY when a cation defect such as Ca^+-O^- trapped a hole.

The two possibilities, O^- and O_2^-, could be distinguished by experiments with ^{17}O as has been demonstrated by Tench and Holroyd[16] and also by Wong and Lunsford[17,18] for oxygen on MgO.

The formation of the oxygen radicals requires an electron-transfer reaction on the surface of the zeolite. In attempting to decide the mechanism of electron donation for the formation of the second oxygen radical, the following factors should be considered. The oxygen radical was formed only on the sodium and the lithium Y-type zeolites which contained impurity transition-metal ions such as iron and copper and the formation of the oxygen

(15) B. D. McNicol and G. T. Pott, *J. Catal.*, **25**, 223 (1972).
(16) A. J. Tench and P. J. Holroyd, *Chem. Commun.*, 471 (1968).
(17) Ning-Bew Wong and J. H. Lunsford, *J. Chem. Phys.*, **55**, 3007 (1971).
(18) Ning-Bew Wong and J. H. Lunsford, *J. Chem. Phys.*, **56**, 2664 (1972).

radical was increased by adding a small amount of Cu(II) or Fe(II) ions. The oxygen radical was formed only at high levels of Na^+ or Li^+ content (or at low concentration of hydrogen ions) on the zeolite surface. There was an inverse relation between the oxygen radical and the Cu(II) ion as illustrated by Figure 5; the spin concentration of the oxygen radical increased and that of Cu(II) ion decreased with increasing Na^+ content in NaHY samples. The same trend was found on copper-exchanged zeolites when the samples were doped with NaOH or LiOH. On the other hand, when the zeolites were treated with higher concentrations of alkali metal hydroxides both the oxygen and copper signals decreased and in the case of KY which formed no oxygen radical there was still a decrease in the Cu(II) signal.

The above observation seems to show that the iron and the copper ions can be the electron donors. The oxidation of Fe(II) ion occurs readily and an electron can be liberated in the step Fe(II) $\rightarrow$ Fe(III) + e^-. In the case of copper-containing zeolites the inverse relationship between Cu(II) and the second oxygen species shown in Figure 5 suggests that the electron-donating reaction is Cu(II) $\rightarrow$ Cu(III) + e^-. The unusual three-valent state of copper is known in the crystalline cuprates;[19] *e.g.*, K Cu(III)O_2 is produced when a mixture of KO_2 and CuO is heated for 24 hr at 400–500° in an atmosphere of oxygen.[20] The decrease in the second oxygen signal accompanying the strongest NaOH treatment (sample CuNaHY(I)–Na(IV), Figure 7) could be due to the inactivation of Cu(II) as an electron donor by this treatment with NaOH, perhaps by the aggregation of Cu(II) ion as an oxide or hydrated oxide which is no longer in a suitable site for electron donation. The corresponding absence of an increase in the Cu(II) signal would be explained by line broadening. In fact a considerable degree of line broadening must be present in all cases because the observed Cu(II) signal was at most only about 4% of the total copper concentration (in the case of the samples containing only impurity copper).

We believe the results given here point strongly to transition metal ions as electron donors in zeolites but the principal question remaining is why is the presence of the most highly mobile lithium or sodium ions in the zeolite structure essential to the electron transfer reaction (or, conversely, how do small traces of protons inhibit this transfer)?

Acknowledgment. The authors thank Dr. K. F. Schulz for continued help and discussions on esr techniques. We are also grateful to Dr. J. H. Lunsford of Texas A & M University for some helpful suggestions. The analyses of the zeolites were made by Mr. M. D. Rawluk.

(19) F. A. Cotton and G. Wilkinson, "Advanced Inorganic Chemistry," Interscience, New York, N. Y., 1966, p 707.
(20) K. Wahland and W. Klemm, *Z. Anorg. Allg. Chem.*, **270**, 69 (1952).

Pressure Dependence of Equilibrium Constants in Aqueous Solutions

Neil A. North

Institute of Oceanography, Dalhousie University, Halifax, Nova Scotia, Canada *(Received May 15, 1972)*

Publication costs assisted by The National Research Council of Canada

An expression for the pressure dependence of equilibrium constants in aqueous solutions is derived by considering solutes to be hydrated and incompressible. The expression so derived agrees well with the experimental data for the ionization of weak acids and bases for pressures of up to 12,000 bars. The pressure dependence of the volume change for a reaction is shown to be a function of the number of solvated water molecules released in the course of the reaction.

The basic equation for the pressure dependence of equilibrium constants is Planck's equation,[1] $RT(\partial \ln K/\partial P)_T = -\Delta V$, which relates the pressure dependence to the difference in the partial molal volumes of the product and reactant species. When this equation is applied to experimental data, ΔV is found to vary with pressure. This pressure dependence is described by the equation $(\partial \Delta V/\partial P)_T = \Delta K$, where ΔK is the difference in the partial molal isothermal compressibilities of the product and reactant species. ΔK is also found experimentally to be pressure dependent.

By assuming that the difference in compressibilities was independent of pressure, for pressures up to 2000 bars, Lown, Thirsk, and Wynne-Jones[2] derived the following equation for the pressure dependence of equilibrium constants

$$RT \ln (K_p/K_0) = -\Delta \overline{V}^0(P - 1) + \tfrac{1}{2}\Delta \overline{K}^0(P - 1)^2 \quad (1)$$

where $\Delta \overline{V}^0$ is the volume difference at atmospheric pressure and $\Delta \overline{K}^0$ is the corresponding partial molal isothermal compressibility difference. This equation was found to provide a good fit, up to 2000 bars, to the experimental data for the ionization of weak acids and bases. Above

(1) M. Planck, *Ann. Phys.*, **32**, 462 (1887).
(2) D. A. Lown, H. R. Thirsk, and L. Wynne-Jones, *Trans. Faraday Soc.*, **64**, 2073 (1968).

2000 bars deviations from eq 1 are observed. Both Planck's and Lown, *et al.*'s, equations are derived from classical thermodynamics and consequently provide no information on the molecular basis of $\Delta\overline{V^0}$ and $\Delta\overline{K^0}$.

In this paper a simple model for hydrated solutes has been used to derive an expression for the pressure dependence of equilibrium constants in aqueous solutions. A solute in aqueous solution is considered to consist of a central solute molecule surrounded by a number of bound water molecules. The number of water molecules bound to the solute molecule and the volume of the hydrated solute, that is the volume of the solute molecule plus that of its hydration shell, are assumed to be independent of pressure. Water molecules released from the solute hydration sheaths during the course of a reaction are treated in the same manner as other product and reactant species. This approach is similar to that adopted by Marshall.[3]

Pressure Dependence of Equilibrium Constants

The partial molal volumes of solutes in aqueous solutions are usually defined as the volume change produced when 1 mol of the anhydrous solute is added to an infinite volume of water. With this definition, the partial molal volume ($\overline{V_k^p}$) of species k at pressure p can be considered to consist of two parts

$$\overline{V_k^p} = V_{k(I)}^p - V_{k(EI)}^p \tag{2}$$

where $\overline{V_{k(I)}^p}$ is the intrinsic volume of the solute molecule and $\overline{V_{k(EI)}^p}$ is the decrease in the volume of the solvated water molecules associated with species k.

The hydrated partial molal volume of species k (V_k) is the volume of the solute molecule plus that of the associated hydration sheath. This volume consists of

$$V_k = V_{k(I)}^p + n_k V_w^p - V_{k(EI)}^p \tag{3}$$

where n_k is the number of water molecules in the hydration sheath of species k and V_w^p is the molal volume of free water at pressure p. In this paper we have considered the hydrated partial molal volumes to be pressure independent. At atmospheric pressure the relationship between the hydrated and the normal partial molal volumes is seen from eq 2 and 3 to be

$$V_k = \overline{V_k^0} + n_k V_w^0 \tag{4}$$

For the general equilibrium

$$\text{reactants (solvated)} \rightleftharpoons \text{products (solvated)} - n\text{H}_2\text{O} \tag{5}$$

in aqueous solution, equilibrium constants can be written which either include the change in the number of solvated water molecules (*e.g.*, Marshall[3]) or omit this change. As the concentration of water is constant, when expressed on a molal basis, these two equilibrium constants will differ only by a constant and will have the same pressure dependence. On a hydrated solute basis the partial molal volume change for eq 5 is given by

$$\Delta V^p = V_{(\text{products})} - nV_w^p - V_{(\text{reactants})} \tag{6}$$

at pressure p. This volume change can be expressed in terms of the usual partial molal volumes by using eq 4

$$\Delta V^p = \Delta\overline{V^0} - n(V_w^p - V_w^0) \tag{7}$$

where $\Delta\overline{V^0}$ is the difference in the normal partial molal volumes at atmospheric pressure of the product and reactant species, excluding the water molecules.

By combining eq 7 with Planck's equation we obtain

$$RT(\partial \ln K/\partial P)_T = -\Delta\overline{V^0} + n(V_w^p - V_w^0) \tag{8}$$

The molal volume of water as a function of pressure is given by the integrated form of Tait's isotherm

$$V_w^p = V_w^0\left(1 - A \ln \frac{B + P}{B + 1}\right) \tag{9}$$

where A and B are constants independent of pressure. The values of A and B have been determined experimentally by Gibson and Loeffler[4] for temperatures between 0 and 85°.

By substituting for V_w^p in eq 8 and integrating with respect to pressure, the equation

$$\frac{RT}{(P-1)} \ln (K_p/K_1) = -\Delta\overline{V^0} + nAV_w^0\left\{1 - \frac{B+P}{P-1} \ln \frac{B+P}{B+1}\right\} \tag{10}$$

is obtained.

Discussion

The validity of eq 10 can readily be tested by plotting the left-hand side of this equation against

$$AV_w^0\left(1 - \frac{B+P}{P-1} \ln \frac{B+P}{B+1}\right)$$

using experimental values for the equilibrium constants. The resulting plot should be linear with a slope of n and an intercept at atmospheric pressure of $-\Delta\overline{V^0}$. Figures 1,[2]2,[5] and 3[6] show these plots for the ionization constants of acetic acid, water, and ammonia, respectively, at 298 K. Figure 4[7] shows the ionization of ammonia at 318 K.

In all cases eq 10 is seen to fit the experimental results very well, even for pressures up to 12,000 bars. The values of $\Delta\overline{V^0}$ and n obtained from these figures are shown in Table I, together with values obtained by other workers from studies at atmospheric pressure. For all of the ionization reactions studied, the value of n was found to be positive. This indicates, as would be expected, that the charged species are more heavily hydrated than are the uncharged species.

Using eq 4, it is possible to express the partial molal isothermal compressibilities in terms of the hydration number. From eq 4

$$\overline{K_k^p} = -\left\{\frac{\partial\overline{V_k^p}}{\partial P}\right\}_T = -\left\{\frac{\partial}{\partial P}(V_k - n_k V_w^p)\right\}_T \tag{11}$$

Since V_k and n_k have been assumed to be independent of pressure

$$\overline{K_k^p} = \frac{-n_k AV_w^0}{(B+P)} \tag{12}$$

and for the overall reaction

$$\Delta\overline{K^p} = \frac{-nAV_w^0}{(B+P)} \tag{13}$$

(3) W. L. Marshall, *J. Phys. Chem.*, **74**, 346 (1970).
(4) R. E. Gibson and O. H. Loeffler, *J. Amer. Chem. Soc.*, **63**, 898 (1941).
(5) S. D. Hamann, *J. Phys. Chem.*, **67**, 2233 (1963).
(6) J. Buchanan and S. D. Hamann, *Trans. Faraday Soc.*, **49**, 1425 (1953).
(7) S. D. Hamann and W. Strauss, *Trans. Faraday Soc.*, **51**, 1684 (1955).

TABLE I: Comparison of the Values of $\Delta\overline{V^0}$, n, and $\Delta\overline{K^0}$ Obtained from the Pressure Dependence of the Equilibrium Constants with Those Obtained by Other Methods

Electrolyte	Temp, K	This work			Literature values	
		ΔV^0, cm^3 mol^{-1}	n	$\Delta K^0 \times 10^3$, cm^3 mol^{-1} bar^{-1}	ΔV^0, cm^3 mol^{-1}	$\Delta K^0 \times 10^3$,[a] cm^3 mol^{-1} bar^{-1}
Water	298	−20.8	5.2	−4.2	−22.1[b]	−5.2
Acetic acid	298	−11.2	2.3	−1.9	−11.5[c]	−1.7
Ammonia	298	−29.4	8.0	−6.6	−29.4[d]	
Ammonia	318	−27.0	5.9	−4.9		

[a] B. B. Owen and S. R. Brinkley, *Chem. Rev.*, **29**, 461 (1941). [b] L. A. Dunn, R. H. Stokes, and L. G. Hepler, *J. Phys. Chem.*, **69**, 2808 (1965). [c] E. J. King, *J. Phys. Chem.*, **67**, 2233 (1963). [d] S. D. Hamann, "High Pressure Physics and Chemistry," Vol 2, R. S. Brandley, Ed., Academic Press, London, 1963.

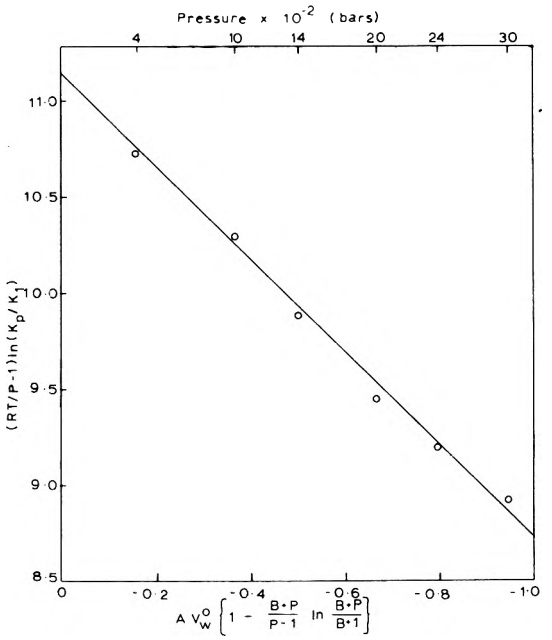

Figure 1. Pressure dependence of the ionization constant of CH_3COOH at 298 K, data taken from ref. 2.

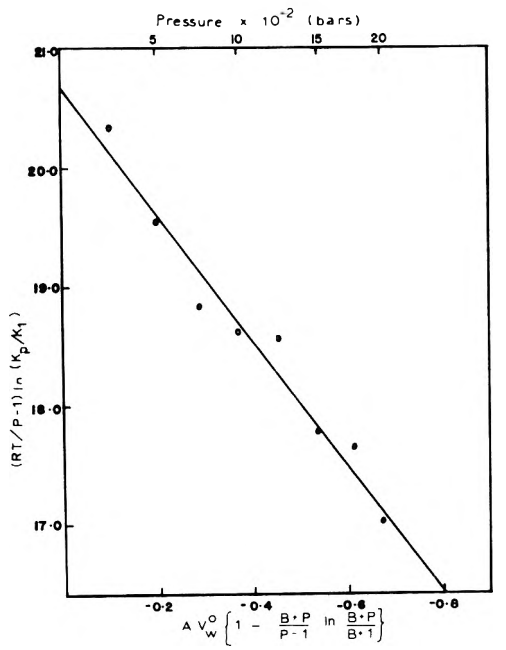

Figure 2. Pressure dependence of the self-ionization of water at 298 K, data taken from ref. 5.

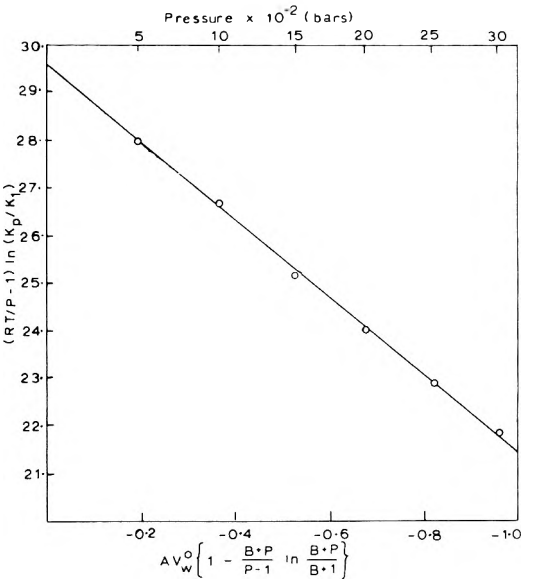

Figure 3. Pressure dependence of the ionization constant of NH_4OH in water at 298 K, data taken from ref. 6.

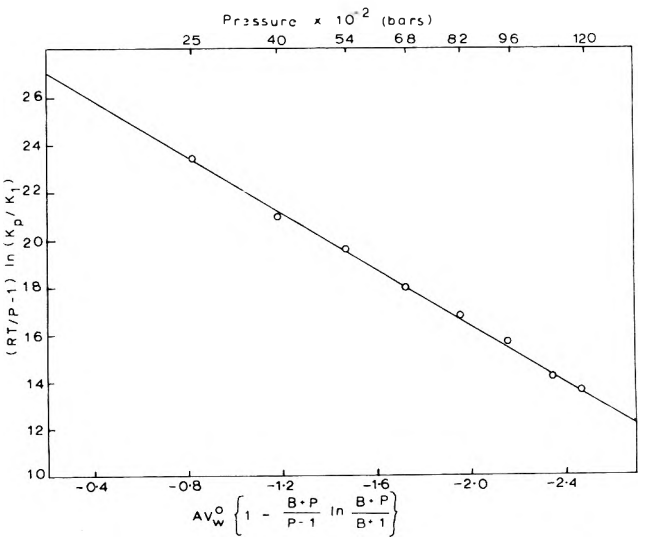

Figure 4. Pressure dependence of the ionization constant of NH_4OH at 318 K, data taken from ref. 7.

The values of $\Delta\overline{K^0}$ for the ionization reactions of water, acetic acid, and ammonia, calculated from eq 13 using the values of n obtained from Figures 1–4, are shown in Table I together with the corresponding values, where known, obtained by other workers from compressibility studies.

The agreement between the two values is seen to be quite good.

According to eq 13, $\Delta\overline{K^p}$ will be pressure dependent. For pressures below 2000 bars, this pressure dependence is small (at 298 K, $\Delta\overline{K^{2000}}$ is approximately 65% of $\Delta\overline{K^0}$) and this allows for the approximation made by Lown, *et al.*, that $\Delta\overline{K^p}$ was independent of pressure up to 2000 bars. At pressures greater than 2000 bars the pressure dependence of $\Delta\overline{K^p}$ becomes significant and consequent deviations from Lown, *et al.*'s, equation are observed. The relationship between $\Delta\overline{V^0}$ and $\Delta\overline{K^0}$ observed by Lown, *et al.*, is seen, from eq 13, to be a relationship between the volume change and the number of solvated water molecules released. A relationship of this nature has been proposed by Marshall.[3]

Conclusion

By considering solutes in aqueous solutions to be hydrated and incompressible, an equation for the pressure dependence of the equilibrium constants was derived. In this equation the parameters are the difference in the partial molal volumes of the product and reactant species at atmospheric pressure and the number of solvated water molecules released in the reaction.

The equation so derived was shown to provide a good fit to experimental data for the ionization of weak acids and bases for pressures up to 12,000 bars. The values of $\Delta\overline{V^0}$ and $\Delta\overline{K^0}$, as determined using this equation, were found to be in agreement with values obtained by other workers using different methods. The value of $\Delta\overline{K^0}$ was shown to be dependent only on the difference in the hydration numbers of the product and reactant species.

Acknowledgments. The author wishes to thank Dr. P. J. Wangersky for comments and suggestions on this work. The author wishes to acknowledge support of a post-doctoral fellowship from Dalhousie University for this study.

Isothermal Diffusion Studies of Water–Potassium Chloride–Hydrogen Chloride and Water–Sodium Chloride–Hydrogen Chloride Systems at 25° [1]

Hyoungman Kim,* Gundega Reinfelds, and Louis J. Gosting[2]

Institute for Enzyme Research, University of Wisconsin, Madison, Wisconsin 53706 *(Received November 2, 1972)*

Publication costs assisted by the National Institute of Arthritis and Metabolic Diseases

Sets of four diffusion coefficients were experimentally obtained for several compositions of systems of H_2O–KCl–HCl and H_2O–NaCl–HCl. These were compared with values predicted according to methods developed by Miller; reasonably good agreement was observed. The calculation of the diffusion coefficients was then extended over the entire composition of H_2O–KCl–HCl and H_2O–NaCl–HCl systems for total concentrations of 1 and 2 *N*. The diffusion behavior of these systems was discussed in light of electrostatic interactions between ions.

Introduction

Aqueous solutions of electrolytes show some of the largest solute–solute flow interactions known so far. The major contribution to this interaction comes from the primary charge effect[3] and the cross-term diffusion coefficients depend to a large extent on the difference in mobilities of the cations and anions.[4] Therefore, it is expected that electrolyte systems containing acids should have particularly large cross-term diffusion coefficients and this has been demonstrated in systems containing weak acids.[5,6] The present study was undertaken to systematically investigate the well-defined systems of H_2O–KCl–HCl and H_2O–NaCl–HCl over a wide range of compositions in order to elucidate the general diffusion behavior of ternary systems which consist of three ionic species.

Diffusion studies of multicomponent systems including acids are also of considerable importance for biological transport because in a number of biological systems cation transport is accompanied by a concomitant transport of protons.[7]

Experimental Section

Materials. Baker and Du Pont reagent grade HCl was used to prepare constant boiling hydrochloric acid. Gravi-

(1) Part of this work was presented at the 162nd National Meeting of the American Chemical Society, Washington, D. C., Sept 1971. This investigation was supported in part by Public Health Service Research Grant No. AM-05177 from the National Institute of Arthritis and Metabolic Diseases.

(2) Deceased May 30, 1971. Recipient of PHS Research Career Award, AM-K6-16,715.

(3) I. J. O'Donnel and L. J. Gosting in "Structure of Electrolytic Solutions," W. J. Hamer, Ed., Wiley, New York, N. Y., 1959, Chapter 11.

(4) L. J. Gosting, *Advan. Protein Chem.*, **11**, 536 (1956).

(5) R. P. Wendt, *J. Phys. Chem.*, **66**, 1279 (1962).

(6) O. W. Edwards, R. L. Dunn, J. D. Hatfield, E. O. Huffman, and K. L. Elmore, *J. Phys. Chem.*, **70**, 217 (1966).

(7) See, for example, R. N. Robertson, "Protons, Electrons, Phosphorylation, and Active Transport," Cambridge University Press, New York, N. Y., 1968.

metric analysis of its chloride content agreed within the experimental error of analysis (±0.1%) with the composition calculated using the atmospheric pressure measured during the preparation of the constant boiling HCl.[8] The same batch of constant boiling HCl was used for all experiments at a given composition of the ternary system. Certified ACS grade Fisher NaCl was recrystallized once from H_2O, centrifugally drained, and fused in a platinum dish. Matheson Coleman and Bell Reagent grade (for calomel cells) KCl was purified using the same procedure as for NaCl. The purity of all three materials was tested by making free diffusion experiments of binary systems. The areas under the fringe deviation graphs for these experiments were all less than 2×10^{-4}. The molecular weights used are 18.016 for water, 74.555 for KCl, 58.443 for NaCl, and 36.461 for HCl.

Solutions. All solutions were prepared with distilled water which had been further purified using a Barnstead water purifier and then saturated with air. The density values used to calculate the air-buoyancy corrections in preparing the solutions were 1.102 for constant boiling HCl, 1.984 for KCl, 2.165 for NaCl, and 8.4 g/ml for the metal weights of the balances.

In order to prepare each solution to a predetermined composition, preliminary density measurements were made to obtain the density derivatives, H_i, of the expression

$$d = d(\tilde{C}_1,\tilde{C}_2) + H_1(C_1 - \tilde{C}_1) + H_2(C_2 - \tilde{C}_2) \qquad (1)$$

where d is the density of the solution; $d(\tilde{C}_1,\tilde{C}_2)$ is the density of a solution in which the molar concentrations of solutes 1 and 2 are $\tilde{C}_1$ and $\tilde{C}_2$, respectively. The densities were measured (usually in triplicate) at 25 ± 0.005° with 30 ml, single-necked Pyrex pycnometers which had been calibrated with air-saturated, Barnstead-purified distilled water. The density of this water was taken as 0.997075 g/ml.

Diffusion. The optical diffusiometer used in this study will be described elsewhere[9] and therefore only a brief account will be given here. This new diffusiometer is similar to the earlier model[10] but was designed to improve precision and versatility. Each optical component is mounted on a rider which is clamped onto dove-tail ways. The stainless steel ways are in turn bolted to a 884-cm-long steel beam.

A GE mercury vapor lamp, a condenser lens, and a Gaertner bilateral adjustable source slit are mounted on a stainless steel tube in the light source assembly. The illuminated source slit can be set to be either horizontal or vertical by rotating the tube. The water bath and stirring motor unit are supported from structural steel tubing which is bolted to the floor and ceiling of the laboratory; thus the bath and motor are isolated from the optical components, *i.e.*, the main collimating lens and the four bath windows. The seal between the windows and water bath is made by rubber bellows which allow minor movements of the water bath relative to the ways without causing strains. The cylinder lens is supported in a lens housing and it can be easily swung in or out of the light path as required for Rayleigh or Gouy optics, respectively. A glass cell (cell thickness a = 2.4938 cm and the optical lever arm b = 308.904 cm) and a fused quartz cell (a = 2.5075 cm, b = 308.868 cm) of Tiselius type were used for the experiments. The general procedure for the diffusion experiments was the same as was used with the previous diffusiometer.[11] In each experiment the initial boundary between the less dense upper solution (denoted by A) and the more dense lower solution (denoted by B) was formed in the cell by sharpening with a single-prong platinum capillary fixed to a T-shaped three-way Teflon stopcock. For both δ corrections and the fractional part of the total number of fringes, J, photographs were made using Kodak Metallographic glass plates. During free diffusion, 6 to 12 photographs of Gouy fringes were taken on Kodak Spectroscopic IIIG glass plates. One or two Rayleigh photographs were also taken.

The measurements of the photographic plates were made with a photoelectric null indicator[12,13] mounted on a Gaertner Model M2001RS-B toolmakers microscope. This microscope is provided with two encoders and each axis position is displayed on a Tyco Digi-Point readout to the nearest 0.0001 cm. The Digi-Point readout is connected to an IBM No 29 keypunch through an interface (Instrumentation Systems Center, University of Wisconsin) and the displayed numbers on the Digi-Point readout were directly punched onto data cards. The necessary calculations were made with a Univac 1108 digital computer at the University of Wisconsin Computation Center. The Fortran program used was a modification of the program kindly provided by Dr. Ellerton.[14] A subroutine for obtaining C_t values from extrapolation of $Y_j/\exp(-\xi_j^2)$ *vs.* Z_j^2 [3] (for fringes j = 0,1, ···, 6,10,15) curves using the least-squares method was incorporated into the main program by Dr. L. A. Loewenstein of this laboratory eliminating the necessity of plotting the curves.[11]

The temperature of the water bath was measured during diffusion with a mercury-in-glass thermometer which had been calibrated against a platinum resistance thermometer. The temperature of the water bath during diffusion runs was within ±0.005 of 25° and never fluctuated by more than 0.002° during a run.

Results

The primary data from the diffusion experiments for two compositions of the H_2O–KCl–HCl system and three compositions of H_2O–NaCl–HCl system will be found in the microfilm edition of this journal.[15] Table I gives the volume-fixed diffusion coefficients, $(D_{ij})_V$, obtained from the primary data. This table also includes the partial molal volumes, $\bar{V}_i$, the refractive index derivatives, R_i, the density derivatives, H_i, and densities, $d(\tilde{C}_1,\tilde{C}_2)$, at the prefixed mean molar concentrations, $\tilde{C}_i$. The solvent-fixed diffusion coefficients, $(D_{ij})_0$, obtained using these data are also given.

The results of the experiments described here were rou-

(8) I. M. Kolthoff and E. B. Sandell, "Textbook of Quantitative Inorganic Analysis," 3rd ed, Macmillan, New York, N. Y., 1956, Table LXX, p 521.
(9) L. J. Gosting, H. Kim, M. A. Loewenstein, G. Reinfelds, and A. Revzin, manuscript in preparation.
(10) L. J. Gosting, E. M. Hanson, G. Kegeles, and M. S. Morris, *Rev. Sci. Instrum.*, **20**, 209 (1949).
(11) See, for example, L. A. Woolf, D. G. Miller, and L. J. Gosting, *J. Amer. Chem. Soc.*, **84**, 317 (1962).
(12) R. P. Wendt, Ph.D. Thesis, University of Wisconsin, 1961.
(13) J. G. Albright, Ph.D. Thesis, University of Wisconsin, 1963.
(14) H. D. Ellerton, Ph.D. Thesis, University of Adelaide, Adelaide, South Australia, 1965.
(15) These tables will appear following these pages in the microfilm edition of this volume of the journal. Single copies may be obtained from the Business Operations Office, Books and Journals Division, American Chemical Society, 1155 Sixteenth St., N.W., Washington, D.C. 20036. Remit check or money order for $3.00 for photocopy or $2.00 for microfiche, referring to code number JPC-73-934.

tinely examined to determine whether the systems had been gravitationally stable throughout the duration of diffusion. Values for gravitational criteria I and II described in earlier publications from this laboratory[16] were calculated for each experiment. The values of these criteria are greater than or equal to zero if there is gravitational stability throughout the cell at all times. In particular, criterion I refers to the ends of the boundary and criterion II to the level of the initial boundary position.[17] All of the experiments were found to satisfy these criteria with the exception of the system H_2O–KCl(1.0 *N*)–HCl(0.1 *N*), where criterion I is violated by all four experiments.

This is the first report of observed gravitational instability in an initially stable ternary free diffusion experiment. Thus it also serves to indicate what experimental abnormalities might be observed due to gravitational instability. The fringe patterns of all four experiments appeared normal and the fringe positions were measured in the usual ways; the extrapolations to obtain values for C_t were also normal. For the experiment with $\Delta C_1 = -0.00003$ and $\Delta C_2 = 0.12999$, however, the plot of $\mathfrak{D}_A'$ *vs.* $1/t'$, instead of being linear as in a normal case, was curved, and the values of the fringe deviations, instead of remaining constant with increasing time, decreased steadily and quite rapidly. Here ΔC_i is the initial concentration difference in moles per liter between upper and lower solutions, $\mathfrak{D}_A'$, is the reduced height-area ratios, and t' is the observed time after formation of a boundary. The last three experiments seemed normal in all respects. Thus, at least in this case, a certain amount of convective mixing due to gravitational instability in the system produces no discernable experimental problems and the $(D_{ij})_v$ values reported here were calculated from these last three experiments. It is reasonable to assume that their values are reliable because the Onsager reciprocal relation holds within experimental error as will be shown in the next section and the experimental values agree as well as is expected with values predicted by Miller's equations, which will also be discussed.

Discussion

Perhaps the most interesting feature of the diffusion coefficients shown in Table I is the large negative size of the $(D_{12})_v$. This may be ascribed to the fact that the mobility of the proton is much greater than that of the chloride ion and the resulting large electrical potential gradient induces the potassium ion to move against its own concentration gradient. For the same composition (0.3 *N* for component 1 and 0.2 *N* for component 2) the value of $(D_{12})_v$ is larger for the H_2O–KCl–HCl system than for the H_2O–NaCl–HCl system despite the fact that the force produced by unit concentration gradient of HCl is about the same in both cases. This is due to the larger mobility of K^+ as indicated also by the fact that $(D_{12})_v/(D_{11})_v$ is about the same in both systems. On the other hand, the larger $(D_{21})_v$ value in the H_2O–NaCl–HCl system is due to the larger force produced by unit concentration gradient because the mobility difference between Na^+ and Cl^- is larger than that between K^+ and Cl^-.

One notices that the main diffusion coefficient, $(D_{22})_v$, is considerably larger than the diffusion coefficient of binary H_2O–HCl which is less than 4×10^{-5} in the concentration range below 2 *N*. In the binary electrolyte systems of H_2O–HCl, the faster proton ion is slowed by the slower chloride ion in order to maintain the macroscopic electroneutrality condition. In the presence of an additional electrolyte, either NaCl or KCl, the electroneutrality condition imposes less restraint on the proton and thus $(D_{22})_v$ may have the observed larger value than the binary diffusion coefficient.

It is of interest to see whether the Onsager reciprocal relations hold for these systems which have enormously large negative cross-term diffusion coefficients. Table II shows the values of the phenomenological coefficients, $(L_{ij})_0$, calculated with respect to the solvent-fixed frame of reference and the intermediate quantities necessary for these calculations. The general procedure of calculating these values has already been described.[18] The activity coefficients were obtained[19] by assuming that the Harned relationship holds for these ternary electrolyte systems. It is recommended that the reader consult the article by Dunlop and Gosting[18] for the definition of symbols. It can be seen that the $(L_{12})_0$ agree with $(L_{21})_0$ within the estimated experimental error, $\%\Delta_{est}$.

In binary electrolyte systems, diffusion coefficients depend only on the concentration for a given temperature. In ternary systems, however, diffusion coefficients are functions of both the concentration ratio and the total concentration of the solutes. Therefore, for a complete description of the diffusion behavior of a ternary electrolyte system, an enormous number of experiments would have to be made. This is impractical because diffusion experiments of ternary systems are very time consuming. Also the present diffusion techniques cannot be used at very low concentrations or for systems with highly concentration dependent diffusion coefficients without introducing appreciable error. Therefore, it is very useful to have a method of predicting diffusion coefficients.

So far the empirical method developed by Miller[20] seems to give the best results. The essence of this method is the assumption that the ionic transport coefficients, l_{ij}, of binary systems stay the same when another ionic species is introduced. This seems to hold for the systems of H_2O–NaCl–KCl, H_2O–LiCl–KCl, and H_2O–LiCl–NaCl which show excellent agreement between experimental and estimated diffusion coefficients. Table III gives the comparison of the experimental and estimated diffusion coefficients for the systems studied here. Miller used two methods[20] for estimating the $(D_{ij})_v$'s. One is denoted as the LN method and it uses ionic transport coefficients, l_{ij}, determined at a binary concentration equal to the total solute concentration of the ternary system. In the second method, which is called the LNI method, the main ionic transport coefficients of cations are taken at the binary concentration equal to the component concentration in the ternary system; the other l_{ij}'s are taken as in the LN method. Despite the fact that the LN method seems more "natural," for the systems he examined, Miller observed better agreement of experimental and calculated coefficients with the LNI method.

The first part of Table III shows the experimental values and the second part has the estimated values using the first approximation method of Gosting[4] which utilizes limiting ionic mobilities. As expected the agreement with

(16) G. Reinfelds and L. J. Gosting, *J. Phys. Chem.*, **68**, 2464 (1964).
(17) H. Kim, *J. Phys. Chem.*, **74**, 4577 (1970), see footnote 9.
(18) P. J. Dunlop and L. J. Gosting, *J. Phys. Chem.*, **63**, 86 (1959).
(19) H. S. Harned and B. B. Owen, "Physical Chemistry of Electrolyte Solutions," 2nd ed, Reinhold, New York, N. Y., 1950, p 467.
(20) D. G. Miller, *J. Phys. Chem.*, **70**, 2639 (1966); **71**, 616 (1967).

TABLE I:[a] Data for the Four Diffusion Coefficients, Partial Molal Volumes, Density Derivatives, and Refractive Index Derivatives

	System				
	H_2O–KCl–HCl		H_2O–NaCl–HCl		
$\bar{C}_1$	0.3	1.0	0.3	0.5	1.9
$\bar{C}_2$	0.2	0.1	0.2	0.5	0.1
$\bar{C}_0$	54.671	53.639	54.840	54.309	53.200
$\bar{V}_1$	28.62	29.99	18.38	19.08	20.93
$\bar{V}_2$	19.17	19.85	19.23	19.71	20.59
$\bar{V}_0$	18.064	18.047	18.064	18.056	18.011
$d(\bar{C}_1,\bar{C}_2)$	1.014569	1.044529	1.012815	1.025889	1.073140
H_1	0.04601	0.04461	0.04011	0.03941	0.03749
H_2	0.01734	0.01665	0.01728	0.01679	0.01586
$R_1 \times 10^3$	9.7155	9.2626	9.8209	9.5608	8.9649
$R_2 \times 10^3$	8.2846	8.0456	8.2874	8.1208	7.7567
$(D_{11})_v \times 10^5$	1.7865	1.8083	1.2946	1.2233	1.4102
$(D_{12})_v \times 10^5$	−0.9797	−2.0378	−0.6869	−0.4700	−1.1021
$(D_{21})_v \times 10^5$	0.1407	0.1782	0.4779	0.7975	0.2747
$(D_{22})_v \times 10^5$	4.8122	6.8153	4.6306	4.3804	5.9441
$(D_{11})_0 \times 10^5$	1.8028	1.8680	1.3046	1.2432	1.4799
$(D_{12})_0 \times 10^5$	−0.9596	−1.9612	−0.6638	−0.4305	−0.9052
$(D_{21})_0 \times 10^5$	0.1516	0.1842	0.4846	0.8174	0.2784
$(D_{22})_0 \times 10^5$	4.8252	6.8230	4.6460	4.4199	5.9545

[a] Units; partial molal volumes $\bar{V}_i$, ml/mol; diffusion coefficients $(D_{ij})_v$ and $(D_{ij})_0$, expressed as cm^2/sec, correspond to the volume-fixed and solvent-fixed frame of reference, respectively.

TABLE II: Test of Onsager Reciprocal Relations

	System				
	H_2O–KCl–HCl		H_2O–NaCl–HCl		
$\bar{C}_1$	0.3	1.0	0.3	0.5	1.9
$\bar{C}_2$	0.2	0.1	0.2	0.5	0.1
μ_{11}/RT	4.9608	1.7744	5.0764	2.9840	1.2031
μ_{12}/RT	1.9559	1.0936	2.0104	1.2536	0.9546
μ_{21}/RT	1.9215	1.1102	1.9775	1.2563	0.9407
μ_{22}/RT	7.1921	11.3543	7.1517	3.4084	11.0887
$(L_{11})_0RT \times 10^9$	4.640	12.353	3.282	5.564	13.873
$(L_{12})_0RT \times 10^9$	−2.596	−2.917	−1.848	−3.308	−2.011
$(L_{21})_0RT \times 10^9$	−2.563	−2.896	−1.765	−3.240	−2.021
$(L_{22})_0RT \times 10^9$	7.406	6.288	6.973	14.157	5.544
$\%\Delta_{expt}$	1.3	0.7	4.6	2.1	0.5
$\%\Delta_{est}$	5.0	6.0	9.9	6.5	4.9

the experimental values is rather poor but this method does indicate general trends of the values and it is useful for systems where ionic transport coefficients are not available. Except for $(D_{21})_v$, the estimated values are higher than the experimental values. The third part contains the estimated values using Miller's LNI method. It is obvious that the agreement with the experimental values is much better than for the first approximation method. There is, however, a distinct pattern. The agreement is very good for the compositions where the C_1/C_2 values are not far from unity. On the other hand the estimated $(D_{ij})_v$ values are less satisfactory for the systems where the C_1/C_2 values are large. This is to be expected because for systems such as H_2O–NaCl–HCl where the concentration of NaCl is 1.9 N and that of HCl is 0.1, the l_{22} value taken at 0.1 N is very much larger than the value at 2 N. The last part contains the estimated $(D_{ij})_v$ values obtained using Miller's LN method. An improvement was achieved for the systems where C_1/C_2 values are large while for the cases of C_1/C_2 being close to unity, less satisfactory estimates were obtained. From the argument given earlier, it is easy to understand why an improvement was obtained for the former compositions, but it is not obvious why the LNI method should give better results for the latter compositions. Still it may be noted that the LN approximation gives overall better values for $(D_{ij})_v$'s.

In order to examine the complete diffusion behavior of these systems, the LN calculations were extended over the entire range of compositions for total concentrations equal to 1 and 2 N. The results are given in Table IV[21] and in the microfilm edition of this journal.[15] The necessary partial molal volumes were calculated from density data obtained using the method described in the Experimental Section. The activity coefficients are obtained using Harned's rule as before.

In Table IV, where the total concentration of the H_2O–KCl–HCl systems is maintained at 1 N, the concentration

(21) For the sake of brevity, the subscript v is omitted from Table IV and from subsequent discussion.

TABLE III: Comparison of Experimental and Calculated Values of $(D_{ij})_v$

	System				
	H_2O–KCl(0.3 *N*)–HCl(0.2 *N*)	H_2O–KCl(1.0 *N*)–HCl(0.1 *N*)	H_2O–NaCl(0.3 *N*)–HCl(0.2 *N*)	H_2O–NaCl(0.5 *N*)–HCl(0.5 *N*)	H_2O–NaCl(1.9 *N*)–HCl(0.1 *N*)
			Exptl		
$(D_{11})_v \times 10^5$	1.79	1.81	1.29	1.22	1.41
$(D_{12})_v \times 10^5$	−0.98	−2.04	−0.69	−0.47	−1.10
$(D_{21})_v \times 10^5$	0.14	0.18	0.48	0.80	0.27
$(D_{22})_v \times 10^5$	4.81	6.82	4.63	4.38	5.94
			Calcd (Gosting[4])		
$(D_{11})_v \times 10^5$	1.97	1.99	1.42	1.40	1.57
$(D_{12})_v \times 10^5$	−1.23	−2.78	−0.89	−0.66	−2.45
$(D_{21})_v \times 10^5$	0.04	0.01	0.40	0.44	0.09
$(D_{22})_v \times 10^5$	5.40	7.99	5.18	4.70	8.41
			Calcd (Miller LNI[18])		
$(D_{11})_v \times 10^5$	1.79	1.77	1.27	1.20	1.39
$(D_{12})_v \times 10^5$	−0.99	−2.25	−0.66	−0.40	−1.64
$(D_{21})_v \times 10^5$	0.17	0.21	0.48	0.84	0.41
$(D_{22})_v \times 10^5$	4.94	7.55	4.60	4.36	7.99
			Calcd (Miller LN[18])		
$(D_{11})_v \times 10^5$	1.77	1.77	1.26	1.13	1.41
$(D_{12})_v \times 10^5$	−0.88	−1.85	−0.56	−0.34	−0.98
$(D_{21})_v \times 10^5$	0.18	0.20	0.50	0.88	0.33
$(D_{22})_v \times 10^5$	4.81	6.70	4.51	4.24	6.21

TABLE IV: Estimated $(D_{ij})_v$ for H_2O–KCl–HCl System for Total Concentration of 1 *N*

C_1	C_2	C_1/C_2	Log (C_1/C_2)	$D_{11} \times 10^5$	$-D_{12} \times 10^5$	$D_{21} \times 10^5$	$D_{22} \times 10^5$	$-D_{12}/D_{11}$	D_{21}/D_{22}
0.0000	1.0000	0.0000	$-\infty$		0.00		3.44		
0.0001	0.9999	0.0001	−4.000	1.76	0.00	0.43	3.45	0.00	0.12
0.0010	0.9990	0.0010	−3.000	1.76	0.01	0.43	3.45	0.01	0.12
0.0100	0.9900	0.0101	−1.996	1.75	0.01	0.44	3.47	0.01	0.13
0.0500	0.9500	0.0526	−1.279	1.75	0.05	0.45	3.54	0.03	0.13
0.1000	0.9000	0.1111	−0.954	1.73	0.10	0.47	3.63	0.06	0.13
0.2000	0.8000	0.2500	−0.602	1.70	0.22	0.49	3.82	0.16	0.13
0.3000	0.7000	0.4286	−0.378	1.68	0.33	0.50	4.06	0.21	0.12
0.4000	0.6000	0.6667	−0.176	1.67	0.48	0.51	4.33	0.29	0.12
0.5000	0.5000	1.0000	0.000	1.66	0.65	0.49	4.59	0.39	0.11
0.6000	0.4000	1.5000	+0.176	1.67	0.85	0.46	4.95	0.51	0.09
0.7000	0.3000	2.3333	+0.378	1.68	1.11	0.41	5.39	0.66	0.08
0.8000	0.2000	4.0000	+0.602	1.71	1.43	0.33	5.95	0.84	0.06
0.9000	0.1000	9.0000	+0.954	1.78	1.86	0.20	6.69	1.04	0.03
0.9500	0.0500	19.0000	+1.279	1.82	2.14	0.11	7.16	1.18	0.02
0.9900	0.0100	99.0000	+1.996	1.86	2.40	0.02	7.59	1.29	0.00
0.9990	0.0010	999.0000	+3.000	1.87	2.50	0.00	7.71	1.34	0.00
0.9999	0.0001	9999.0000	+4.000	1.88	2.50	0.00	7.73	1.32	0.00
1.0000	0.0000	$+\infty$	$+\infty$	1.89		0.00	7.70		

of KCl increases from zero to 1 *N* downward while the concentration of HCl decreases from 1 *N* to zero. The D_{22} value at $C_2 = 1.0$ is the binary diffusion coefficient of HCl at this concentration and the D_{11} value at $C_1 = 1.0$ is the binary diffusion coefficient of KCl at this concentration. These are taken from the literature.[22] The D_{22} at $C_1 = 1.0$ is the tracer diffusion coefficient and it is also given in the same monograph.[23]

As C_1 approaches 1 *N*, it is expected that the value of D_{11} will approach the binary diffusion coefficient and the excellent agreement of the calculated values with this expectation indicates that the estimated D_{11} values are reliable. As C_2 approaches 1 *N*, D_{11} becomes the diffusion coefficient of a tracer amount of KCl in a 1 *N* HCl solution, and the limiting value of D_{11} should be the tracer diffusion coefficient. Unfortunately an experimental value for this tracer diffusion coefficient is not available. The calculated D_{11} value at this limiting concentration is smaller than the corresponding binary diffusion coefficient (1.999×10^{-5}).[22] This is as expected because, in binary diffusion the K^+ ion is accelerated by the faster moving Cl^- ion. Therefore, the D_{11} values increase as they approach the limiting value at 1 *N*.

(22) R. A. Robinson and R. H. Stokes, "Electrolyte Solutions," 2nd revised ed, Butterworths, London, 1959, p 515.
(23) Reference 22, p 317, Table 11.7.

From the flow equations it is apparent that

$$D_{12} \longrightarrow 0 \text{ as } C_1 \longrightarrow 0 \quad (2a)$$

$$D_{21} \longrightarrow 0 \text{ as } C_2 \longrightarrow 0 \quad (2b)$$

From Table IV it is clear that these conditions are met. Each calculated cross-term diffusion coefficient is, therefore, sensitive to the concentration of the corresponding component and it approaches zero as the appropriate component concentration approaches zero. It should be noted that the D_{21} value is large despite the fact that the difference between the mobilities K^+ and Cl^- is very small. This is because cross-term diffusion coefficients, D_{ij}, also depend on the mobility of component i and the mobility of the proton is very large.

As in the case of D_{11}, D_{22} should approach the value of the binary diffusion coefficient as $C_1 \rightarrow 0$ and approach the tracer diffusion coefficient as $C_2 \rightarrow 0$. In both cases the limiting values of the estimated D_{22} agree very well with these experimental values. As the cross-term diffusion coefficients themselves, the ratios D_{12}/D_{11} *and* D_{21}/D_{22} also approach certain limiting values.

At a total concentration of 2 N for the same system,[15] the limiting values of D_{ij} again agree well with either the binary diffusion coefficients or the tracer diffusion coefficients. Qualitatively the diffusion behavior is the same as it was for the case where the total concentration was 1 N. For the system of H_2O-NaCl-HCl at total concentrations of 1 and 2 N,[15] the agreement between the binary diffusion coefficients and the limiting D_{11} and D_{22} values is very good. However, there are discrepancies of about 10% between the tracer diffusion coefficients of the proton and the limiting value of D_{22}.

Figure 1 summarizes the diffusion behavior of the H_2O-KCl-HCl and H_2O-NaCl-HCl systems, each up to a total concentration of 2 N. The solid lines represent the estimated values of $(D_{ij})_v$ using Gosting's first approximation method.[4] Therefore, these are the limiting cases at infinite dilution. The dashed and the broken lines represent estimated values at 1 and 2 N total concentration, respectively, using Miller's LN method.[20] Some of the experimental values are also included to compare with those of calculated values.

Figure 1a is a plot of the estimated $(D_{11})_v$ *vs.* log (C_1/C_2) and the extreme left-hand side represents the tracer diffusion coefficient of KCl; the extreme right-hand side represents the binary diffusion coefficient of KCl. As the C_1/C_2 value increases from left to right, both the 1 and 2 N lines dip down initially, bottom out, and then cross each other. There is only minor variation in the solid line which is close to horizontal and reflects the closeness of the mobilities of K^+ and Cl^-. For the case of 1 N the magnitude of the initial decrease in D_{11} is not much larger than the error of estimation, but the decrease is much larger for the 2 N case. One would expect this kind of behavior if the replacement of H^+ by equal molar concentration of K^+ increases the solution viscosity appreciably. The crossover occurs simply because the binary diffusion coefficient of KCl at 2 N is larger[22] than that at 1 N. The former value is smaller than the value at infinite dilution and there is no cross over between the curves for infinite dilution and for 2 N total concentration.

The values of D_{22} estimates are plotted in Figure 1b and the extreme left-hand side represents the binary diffusion coefficient of the HCl solution; the extreme right-hand side represents the tracer diffusion coefficient of HCl in KCl solutions. Here the tracer diffusion coefficient is very sensitive to the concentration of KCl. The crossover is complete here because the binary diffusion coefficient of HCl at 2 N is larger than that at 1 N which is larger than the value at infinite dilution.

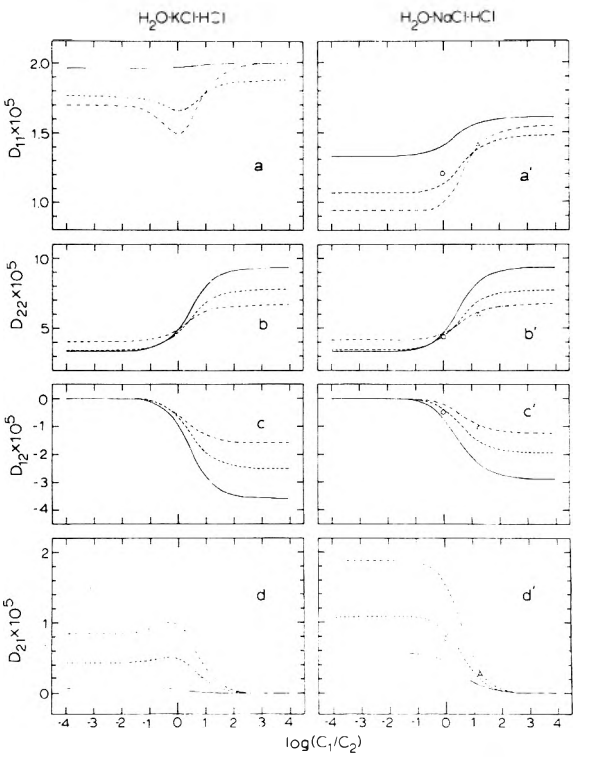

Figure 1. Estimated $(D_{ij})_v$ plotted against log (C_1/C_2): (——) limiting diffusion coefficients for $N \rightarrow 0$; (- - - - -) $N = 1$; (—·—·—·—·—·—·) $N = 2$; Δ, experimental $(D_{ij})_v$ for $C_1 = 1.9$, $C_2 = 0.1$; O, for $C_1 = C_2 = 0.5$.

Figures 1c and 1d give the cross-term diffusion coefficients of H_2O-KCl-HCl as functions of log (C_1/C_2). Perhaps the most interesting feature here is that $-D_{12}$ values decrease with increasing total concentration while the reverse is true for D_{21}. In general, the magnitudes of the cross-term diffusion coefficients, D_{ij}, depend on three factors: concentration of component i, the mobility of component i, and the force produced by a unit concentration gradient of component j. For a given value of C_1/C_2, the component concentration increases as the total concentration increases, making the cross-term diffusion coefficient larger. The contribution due to this effect should be about the same for $-D_{12}$ and D_{21}. As the total concentration increases, however, the mobilities of ions generally decrease and from Figures 1a and 1b it is clear that the extent of this decrease is much larger for H^+ than for K^+. This effect alone will decrease the cross-term diffusion coefficients with increasing total concentration, but the values of D_{21} show that this effect is not big enough to offset the concentration effect. If the decrease in the self-diffusion coefficient of Cl^- going from a 1 to a 2 N solution of HCl is comparable to the decrease in the tracer diffusion coefficient of KCl going from a 1 to 2 N HCl solution, the electrical potential gradient produced by a unit concentration gradient of KCl is not very sensitive to the total concentration whereas the electrical potential gradient produced by a unit concentration gradient of HCl decreases drastically as the total concentration increases.

This effect may be large enough to overcome the concentration effect and make $-D_{12}$ smaller as the total concentration is increased.

Figure 1a' gives the D_{11} values of the H_2O-NaCl-HCl system as a function of log (C_1/C_2). It may be seen that the behavior of main diffusion coefficient, D_{11}, is similar to that for the H_2O-KCl-HCl system. The lack of minima in D_{11} *vs.* log (C_1/C_2) curves for the present system may be due to the fact that the difference between the binary diffusion coefficients of NaCl and the tracer diffusion coefficients of NaCl in HCl for a given total concentration are much larger than those between the binary diffusion coefficient of KCl and the tracer diffusion coefficient of KCl in HCl solution. Figure 1b' gives the D_{22} as a function of log (C_1/C_2) and the curves are similar to the curves for system of H_2O-KCl-HCl.

Figures 1c' and 1d' give the cross-term diffusion of H_2O-NaCl-HCl system plotted against log (C_1/C_2). Here again the $-D_{12}$ decreases with increase in total concentration while opposite effect is observed for D_{21}. The explanation given for the concentration dependence of the cross-term diffusion coefficients in H_2O-KCl-HCl should apply here. This explanation also predicts that in H_2O-NaCl-KCl both cross-term diffusion coefficients should increase with increasing total concentration. The cross-term diffusion coefficients of this system have been determined experimentally[3,24] at a C_1/C_2 value of 1 and total concentrations of 0.5, 1, and 3 *N*, and the experimental values are in agreement with the above prediction.

Conclusion

The complete diffusion behavior of two ternary electrolyte systems was examined for the first time here. This was possible because of the success of Miller's approximation method.[20] Although the differences between the experimental $(D_{ij})_v$'s and the predicted values amount as much as 20% for small cross-term diffusion coefficients, the predicted values do provide a reasonably good overall picture of diffusion of two electrolytes with a common ion. The success of predicting ternary transport properties from the binary transport properties also indicates that the mixing of these electrolytes does not bring about gross changes in ion transport behavior even for protons. The transport of protons is expected to be sensitive to the structure of water. However, the modification of water structure caused by the introduction of either K^+ or Na^+ does not appear to be severe enough to change the proton mobility drastically.

The analysis given under Discussion suggests that a qualitative picture of diffusion behavior of simple ternary electrolyte systems may be obtained from the binary and tracer diffusion coefficients as a function of concentration.

Acknowledgments. The expert technical assistance of Mr. John L. Straughn is very much appreciated. We also thank Dr. Donald G. Miller of Lawrence Livermore Laboratory for reading the manuscript.

(24) P. J. Dunlop, *J. Phys. Chem.*, **63**, 612 (1959).

Vacuum Sublimation of Ammonium Perchlorate

S. P. Tang and J. B. Fenn*

Department of Engineering and Applied Science, Yale University, New Haven, Connecticut 06520 *(Received November 7, 1972)*

Publications costs assisted by The Office of Naval Research through Project SQUID

Time-of-flight measurements have been made on the flux of molecules from the surface of ammonium salts vaporizing under vacuum. As expected with ammonium halides and ammonium bisulfate the TOF distributions correspond to equimolar fluxes of ammonia and the corresponding acid. In the case of ammonium perchlorate the vapor subliming from a single crystal surface comprised ammonia and perchloric acid. When the source was compressed powder the vapor was a mixture of lower molecular weight species. This result seems best explained in terms of decomposition of the vapor after dissociative sublimation in the subsurface interstices of the pressed material.

Introduction

If man ever decides to obliterate himself in a nuclear cataclysm one of the first steps in the overall process may well be the vaporization of thousands of tons of ammonium perchlorate (NH_4ClO_4 hereafter referred to as AP). As the oxidizer in most solid fuel rockets AP comprises perhaps half the total weight of most ballistic missiles. This vital role has made its vaporization and thermal decomposition the object of intensive and extensive investigation. In their comprehensive review Keenan and Sigmund cite some 137 references to previous work on this subject.[1] In spite of, or perhaps because of, all this study there are still very few unequivocal assertions which can be made about the several steps in the sequence by which granules of AP in the propellant grain finally emerge from the rocket nozzle as combustion products. We address

(1) A. G. Keenan and R. F. Sigmund, *Quart. Rev., Chem. Soc.*, **23**, 430 (1969).

ourselves here to what is probably the first major step, the vaporization or sublimation of crystalline AP. More specifically we are concerned with the composition of the vapor which leaves the crystal surface.

Because it is thermodynamically unstable relative to H_2O, O_2, HCl, and N_2, AP can decompose exothermically before, during, and/or after vaporization. At the pressures and temperatures encountered in rocket motors pure AP can sustain its own decomposition flame in a steady deflagration. Under these conditions it is not clear that the vaporization step is the same as for sublimation under vacuum or low-pressure inert gas. It might be argued, therefore, that from the standpoint of practice the study of high-pressure vaporization would be more appropriate. On the other hand, some kinds of experiments, including those we report here, can only be done *in vacuo*. Confident that such experiments are of interest *per se* we also can hope that they will cast light on the practical process. As Guirao and Williams suggest in their analysis of models for the sublimation of AP, the mechanisms deserve elucidation whether the investigator's motives are pure or applied.[2]

The possible mechanisms for AP can be conveniently divided into three classes: (1) *associative sublimation* in which AP molecules leave the surface intact; (2) *dissociative sublimation* in which the species leaving the surface are NH_3 and $HClO_4$; and (3) *destructive sublimation* in which the species leaving the surface comprise some distribution of thermodynamically more stable decomposition products. The best choice seems to be between 1 and 2. There have been any number of experiments which show that the product obtained by condensing the vapors of subliming AP is itself AP. This result undermines the credibility of 3. The recently obtained mass spectra of AP vapor which show a wide range of fragments are most easily explained by decomposition in the ion source of the mass spectrometer.[3-5] To distinguish between 1 and 2 is more difficult because most experimental results can be explained by either mechanism. Guirao and Williams conclude that 2 is the most likely candidate and they assume dissociative sublimation under all conditions even though they warn that the case for this mechanism is not airtight, even at low pressures. The results reported here may help to plug some of the leaks remaining in that case.

Experimental Section

Although there have been relatively few experimental demonstrations since the classic experiments of Stern in 1920, there seems to be little doubt that vaporizing species leave their source surface with a Maxwellian velocity distribution corresponding to the surface temperature.[2,6,7] Our own recent results with sulfur and benzene hexachloride, in which we took particular pains to determine the surface temperature, confirm this generally accepted premise.[8] If the surface temperature is known independently, velocity distribution measurements on the vaporizing flux can provide information on the mass of the vaporizing species. In this way Rothberg, Eisenstadt, and Kusch were able to determine the mole fractions of dimers and trimers in the vapor from alkali halide crystals.[9] Velocity distribution measurements as a means of mass spectrometry cannot provide very high resolution but they do avoid distortions and uncertainties due to fragmentation during ionization in conventional mass spectrometers. Therefore, we undertook to determine the velocity distribution of species in the vapor of subliming AP. In order to prove the method and to provide some calibration we also made measurements on NH_4Cl, NH_4Br, NH_4I, and NH_4HSO_4.

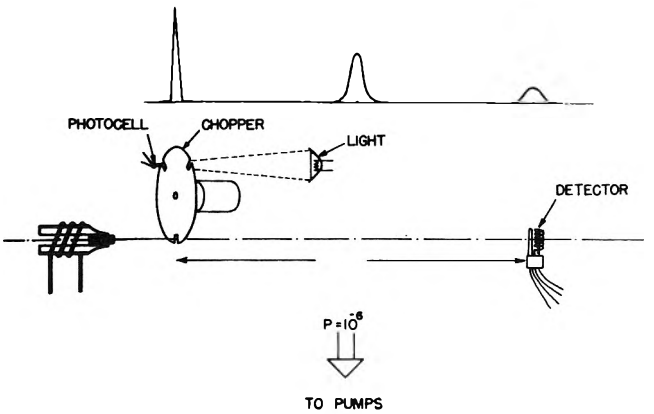

Figure 1. Schematic representation of apparatus.

The approach was to measure time-of-flight distributions (TOF) over a known path length. In essential features the equipment is the same as that previously used in our laboratory for the TOF analysis of molecular beams from free jet sources.[10] It is shown schematically in Figure 1. The only essential change has been the addition of a signal averager. The detector is a simple nude ionization gauge in the Bayard-Alpert configuration. The grid defining the effective ionization region was 1 cm in diameter and was located 36.8 cm from a rotating shutter mounted on the shaft of a synchronous motor energized by a variable-frequency power supply. We were able to overcome some noise problems due to vibration by mounting the detector on a heavy plate suspended by four soft springs, one at each corner. The shutter was an aluminum disk 19 cm in diameter and 0.6 mm thick. There were three 5 × 25 mm slots on the periphery at 120° intervals. For the experiments reported here the shutter was rotated at 85 rps giving a "beam on" time of about 50 μsec. The velocity distributions were so broad that no attempt was made to account for this small but finite spread in effective time zero. The shutter speed was high enough so that there was no change with speed in the shape of the observed waveform.

The signal from the detector was introduced immediately to a field-effect transistor amplifier in the vacuum tank. Its output outside the tank was fed through two more amplifiers in sequence (Tektronix-123 and PAR CR4A) before going into the signal averager (PAR-Waveform Eductor-TDH-9). Readout was by means of Polaroid photographs of the trace on an oscilloscope (Tektronix-502A). Zero time and triggering pulses were obtained from a photodiode exposed to a light source by the slots in the shutter disk. Measurements were made with the shutter rotating in both directions in order to verify the location of the zero time pulse. The photodiode signal was also fed into a counter (Hewlett-Packard 5215 A) to determine the

(2) C. Guirao and F. A. Williams, *J. Phys. Chem.*, **73**, 4302 (1969).
(3) G. A. Heath and J. R. Majer, *Trans. Faraday Soc.*, **60**, 783 (1964).
(4) G. L. Pellett, *AIAA J.*, **8**, 1560 (1970).
(5) W. A. Guillory and M. King, *AIAA J.*, 1134 (1970).
(6) O. Stern, *Z. Phys.*, **2**, 49 (1926); **3**, 417 (1920).
(7) H. Saltsburg, *J. Chem. Phys.*, **42**, 1303 (1965).
(8) S. P. Tang, R. J. Gallagher, and J. B. Fenn, *Entropie*, **42**, 51 (1971).
(9) G. M. Rothberg, M. Eisenstadt, and P. Kusch, *J. Chem. Phys.*, **30**, 517 (1959).
(10) J. B. Anderson and J. B. Fenn, *Phys. Fluids*, **8**, 780 (1965).

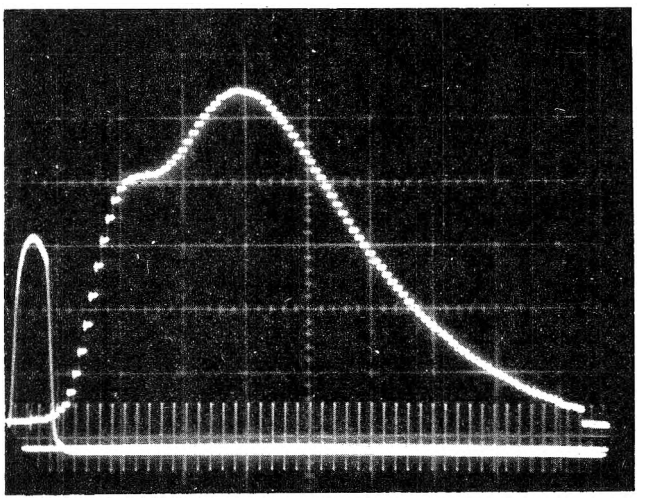

Figure 2. Oscillogram of averaged TOF distribution for vapor from (210) surface of an ammonium perchlorate single crystal.

shutter speed. A 25-kHz time-mark generator provided a time scale on each oscillogram. Typical results are shown in Figure 2.

For the experiments with ammonium bisulfate and the halides the source was a rectangular wafer of reagent grade powder compressed to between 100 and 200 kg/cm^2. The cross section of the wafer, *i.e.*, the surface from which evaporation occurred, was 4 × 20 mm in dimension. The remaining surfaces were treated with a colloidal dispersion of graphite in alcohol (Acheson Colloids, Port Huron, Mich.) to inhibit evaporation. Two holes 0.25 mm in diameter were drilled in the narrow lateral surface of the wafer at about 3 and 7 mm from the evaporating surface. Chromel–alumel thermocouple junctions were packed into these holes. Readings of these thermocouples established the gradient of temperature in the direction of the evaporating surface and permitted a fairly accurate estimate of the surface temperature.

In the case of AP three kinds of samples were used. Two were cut from ground perchlorate strands kindly furnished by A. Macek of Atlantic Research Corp. One had been compressed to 333 kg/cm^2. The other had been compressed to 1200 kg/cm^2. The areas of the evaporating surfaces were about 4 × 20 mm in each case. Experiments were also done with single crystal AP grown by neutralizing $HClO_4$ with NH_4OH and very kindly furnished by W. McBride at the U. S. Naval Weapons Center. TOF distributions were measured on the vaporizing flux from both (001) and (210) faces. The area of the (001) surface was 10 × 3.8 mm. For the (210) faces the areas were about 12 × 1.5 and 8 × 1.2 mm. All other surfaces were coated with graphite. For the case of evaporation from the (210) faces two thermocouples were inserted in small holes drilled in the crystals to determine the temperature gradient toward the surface. Because the total thickness of the crystal in the direction normal to the (001) surface was only about 1.5 mm only one thermocouple could be used. We assumed that the temperature gradient during evaporation was the same as in the case of the 210 surface.

For an evaporation experiment the source wafers were held between two jaws of stainless steel which were in good thermal contact with the broad sides of the wafer. Each jaw was inset in the end of one side of a split cylindrical copper bar 3 cm in diameter and 10 cm long surrounded by a resistance heater which provided control over the surface temperature. The two halves of the copper bar were clamped together to provide a firm grip on the salt wafer.

The stage on which these various elements of apparatus performed their roles was in a vacuum chamber about 80 cm in diameter and 1 m long exhausted by a 70-cm oil diffusion pump. There was a flat Freon-cooled optical baffle between the pump and the chamber which halved the nominal pumping speed of 30,000 l./sec. Background pressure was usually between 10^{-6} and 10^{-7} Torr during the experiments.

Results with Ammonium Halides

It is appropriate to consider first the evaporation of NH_4Cl, NH_4Br, and NH_4I. Unlike AP, these compounds and their dissociation products, NH_3 and HX, do not offer the possible complication of exothermic decompositon to simpler molecules. It is generally believed that their sublimation is dissociative. On this basis we can assume that the vaporizing flux comprises NH_3 and HX in equal amounts, each with a Maxwellian velocity distribution corresponding to the surface temperature. The signal, S (ordinate on oscilloscope trace), is proportional to the number density of molecules at the detector. For a Maxwellian distribution the signal contribution for a single species can be expressed as

$$S = CQ(t_\alpha/t)^4 \exp[-(t_\alpha/t)^2]$$

where $t_\alpha = z/(2kT/m)^{1/2}$ and z is the distance from the shutter to the detector.[7] The constant C depends upon source intensity as well as geometric factors. It can be considered the same for all species in a particular experiment. The factor Q relates to the sensitivity of the detector for a particular species. The total signal for an equimolar flux of two species is simply the sum of the signals for each one. If the coordinates of the signal trace at any point are normalized to the coordinates at its maximum value the normalized total signal at any normalized time $\tau = t/t_m$ becomes

$$\frac{S}{S_{t_m}} = \frac{\theta(t_{\alpha_1}/\tau)^4 \exp[-(t_{\alpha_1}/\epsilon_n\tau)^2] + (t_{\alpha_2}/\tau)^4 \exp[-(t_{\alpha_2}/t_n\tau)^2]}{\theta(t_{\alpha_1})^4 \exp[-(t_{\alpha_1}/t_m)^2] + (t_{\alpha_2})^4 \exp[-(t_{\alpha_2}/t_m)^2]}$$

where θ is simply the ratio of Q_1/Q_2. The subscripts refer to a particular species. If we know θ we can compute a normalized signal trace for an equimolar flux of say NH_3 and HX from the vaporizing surface assuming that each species has a Maxwellian velocity distribution. The problem is to determine θ, *i.e.*, $Q(NH_3)/Q(HX)$. As we have already noted, Q represents the relative sensitivity of our detector to a particular species. Because the detector is in effect simply an ionization gauge we could use with some confidence measured values of ion gauge sensitivity from the literature. Unfortunately, we were unable to find values of overall ion gauge sensitivity for ammonia and the hydrogen halides under comparable conditions. We did find comparable values for total ionization cross sections for NH_3 and HCl at an electron energy of 75 eV, 25 V less than the electron energy in our detector.[10] We simply assumed that θ could be taken as the ratio of these total ionization cross sections, 0.745. In Figure 3 the solid curve is the calculated TOF curve normalized to the coordinates of the maximum signal. It assumes in addition equimolar fluxes of NH_3 and

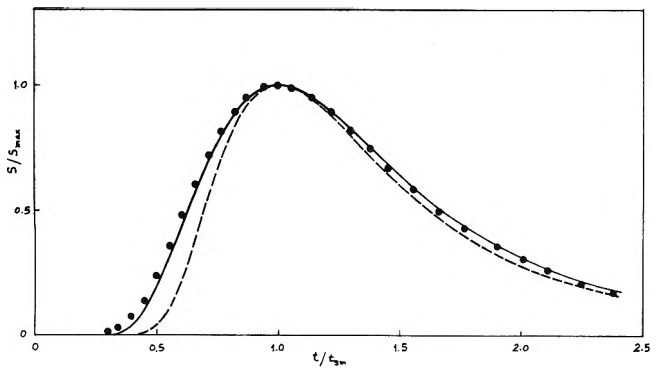

Figure 3. TOF results for ammonium chloride. The solid curve is a calculated Maxwellian distribution normalized to the maximum signal, assuming equimolal fluxes of NH_3 and HCl. The dashed curve represents a Maxwellian distribution for a single species, *i.e.*, NH_4Cl.

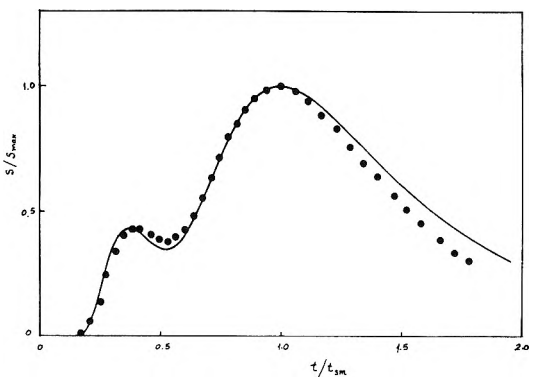

Figure 4. TOF results for ammonium iodide. The solid curve is a calculated Maxwellian distribution normalized to the maximum signals, assuming equimolal fluxes of NH_3 and HI.

HCl having a Maxwellian velocity distribution corresponding to a surface temperature of 358°K. The points are taken from an oscillogram made at that surface temperature. The agreement seems good enough to justify all of the assumptions which underly the calculation and the measurement. At least, the net result of all the assumptions is a fair approximation of reality.

The only pertinent data we could find for NH_3 and HI were the relative ionization efficiencies by Frost and McDowell.[11] These were linear functions of the electron energy over the range studied, 1–15 eV. We made the bold extrapolation to 100 eV to obtain the ratio 0.45 (NH_3/HI) which we used in calculating the solid curve in Figure 4. The points were taken from an oscillogram made at 396°K, the temperature assumed in the calculation. Once again the agreement is good enough to support the underlying assumptions. The observed deficiency in signal at long flight times is commonly encountered and is doubtless due to self-scattering of the slow particles. Such scattering losses become noticeable with high molecular weight particles because of their somewhat larger cross section and their relatively low velocity which gives a longer time in the line of fire.

For NH_4Br we could find no appropriate ionization data. Consequently, we simply interpolated on the basis of total number of electrons in the molecules between the already mentioned values for NH_4Cl and NH_4I to obtain 0.598 as a value of θ for NH_4Br. Figure 5 shows the solid curve obtained with this approximation assuming a surface temperature of 390°K, the points being taken from

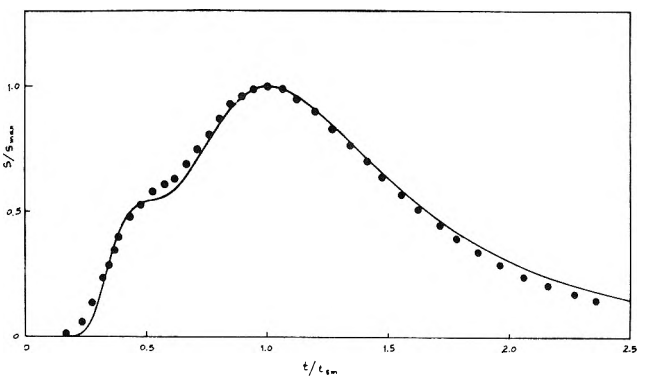

Figure 5. TOF results for ammonium bromide. The solid curve is a calculated Maxwellian distribution normalized to the maximum signal, assuming equimo al fluxes of NH_3 and HBr.

the corresponding oscillogram. The agreement is reasonably good. Note that the scattering loss of slow particles is less than for NH_4I but greater than for NH_4Cl.

These results with the ammonium halides persuaded us that our general approach was sound. Let's now consider AP. We could find no ionization data for $HClO_4$. Moreover, there is a good deal of evidence that a substantial amount of fragmentation occurs during electron bombardment in the ion source of a mass spectrometer.[3-5] Consequently, we did not even know how to guess at a value of θ. A possible solution to this problem occurred to us and turned out to be fruitful. In the thermal decomposition of ammonium bisulfate (ABS) there are only two reasonable possibilities: to NH_3 and H_2SO_4 or to H_2O and NH_2SO_3H.[12] Both sulfuric acid and sulfamic acid are isoelectronic with perchloric acid. There is an old rule of thumb which says that ionization gauge sensitivity to a particular species is directly proportional to the total number of electrons in that species. Moreover, the mass resolution of our version of TOF spectroscopy could not distinguish between NH_3 and H_2O or between $HClO_4$, H_2SO_4, and NH_2SO_3H. Consequently, we reasoned that vaporization of NH_4HSO_4 should be a good model for the vaporization of NH_4ClO_4 if the latter undergoes dissociative sublimation into NH_3 and $HClO_4$ and if the number of positive ions formed in the detector per parent molecule was the same for both $HClO_4$ and H_2SO_4 or NH_2SO_3H.

Figure 6 tells the story. The open circle points were obtained from an oscillogram taken during vaporization from the (210) surface of single crystal AP at a surface temperature of 454°K. The solid circles were obtained from a wafer of compressed ammonium bisulfate powder. In both cases the signal strength and the time were normalized to the coordinates of the maximum signal. Because the bisulfate is so hygroscopic we were unable to drill holes and embed thermocouples in the pressed wafer. Therefore, we do not have independent knowledge of the sulfate surface temperature. In terms of normalized coordinates a Maxwellian distribution will give the same curve no matter what the temperature. However, we also note that the *real* time of flight to the maximum signals was the same within experimental error for both the AP and the sulfate experiments shown on Figure 6. We conclude that the surface temperatures were the same. In Figure 6 the signal corresponding to flight time for HN_3 is

(11) D. C. Frost and C. A. McDowell, *Can. J. Chem.*, **36**, 39 (1958).
(12) R. Kiyoura and K. Urano, *Ind. Eng. Chem.*, **9**, 489 (1970).

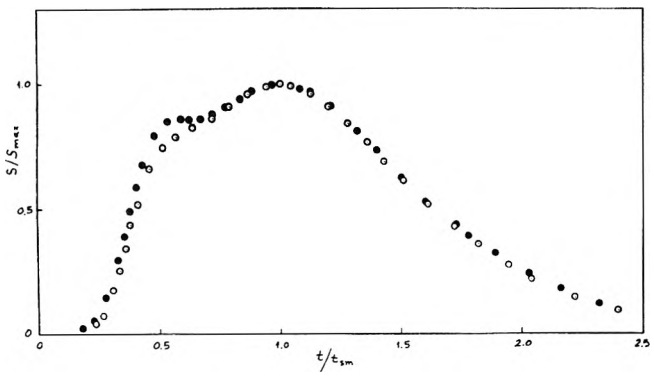

Figure 6. TOF results for ammonium perchlorate and ammonium bisulfate. The open circles are for AP, the solid circles for ABS. Coordinates of all points are normalized to the maximum signal.

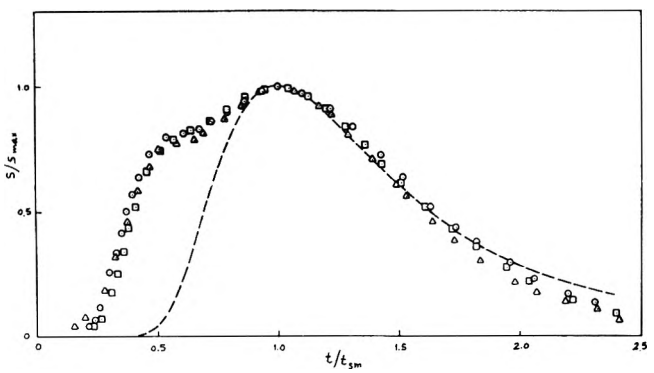

Figure 7. Normalized TOF results for ammonium perchlorate. Circles and squares are for vapor from (210) surfaces. Triangles are for (001) surface. The dashed curve represents a Maxwellian distribution for a single species.

higher for ABS than for AP. We were bothered by this apparent discrepancy until we noted that the excess signal decreased with time. We then realized that it was due simply to vaporization of water which had been absorbed by the ABS during preparation of the source wafer. The molecular weights of H_2O and NH_3 are too close for resolution by this experiment.

In Figure 7 are results from three different surfaces of an AP single crystal, two of them being crystallographically identical. It would seem that the sublimation process is the same in each case. We found essentially the same shape for the TOF curves over a temperature range from about 425 to about 525°K. At lower temperatures there was too little signal. At higher temperatures there were enough collisions that the structure of the curve began to be washed out. For comparison purposes we show by the dashed curve in Figure 7 a Maxwellian distribution for a single species. We cannot provide a calculated curve for the bimodal case because we have no idea what value to choose for θ, the relative gauge sensitivity for the two species involved. We simply assume that ABS sublimation gives rise to equimolal fluxes of NH_3 and H_2SO_4. The similarity between ABS and AP in Figure 6 persuades us that AP sublimes in an analogous way.

The results with the compressed perchlorate powder were quite different from those obtained with single crystal AP. They are shown in Figure 8. The solid curve represents a Maxwellian TOF distribution. The solid circles are

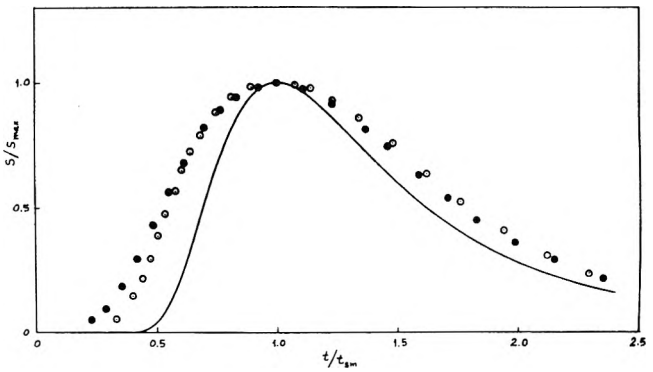

Figure 8. Normalized TOF results for vapor from surface of a pellet of ammonium perchlorate powder. The solid circles were obtained from powder compressed to 1200 kg/cm^2. The open circles were obtained from powder compressed to 333 kg/cm^2. The curve represents a Maxwellian distribution for a single species.

from an experimental oscillogram with a wafer cut from a strand which had been compressed to about 1200 kg/cm^2. The open circles were obtained with a sample which had been compressed to about 333 kg/cm^2. It is obvious that neither case corresponds to a Maxwellian distribution for a single species as represented by the solid curve. Nor are they in any way similar to the single crystal results which can most easily be explained in terms of dissociative sublimation into NH_3 and $HClO_4$. As a very crude representation of what happened we can relate the absolute TOF of the maximum signal to that which would be expected for a Maxwellian distribution for a single species. On this basis the results represented by the open circles correspond to an average molecular weight of 34. The solid circles correspond to an average molecular weight of 43. In other words the more highly compressed material underwent less decomposition than the less highly compressed material. In the limiting case of the single crystal material there was no decomposition. We speculate that because the temperature was higher in the bulk of the sample than at the surface, there was vaporization beneath the surface followed by decomposition in the interstitial voids as the vapors worked their way out to the surface. By this interpretation, the first step in the gasification of AP even when it occurs in the bulk material beneath the surface, is dissociative sublimation into ammonia and perchloric acid. Any further decomposition occurs as a result of subsequent gas–gas or gas–surface collisions of NH_3 and $HClO_4$. This speculation is supported by some recent results of Kung and Roberts.[13] They also examined TOF distributions from vaporizing salts. Instead of heating "from behind" by conduction, they heated the surface by radiation. Consequently, the surface temperature was above the bulk temperature instead of *vice versa*. In an experiment with compressed AP powder they found the same bimodal TOF distribution that we obtained with single crystal material. It would seem, therefore, that the decomposition we observed with samples of compressed powder did indeed take place in the interstices below the "surface" of the subliming wafer.

Acknowledgment. This work was supported in part by the National Science Foundation under Grant No. GK 4329 and in part by the Office of Naval Research through Project SQUID (Contract No. N00014-67-0226-0005, NR-098-038).

(13) Kung and Roberts, private communication.

Electron Spin Resonance Spectra of Manganese(II) in Five Isomorphic Host Lattices of Hexakisantipyrine Metal Perchlorates

Gerald M. Woltermann and John R. Wasson*

Department of Chemistry, University of Kentucky, Lexington, Kentucky 40506 *(Received August 28, 1972)*

Electron spin resonance (esr) spectra of manganese(II) in a number of isomorphic hexakisantipyrine divalent metal perchlorates were analyzed in order to determine the effect of variation of the host metal ion on the spin Hamiltonian parameters. Results are inconclusive for $(a - F)$ parameters since the F term was not determined separately. However, D values showed a marked decrease with increasing size of the host metal ion. The manganese electron spin–nuclear spin hyperfine coupling constant was unaffected by changes in the lattice and its magnitude indicative of some covalency in the manganese–oxygen bonding. Esr spectra of powdered samples of a number of the complexes were measured in order to analyze forbidden ($\Delta m_I = \pm 1$) doublet transitions not observed in the single-crystal spectra. Agreement between theory and experiment was excellent. No splitting of the main hyperfine lines was observed in the powder spectra, probably due to the small magnitude of the zero-field splitting parameter, D. The esr spectrum of hexakisantipyrinemanganese(II) perchlorate in methylene chloride yielded a nuclear hyperfine coupling constant in agreement with single-crystal data.

Introduction

Hexakis- and pentakisantipyrine metal perchlorate complexes have been the subject of a number of recent investigations. The electron spin resonance (esr) spectra of both the pentakisantipyrinecopper(II) complex,[1] $Cu(apy)_5(ClO_4)_2$ (apy = antipyrine (I)), and the hexakisantipyrinemanganese(II) complex,[2] $Mn(apy)_6(ClO_4)_2$, have been reported. Both complexes behaved as though they were axially symmetric. The electron spin–nuclear spin hyperfine coupling constant for the manganese(II) complex indicated some manganese–oxygen covalency although the complex could be considered more ionic than the corresponding hexaaquo complex. The axial field splitting parameter, D, was found[2] to be quite small and the cubic zero-field splitting parameter, a, was even smaller. The metal–oxygen bond in the copper(II) complex was estimated[3] to contain about 13% covalent character, a result consistent with the data for the manganese compound. Electronic spectra data[4,5] for transition metal complexes indicate that antipyrine lies above water and dimethyl sulfoxide in the spectrochemical series but that metal–ligand covalency is less than with these other ligands. Magnetic susceptibility data for metal antipyrine complexes show that they are high spin in all cases. Single-crystal magnetic susceptibility studies of cerium and ytterbium hexakisantipyrine complexes demonstrated[6,7] that they behave magnetically as trigonally elongated octahedra with high-spin configurations. Hexakisantipyrine complexes of divalent magnesium, calcium, zinc, and lead perchlorates are isomorphic,[8] being hexagonal (space group $P\bar{3}$),[9,10] with one molecule per unit cell and nearly identical lattice parameters ($a \sim 14$ Å, $c \sim 10$ Å) for the different salts. Each metal ion is surrounded by a trigonally distorted octahedral array (trigonal axis is crystal c axis) of carbonyl oxygens of antipyrine which are the donor atoms. This is consistent with the reduction of the carbonyl stretching frequency in the infrared spectra. The isomorphism (surprising, in view of the size difference between Mg and Pb ions) makes this series of complexes convenient for studies of the effect of the host lattice on esr spectra.

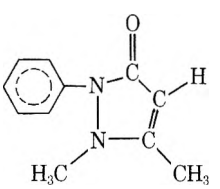

antipyrine = 1-phenyl-2,3-dimethyl-5-pyrazolone

Lattice effects of the esr spectra of high-spin manganese(II) compounds have been of considerable interest. A number of workers have noted[11-13] the regular variation of g, a, D, and A values with changing host metal ions in isomorphic systems and they have offered qualitative interpretations of these results. Others[14-19] have attempted to lay a theoretical basis for the magnitude of the zero-

(1) R. Srinivasan and C. K. Subramanian, *Indian J. Pure Appl. Phys.*, **8**, 817 (1970).
(2) R. Srinivasan and C. K. Subramanian, *Indian J. Pure Appl. Phys.*, **9**, 21 (1971).
(3) J. Gopalakrishnan and C. C. Patel, *Indian J. Chem.*, **5**, 389 (1967).
(4) A. Ravi, J. Gopalakrishnan, and C. C. Patel, *Indian J. Chem.*, **5**, 356 (1967).
(5) D. M. Sathyanarayana and C. C. Patel, *Indian J. Chem.*, **5**, 360 (1967).
(6) M. Gerloch and D. J. Mackey, *J. Chem. Soc. A*, 3030 (1970).
(7) M. Gerloch and D. J. Mackey, *J. Chem. Soc. A*, 3040 (1970).
(8) M. Vijayan and M. A. Viswamitra, *Z. Kristallogr.*, **122**, 153 (1965).
(9) M. Vijayan and M. A. Viswamitra, *Acta Crystallogr.*, **23**, 1000 (1967); *Acta Crystallogr., Sect. B*, **24**, 1067 (1968).
(10) M. Vijayan and M. A. Viswamitra, *Acta Crystallogr.*, **21**, 522 (1966).
(11) C. Kikuchi and G. H. Azarbayejani, *J. Phys. Soc. Jap., Suppl. B-I*, 2503 (1962).
(12) R. S. Title, *Phys. Rev.* **131**, 2503 (1963).
(13) R. S. Title, *Phys. Rev.* **130**, 17 (1963).
(14) H. Watanabe, *Progr. Theort. Phys.*, **18**, 405 (1957).
(15) M. J. D. Powell, J. R. Gabriel, and D. F. Johnston, *Phys. Rev. Lett.*, **5**, 145 (1960).
(16) J. R. Gabriel, D. F. Johnston, and M. J. D. Powell, *Proc. Roy. Soc. (London)*, **264**, 503 (1961).
(17) A. Shuskus, *Phys. Rev.*, **17**, 1529 (1962).
(18) T. P. P. Hall, W. Hayes, and F. I. B. Williams, *Proc. Phys. Soc. Ser. A*, **78**, 883 (1961).
(19) E. Simanek and K. A. Mueller, *Chem. Phys. Lett.*, **4**, 482 (1970).

field splitting parameters and their variation with host lattice while subsequent work attempted to verify these theories experimentally by observing pressure effects on the esr spectra. Qualitatively, all relevant work has shown that the absolute magnitude of the zero-field constants should decrease with increasing size of the host metal ion in an isomorphic series, while g and A values show little if any change.

Experimental Section

Antipyrine was obtained from Eastman Chemical Co., Rochester, N. Y., and hydrated magnesium(II), manganese(II), cobalt(II), and cadmium perchlorates were obtained from Alfa Inorganics, Beverly, Mass. The calcium and lead perchlorates were prepared by dissolving the metal carbonates (Matheson Coleman and Bell) in perchloric acid (J. T. Baker Chemical Co.).

Doped samples of hexakisantipyrine divalent metal perchlorates were prepared by addition of stoichiometric amounts of antipyrine and hydrated metal perchlorate to water along with a small (~1%) amount of manganese(II) perchlorate hexahydrate. Crystals formed upon slow evaporation of the aqueous solutions. The crystals were hexagonal with well-developed faces.

Electron spin resonance spectra were measured with a Magnion Model MVR-12X X-band esr spectrometer (O. S. Walker Co., Worcester, Mass.) operating at about 9.4 GHz using 6-kHz field modulation and a 12-in. electromagnet. The frequency was monitored with a calibrated absorption wavemeter incorporated in the microwave unit. Field calibration was checked using diphenylpicrylhydrazyl (DPPH) free radical for which $g = 2.0036$. Single-crystal spectra at ambient room temperature were obtained by mounting a crystal on a quartz rod with Duco cement and placing the mounted crystal in a device which could control the degree of orientation to within ±1°. Spectra for several crystals at several orientations with respect to the applied magnetic field were obtained. Reproducibility of spectra from crystal to crystal and at different levels of doping was excellent.

Results and Discussion

The esr spectrum of a metal ion with a ^6S ground state in an axially symmetric crystalline field can be fit to the following spin Hamiltonian

$$H = g\beta H + D(S_z^2 - 1/3S(S+1)) + 1/6a[(S_1^4 + S_2^4 + S_3^4) - 1/5S(S+1)(3S^2 + 3S - 1)] + 1/180F[35S_z^4 - 30S(S+1)S_z^2 + 25S_z^2 - 6S(S+1) + 3S^2(S+1)^2] + AS\cdot I$$

where $S = 5/2$ and S_1, S_2, and S_3 are the spin operators with respect to the cube axes. The terms in D, a, and F give rise to the fine structure of the spectrum and the A term to the hyperfine structure. D and F are zero-field splitting terms due to the axial field and a is the zero-field splitting term due to the cubic field.

If the applied field is directed at some arbitrary angle θ to the trigonal axis, the fine line field positions can be determined by rotating the coordinate system by an angle θ about the y axis of the molecule and expressing the S_z' of the new coordinate system in terms of the S_z of the old coordinate system. The resonant field positions of the fine lines are then calculated to the first-order by operating on the spin states with the Hamiltonian and ignoring any off-diagonal terms. Subsequently, the energies are corrected to a second-order in D by use of non-degenerate second-order perturbation theory. The results given by these operations are as follows

$$\Delta m_s = \pm 5/2 \longleftrightarrow \pm 3/2 \quad H = H_0 \mp [2D(3\cos^2\theta - 1) \pm \frac{32D^2}{H_0}\sin^2\theta\cos^2\theta \mp \frac{D^2}{H_0}\sin^4\theta + \frac{1}{6}F(35\cos^4\theta - 30\cos^2\theta + 3) + 2pa] \quad (1)$$

$$\Delta m_s = \pm 3/2 \longleftrightarrow \pm 1/2 \quad H = H_0 \mp [D(3\cos^2\theta - 1) \mp \frac{4D^2}{H_0}\sin^2\theta\cos^2\theta \pm \frac{5}{4}\frac{D^2}{H_0}\sin^4\theta - \frac{5}{24}F(35\cos^4\theta - 30\cos^2\theta + 3) - \frac{5}{2}pa] \quad (2)$$

$$\Delta m_s = -1/2 \longleftrightarrow +1/2 \quad H = H_0 + 16\frac{D^2}{H_0}\sin^2\theta\cos^2\theta - \frac{2D^2}{H_0}\sin^4\theta \quad (3)$$

where $H_0 = h\nu/gB$ and D, a, and F are expressed in oersteds. In the above expression $p = 1\text{-}5\phi$ where $\phi = l^2m^2 + m^2n^2 + n^2l^2$ and l, m, and n are the direction cosines with respect to the cubes axes. When H is directed along the threefold axis, $\theta = 0°$ and $p = -2/3$ and the above equations reduce to

$$\Delta m_s = \pm 5/2 \longleftrightarrow \pm 3/2 \quad H = H_0 \mp [4D - \frac{4}{3}(a - F)] \quad (4)$$

$$\Delta m_s = \pm 3/2 \longleftrightarrow \pm 1/2 \quad H = H_0 \mp [2D - \frac{5}{3}(a - F)] \quad (5)$$

$$m_s = -1/2 \longleftrightarrow +1/2 \quad H = H_0 \quad (6)$$

It can be seen from the above equations the fine structure parameters should give rise to five fine lines. If the hyperfine term from the Hamiltonian is included, the following term must be added to the above fine line energies

$$-Am_I - (B^2/2H_0)(35/4 - m_I^2 + m_I(2m_s - 1)) \quad (7)$$

The parameters D, and $(a - F)$ can be obtained experimentally by taking the esr spectra with H parallel to the

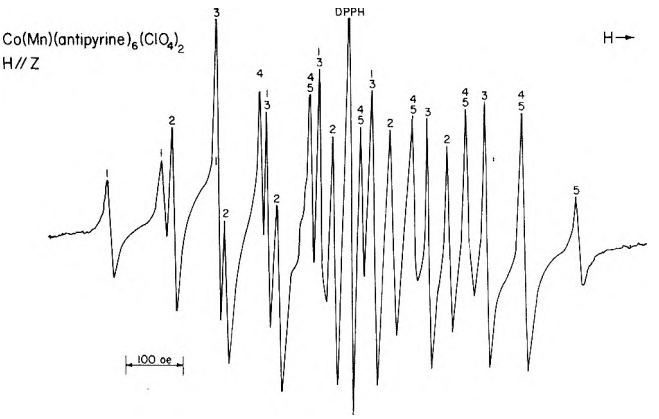

Figure 1. Esr spectrum of Mn(II)-doped $Co(apy)_6(ClO_4)_2$ with the magnetic field along the trigonal axis. The nuclear hyperfine lines associated with the five fine lines are indicated.

trigonal axis and measuring the fine line positions at the center of the hyperfine sextets. A is determined by taking the average of all the hyperfine line separations since this varies with changing field due to the second-order terms in B. The sign of D and hence $(a - F)$ can be determined from this variation in hyperfine splitting if A is assumed negative as is always the case for Mn(II). If the splitting increases with increasing field, then D is positive. The fine line parameters can be checked by rotating the crystal by 90° to obtain the perpendicular spectrum, and then comparing experimental fine line separations with those calculated using D and $(a - F)$ values obtained from the parallel spectrum. With $\theta = 90°$ $p = -\frac{1}{4}$ and eq 1-3 reduce to

$$\Delta m_s = \pm 5/2 \longleftrightarrow \pm 3/2 \quad H = H_0 \pm 2D + \frac{D^2}{H_0} \pm 1/2(a - F)$$

$$\Delta m_s = \pm 3/2 \longleftrightarrow \pm 1/2 \quad H = H_0 \pm D - \frac{5D^2}{4H_0} \mp \frac{5}{8}(a - F)$$

$$\Delta m_s = -1/2 \longleftrightarrow +1/2 \quad H = H_0 - \frac{2D^2}{H_0}$$

In Figures 1 and 2 the parallel and perpendicular spectra for manganese doped into the cobalt complex are shown. The expected five sets of hyperfine sextets are observed in each case with considerable overlap of hyperfine lines due to the small magnitude of the zero-field splitting. Compression of the spectra on going from parallel to perpendcular orientation is also observed. In Table I the spin Hamiltonian parameters for manganese in the five host lattices are given with ionic radii of the host metal ions. In Table II the calculated and experimental fine line separations are compared, and in all cases agreement between theory and experiment is excellent.

The esr of Mn(II) in the magnesium host lattice has been studied previously[2] and the literature results are in good agreement with ours. The fine line splitting showed D and $(a - F)$ to be of opposite sign, and, since the hyperfine splitting decreased with increasing field, the sign of D was determined to be negative and $(a - F)$ positive. The positive value of a is in agreement with other values reported in the literature and agrees with both the calculations of Watanabe[14] and Powell[15] who predicted positive a values for reasonable values of Dq.

As is illustrated by the values in Table I, the axial zero-field splitting parameter, D, shows the most pronounced change upon changing host metal ion. The change in $(a - F)$ is, however, both small and random. Both Kikuchi[11] and Title[12] found the cubic field splitting parameter, a, to decrease with increasing size of host lattice metal ion. Our experiments, however, give only the value of $(a - F)$ as we are working with an axially symmetric field instead of a cubic field. Hall, *et al.*,[18] considered the F term to be negligible for axially symmetric cases and postulated that the term $(a - F)$ ought to exhibit the same trend as a itself. Our data indicates this is not the case, at least in the antipyrine series under study here. In fact, the F value appears to be large enough to alter the expected decrease of $(a - F)$ with host metals of larger ionic radius.

For the hyperfine coupling constants no change in the A values accompanied the change of host lattice. Although Title[12] and Kukuchi[11] did observe a small increase in A with increasing size of the host ion, these increases were

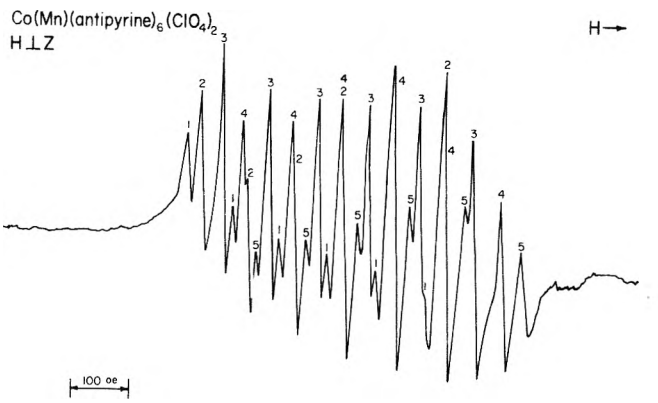

Figure 2. Esr spectrum of Mn(II)-doped $Co(apy)_6(ClO_4)_2$ with the magnetic field perpendicular to the trigonal axis. The nuclear hyperfine lines associated with the five fine lines are indicated.

TABLE I: Spin-Hamiltonian Parameters for Mn-M $(apy)_6(ClO_4)_2$

M	Ionic radius, Å[a]	g	A, Oe	B, Oe	D, Oe	$(a - F)$, Oe
Mg^{2+}	0.66 (0.14)[b]	2.008	−93	−93	−47.5	+7.1
Co^{2+}	0.72 (0.08)	2.011	−94	−95	−44.0	+9.0
Cd^{2+}	0.97 (0.17)	2.008	−93	−95	−30.1	+5.3
Ca^{2+}	0.99 (0.19)	2.009	−93	−95	−34.2	+7.2
Pb^{2+}	1.20 (0.40)	2.008	−93	−94	−9.3	+5.8

[a] R. T. Sanderson, "Inorganic Chemistry," Reinhold, New York, N. Y., 967, p 136. Manganese(II) has an ionic radius of 0.80 Å. [b] $|r_{M^{2+}} - r_{Mn^{2+}}|$ where r indicates the ionic radius.

on the order of 1 or 2 G. Furthermore, Hall, *et al.*,[18] saw no change in A when the host lattice was changed from $MgCl_2$ to $CdCl_2$. Similarly Liebler[20] observed no change in A for Mn(II) in the series of mixed crystals CdTe-HgTe. In agreement with these results, Simanek[19] concluded from a study of ionic-covalent transitions in solids that A values would be to a large degree unaffected by changes in lattice parameters, but rather, would be affected more by local effects such as covalency changes in the metal-ligand bond. Presumably, in the series under investigation here, the covalency in the MnO bond would remain constant, since change in the host lattice would not be expected to change the nature of the Mn-O bond. It was also noted by Feher[21] that uniaxial pressure left A relatively unaffected. Thus, it seems that change in lattice will at best have only a very small affect on A, or, according to our results, will have none at all. The magnitude of the A values, as noted in the earlier esr study in the magnesium host lattice,[2] indicate some covalent character to be present in the Mn-O bonds. Nevertheless, a value of about −93 G for A indicates the complex to be more ionic than the corresponding hexaaquo complex of Mn(II) which gives an A value of −91 G. This is in line with the results of the optical spectra studies which indicate antipyrine to be more covalent than either water or dimethyl sulfoxide.[4,5]

The axial field splitting parameter, D, as noted above, shows the most pronounced variation with change in host

(20) K. Liebler, Summer School on Magnetic Resonance and Related Phenomena, Mangalia, Rumania, 1969, cited in ref 19.
(21) E. R. Feher, *Phys. Rev.*, *A* **136**, 145 (1964).

TABLE II: Calculated and Experimental Separations of Forbidden Doublets

Metal	m_I	ΔH_{expt}, Oe	ΔH_{calcd}, Oe	ΔH_{calcd}, Oe
			$P = 0.0$	$P = 0.11$
Co^{2+}	−3/2	22.6	21.9	22.7
	−1/2	24.4	24.0	24.5
	1/2	26.0	26.1	26.1
	3/2	27.8	28.2	27.8
	5/2	29.4	30.3	29.4
			$P = 0.0$	
Mg^{2+}	−3/2	21.7	21.8	
	−1/2	22.6	22.7	
	1/2	24.5	24.5	
	3/2	26.4	26.4	
	5/2	28.2	28.3	
			$P = 0.0$	$P = 0.03$
Ca^{2+}	−3/2	21.2	21.0	21.2
	−1/2	3.4	23.2	23.3
	1/2	25.5	25.5	25.5
	3/2	27.7	27.9	27.7
	5/2	29.8	30.0	29.8
			$P = 0.0$	$P = 0.09$
Pb^{2+}	−3/2	20.2	19.3	20.1
	−1/2	22.9	22.5	22.9
	1/2	24.8	24.8	24.8
	3/2	26.8	27.1	26.8
	5/2	28.7	29.4	28.7

lattice. Watanabe[14] and Nicholson[22] found D to depend at least crudely on the axial crystal field. From this result it would seem reasonable that as metal–ligand distance is increased the axial field potential would decrease, thus, giving rise to a smaller D term. Hutchings[23] proposed D and E to be functions of $1/r_i^3$ where r_i is the metal–ligand distance. Obviously, D would then decrease with increasing size of the host metal ion. Feher[21] found that D values increased with increasing uniaxial pressure of the crystal. Decreasing the size of the metal ion of the host lattice would have an effect similar to exerting pressure on the crystal and, in accord with the results of Feher,[21] the D value increases with decreasing size of the host metal ion.

In a more simplistic view, the magnitude of the D value can be considered to be indicative of the extent of distortion of the complex from octahedral symmetry. Since antipyrine is a rather bulky ligand, six of these ligands around a central metal ion probably involve considerable steric hindrance and this would necessarily distort the complex from pure octahedral symmetry. However, when the size of the host metal ion is increased, the steric effect would be relaxed. This would result in a decrease in the magnitude of D with increasing size of host metal ion in agreement with experimental results. In all of these speculations it is necessary to assume that no local contractions around the manganese impurity occur. This is directly opposed to the reasoning of Title[12,13] who assumes local expansions or contractions occur in order to explain his results. Our results indicate this not to be the case. Thus, there are a number of ways that the effect on D can be viewed, all of which yield the same result, that is, that D will decrease with increasing size of host metal. Any attempts, then, to calculate D or a on a theoretical basis must take into account the effects of different lattices on the cubic and axial potentials surrounding the impurity ion, as well as covalency effects.

Powder Spectra and Forbidden Lines

Bleaney and Ingram[24] first noticed lines of small intensity appearing as doublets between the main hyperfine lines in their study of two Tutton salts of Mn(II). These lines were attributed to $\Delta m_I = \pm 1$ forbidden transitions arising out of admixture of the nuclear spin states by off-diagonal terms in the spin Hamiltonian matrix. These lines had zero intensity when the applied field was parallel or perpendicular to the threefold axis, but had finite intensities at other orientations of the field. Due to the small magnitude of the zero-field splitting in the antipyrine complexes, these lines were masked by the allowed hyperfine transitions and the esr spectra of powdered samples were taken in order to observe them.

If we consider the central $-\frac{1}{2} \rightarrow \frac{1}{2}$ Δm_s transition, the second- and third-order energy corrections to the hyperfine term are as follows if D is much less than $g\beta H$

$$E_{1/2,\,m_I} = -\left(\frac{9A^2}{4H_0}\right)\left(\frac{35}{4} - m_I(m_I+1)\right) + \left(\frac{8A^2}{4H_0}\right)\left(\frac{35}{4} - m_I(m_I-1)\right) + \left(\frac{A^3}{4H_0^2}\right)\left[8\left(\frac{3}{2} - m_I\right)\right]\left[\frac{35}{4} - m_I(m_I-1)\right] + \left(\frac{A^3}{4H_0^2}\right)\left[9(1/2+m_I)\left(\frac{35}{4} - m_I(m_I+1)\right)\right] + \left(\frac{A^2D}{H_0^2}\right)\left[4\left(\frac{35}{4} - m_I(m_I-1)\right)\right]$$

$$E_{-1/2,\,m_I} = -\left(\frac{9A^2}{4H_0}\right)\left[\frac{35}{4} - m_I(m_I-1)\right] - \left(\frac{8A^2}{4H_0}\right)\left[\frac{35}{4} - m_I(m_I+1)\right] + \left(\frac{9A^3D}{4H_0^2}\right)\left[\frac{35}{4} - m_I(m_I-1)\right](1/2-m_I) + \left(\frac{8A^3}{4H_0^2}\right)\left[\left(\frac{35}{4} - m_I(m_I+1)\right]\left(\frac{3}{2}+m_I\right) + \left(\frac{A^2D}{H_0^2}\right)\left[4\left(\frac{35}{4} - m_I(m_I+1)\right)\right]$$

Solving for the energies of the $-\frac{1}{2}$, $m_I - 1 \rightarrow \frac{1}{2}$, m_I and $-\frac{1}{2}$, $m_I \rightarrow {}^1\!2$, $m_I - 1$ transitions, and noting that $\Delta E = g\beta H$ and solving for H or the field position, we arrive at the following equation for the separation of the forbidden doublets

$$\Delta H = \frac{17A'^2}{2H_0} - \left[\frac{67A'^3}{4H_0^2} - \frac{8A'^2D}{H_0^2}\right](2m_I - 1)$$

If the nuclear Zeeman and nuclear quadrupole energies are included the equation becomes the following

$$\Delta H = \frac{17A'^2}{2H_0} + \frac{2g_I}{g}H_0 - \left[\frac{67A'^3}{4H_0^2} - \frac{8A'^2D}{H_0^2} + 2P'\right](2m_I - 1)$$

where the primes indicate that the parameters are expressed in Gauss. This holds strictly only if the angle of the field with the trigonal axis is small since the term in D has a $(3\cos^2\theta - 1)$ term associated with it. However, due to the small magnitude of D in this series, the above equation is still applicable to the powder spectrum. In

(22) W. J. Nicholson and G. Burns, *Phys. Rev.*, **129**, 2490 (1963).
(23) M. T. Hutchings, *Solid State Phys.*, **16**, 227 (1964).
(24) B. Bleaney and D. J. E. Ingram, *Proc. Roy. Soc., Ser. A*, **205**, 336 (1951).

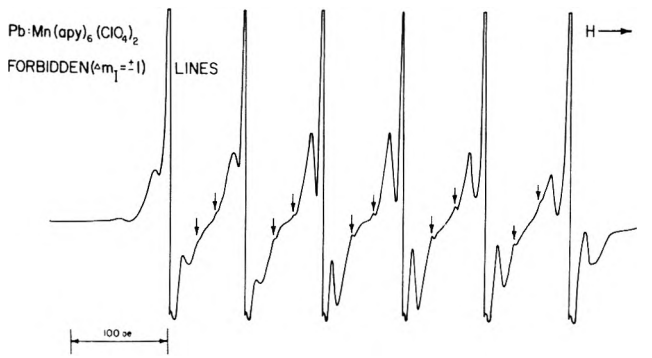

Figure 3. Forbidden lines in the powder esr spectrum of Mn(II)-doped Pb(apy)$_6$(ClO$_4$)$_2$.

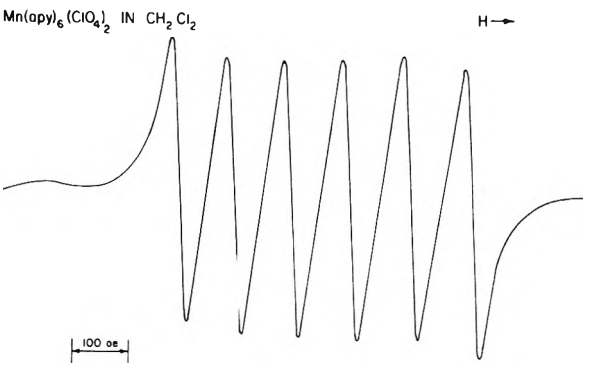

Figure 4. Esr spectrum of Mn(apy)$_6$(ClO$_4$)$_2$ in methylene chloride solution.

Table II the experimental and calculated doublet separations for Mn(II) in four of the host lattices are reported, while Figure 3 shows the forbidden doublets in the lead lattice. For the cadmium complex the doublets were not observed due to masking by other lines present in the spectrum. From the results given in Table II, agreement between theory and experiment is seen to be quite good. In several cases a small nuclear quadrupole term was included in the splitting. As expected for lattices in which the distortion from cubic symmetry is small, the quadrupole coupling constant is quite small. In none of the powder spectra studied was splitting of the main hyperfine lines observed. Bleaney and Rubins[25] observed this in the powder spectra of Mn(II) in moceling clay and calculated the magnitude of this splitting. The splitting was found to always increase with increasing field and was largely dependent on the magnitude of D. Because the values of D are so small for the antipyrine series, their splitting was not observed. The equation derived by Bleaney and Rubins[25] for the separation is as follows

$$\Delta H = x^2\left(1 - \frac{y^2}{4y^2 + 1}\right)$$

where $x = (D'^2/16H_0)[4S(S + 1) - 3]$ and $y = 8(1 - \delta)$ and $\delta = (A'm_I/4H_0)[4S(S + 1) + 1]$. If we utilize this expression to calculate the splitting for the $m_I = \frac{5}{2}$ line of the Mn(II) doped magnesium antipyrine complex which has the largest D value in the series, the separation is calculated to about 4 G. A splitting of this size in a powder spectrum only would broaden the allowed lines, and the broadening should increase with increasing field. This is what is observed for our spectra.

Finally, from our work it was found that even pure crystals of the manganese antipyrine complex allowed resolution of the hyperfine sextet, that is, it was magnetically dilute even in the pure form. This is undoubtedly due to the large size of the antipyrine molecules which brings about large separation of the paramagnetic ions. Studies[26] in this laboratory have indicated that large ligands of this type, when bonded to copper(II) or vanadyl(IV) ions, retard tumbling time in solution to such an extent that powder spectra are observed for free-flowing solutions. We thought it would be of interest to look at esr spectrum of Mn(antipyrine)$_6$(ClO$_4$)$_2$ in methylene chloride. Figure 4 shows the symmetric six-line spectra normally observed for Mn(II) in solution. Hence it seems that Mn(II) is not as sensitive to changes in tumbling time as the other two ions. The isotropic hyperfine coupling constant of −94 G is very close to the values found in single-crystal studies. This lends support to the conclusion that A is relatively unaffected by change of host metal ion, but is much more dependent on local environment.

Acknowledgment. This work was supported by the University of Kentucky Research Foundation and Project Themis DAAB07-69-C-0366. The esr instrument was purchased with the aid of National Science Foundation Grant No. GP-18397.

(25) B. Bleaney and R. S. Rubins, *Proc. Phys. Soc. (London)*, **77**, 103 (1961).
(26) H. J. Stoklosa, H. L. Huffman, and J. R. Wasson, *J. Inorg. Nucl. Chem.*, in press.

Order-Related Properties of Some Nematic Liquids

I. Haller,* H. A. Huggins, H. R. Lilienthal, and T. R. McGuire

IBM Thomas J. Watson Research Center, Yorktown Heights, New York 10598 *(Received September 22, 1972)*

Publication costs assisted by the IBM Corporation

The refractive indices, density, and diamagnetic susceptibility are reported as a function of temperature for three materials that exhibit nematic liquid crystalline phases in the vicinity of room temperature. The temperature dependence of the nematic order parameter is essentially identical for the three materials. The applicability of models used in the computation of polarization fields of anisotropic molecules is evaluated.

Introduction

In recent years several materials became available that exhibit a nematic liquid crystalline phase in the vicinity of room temperature. Existing measurements of important physical properties of these materials are scarce. We wish to report here on our measurements of the ordinary refractive index, birefringence, density, and diamagnetic susceptibility, as a function of temperature, of three materials: 4-*n*-butyl-4′-ethoxy-α-chlorostilbene (I),[1] 4-*n*-octyl-4′-ethoxy-α-chlorostilbene (II),[1] and the mixture (III) of the isomers (IIIa and IIIb) of 4-methoxy-4′-butylazoxybenzene.[2,3]

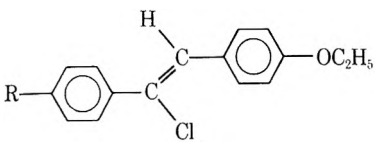

I, R = C_4H_9
II, R = C_8H_{17}

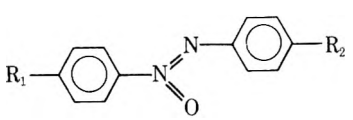

IIIa, R_1 = CH_3O, R_2 = C_4H_9
IIIb, R_1 = C_4H_9, R_2 = CH_3O

The magnetic measurements were also carried out on 4-methoxybenzylidene-4′-*n*-butylaniline (IV).[4]

In addition to the general need for the optical and magnetic data in interpreting other measurements[5,6] on liquid crystals, the measurements reported here are of interest for several reasons. The anisotropy of the diamagnetic susceptibility and, except for possible local-field effects,[7] the anisotropy of the optical dielectric constant are proportional to the order parameter $Q = \frac{1}{2}\langle 3\cos^2\theta - 1\rangle$, where θ is the angle between the long axis of a molecule and the optic axis of nematic liquid. Hence their temperature dependence represents, in the first approximation, the temperature dependence of the order parameter. The proportionality constants are simply the anisotropies of the susceptibility and of the dielectric constant for the (hypothetical) completely ordered liquid crystal. The availability of optical and density data over a wide temperature range including the ordered and the isotropic phases allows evaluation of models proposed for taking account of local fields in the calculation of polarizabilities in nematic liquids.

Experimental Section

The refractive index in the isotropic phase and the ordinary index in the nematic phase were measured with an Abbe refractometer. Birefringences were obtained by measuring the spacings of extinction bands of wedge-shaped samples. The methods have been described in detail earlier.[8]

The diamagnetic susceptibilities were measured and the anisotropy derived in a manner similar to the method of Foex.[9] The liquid crystal samples were degased and sealed *in vacuo* in commercial glass ampoules (Coby Glass Products) and were weighed. The ampoules had been preselected for uniformity in shape and wall thickness; the variation in the weight of glass in the sealed samples amounted to 1%. They were suspended by copper wires in the uniform field gradient region of the automatic balance magnetometer[10] and the gross force measured at five fields ranging from 6 to 14 kOe. The net forces on the samples (which were about half of the gross) were obtained by subtracting the forces on an empty ampoule measured separately at each temperature.

The density measurements were carried out in a Pyrex bicapillary pycnometer[11] on approximately 1 ml size samples.

Compounds I, II, and IV were obtained from W. R. Young of this Laboratory. Material III was purchased from E. M. Laboratories under the trade name Nematic Phase IV (16/76) Licristal. The nematic–isotropic transition temperatures were 57.5–57.7° for I, 61.5–61.7° for II, 74.6–75.0° for III, and 47.0° for IV.

Results

Optical Measurements. The refractive indices and birefringences at 589.3- and 632.8-nm wavelengths are presented in Table I for the three materials investigated. Since the degree of order and consequently the optical proper-

(1) W. R. Young, A. Aviram, and R. J. Cox, *Angew. Chem., Int. Ed. Engl.*, **10**, 410 (1971); *J. Amer. Chem. Soc.*, **94**, 3976 (1972).
(2) H. Kelker, B. Scheurle, R. Hatz, and W. Bartsch, *Angew. Chem., Int. Ed. Engl.*, **9**, 962 (1970).
(3) R. Steinstrasser and L. Pohl, *Tetrahedron Lett.*, 1921, (1971).
(4) H. Kelker and B. Scheurle, *Angew. Chem., Int. Ed. Engl.*, **8**, 884 (1969).
(5) I. Haller and J. D. Litster, *Phys. Rev. Lett.*, **25**, 1550 (1970).
(6) A. Saupe, *Z. Naturforsch. A*, **15**, 81 (1960).
(7) P. G. De Gennes, *Mol. Cryst. Liquid Cryst.*, **12**, 193 (1971).
(8) I. Haller, H. A. Huggins, and M. J. Freiser, *Mol. Cryst. Liquid Cryst.*, **16**, 53 (1972).
(9) G. Foex, *Trans. Faraday Soc.*, **29**, 958 (1933).
(10) T. R. McGuire and P. J. Flanders in "Magnetism and Metallurgy," Vol. 1, A. E. Berkowitz and E. Kneller, Ed., Academic Press, New York, N. Y., 1969, p 175.
(11) ASTM Standard D 1481-62.

TABLE I: Refractive Indices and Birefringences of Three Nematic Liquids as a Function of Reduced Temperature

	Butylethoxychlorostilbene				Octylethoxychlorostilbene				Methoxybutylazoxybenzene			
τ	λ=589.3 nm		λ=632.8 nm		λ=589.3 nm		λ=632.8 nm		λ=589.3 nm		λ=632.8 nm	
	n	Δn	n	Δn	n	Δn	n	Δn	n	Δn	n	Δn
0.0235	--	0	--	0	1.5717	0	1.5651	0	--	0	--	0
0.0150	1.6003	0	1.5931	0	1.5733	0	1.5668	0	1.6181[a]	0	1.6076[a]	0
0.0100	1.6011	0	1.5937	0	1.5741	0	1.5675	0	1.6191	0	1.6085	0
0.0050	1.6020	0	1.5946	0	1.5749	0	1.5684	0	1.6200	0	1.6095	0
0.0010	1.6027	0	1.5952	0	1.5756	0	1.5692	0	1.6207	0	1.6101	0
-0.0005	1.5644	0.107	1.5591	0.103	1.5451	0.094	1.5395	0.091	--	0.121	--	0.114
-0.0012	1.5636	0.117	1.5578	0.112	1.5435	0.100	1.5378	0.096	1.5777	0.132	1.5670	0.124
-0.0025	1.5613	0.120	1.5562	0.121	1.5411	0.110	1.5356	0.106	1.5746	0.142	1.5664	0.134
-0.0040	1.5604	0.134	1.5544	0.129	1.5392	0.116	1.5341	0.112	1.5722	0.149	1.5646	0.141
-0.0060	1.5583	0.141	1.5526	0.137	1.5372	0.124	1.5323	0.118	1.5701	0.158	1.5619	0.151
-0.0080	1.5571	0.147	1.5511	0.144	1.5360	0.130	1.5308	0.125	1.5686	0.165	1.5602	0.157
-0.0100	1.5560	0.152	1.5501	0.148	1.5350	0.135	1.5298	0.129	1.5674	0.171	1.5592	0.163
-0.0150	1.5535	0.163	1.5478	0.158	1.5330	0.144	1.5280	0.139	1.5644	0.183	1.5568	0.175
-0.0200	1.5517	0.171	1.5461	0.166	1.5314	0.151	1.5266	0.147	1.5627	0.191	1.5551	0.184
-0.0300	1.5493	0.184	1.5438	0.177	1.5297	0.162	1.5248	0.155	1.5597	0.206	1.5522	0.200
-0.0400	1.5478	0.194	1.5424	0.187	1.5286	0.172	1.5239	0.165	1.5578	0.216	1.5504	0.209
-0.0500	1.5467	0.202	1.5417	0.195	1.5278	0.179	1.5231	0.172	1.5560	0.228	1.5489	0.219
-0.0600	1.5461	0.210	1.5409	0.203	1.5275	0.186	1.5228	0.178	1.5547	0.237	1.5478	0.227
-0.0800	1.5455	0.223	1.5405	0.215	1.5270	0.196	1.5226	0.189	1.5534	0.253	1.5467	0.241
-0.1000	1.5454	0.231	1.5407	0.228	1.5271	0.207	1.5231	0.200	1.5528	0.265	1.5461	0.253
-0.1200	1.5458[b]	0.240[b]	1.5408[b]	0.232[b]	1.5271[c]	0.212[c]	1.5231[c]	0.204[c]	1.5527	0.276	1.5461	0.262
-0.1400	--	--	--	--	--	--	--	--	1.5527	0.285	1.5464	0.271
-0.1600	--	--	--	--	--	--	--	--	1.5532	0.295	1.5465	0.279
-0.1710	--	--	--	--	--	--	--	--	--	0.299	--	0.286

[a] At τ = 0.160. [b] At τ = −0.1136. [c] At τ = −0.1165.

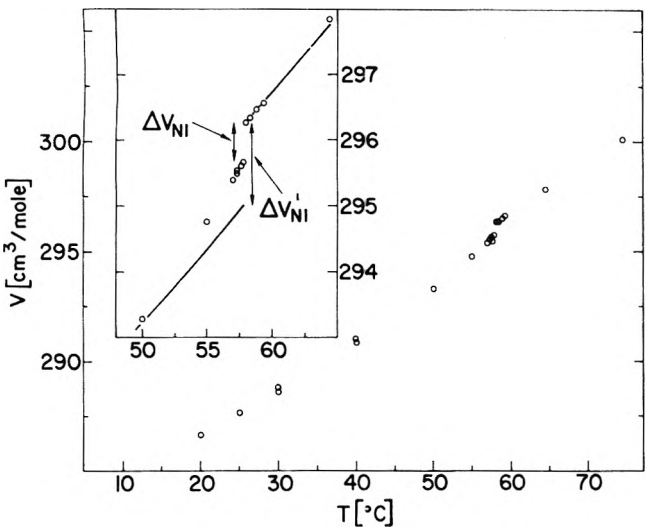

Figure 1. Molar volume of compound I as a function of temperature.

ties vary most rapidly near the transition temperature, t_{NI}, and since t_{NI} can vary from sample to sample, it is more meaningful to inspect the data in terms of a reduced temperature, $\tau = (t - t_{NI})/(t_{NI} + 273.2)$. The data presented in the table have been interpolated from the original numbers[12] to round numbers in the reduced temperature.

The refractive indices represent n_{iso} above the transition temperature, and the ordinary refractive index, n_o in the nematic phase.[8] The systematic error of the refractometer, as checked by calibration with benzene at several temperatures, is less than 0.0002. Random errors in the nematic phase are about twice as large. This is mainly due to a slight blurring of the boundary line corresponding to the critical angle of total internal reflection in the anisotropic liquid.

In the birefringence measurements the random error appears to be ±0.002, while the systematic error due to the wedge angle measurements is estimated, as before,[8] to be 1%. The uncertainty in t_{NI} due to the width of the transition and to temperature gradients is less than 0.2°.

Densities. The molar volume of I as a function of temperature is shown in Figure 1. In the nematic phase, deviations from linearity become noticeable at about 6° below the transition temperature. The behavior of the other two materials investigated was analogous. The densities, volume expansion coefficients [$\beta \equiv (\partial \ln V/\partial T)_p$], and the per cent transition volume changes (as defined in Figure 1) are summarized for all three materials in Table II.

Magnetic Susceptibilities. The diamagnetic susceptibility of the four materials investigated is shown in Figure 2 as a function of temperature. Random errors are approximately ±1%. In the case of compound IV, for which susceptibility data have been reported,[13] the agreement with earlier measurement is satisfactory.

Discussion

Optical Data. In order to calculate the polarizability and its ansiotropy in the nematic phase, specific models taking account of the polarization field in an anisotropic medium need to be considered. We have applied to our data two models[14,15] that have been used previously for *p*-azoxyanisole (PAA). Both models involve severe assumptions.

(12) The original refractive index and birefringence data will appear following these pages in the microfilm edition of this volume of the journal. Single copies may be obtained from the Business Operations Office, Books and Journals Division, American Chemical Society, 1155 Sixteenth St., N.W., Washington, D. C. 20036. Remit check or money order for $3.00 for photocopy or $2.00 for microfiche, referring to code number JPC-73-950.

(13) H. Gasparoux, B. Regaya, and J. Prost, *C. R. Acad. Sci., Ser. B*, **272**, 1168 (1971).

(14) (a) A. Saupe and W. Maier, *Z. Naturforsch. A*, **16**, 816 (1961); (b) H. E. J. Neugebauer, *Can. J. Phys.*, **32**, 1 (1954).

(15) (a) S. Chandrasekhar and N. V. Madhusudana, *J. Phys. (Paris), Suppl.*, **30**, C4-24 (1969); (b) M. F. Vuks, *Opt. Spektrosk.*, **20**, 644 (1966).

TABLE II: Densities and Expansion Coefficients for the Nematic and Isotropic Phases, and the Fractional Volume Changes of the Phase Transition

Material	$d_{N,25}$, g cm^{-3}	$10^3\beta_N$[a], °C^{-1}	$d_{I,75}$, g cm^{-3}	$10^3\beta_I$[b] °C^{-1}	$\Delta V_{NI}/V$, %	$\Delta V'_{NI}/V$, %
I	1.0945	0.77	1.0486	0.79	0.17	0.42
II	1.0508	0.80	1.0055	0.82	0.12	0.40
III	1.1174	0.73	1.0732	0.78	0.16	0.36

[a] From least-squares fit of ln V vs. t of all points with $t < t_{NI-6}$. [b] From least-squares fit of all points in the isotropic phase.

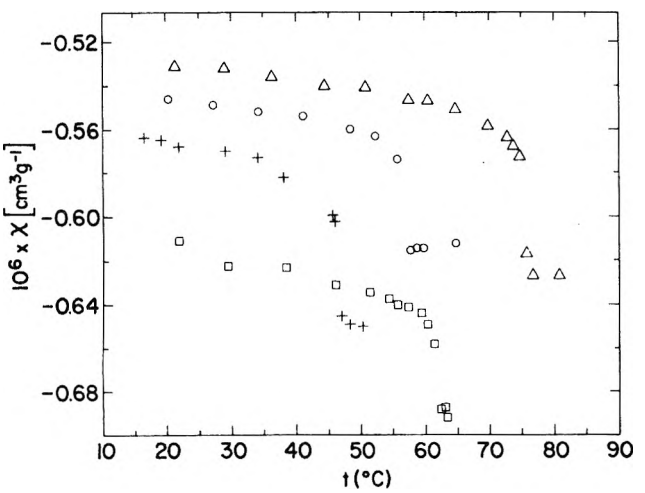

Figure 2. Magnetic susceptibility in the nematic and isotropic phases: compound I, circles; compound II, squares; material III, triangles; compound IV, crosses.

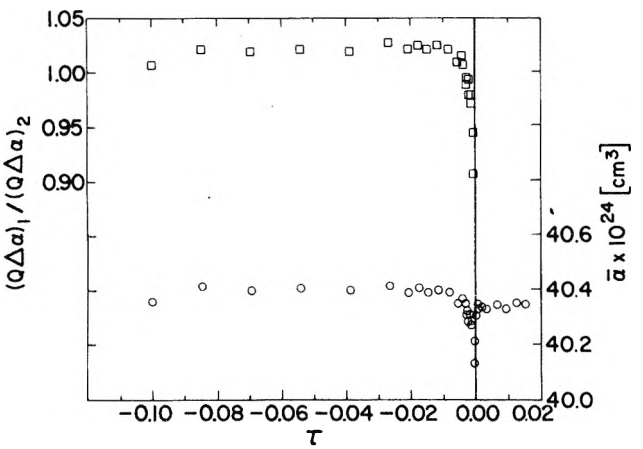

Figure 3. The mean polarizability (circles, scale on right), and the ratio of the polarizability anisotropy from two sets of data (squares, scale on left) for compound I.

The Saupe-Maier-Neugebauer (SMN) model[14] provides a local field correction with the use of a quantity a expressed as a function of the coordinates of the molecules within the Lorentz sphere. It is thus a purely geometric factor which, in the absence of precise structural information, becomes an adjustable parameter. Consequently the only test of consistency of the SMN method is to examine whether the variations in a are reasonable. As with PAA, this parameter for all three compounds appears to be independent of wavelength within experimental error. In contrast to PAA, however, the a values as a function of temperature in all cases exhibit a minimum at about $\tau = -0.01$. This is contrary to the reasonable expectation[14a] that the correction parameter should decrease monotonically as the anisotropy of the local field decreases with increasing temperature.

The Chandrasekhar-Madhusudana-Vuks (CMV) approach[15] assumes that the Lorentz-Lorenz type equations

$$(n_e^2 - 1)/(\bar{n}^2 + 2) = 4/3\pi N(\bar{\alpha} + 2/3Q\Delta\alpha) \quad (1)$$

and

$$(n_o^2 - 1)/(\bar{n}^2 + 2) = 4/3\pi N(\bar{\alpha} - 1/3Q\Delta\alpha) \quad (2)$$

are valid for the principal axes of polarizability of the nematic medium and that the polarizabilities obtained from eq 1 and 2 are those of the isolated molecule, *i.e.*, independent of temperature and of the state of matter. In these equations n_e and n_o are the extraordinary and ordinary refractive indices $\bar{n}^2 = \frac{1}{3}(n_e^2 + 2n_o^2)$, $\bar{\alpha} = \frac{1}{3}(\alpha_{\parallel} + 2\alpha_{\perp})$, $\Delta\alpha = \alpha_{\parallel} - \alpha_{\perp}$, and N is the number of molecules per cm^3.

In Figure 3 we plot, as a function of temperature, $\bar{\alpha}$ of compound I at 589 nm, obtained by combining eq 1 and 2 and using the experimentally determined refractive indices, birefringences, and densities. A more severe test of the CMV method is to compare $Q\Delta\alpha$ computed separately from eq 1 and 2 by taking $\bar{\alpha} = \alpha_{iso}$.[16] As seen from Figure 3, at temperatures lower than 1° below T_{NI} the mean polarizability is constant and the ratio of the independently computed $Q\Delta\alpha$'s is not significantly different from unity. The discrepancy in the immediate vicinity of the transition temperature may be caused by error due to the difficulties in assigning T_{NI} for a transition with a breadth of about 0.1°. Entirely analogous results were obtained with the data for the other two compounds and also at 633-nm wavelength. Our data support the validity of the assumptions of the CMV method, implying either[15b] that the internal field is isotropic in all states of matter, or at least that it does not change in the isotropic to nematic transition. To the extent that the major contribution to the internal field around a molecule arises from near neighbors and that short-range order persists[7] to well above the transition temperature, the second implication is indeed highly plausible.

In the absence of solid-state optical and X-ray data, $\Delta\alpha$ is not known, and the order parameter cannot be separated. Its temperature dependence is given, however, by $Q\Delta\alpha$, and this quantity, obtained by subtracting eq 2 from 1, and from the data at 589 nm, is given in Figure 4. The curves for the three materials are remarkable similar, in fact if $Q\Delta\alpha(\tau)$ is scaled at a conveniently chosen temperature, as is done in Figure 5 for the data at 633 nm, within experimental error the points for all three materials fall on a single line. At least for the materials investigated here, the order parameter is apparently a universal function of the reduced temperature.

(16) If, for example, in eq 1 and 2 $\bar{n}$ were replaced by n_e and n_o, respectively, the variation in the mean polarizability would still be less than 1%, but the ratio of the two separately computed $Q\Delta\alpha$'s would vary from 0.32 to 0.37 over the same temperature range.

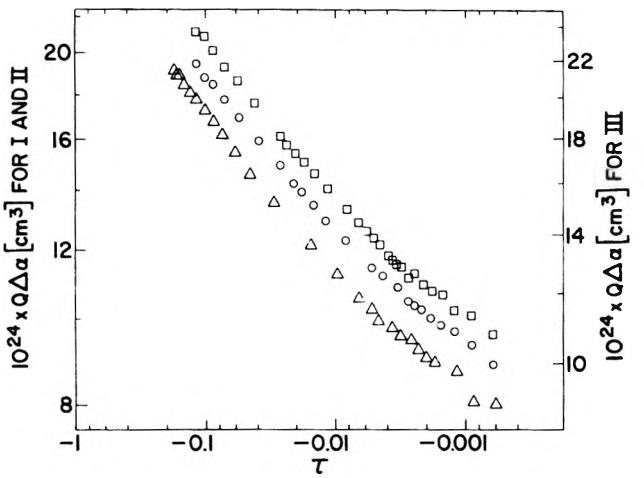

Figure 4. Log–log plot of $Q\Delta\alpha$ at 589 nm *vs.* reduced temperature: circles, compound I; squares, compound 2 (scale on left side); triangles, material III (scale on right)

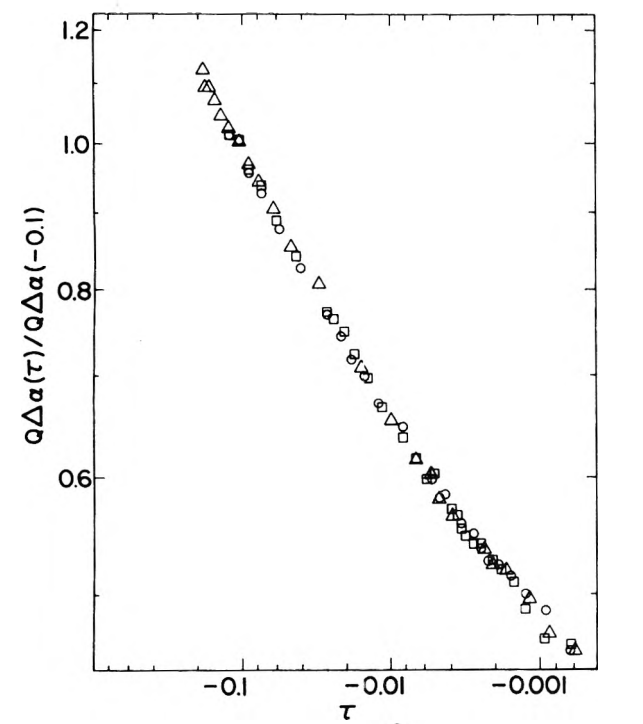

Figure 5. Log–log plot of the scaled polarizability anisotropy at 633 nm *vs.* reduced temperature: circles, compound I; squares, compound II; triangles, material III.

In the low-temperature region of Figure 4, log $Q\Delta\alpha$ appears to be proportional to log $(-\tau)$. The slopes of the linear least-squares fits for data points with $\tau < -0.01$ are shown in Table III. The slightly higher slopes for material III is of marginal significance.

If one assumes that the straight line sections of the curves in Figure 4 can be extrapolated to $T = 0°K$ ($\tau = -1$), where the order parameter is unity, the intercept should yield the anisotropy of the polarizability. These numbers are also included in Table III. A similar extrapolation for PAA, using optical and density data from the literature,[17,18] yields $\Delta\alpha = 31.4 \times 10^{-24}$ cm^3, compared to 34.7×10^{-24} cm^3 obtained from the solid-state optical constants.[15a,19] The 10% discrepancy casts some doubt on the utility of the extrapolation process, although it is highly probable that inner field effects, which appear negligible at the nematic–isotropic transition, would play a role at the solid–nematic transition.

TABLE III: Slopes of the Low-Temperature Sections of Log $Q\Delta\alpha$ *vs.* Log $(-\tau)$ Plots and the Anisotropies of the Polarizabilities Obtained by Extrapolating to Absolute Zero

	d log $Q\Delta\alpha$/d log $(-\tau)$		$10^{24}\Delta\alpha$, cm^3	
Material	589 nm	633 nm	589 nm	633 nm
I	0.177	0.181	28.5	27.9
II	0.179	0.179	31.1	30.0
III	0.190	0.184	30.0	28.1

TABLE IV: Polarizabilities and the Dispersion of the Polarizability Anisotropy

	$10^{24}\bar{\alpha}$, cm^3				
	Nematic[a]		Isotropic		
Material	589	633	589	633 nm	$Q\Delta\alpha_{589}{}^a/Q\Delta\alpha_{633}$
I	40.39	39.98	40.34	39.93	1.035
II	47.91	47.46	47.85	47.41	1.037
III	36.98	36.48	36.95	36.44	1.048

[a] Disregarding points with τ between 0 and −0.003.

Table IV summarizes the mean polarizabilities in the nematic and isotropic phases at 589 and 633 nm, and the ratio of $Q\Delta\alpha$ at the two wavelengths, averaged over the proper temperature range, for the three materials studied. The anisotropy of the polarizability is seen to exhibit a much larger per cent dispersion than the mean polarizability in accordance with the expectation that the transition moment of the first absorption band of these compounds lies along the molecular axis. The increment in the mean polarizability per methylene group (1.88×10^{-24} cm^3) obtained by comparing compounds I and II is in good agreement with quoted values.[20-22]

Molar Volumes. If additivity of atomic volumes is assumed, from the difference in the molar volumes of the octyl and the butylethoxychlorostilbenes, the contribution of a single methylene group is calculated to be 16.34 cm^3/mol at 25° in the nematic phase. This number is only slightly lower than the contribution of a methylene group in *n*-alkanes,[23] alkylbenzenes,[21] or alkylbiphenyls[22] (16.4, 16.6, and 17.1 cm^3/mol, respectively) in the isotropic phase, and it is substantially higher than *n*-alkanes in the solid state[23] (14.5). This indicates that in the nematic phase the packing of alkyl wing groups (as well as that of the aromatic cores of the molecules) is closer to the isotropic than to the solid phase.

The fractional volume change associated with the nematic–isotropic transition is remarkably small in all three compounds investigated. Wulf and De Rocco[24] examined the statistical mechanics of semiflexible molecules as a model for nematic liquids. Their model predicts an

(17) M. Brunet-Germain, *Mol. Cryst. Liquid Cryst.*, 11, 289 (1970).
(18) W. Maier and A. Saupe, *Z. Naturforsch. A*, 15, 287 (1960).
(19) P. Chatelain, *C. R. Acad. Sci.*, 203, 1169 (1936).
(20) A. I. Vogel, W. Cresswell, G. Jeffery, and I. Leicester, *Chem. Ind.*, 376 (1951).
(21) J. Timmermans, "Physico-chemical Constants of Pure Organic Compounds," Elsevier Publishing Co., Amsterdam, 1965.
(22) I. A. Goodman and P. K. Wise, *J. Amer. Chem. Soc.*, 72, 3076 (1950).
(23) S. S. Kurtz in "The Chemistry of Petroleum Hydrocarbons," Vol. 1, B. T. Brooks, *et al.*, Ed., Reinhold, New York, N. Y., 1954, p 275.
(24) A. Wulf and A. G. De Rocco, *J. Chem. Phys.*, 55, 12 (1971).

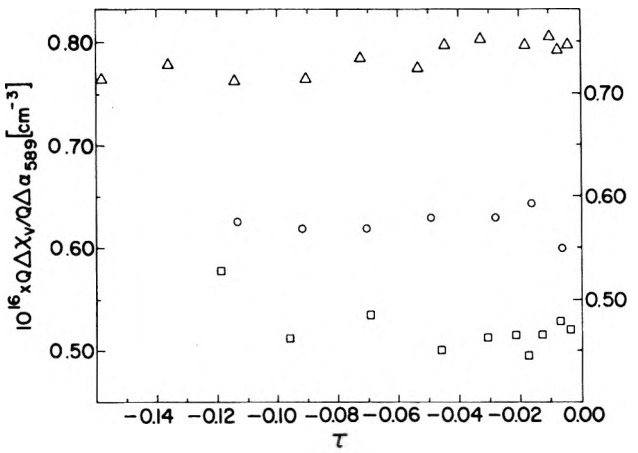

Figure 6. Test of identity of the temperature dependence of the nematic order parameter from optical and diamagnetic measurements: circles, compound I (scale on right); squares, II; triangles, III (scale on left).

inverse relation between the flexibility of the molecules and the relative volume change at the nematic–isotropic phase transition. The fact that the $\Delta V_{NI}/V$ values of the compounds studied here are significantly less than the transition volume change in PAA[18,25,26] could be accommodated in the framework of their model implying that much of the flexibility resides in the wing groups. This is consistent with our previous conclusion[27] that alkyl wing groups of molecules in the nematic phase should not be regarded as occupying a single, elongated conformation.

It is also noteworthy that the direct volume change is but a small fraction of the total volume change as estimated from the extrapolation of data more than 6° below the transition temperature. That is $\Delta V_{NI}/\Delta V_{NI}'$ varies from 0.3 to 0.45 for the three materials. It is clear from the optical data, that in the corresponding temperature range the order parameter does not diminish by a comparable factor.

Diamagnetic Anisotropy. Our experiments measure the highest susceptibility, which in the isotropic phase is the mean molecular susceptibility, $\bar{\chi} = \frac{1}{3}(\chi_{\parallel} + 2\chi_{\perp})$, and in the nematic phase the axial susceptibility, $\chi_n = \bar{\chi} + \frac{2}{3} Q\Delta\chi$, where $\Delta\chi = \chi_{\parallel} - \chi_{\perp}$. By combining the data in the two phases, numerical values of $Q\Delta\chi$ can be obtained as a function of temperature.

It has been pointed out by De Gennes[7] that the definition of the order parameter through the diamagnetic anisotropy is theoretically preferable since the complications due to electrical interactions between molecules do not arise. Unfortunately the inherent precision of diamagnetic susceptibility measurements is far worse than that of optical measurements. With this limitation in mind, however, we can compare the temperature dependence of the order parameter obtained from the optical and from the magnetic data.

In Figure 6 the ratio of $Q\Delta\chi$ (multiplied by the density to convert to unit volume) to $Q\Delta\chi_{589}$ is plotted for the three nematic liquids investigated as a function of reduced temperature. While the scatter is substantial, no trend with temperature is apparent within experimental error. This confirms the conclusion that the assumptions in the CMV treatment of the optical data are adequately satisfied.

Acknowledgments. We wish to thank Dr. W. R. Young for providing materials, and Dr. M. J. Freiser for valuable comments.

(25) E. McLaughlin, A. Shakespeare, and R. Ubbelohde, *Trans. Faraday Soc.*, **60**, 25 (1964).
(26) F. P. Price and J. H. Wendorff, *J. Phys. Chem.*, **76**, 2605 (1972).
(27) W. R. Young, I. Haller, and A. Aviram, *Mol. Cryst. Liquid Cryst.*, **13**, 372 (1971).

Intramolecular Energy Relaxation in the Photodissociation of Cyclobutanone

F. H. Dorer

Chemistry Department, California State University, Fullerton, California 92634 *(Received September 22, 1972)*

Publication costs assisted by The National Science Foundation

The product energy distribution indicates that there is random intramolecular energy relaxation in the cyclopropane-forming reaction when cyclobutanone is photolyzed by wavelengths ≤313 nm. In addition, there appear to be two mechanisms by which the cyclopropane fragment is formed; the relative importance of the two mechanisms is wavelength dependent. The results also illustrate that internal vibrational energy randomization occurs in less than 10^{-10} sec.

Introduction

Although it has been recognized that the characterization of how energy is partitioned to the reaction products might offer some insight into the mechanistic details of photofragmentation reactions,[1-4] there are at least two major problems in interpreting the product energy distri-

(1) S. H. Bauer, *J. Amer. Chem. Soc.*, **91**, 3688 (1969).

butions observed on photolysis of relatively complex molecules. A problem encountered with cyclic azo compounds has been that more than one electronic state of the reactant can produce the same product,[4,5] and the product energy distribution may reflect unknown contributions of different reactant states. Another problem is that the lifetime of the decomposition state may be sufficiently long such that some intermolecular energy relaxation occurs prior to the fragmentation reaction.[2,4] Collisional relaxation problems produce a distribution of vibronic states of the reactant, the nature of which will depend on the pressure of the system, and the product energy distribution loses some of its feasibility for elucidating characteristics of the potential surface on which the reaction proceeded.

An ideal system for studying energy partitioning would be one for which the product arises from only one electronic state of the reactant, or at least the relative importance of any other electronic state is well documented, and the lifetimes of the dissociative states are less than the collisional relaxation time. Lee and his coworkers have demonstrated that at least 85% of the cyclopropane produced on photolysis of cyclobutanone by wavelengths ≤313 nm arises by direct dissociation of the S_1 state with a lifetime of $<10^{-10}$ sec.[6-8] At ordinary pressures collisional relaxation of the initially prepared state of the reactant does not occur.

Since the purity of the reactant state is relatively high,[9] and there are no intermolecular energy relaxation problems, we have, using the extensive experimental data of Lee and coworkers,[6b] characterized how the available energy is partitioned to the internal degrees of freedom of the cyclopropane fragment produced on photolysis of cyclobutanone. Although energy partitioning in cyclobutanone photolysis has previously been investigated,[10] there are now more extensive data available, and the present treatment of the data and our conclusions differ significantly from the earlier study.

A mechanism used to describe the cyclopropane product formation from cyclobutanone on photolysis by wavelengths below 319 nm is one in which the S_1 state rapidly predissociates to an intermediate, which may be a singlet 1,4 biradical, and the intermediate decarbonylates to form cyclopropane and carbon monoxide (Scheme I).[6-8] The asterisk in Scheme I denotes a vibrationally excited species. From a detailed study of the *cis*- and *trans*-2,3- and *cis*-

Scheme I

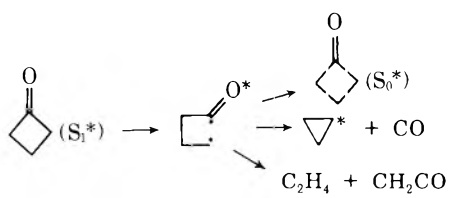

and *trans*-2,4-dimethylcyclobutanones it has been determined that the short lived ($<10^{-10}$ sec) singlet 1,4 biradical intermediate undergoes cyclization, decarbonylation, and bond rotation on a competitive time scale.[7] Therefore, for this system, one is probably dealing with intramolecular vibrational energy relaxation of a monoenergetic vibrationally excited intermediate in its lowest electronic singlet state that decomposes to ground electronic state products with a rate at least as great as the rate of internal bond rotations ($>10^{10}$ sec^{-1}). The photochemical decomposition of cyclobutanone provides a system in which one can characterize intramolecular vibrational energy relaxation on very short time scales in a novel manner. This aspect of the work is discussed in a following section of this paper.

Results and Discussion

Experimental and Calculated Rate Constants for Isomerization of the Vibrationally Excited Cyclopropane. The experimental data that we have used for this work are the relative amounts of C_3H_5T and c-C_3H_5T produced on photolysis of cyclobutanone-2-*t*, CBT, as a function of pressure and wavelength of photolysis. These data are contained in ref 6b.[11]

It has generally been accepted that all of the proplyene formed on photolysis of cyclobutanone arises from the isomerization of the vibrationally excited cyclopropane formed in the primary process.[6,10,12] However, we illustrate in Figures 1 and 2 the C_3H_5T:c-C_3H_5T ratio resulting from photolysis of CBT at higher pressures. Since the limiting high-pressure C_3H_5T:c-C_3H_5T ratio is not zero at any of these photolysis wavelengths, there does appear to be a small, but relatively important, amount of propylene formed in the primary photodissociation process.

The amount of propylene formed in the primary process is wavelength dependent. Consequently, the scheme from which one must calculate the experimental values for the unimolecular rate constants for the isomerization of c-C_3H_5T* is

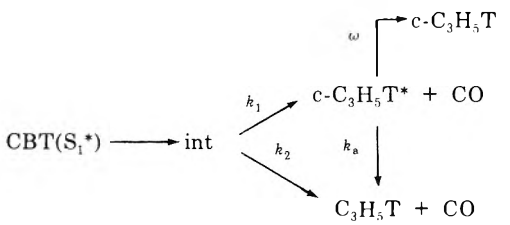

In this scheme ω is the collisional vibrational deactivation rate of c-C_3H_5T* by the bath molecules (propylene and CBT in the present case). Equation 1 is then appropriate for calculating the experimental values of k_a from the measured C_3H_5T:c-C_3H_5T ratios.

(2) (a) T. F. Thomas, C. I. Sutin, and C. Steel, *J. Amer. Chem. Soc.*, **89**, 5107 (1967); (b) B. S. Solomon, T. F. Thomas, and C. Steel, *ibid.*, **90**, 2249 (1968).
(3) (a) F. H. Dorer, E. Browr, J. Do, and R. Rees, *J. Phys. Chem.*, **75**, 1640 (1971); (b) F. H. Dorer and S. N. Johnson, *ibid.*, **75**, 3651 (1971).
(4) G. L. Loper and F. H. Dorer, *J. Amer. Chem. Soc.*, **95**, 20 (1973).
(5) R. Moore, A. Mishra, and R. J. Crawford, *Can. J. Chem.*, **46**, 3305 (1968).
(6) (a) J. C. Hemminger and E. K. C. Lee, *J. Chem. Phys.*, **56**, 5284 (1972); (b) N. E. Lee and E. K. C. Lee, *ibid.*, **50**, 2094 (1969); (c) H. O. Denschlag and E. K. C. Lee, *J. Amer. Chem. Soc.*, **90**, 3628 (1968).
(7) (a) J. C. Hemminger, H. A. J. Carless, and E. K. C. Lee, *J. Amer. Chem. Soc.*, **95**, 682 (1973); (b) H. A. J. Carless and E. K. C. Lee, *ibid.*, **92**, 4482, 6683 (1970); (c) H. A. J. Carless, J. Metcalfe, and E. K. C. Lee, *ibid.*, **94**, 7221 (1972).
(8) H. A. J. Carless and E. K. C. Lee, *J. Amer. Chem. Soc.*, **94**, 1 (1972).
(9) The purity of the reactant state in the photolysis system has been supported by a recent study in which it was found that chemically activated methylcyclobutanone with internal energy ~100 kcal mol^{-1}, produced by methylene insertion into the CH bonds of cyclobutanone, yields a total of only 10% C_4H_8 isomers relative to the C_2H_4 and C_3H_6 products. Unpublished data of R. B. Wollenberg and F. H. Dorer.
(10) (a) R. J. Campbell and E. W. Schlag, *J. Amer. Chem. Soc.*, **89**, 5103 (1967); (b) R. F. Klemm, D. N. Morrison, P. Gilderson, and A. T. Blades, *Can. J. Chem.*, **43**, 1934 (1965); (c) R. J. Campbell, Ph.D. Thesis, Northwestern University, 1967.
(11) A tabulated summary of the data was generously provided by Professor E. K. C. Lee.
(12) R. J. Campbell, E. W. Schlag, and B. Ristow, *J. Amer. Chem. Soc.*, **89**, 5098 (1967).

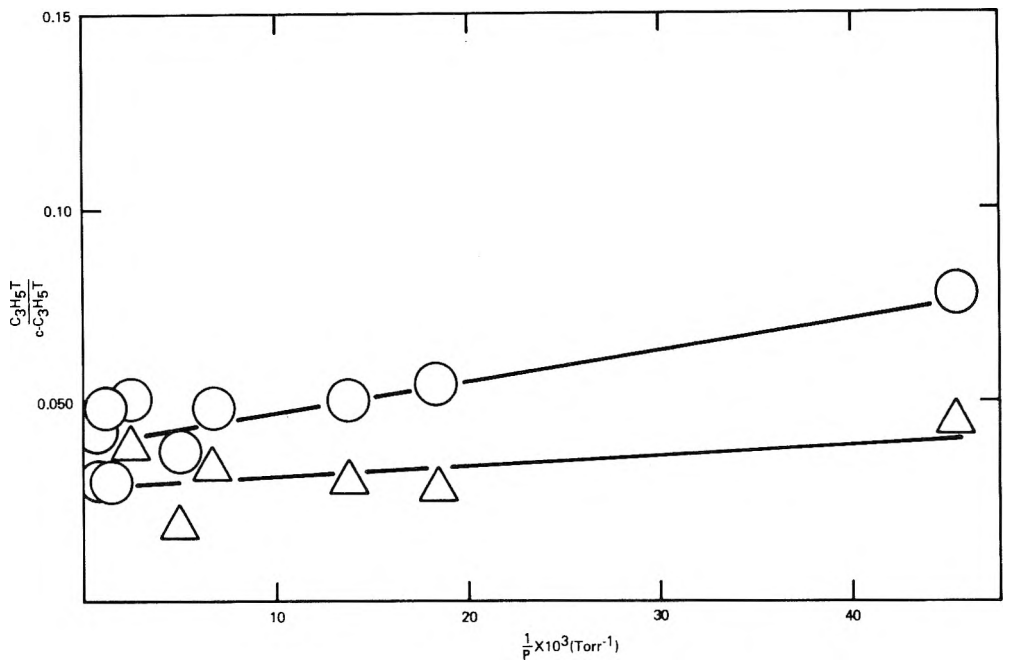

Figure 1. Pressure dependence of the C_3H_5T:c-C_3H_5T ratio in the high-pressure region; △, 313-nm photolysis; ○, 302-nm photolysis.

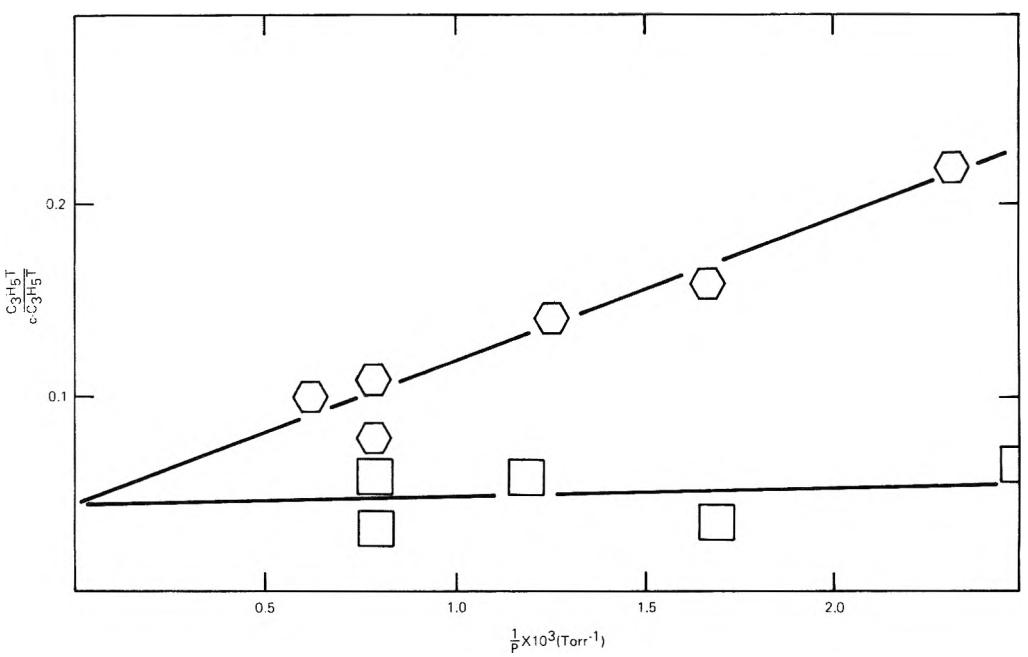

Figure 2. Pressure dependence of the C_3H_5T:c-C_3H_5T ratio in the high-pressure region; □, 289.4-nm photolysis; ⬡ 253.7-nm photolysis.

$$k_a = \omega \frac{C_3H_5T/c\text{-}C_3H_5T - k_2/k_1}{1 + k_2/k_1} \qquad (1)$$

The values of k_2/k_1, obtained by extrapolation of the data in Figures 1 and 2, are 0.05 (253.7 nm), 0.05 (289 nm), 0.04 (302 nm), and 0.03 (313 nm).

There appears to be sufficient evidence to conclude that a vibrationally excited cyclopropane with internal energy content in the range of 100 kcal mol^{-1} will lose at least 10 kcal mol^{-1} of its internal energy on collision with a bath molecule of the complexity of propylene at room temperature.[6b,13] Since the most probable internal energy content of the cyclopropane fragment produced in this system is between 66 and 83 kcal mol^{-1}, depending on photolysis wavelength, the unit efficiency collisional deactivation assumption would seem to be particularly appropriate, except perhaps for photolysis by 253.7-nm radiation at the lowest pressures. Consequently, ω can be calculated from gas kinetic theory using Lennard-Jones force constants and the $\Omega^{(2,2)}$ integral to calculate the collision cross sections.[10a,14]

(13) (a) J. D. Rynbrandt and B. S. Rabinovitch, *J. Phys. Chem.*, **74**, 1679 (1970); (b) W. G. Clark, D. W. Setser, and E. E. Siefert, *ibid.*, **74**, 1670 (1970); (c) B. S. Rabinovitch, H. F. Carroll, J. D. Rynbrandt, J. H. Georgakakos, B. A. Thrush, and R. Atkinson, *ibid.*, **25**, 3376 (1971); (d) D. W. Setser, B. S. Rabinovitch, and J. W. Simons, *J. Chem. Phys.*, **40**, 1751 (1964); (e) J. W. Simons, B. S. Rabinovitch, and D. W. Setser, *ibid.*, **41**, 800 (1964).

(14) J. O. Hirschfelder, C. F. Curtis, and R. B. Bird, "Molecular Theory of Gases and Liquids," Wiley, New York, N. Y., 1954.

The experimental unimolecular rate constant for the isomerization of c-$C_3H_5T^*$ is related to the microscopic unimolecular rate constants for isomerization of c-$C_3H_5T^*$ with energy E, k_E, by

$$k_1 = \omega \sum^{E_T} \frac{k_E}{k_E + \omega} f(E) / \sum^{E_T} \frac{\omega}{k_E + \omega} f(E) \quad (2)$$

In eq 2 $f(E)$ is the internal energy distribution function of the vibrationally excited c-$C_3H_5T^*$ formed in the primary process. For the fragmentation of cyclobutanone to cyclopropane it appears that the most suitable form for $f(E)$ is a statistical distribution function.[3,10a,15]

$$f(E) = \frac{N(E^+ - E_R) \sum^{E_R} P_R(E_R)}{\sum P^+(E^+)} \quad (3)$$

In eq 3, $N(E^+ - E_R)$ is the density of energy eigenstates for those internal degrees of freedom of the activated complex for the decomposing intermediate that will be associated with the internal degrees of freedom of the cyclopropane or trimethylene biradical product. The $\Sigma P_R(E_R)$ term is the sum of energy eigenstates for those degrees of freedom of the activated complex that are to become the carbon monoxide stretching frequency and the three relative translation and two additional rotational degrees of freedom of the newly formed products. The normalization term in the denominator is the sum of energy eigenstates over all of the internal degrees of freedom of activated complex derived from the 1,4 biradical intermediate, allowing one C-C stretching frequency to be the reaction coordinate (*i.e.*, a C-C stretching frequency becomes a relative translation). The product energy distribution is relatively insensitive to the details of the frequency assignment. The k_E values in eq 2 were calculated using RRKM Theory,[16] allowing all of the internal degrees of freedom of the cyclopropane to be active. The evaluation of the sum and density terms in eq 2 and 3 as made by using an exact sum computer program[17] in the lower energy region and the approximation of Whitten and Rabinovitch[18] in the higher energy region.

The frequency assignments for the 1,4 biradical activated complex and c-C_3H_5T were constructed from the known assignments for cyclobutanone,[19] c-C_3H_6, and c-C_3D_6.[20] The c-C_3H_5T vibrational frequency assignment was constructed with the aid of the Teller-Redlich product rule,[21] and the activated complex model for the cyclopropane to propylene isomerization was consistent with the thermal data[22] for c-C_3H_5T isomerization. The k_E values calculated for c-C_3H_5T isomerization were a factor of 1.7 lower than those calculated for c-C_3H_6 at the same energy; a not unreasonable magnitude for the sum of the primary and secondary isotope effects.[23]

The total energy to be distributed to the reaction products is the sum of the absorbed light energy, the exothermicity of the reaction at 0°K, and the thermal energy of the cyclobutanone reactant. After estimating the enthalpy of formation of cyclobutanone at 0°K from an approximate value for its enthalpy of formation at 298.2°K,[6b] the total energy available to the cyclopropane and carbon monoxide fragments that are produced on photolysis of cyclobutanone is

$$E_T = E_{ex} - 3.6 \text{ kcal mol}^{-1} \quad (4)$$

where E_{ex} is the energy of the absorbed radiation in units of kcal mol^{-1}.

Two mechanisms for statistical energy relaxation might be appropriate in the cyclobutanone system. Mechanism I is one in which all of the available energy given by eq 4 can be statistically redistributed to the reaction products. If a singlet 1,4 biradical is an intermediate, mechanism I would imply that the biradical undergoes simultaneous loss of CO and cyclopropane ring formation, and even the energy released on going from the activated complex to reaction products is randomly distributed to the degrees of freedom of the CO and cyclopropane fragments.

Mechanism II is one in which loss of CO from the intermediate and cyclopropane formation are sequential and the trimethylene biradical is actually a second intermediate in the cyclopropane forming reaction. The potential energy of trimethylene has been estimated at 52–64 kcal above cyclopropane.[24] For the present we will take the lowest value; the consequences of using a higher value for the enthalpy of formation of trimethylene on the energy distribution calculations will be illustrated. If the 1,3 biradical were an intermediate the amount of energy available for statistical redistribution to the trimethylene and carbon monoxide fragments, E^+, is the light energy absorbed by the cyclobutanone minus 56–58 kcal mol^{-1}. The intermediate is ~58 kcal above cyclobutanone in energy.[7c,25a] Of course, one must add 52 kcal mol^{-1} to the amount of energy partitioned to the trimethylene fragment in order to obtain the internal energy of the formed cyclopropane.

The first question that must be answered is does a statistical model for energy relaxation fit the experimental results? In Figures 3–6 are illustrated the experimental and calculated values of k_a for four photolysis wavelengths. The recently measured enthalpy of combustion of cyclobutanone[25b] indicates that its enthalpy of formation can be 4 kcal mol^{-1} more exothermic than the value given in ref 6b. Calculational results are also given in Figures 3–5 using this new value for the enthalpy of formation of cyclobutanone. In view of the uncertainties in the energetics collisional deactivation rate, k_a, and the magnitude of the calculated k_E values, one would conclude that the experimental data for 313- and 302-nm photolysis are fitted about as well as can be expected by mechanism I. Mechanism II yields rate constants that are a factor of 5–10 higher than the experimental results, depending on the value of E_T used, if the energy of the trimethylene is taken to be 52 kcal above cyclopropane. Raising the energy of the trimethylene biradical would only make the calculated rates even greater. It appears that on photolysis of

(15) Y. N. Lin and B. S. Rabinovitch, *J. Phys. Chem.*, **74**, 1769 (1970).
(16) (a) R. A. Marcus, *J. Chem. Phys.*, **20**, 359 (1952); (b) R. A. Marcus and O. K. Rice, *J. Phys. Colloid. Chem.*, **55**, 894 (1951).
(17) Kindly supplied by Professor B. S. Rabinovitch.
(18) G. Z. Whitten and B. S. Rabinovitch, *J. Chem. Phys.*, **38**, 2466 (1963).
(19) K. Frei and Hs. H. Gunthard, *J. Mol. Spectrosc.*, **5**, 218 (1960).
(20) S. J. Cyvin, *Spectrochim. Acta*, **16**, 1022 (1960).
(21) E. B. Wilson, J. C. Decius, and P. C. Cross, "Molecular Vibrations," McGraw-Hill, New York, N. Y., 1955, p 183.
(22) R. H. Lindquist and G. K. Rollefson, *J. Chem. Phys.*, **24**, 725 (1956).
(23) (a) K. Dees and D. W. Setser, *J. Chem. Phys.*, **49**, 1193 (1968); (b) F. H. Dorer and B. S. Rabinovitch, *J. Phys. Chem.*, **69**, 1973 (1965); (c) J. W. Simons and B. S. Rabinovitch, *ibid.*, **68**, 1322 (1964); (d) J. W. Simons, B. S. Rabinovitch, and R. F. Kubin, *J. Chem. Phys.*, **40**, 3343 (1964); (e) B. S. Rabinovitch and J. H. Current, *Can. J. Chem.*, **40**, 557 (1962).
(24) (a) P. J. Hay, W. J. Hunt, and W. A. Goddard, *J. Amer. Chem. Soc.*, **94**, 638 (1972); (b) L. Salem and C. Rowland, *Angew. Chem., Int. Ed. Engl.*, **11**, 92 (1972), and references cited therein; (c) H. E. O'Neal and S. W. Benson, *J. Phys. Chem.*, **72**, 1866 (1968).
(25) (a) A. T. Blades, *Can. J. Chem.*, **47**, 615 (1969); (b) G. Wolfe, *Helv. Chim. Acta*, **55**, 1446 (1972).

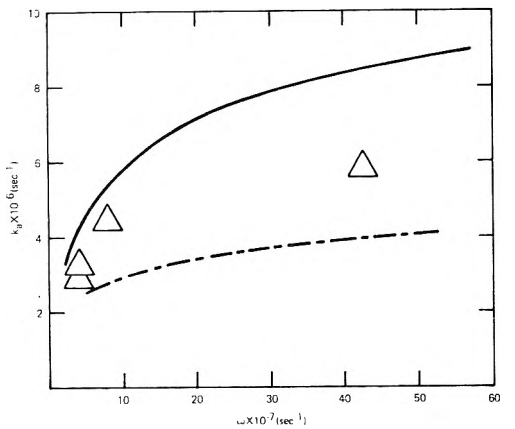

Figure 3. Experimental and calculated values of k_a as a function of ω resulting from 313-nm photolysis of CBT. The solid line is a calculated curve for $E^+ = 88$ kcal mol^{-1}. The broken line is a calculated curve for $E^+ = 84$ kcal mol^{-1}. Mechanism II yields rate constants that are a factor of ~7–8 greater than the calculated rate constants for mechanism I.

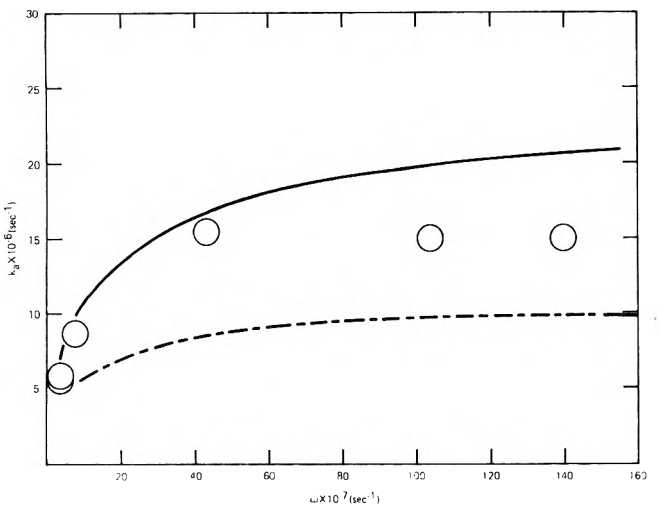

Figure 4. Experimental and calculated values of k_a as a function of ω resulting from 302-nm photolysis of CBT. The solid line is a calculated curve for $E^+ = 91$ kcal mol^{-1}. The broken line is a calculated curve for $E^+ = 88$ kcal mol^{-1}. Mechanism II yields rate constants that are a factor of ~7–8 greater than the calculated rate constants for mechanism I.

cyclobutanone at longer wavelengths in its first singlet band there is statistical relaxation of all of the available energy to the reaction products.

The situation changes somewhat on photolysis at shorter wavelengths. Mechanism I begins to give calculated values below the experimental results at 289 nm and the disagreement is quite pronounced at 253.7 nm. However, even at these shorter wavelengths mechanism II yields results considerably greater than the experimental values. A plausible explanation is that the intermediate formed by photolysis of cyclobutanone at shorter wavelengths begins to be able to lose the carbon monoxide fragment before 1,3 ring closure can occur, and the trimethylene biradical is actually an intermediate in the cyclopropane forming reaction. That is, at shorter wavelengths both mechanisms, I and II, are operating, and both exhibit statistical intramolecular energy relaxation. From the data in Figure 6 it is obvious that a bimodal distribution function constructed from mechanisms I and II could be made to fit the data. Primarily because of the uncertainty in the energetics, such a calculation could give only a very rough

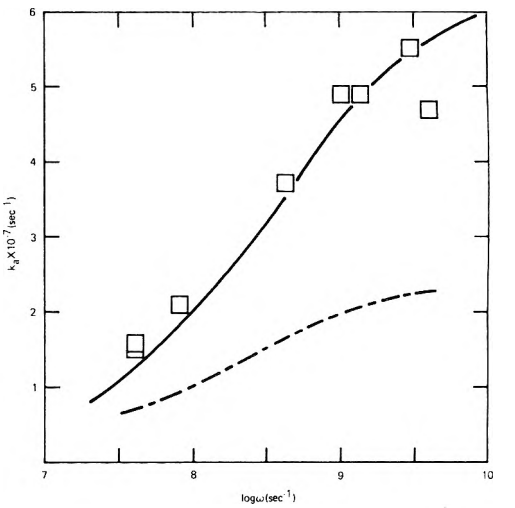

Figure 5. Experimental and calculated values of k_a as a function of ω resulting from 289.4-nm photolysis of CBT. The solid line is a calculated curve for $E^+ = 95$ kcal mol^{-1}. The broken line is a calculated curve for $E^+ = 91$ kcal mol^{-1}. Mechanism II yields rate constants that are at least a factor of 5.5 greater than the calculated rate constants for mechanism I.

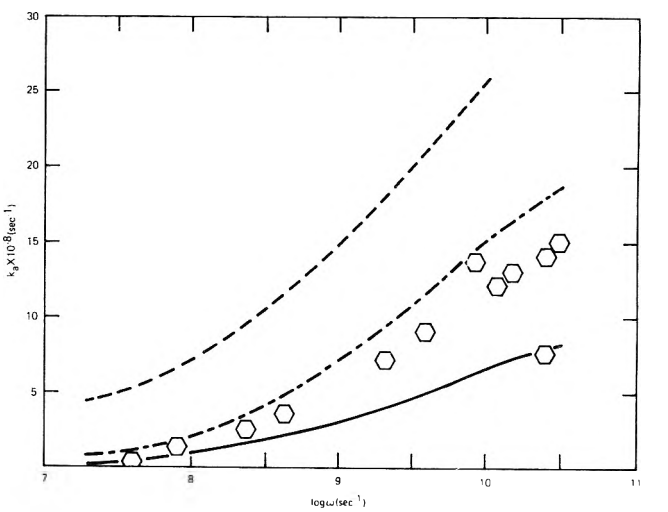

Figure 6. Experimental and calculated values of k_a as a function of ω resulting from 253.7-nm photolysis of CBT. The solid line is a calculated curve for $E^+ = 109$ kcal mol^{-1} (mechanism I); the dashed line (– – – –) is a calculated curve for mechanism II for $E_T = 109$ kcal mol^{-1}; the broken line (– – –) is a calculated curve for a bimodal distribution function that weighs mechanisms I and II equally.

estimate of the relative contributions of the two reaction channels.

Moreover, using the approximation[26]

$$E_{Tr} = E^+/N \qquad (5)$$

for calculating the energy released along the reaction coordinate, where N is taken to be roughly one-half of the total number of vibrational degrees of freedom of the intermediate, there would be 6–8 kcal mol^{-1} of energy that might be released to translation of the separating fragments. This means that the deactivation rate, ω, used in calculating k_a from eq 1 could be as much as a factor of 1.6 too low;[27] therefore, the experimental rate constants in Figures 3–5 probably should be raised by this factor. Al-

(26) (a) M. A. Haney and J. L. Franklin, *J. Chem. Phys.*, **48**, 4093 (1968); (b) C. E. Klots, *ibid.*, **41**, 117 (1964).
(27) S. W. Benson, "The Foundations of Chemical Kinetics," McGraw-Hill, New York, N. Y., 1960, p 152.

though this still does not affect the general conclusion that there is a random redistribution of the available energy in the cyclopropane-forming reaction, it does add complexity to the problem of determining the relative contributions of mechanisms I and II.

These conclusions contained in this study about the nature of energy partitioning in cyclobutanone photolysis differ substantially from the work of Campbell and Schlag.[10a,c] The primary reasons that the results of these two studies are not the same is because of the considerable difference in the magnitude of the total energy assumed to be available for redistribution to the degrees of freedom of the reaction products, and the previous study assumed no propylene is formed in the primary process.

It has been shown that there is diminishing stereospecificity in the dimethylcyclopropanes produced on photolysis of *cis*- and *trans*-2,3- and *cis*- and *trans*-2,4-dimethylcyclobutanones at shorter wavelengths.[7c] The loss of stereospecificity in the cyclopropane-forming reaction could be due to faster randomizing of the internal rotations in the 1,4 biradical before loss of CO. However, the results of this work indicate an alternate explanation might be that decarbonylation of the intermediate occurs rapidly enough at shorter wavelengths such that some of the decomposition events actually yield a vibrationally excited trimethylene biradical, and the trimethylene biradical subsequently yields cyclopropanes of a different stereochemistry.

Implications Concerning the Rate of Intramolecular Vibrational Energy Relaxation. A fundamental assumption contained in the Rice, Ramsperger, Kassel, and Marcus (RRKM) theory[16,28] of unimolecular decomposition is that internal energy relaxation occurs on a shorter time scale than does decomposition. During recent years there have been various experimental tests[28-34] and theoretical examinations[28,35-36] of this postulate that have supported its validity. More recently Rynbrandt and Rabinovitch[30] have observed nonrandom intramolecular energy relaxation for the decomposition of chemically activated hexafluorobicyclopropyl. From this work they were able to extract the rate of intramolecular energy relaxation for that system to be 1.1×10^{12} sec^{-1}. Intramolecular energy relaxation appears to be even faster when chemically activated *sec*-butyl radicals decompose.[31]

The cyclobutanone system also offers some insight into the rate of intramolecular vibrational energy relaxation. On photolysis by wavelengths $\leq$313 nm the initially prepared S_1 state predissociates with a lifetime of 10^{-10} to $\sim 10^{-12}$ sec,[6a] depending on λ_{ex}, to form an intermediate, presumably a vibrationally excited singlet 1,4 biradical, that in turn has a lifetime of less than 10^{-10} sec.[6-7] In view of the results obtained for other systems one might expect that a vibrationally excited intermediate with a lifetime of 10^{-10} sec should exhibit a random distribution of its excess vibrational energy to the degrees of freedom of its reaction products, and the results for the present system are not surprising.

However, the results for this system indicate that not only the excess vibrational energy of the intermediate is randomly redistributed to the reaction products, but also the energy released on going from the intermediate to cyclopropane and carbon monoxide is statistically distributed to the degrees of freedom of the products. Again, for random intramolecular energy relaxation the average energy contained in the reaction coordinate would be 6-8 kcal mol^{-1} (eq 5). The frequency of passage through the critical configuration to products,[36b] t^{-1}, is given by $(E_{rr}/2\mu)^{1/2}\delta^{-1}$ where δ is the extension of the critical configuration that must be reached such that the system has attained the energy level of the products, and μ is the reduced mass of the separating fragments. If one makes a liberal estimate of 10 Å for δ the fragments should separate in $\sim 10^{-12}$ sec, and intramolecular vibrational energy relaxation must be at least this rapid. This is, of course, a lower limit to the time scale since energy is being released as the fragments separate.

Acknowledgments. This work has been supported by the National Science Foundation. The author wishes to express his gratitude to Professor E. K. C. Lee of the University of California, Irvine, for providing preprints of some of the work carried out in his laboratory and for his many valuable comments. In addition, this work was greatly facilitated by the expert assistance of Mr. P. B. Do with the computer calculations.

(28) For a review see L. D. Spicer and B. S. Rabinovitch, *Annu. Rev. Phys. Chem.*, **21**, 349 (1970).
(29) Y. Y. Su and Y. N. Tang *J. Phys. Chem.*, **76**, 2187 (1972).
(30) (a) J. D. Rynbrandt and B. S. Rabinovitch, *J. Phys. Chem.*, **75**, 2164 (1971); (b) J. D. Rynbrandt and B. S. Rabinovitch, *J. Chem. Phys.*, **54**, 2275 (1971).
(31) (a) I. Oref, D. Schuetzle, and B. S. Rabinovitch, *J. Chem. Phys.*, **54**, 575 (1971); (b) D. W. Placzek, B. S. Rabinovitch, and F. H. Dorer, *ibid.*, **44**, 279 (1966).
(32) J. N. Butler and G. B. Kistiakowsky, *J. Amer. Chem. Soc.*, **82**, 759 (1960).
(33) W. Von E. Doering, J. C. Gilbert, and P. A. Leermakers, *Tetrahedron*, **24**, 6863 (1968).
(34) M. L. Dutton, D. L. Bunker, and H. H. Harris, *J. Phys. Chem.*, **76**, 2614 (1972).
(35) (a) R. C. Baetzold and D. J. Wilson, *J. Phys. Chem.*, **68**, 3141 (1964); (b) F. P. Buff and D. J. Wilson, *J. Amer. Chem. Soc.*, **84**, 4063 (1962).
(36) (a) D. L. Bunker, *J. Chem. Phys.*, **40**, 1946 (1964); (b) D. L. Bunker and M. Pattengill, *ibid.*, **48**, 772 (1968).

Nuclear Magnetic Resonance Study of the Proton Exchange Reaction of Hexaammineruthenium(III)

Daniel Waysbort and Gil Navon*

Department of Chemistry, Tel-Aviv University, Ramat-Aviv, Israel *(Received October 13, 1972)*

Water nmr line widths, shifts, and longitudinal relaxation times due to the presence of dissolved $Ru(NH_3)_6Cl_3$ were measured. The marked pH and temperature dependence of these quantities was explained by a base-catalyzed chemical exchange of the ammine protons of the complex ions. The measured parameters for the apparent second-order rate constant were $k = 2.0 \times 10^9$ l. (g-atom)$^{-1}$ sec^{-1} at 25°, $\Delta H^* = 20.0$ kcal mol^{-1}, and $\Delta S^* = 51$ eu, based on the exchange rate of a single NH proton. An assumption of a single-step exchange mechanism leads to a bimolecular rate constant of $18k = 3.6 \times 10^{10}$ M^{-1} sec^{-1} for the reaction between $Ru(NH_3)_6^{3+}$ and OH^-. This value is close to the diffusion controlled limit and is incompatible with the high observed activation energy. A multistep mechanism was postulated which involves formation of ion pairs and deprotonated species as the first two steps followed by proton exchange, between the deprotonated species and the bulk water, which might be assisted by a Grotthuss type mechanism. Small values of chemical shifts and longitudinal relaxation rates of water protons were observed in the absence of proton exchange with the complex, and were tentatively assigned to water molecules in the second coordination sphere.

Introduction

Recently there has been a great deal of interest in the chemistry of ruthenium complexes, particularly since the discovery of the nitrogenpentaammine ruthenium complex.[1,2] While the low spin d^5 hexaammineruthenium(III) complex is known to be relatively inert to substitutions, it does undergo a very fast proton exchange reaction which has been found to be proportional to hydroxide ion concentration.[3,4] This has been linked to a probable high acidity of these ions.[5] In a previous investigation[6] the deprotonated species $Ru(NH_3)_5NH_2^{2+}$ was characterized by its optical spectrum and its formation constant. Thus, $Ru(NH_3)_6^{3+}$ can serve as an example where the deprotonated species can be quantitatively implicated in the mechanism of the proton exchange and substitution reactions. In the present paper, the nmr method was applied to the study of the proton exchange of this ion. This is part of a general nmr investigation of the chemical and electronic properties of ruthenium complexes. After evaluating the line width and chemical shift parameters from the water nmr which are given in the present paper, it was concluded that the nmr of the ammine protons of $Ru(NH_3)_6^{3+}$ might be seen directly. This has now been observed using wide-line techniques; the results and interpretation will be given in a later publication.[7] Some use of these wide-line results is made in the present paper.

Experimental Section

$Ru(NH_3)_6Cl_3$ was supplied by Johnson Matthey Chemicals (Batch No. 7). Some of the material was doubly recrystallized from 1 *N* HCl solutions.[4] Both uv spectrum and nmr results using the recrystallized material were found to be identical with the results obtained with the unrecrystallized material. Therefore, unrecrystallized material of the above-mentioned batch was subsequently used.

Solutions were prepared by dissolving a weighed amount of $Ru(NH_3)_6Cl_3$ in water and diluting the parent solution with various ammoniacal buffers in the pH range 7.5–10. The pH values of the solutions were measured as a function of temperature thus avoiding the need for corrections imposed by the temperature dependence of the ionization constant of the ammoniacal buffers. Hexaammineruthenium ions undergo a slow decomposition process in basic solutions. This decomposition is due to a base-catalyzed aquation reaction. In order to ensure that this reaction does not affect our results, the rate constant for the aquation reaction was measured spectrophotometrically. The results, which will be presented and discussed separately, show that no appreciable aquation took place during the time of the nmr measurements. The solutions were freshly prepared and were kept in ice until the measurement. As a further check, line width measurements of some of the solutions were repeated several times during 1 hr, keeping the sample at the probe temperature. No detectable changes were observed in the results. Each solution studied by high resolution nmr contained 1.4% (by volume) of dioxane as an internal reference. No difference in results was found for solutions containing up to 15% (by volume) of dioxane.

All nmr spectra were taken using a Varian HA 100 instrument. The probe temperature was controlled by a V-6040 variable temperature unit and was measured using the peak separation in methanol and ethylene glycol standard samples. The accuracy of temperature measurement was ±0.5° in the low-temperature range and ±1.0° in the high-temperature range. A capillary of hexamethyldisiloxane was used to obtain an external lock.

(1) A. D. Allen and F. Bottomley, *Accounts Chem. Res.*, **1**, 360 (1968).
(2) A. D. Allen and C. V. Senoff, *Chem. Commun.*, 621 (1965).
(3) J. W. Palmer and F. Basolo, *J. Inorg. Nucl. Chem.*, **15**, 275 (1960).
(4) T. J. Meyer and H. Taube, *Inorg. Chem.*, **7**, 2369 (1968).
(5) F. Basolo and R. G. Pearson, "Mechanisms of Inorganic Reactions," 2nd ed, Wiley, New York, N. Y., 1967, Chapter 3.
(6) D. Waysbort and G. Navon, to be published. For preliminary results see *Chem. Commun.*, 1410 (1971).
(7) D. Waysbort and G. Navon, to be published.

Measurements of the longitudinal relaxation time of water protons were performed using a spin-echo attachment[8] to the Varian HA 100 spectrometer, by the 180 − 90° null method.[9]

Results

The nmr signal of water protons was found to be appreciably broadened and shifted by small concentrations of added $Ru(NH_3)_6Cl_3$ at high pH values. Both line widths and chemical shifts were measured as a function of pH and temperature. Buffer solutions which did not contain the ruthenium complex were run in parallel. Line widths and chemical shift differences between the solutions and the corresponding buffers will be denoted by $\Delta\nu_p$ and δ_p, respectively. The transverse relaxation rates due to the paramagnetic solute are calculated using the relation $T_{2p}^{-1} = \pi\Delta\nu_p$. The results are shown in Figures 1 and 2.

The following expressions for the relaxation rates and shifts for nuclei exchanging between two sites with one in a large excess on the other were derived by Swift and Connick[10]

$$T_{2p}^{-1} = \frac{f}{\tau_M}\frac{T_{2M}^{-2} + (T_{2M}\tau_M)^{-1} + \Delta\omega_M^2}{(\tau_M^{-1} + T_{2M}^{-1})^2 + \Delta\omega_M^2} \quad (1)$$

$$\Delta\omega_p = \frac{f}{\tau_M^2}\frac{\Delta\omega_M}{(\tau_M^{-1} + T_{2M}^{-1})^2 + \Delta\omega_M^2} \quad (2)$$

T_{2M}, $\Delta\omega_M$, and τ_M are the transverse relaxation time, the chemical shift, and the exchange lifetime, respectively, of the amine protons in the ruthenium complex; f is the ratio of protons in the complex and in the solvent.

Since the exchange rate of the ammine protons is proportional to the OH^- concentration, one can write

$$\tau_M^{-1} = k[OH^-] \quad (3)$$

This dependence enabled us to vary τ_M at a constant temperature (so that T_{2M} and $\Delta\omega_M$ remained constant) simply by variation of OH^- concentration.

It can be seen that the dependence of T_{2p}^{-1} with pH and temperature given in Figure 1 is similar to what is expected from eq 1 and 3. Generally, the line widths increase with pH as the exchange rate becomes faster. It can be shown by differentiating eq 1 that the plot of T_{2p}^{-1} *vs.* pH will have a maximum when the following equality holds

$$(\tau_M^{-1})_{at\ max} = \frac{\Delta\omega_M^2 + T_{2M}^{-2}}{\Delta\omega_M - T_{2M}^{-1}}$$

One conclusion is that such a maximum will appear only in cases where $\Delta\omega_M > T_{2M}^{-1}$. Also, it is obvious from the above equality that $\tau_M^{-1} \geq \Delta\omega_M$ at the maximum. The existence of maxima in Figure 1 implies that the inequality $\Delta\omega_M > T_{2M}^{-1}$ is valid in the present case. The maxima are shifted to lower pH values at higher temperatures, as expected.

Initially, T_{2p}^{-1} results were used for simultaneous fitting of the three parameters T_{2M}^{-1}, $\Delta\omega_M$, and k to eq 1 and 3. However, the fitted $\Delta\omega_M$ and particularly T_{2M} showed a slightly irregular dependence on temperature. This is understandable since T_{2p} is dominated by τ_M within the major portion of the pH range used in this experiment. Therefore, directly measured values of T_{2M} and $\Delta\omega_M$ have been used (Table I), and thus the curves in Figure 1 were fitted with k as the only adjustable parameter.

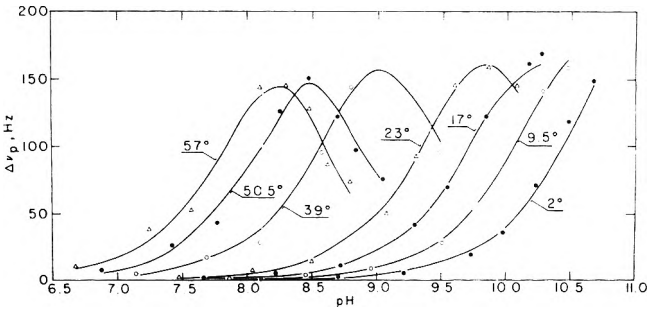

Figure 1. pH and temperature dependence of water proton nmr line widths in solutions of $6.5 \times 10^{-2}M$ $Ru(NH_3)_6Cl_3$ and NH_3–NH_4Cl buffer. NH_3 concentration was 0.1 *M*. The curves were calculated using the fitted rate constant k as explained in the text.

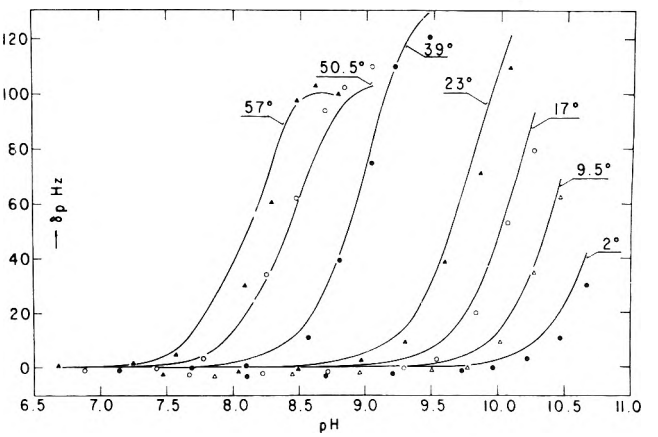

Figure 2. pH and temperature dependence of water protons chemical shifts in $Ru(NH_3)_6Cl_3$ solutions relative to the buffer solutions. Solutions are the same as in Figure 1. 1.4% dioxane was used as an internal reference. Curves were calculated using the fitted parameters of Figure 1 without any correction for the second sphere chemical shift.

TABLE I

t, °C	10^4T_{1M},[a] sec	$10^{-2}C$,[a] sec^{-1}	10^4T_{2M},[b] sec	$10^{-4}\Delta\omega_M$,[b] rad/sec
2	2.23	1.57	2.05	10.1
9.5	2.38	1.50	2.14	9.93
17	2.27	1.33	2.19	9.80
23	2.55	1.25	2.24	9.67
39	2.85	1.21	2.41	9.39
45.5	2.99	0.942	2.41	9.28
50.5	3.16	0.756	2.31	9.20
57	2.93	0.916	2.48	9.09

[a] Best fit parameters to eq 5 of the results given in Figure 4. [b] Values obtained from direct observation of $Ru(NH_3)_6^{3-}$ protons by wide-line nmr measurements at 100 MHz.[7]

The lack of dependence of the three parameters on the ruthenium concentration is demonstrated in Figure 3. In this experiment, $\Delta\nu_p$ was measured at a constant pH and temperature. It was found to be proportional to the ruthenium concentration, as is seen from the constancy of the ratio $\Delta\nu_p/f$. In order to eliminate any effect which might arise from the ionic strength variation during the $Ru(NH_3)_6Cl_3$ concentration increase, a measurement for

(8) A. Ginsburg, A. Lipman, and G. Navon, *J. Phys. E.*, **3**, 699 (1970).
(9) H. Y. Carr and E. M. Purcell, *Phys. Rev.*, **94**, 630 (1954).
(10) T. J. Swift and R. E. Connick, *J. Chem. Phys.*, **37**, 307 (1962).

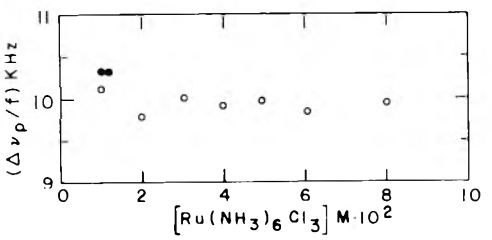

Figure 3. Concentrations dependence of water proton nmr line widths of $Ru(NH_3)_6Cl_3$ in NH_3–NH_4Cl buffer solutions at pH 9.3: ●, ionic strength adjusted to 0.36 with NaCl; O, no NaCl added.

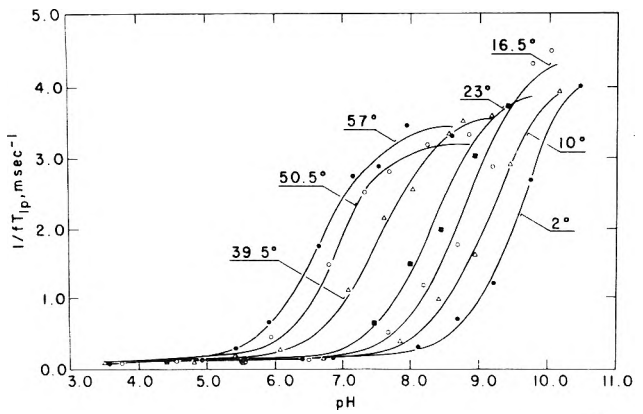

Figure 4. pH and temperature dependence of normalized longitudinal relaxation rates of water protons in solutions of $Ru(NH_3)_6Cl_3$. Concentration of $Ru(NH_3)_6Cl_3$ was in the range 0.06–0.1 *M*.

one $Ru(NH_3)_6Cl_3$ concentration was repeated with added NaCl (black circles in Figures 3). The observed effect was well within the experimental error and was thus ignored.

The chemical shift of the water protons absorption is dependent on the pH in a manner described in Figure 2 for several temperatures. The curves shown in the figure are calculated using eq 2 and 3, the measured $\Delta\omega_M$ and T_{2M} values (Table I), and the k values which were obtained by the fitting of the T_{2p}^{-1} data. It is seen that the diamagnetic shift which is observed at low pH values persists at high pH values as well. Thus a correction for this shift would improve the fit between the experimental points and the curves calculated on the basis of the T_{2p}^{-1} data. Tentatively this shift can be assigned to water molecules bound in the second coordination sphere. A discussion of this point will be given in a later publication.[7]

The pH dependence of $(fT_{1p})^{-1}$ at various temperatures is shown in Figure 4. T_{1p}^{-1} increases monotonically with increasing exchange rates attainable both by pH and temperature rise. This is expected on the basis of eq 3 and the following relation

$$T_{1p}^{-1} = f(T_{1M} + \tau_M)^{-1} \quad (4)$$

Yet, extrapolations to low pH values gave us nonzero T_{1p}^{-1} values rather than vanishing as is expected from eq 4. The results could be fitted using the following expression

$$(fT_{1p})^{-1} = (T_{1M} + \tau_M)^{-1} + C \quad (5)$$

where τ_M is given by eq 3 and C is a constant. The fitted parameters T_{1M} and C for the various temperatures are given in Table I. The fitted values of k are shown in Figure 5 together with the values obtained from the line width data. These two completely independent sets of measurements of k show a reasonably good agreement. The average Arrhenius activation energy is 20.6 ± 1.0 kcal mol^{-1}, the enthalpy of activation ΔH^* is 20.0 ± 1.0 kcal mol^{-1}, and the entropy of activation ΔS^* is 51 ± 3 eu.

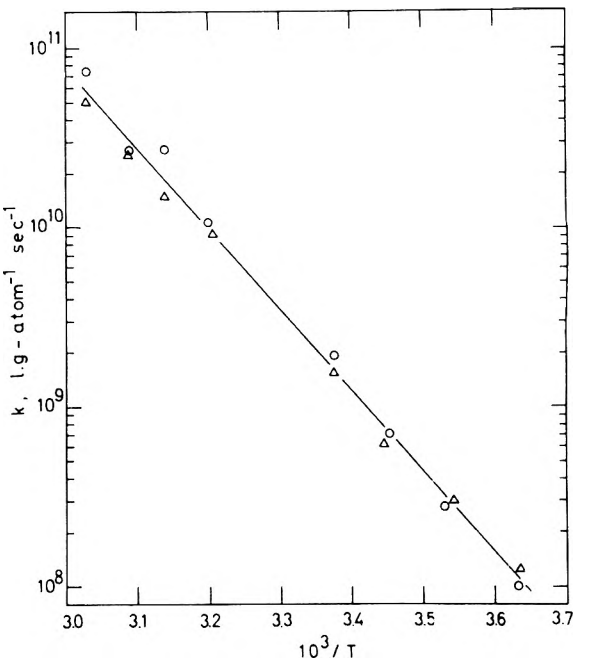

Figure 5. Arrhenius plot of the proton exchange rate constant: Δ, k fitted to the T_{2p}^{-1} data; O, k fitted to the T_{1p}^{-1} data.

Discussion

The value obtained here by the nmr method for the bimolecular rate constant $k = 2.0 \times 10^9$ l.(g-atom)$^{-1}$ sec^{-1} at 25° compares favorably with the values 6×10^8 [3] and 2.1×10^9 l.(g-atom)$^{-1}$ sec^{-1} [4] obtained for proton exchange of $Ru(NH_3)_6^{3+}$ ion with water deuterons as measured by ir. However, the activation energy for this process was not measured by these authors.

Let us consider the following bimolecular reaction

$$Ru(\overset{*}{N}H_3)_6^{3+} + OH^- \underset{k_{-6}}{\overset{k_6}{\rightleftharpoons}} Ru(NH_3)_5\overset{*}{N}H_2^{2+} + \overset{*}{H}_2O \quad (6)$$

which is the simplest mechanism for base-catalyzed proton exchange. Our measured k is the bimolecular rate constant for a proton exchange of a single N-H proton. Since there are 18 such protons in a $Ru(NH_3)_6^{3+}$ ion, and since only one of them is exchanged in each cycle of reaction 6, $k_6 = 18k = 3.6 \times 10^{10}$ M^{-1} sec^{-1} at 25°. The diffusion-controlled limit for the rate constant k_6 can be estimated as 1.0×10^{11} M^{-1} sec^{-1}, using the Debye equation[11] with $D = 1 \times 10^{-5}$ and 5.3×10^{-5} cm^2 sec^{-1} for the diffusion coefficient of $Ru(NH_3)_6^{3+}$ and OH^-, respectively, and with 4.4 Å for the distance of closest approach. The activation energy for diffusion-controlled reactions with large and negative electrostatic energy is determined by the temperature variation of the solvent viscosity. For aqueous solutions it is 4 kcal mol^{-1}. The activation energy obtained in the present work for the proton exchange reaction is much too high for a rate constant

(11) P. Debye, *Trans. Electrochem. Soc.*, **82**, 265 (1942).

so close to the diffusion-controlled limit. Therefore reaction 6 cannot be solely responsible for the proton exchange process.

In order to explain the high activation energy for such a rapid proton exchange, a composite rather than a single-step mechanism seems plausible. Since the deprotonated species of $Ru(NH_3)_6^{3+}$ has been characterized previously, by its absorption spectrum in basic solutions, it is suggested here as an intermediate in the proton exchange reaction. Also, since the proton dissociation reaction occurs only at high pH values, introduction of ion pair formation to the mechanism seems reasonable. Therefore, the following set of reactions can be proposed as leading to proton exchange

$$Ru(NH_3)_6^{3+} + OH^- \overset{K_{IP}}{\rightleftharpoons} Ru(NH_3)_6^{3+}\cdot OH^- \quad (7)$$

$$Ru(\overset{*}{N}H_3)_6^{3+}\cdot OH^- \underset{k_{-8}}{\overset{k_8}{\rightleftharpoons}} [Ru(NH_3)_5NH_2\cdot\overset{*}{H}OH]^{2+} \quad (8)$$

$$[Ru(NH_3)_5NH_2\cdot\overset{*}{H}OH]^{2+} + H_2O \overset{k_H}{\rightleftharpoons} [Ru(NH_3)_5NH_2\cdot HOH]^{2+} + \overset{*}{H}_2O \quad (9)$$

By analogy with the results on the proton exchange in solutions of methylammonium ions,[12] the following reaction could also be included

$$Ru(\overset{*}{N}H_3)_6^{3+} + \underset{H}{\overset{H}{O}}-H + \underset{H}{\overset{H}{N}}-Ru(NH_3)_5^{2+} \longrightarrow$$

$$Ru(NH_3)_5NH_2^{2+} + \overset{*}{H}-\underset{H}{\overset{H}{O}} + H-\underset{H}{\overset{H}{N}}-Ru(NH_3)_5^{3+} \quad (10)$$

However, the lack of dependence of τ_M on the ruthenium concentration (see Figure 3) rules out this possibility. This is reasonable in view of the positive charges on the two reactants in eq 10.

Reaction 7 can be safely taken as a fast preequilibrium, since the formation rate constants of ion pairs were found to be diffusion controlled.[13] Applying the steady-state condition for the deprotonated species, the following expression is calculated for the proton exchange rate

$$\frac{d[\overset{*}{H}_2O]}{dt} = \frac{K_{IP}k_8k_H}{k_{-8} + k_H}[Ru(NH_3)_6^{3+}][OH^-] \quad (11)$$

Since τ_M is the exchange lifetime of an NH* proton, and since each such exchange leads to an *HOH formation

$$\tau_M^{-1} = \frac{1}{18[Ru(NH_3)_6^{3+}]}\frac{d[\overset{*}{H}_2O]}{dt} \quad (12)$$

Using eq 3 we obtain from the above two equations

$$k = \frac{K_{IP}k_8k_H}{18(k_{-8} + k_H)} \quad (13)$$

In order to estimate the relative magnitudes of the rate constants, the values of the equilibrium constants K_{IP} and $K_8 = k_8/k_{-8}$ are necessary. In our spectrophotometric work on the formation equilibrium constant of the deprotonated species, a value of $K_{IP}K_8 = 8\ M^{-1}$ at 25° was estimated with apparent thermodynamic parameters for this product of $\Delta H° = 8.5$ kcal mol^{-1} and $\Delta S° = 33$ eu.[6] K_{IP} is likely to be of the same order of magnitude as the $Ru(NH_3)_6^{3+}$-Cl^- pair association constant, which was found to be 3.9 M^{-1} at 25° and ionic strength of 0.1 M[14] $\Delta H_{IP}°$, the enthalpy of the ion pair formation reaction, is assumed to be in the range 0–4 kcal mol^{-1}. This assumption is based on values such as $\Delta H° = 0.8$ kcal mol^{-1} for the $Co(en)_3^{3+}$-OH^- ion pair formation constant, which could be estimated from the results of Chan;[15] $\Delta H° = 2.3$ kcal mol^{-1} for the $Ru(NH_3)_6$-Cl^- ion pair formation constant,[14] and $\Delta H° = 3.7$ kcal mol^{-1} reported for the $Co(NH_3)_6^{3+}$-Cl^- ion pair formation constant.[16]

In eq 13, two limiting cases can be distinguished.

(a) $k_H \gg k_{-8}$, *i.e.*, the formation of the deprotonated species from the contact ion pair is the rate-limiting step. In this case

$$k = \frac{1}{18}K_{IP}k_8$$

Substituting the above-estimated value of K_{IP}, k_8 will be of the order of 1×10^{10} with ΔH^* in the range 16–20 kcal mol^{-1} and ΔS^* about 47 eu. Again the activation energy for k_8 seems to be too high for such a fast rate constant.

(b) $k_H \ll k_{-8}$, *i.e.*, the dissociation of the bound water molecule is the rate-limiting step. In this case

$$k = \frac{1}{18}K_{IP}K_8k_H$$

Inserting our measured thermodynamic parameters for $K_{IP}K_8$ we obtain for this limiting case $k_H = 4.5 \times 10^9$ sec^{-1} with $\Delta H_H^* = 11.5$ kcal mol^{-1} and $\Delta S^* = 23$ eu. The calculated enthalpy of activation seems too high for a reaction (eq 9) which involves only exchange of water molecules from the second coordination sphere. It should be noted that the condition $k_{-8} \gg k_H$ implies the approximate inequality $k_8 \gg 1 \times 10^{10}$ sec^{-1}. Since the activation energy for this reaction cannot be estimated in this limit, such a value for k_8 cannot automatically be excluded on this basis.

It is possible to envisage a Grotthuss type mechanism as another path for the proton exchange between the coordinated ammonia in the deprotonated species and bound water molecules

$$(H_3N)_4Ru(-NH_2)(-\underset{H}{\overset{H}{N}}-\overset{*}{H}\ \ O-H) \overset{k_G}{\underset{k_{-G}}{\rightleftharpoons}} (H_3N)_4Ru(-NH_3)(-\underset{H}{\overset{H}{N}}\ \ \overset{*}{H}-O-H) \quad (14)$$

Incorporating this reaction into the previous set of reactions, we obtain

$$k = \frac{K_{IP}K_8k_H(k_{-8} + k_G)}{18(k_{-8} + k_H + 2k_G)} \quad (15)$$

Obviously, this expression reduces to eq 13 when $k_G \ll$

(12) E. Grunwald, A. Loewenstein, and S. Meiboom, *J. Chem. Phys.*, **27**, 630 (1957).
(13) A. Elder and S. Petrucci, *Inorg. Chem.*, 9, 19 (1970).
(14) D. Waysbort, M. Evenor, and G. Navon, to be published.
(15) S. C. Chan, *J. Chem. Soc. A*, 2104 (1967).
(16) Although King, *et al.*,[17a] have questioned the K_{IP} reported by Evans and Nancollas,[17b] they seemed to agree with the values of $K_{IP}\epsilon_{IP}$. Because ϵ_{IP} is not expected to vary considerably with temperature, the temperature dependence of the optical density is likely to be due to variations of K_{IP} with temperature and $\Delta H°$ was therefore included in our considerations.

k_{-8}. The effect of the Grotthuss mechanism will be significant only when $k_G \gg k_{-8}$. Here too we can distinguish between two limiting cases.

(c) $k_G \gg k_H, k_{-8}$, then

$$k = \frac{1}{36} K_{IP} K_8 k_H$$

The resulting expression differs only by a factor of 2 from case b which was discussed previously, *i.e.*, in this case the assumption of a fast k_G merely gives a calculated k_H which is twice the previous value.

(d) $k_{-8} \ll k_G \ll k_H$, then

$$k = \frac{1}{18} K_{IP} K_8 k_G$$

k_G is the rate-determining step and therefore has the numerical value calculated in case b for k_H; $k_G = 4.5 \times 10^9$ sec^{-1} with $\Delta H^* = 11.5$ kcal mol^{-1} and $\Delta S^* = 23$ eu.

The assignment of such an activation enthalpy to k_G seems more reasonable than to k_H, since this reaction involves breaking of covalent bonds, while the other involves only cleavage of hydrogen bonds.

A value of 7.7×10^6 sec^{-1} was reported[18] for the proton exchange in $Cr(H_2O)_5OH^{2+}$. It was attributed to a Grotthuss type exchange reaction, while a fast k_H, and thus not a rate-limiting step, was tacitly assumed. Such an assignment leads to a numerical value of 7.7×10^6 sec^{-1} for k_G, and it seems very plausible that k_H is much faster indeed. Unfortunately, the activation energy was not measured and therefore it does not allow a further comparison with the present results. In a study of the proton exchange in $Pt(NH_3)_5NH_2^{3+}$ solutions, a value of 2×10^8 sec^{-1} was reported for the rate constant of the proton exchange.[19] In this report the value was assigned to k_H with a fast internal proton exchange *via* a Grotthuss type mechanism. However, since no further details were given, it is again difficult to have a direct comparison with the results presented here.[20]

In conclusion, we can say that the apparent high activation energy for the base-catalyzed proton exchange rate constant of $Ru(NH_3)_6^{3+}$ ion can be accounted for by a preequilibrium leading to a deprotonated species as a fast proton-exchanging intermediate. The proton exchange reaction of the deprotonated species is best explained by a Grotthuss type mechanism, although, of course, other alternatives can not be conclusively ruled out at present.

(17) (a) E. L. King, J. H. Espenson, and R. E. Visco, *J. Phys. Chem.*, **63**, 755 (1959); (b) M. G. Evans and G. H. Nancollas, *Trans. Faraday Soc.*, **49**, 363 (1953).
(18) B. F. Melton and V. L. Pollak, *J. Phys. Chem.*, **73**, 3669 (1969).
(19) D. W. Fong and E. Grunwald, unpublished work quoted by E. Grunwald and E. K. Ralph, *Accounts Chem. Res.*, **4**, 107 (1971).
(20) Note Added in Proof. Since the submission of our manuscript Grunwald and Fong's full report has appeared (E. Grunwald and D. W. Fong, *J. Amer. Chem. Soc.*, **94**, 7371 (1972)). The activation parameters of the rate constant, which they assign as k_H, are $\Delta H^* = 0.7$ kcal mol^{-1} and $\Delta S^* = -18$ eu. The large differences between these values and those found by us for the ruthenium system seem to support our conclusion that k_G (eq 14) is the rate-limiting step in the proton exchange reaction of $Ru(NH_3)_5NH_2^{2+}$.

Binding Energy Shifts in the X-Ray Photoelectron Spectra of a Series of Related Group IV-a Compounds

Wayne E. Morgan and John R. Van Wazer*

Department of Chemistry, Vanderbilt University, Nashville, Tennessee 37235 *(Received September 1, 1972)*

X-Ray photoelectron spectroscopy was used to determine the binding energies of the $2p_{3/2}$ electrons in germanium compounds, the $3d_{3/2}$ and $3d_{5/2}$ electrons in tin compounds, the $4f_{5/2}$ and $4f_{7/2}$ electrons in lead compounds, and the 2p electrons in some related silicon compounds. Analogous chemical environments were compared experimentally for carbon, silicon, germanium, tin, and lead, and the observed decrease in chemical shift with increasing atomic size was found to be similar to that obtained theoretically from atomic SCF calculations. In addition, data are presented for the binding energies of several core electrons of the same element for a few representative compounds of germanium, tin, and lead.

Introduction

Since the recent practical introduction[1] of X-ray photoelectron spectroscopy, core-electron binding energies have been measured by this method for nearly half of the elements.[2] Distinguishable chemical shifts,[3] in the range of 1 to 10 eV, have also been reported for elements scattered throughout the entire periodic table. It is the purpose of the work reported here to complement the relative chemical shift comparison of the group V-a compounds[4,5] with an investigation of a carefully selected array of representative group IV-a compounds. Additionally, a particular concern of this study lies in apportioning the smaller-than-expected substituent effects in molecular systems (not based on first-row elements) between a reduction of

(1) K. Siegbahn, C. Nordling, A. Fahlman, R. Nordberg, K. Hamrin, J. Hedman, G. Johansson, T. Bergmark, S. Karlsson, I. Lindgren, and B. Lindberg, "ESCA Atomic Molecular and Solid State Structure Studies by Means of Electron Spectroscopy," Almqvist and Wiksells, Uppsala, 1967.
(2) T. A. Carlson, *Phys. Today*, **25**(1), 30 (1972).
(3) D. M. Hercules, *Anal. Chem.*, **44**, 106R (1972).
(4) W. J. Stec, W. E. Morgan, R. G. Albridge, and J. R. Van Wazer, *Inorg. Chem.*, **11**, 219 (1972).
(5) W. E. Morgan, W. J. Stec, and J. R. Van Wazer, *Inorg. Chem.*, in press.

chemical shift due to molecular effects, such as charge equalization[6-12] through π bond feedback, and a reduction simply due to inherent atomic properties.

Experimental Section

The inner-orbital binding energies reported herein were obtained from a Varian IEE-15 spectrometer equipped with an aluminum Kα X-ray source (1486.6 eV). This is a computer-regulated system with a spherical electrostatic analyzer[13] of 10 cm radius and a fixed instrumental resolution of 1%. The high reproducibility of this instrument has been previously demonstrated.[4,14] Samples were mounted on a cylindrical sample holder using double-sided adhesive tape. Representative compounds from each series upon which several replicate measurements were taken yielded a standard deviation of *ca.* ±0.2 eV; however, the absolute values of the binding energies are probably known with less certainty.

Nearly all of the samples studied in this work were commercially available. Two compounds, GeS and GeS_2, were prepared according to standard methods.[15,16] All of the compounds were materials of high purity.

Atomic SCF calculative procedures[17] were applied to carbon, silicon, germanium, tin, and lead as neutral atoms and as their +1 and +2 ions in the lowest Hund's rule energy states. The corresponding valence-electron configurations are $s^2p^2(^3P)$, $s^2p^1(^2P)$, and $s^2(^1S)$, respectively. The results from some of these calculations were compared with values from a tabulation of near-limit Hartree-Fock atomic wave functions[18] and were found to be essentially identical.

Results and Discussion

By precisely measuring the kinetic energy of the electrons photoejected from the sample being investigated and supplying this information plus the necessary constants to the usual energy conservation relationship,[1,4] a "direct" binding energy is obtained. This value is found to vary, depending on the surface charging of the particular sample, and it is present practice to obtain a "corrected" binding energy by carrying out a simultaneous kinetic energy measurement on a comparison substance (of known or arbitrarily assigned binding energy) which is believed to exhibit the same surface charge under the experimental conditions. Although there is as yet no consensus concerning the proper choice and physical form of this reference substance, the carbon 1s line resulting from the ubiquitous surface layer of adsorbed hydrocarbon has widely been employed[1,19] as the binding energy reference and the results obtained with its use generally appear to be sensible and reproducible. This technique has been employed in the work reported here, using an assigned value[20] of 285.0 eV for the C 1s line.

Binding energy data arising from selected intense photoelectron spectral lines[21] for the compounds of germanium, tin, and lead are reported in Tables I-III. In each of these tables, the first column of binding energy data corresponds to the directly measured carbon 1s binding energy and the second column to the similar direct measurements on the sample under investigation. For sample compounds which do not contain organic groups, the observed C 1s line corresponds solely to the adsorbed hydrocarbon, as evidenced by the fact that its intensity increases with time. In the case of sample compounds having organic groups, the C 1s line is dominated by these groups. Nevertheless, the same value of 285.0 eV is assigned to the C 1s line, since it has been shown[6,20] that this value applies to the aliphatic and aromatic hydrocarbon environments corresponding to the majority of the carbon atoms in the organic groups of the compounds used in this work. The corrected values for the binding energies shown in Tables I-III are obtained by subtracting from the respective directly measured value for the test sample the difference between the measured (direct) C 1s binding energy and the assumed value of 285.0 eV.

TABLE I: Experimental Binding Energies of Various Germanium Compounds

Compd	Measured binding energy, eV		
	C 1s	Ge $2p_{3/2}$	
	direct	Direct	Corrected[a]
K_2GeF_6	289.3	1225.2	1220.9
	288.8	1224.7	1220.9
GeF_2	287.5	1223.4	1220.9
GeO_2	287.7	1222.9	1220.2
	287.0	1222.5	1220.5
Na_2GeO_3	286.7	1220.8	1219.1
GeO	286.1	1222.8	1221.7
GeI_2	286.7	1220.1	1218.4
GeS_2	285.8	1220.8	1220.0
GeS	286.1	1220.4	1219.3
$(C_6H_5)_4Ge$	284.2	1218.2	1219.0
	283.6	1217.7	1219.1
Ge	286.2	1218.8	1217.6[b]

[a] Measurements referenced to hydrocarbon-contaminant C 1s line, assuming a value of 285.0 eV. [b] An additional Ge $2p_{3/2}$ peak was found at 1220.9 eV due to the presence of the oxide.

The corrected binding energy data reported in Tables I-III show the expected general increase with increasing substituent electronegativity.[4,20,22-26] As previously ob-

(6) W. E. Morgan, W. J. Stec, R. G. Albridge, and J. R. Van Wazer, *Inorg. Chem.*, **10**, 926 (1971).
(7) J. R. Blackburn, R. Nordberg, F. Stevie, R. G. Albridge, and M. M. Jones, *Inorg. Chem.*, **9**, 2374 (1970).
(8) G. Kumar, J. R. Blackburn, R. G. Albridge, W. E. Moddeman, and M. M. Jones, *Inorg. Chem.*, **11**, 296 (1972).
(9) W. E. Moddeman, J. R. Blackburn, G. Kumar, K. A. Morgan, R. G. Albridge, and M. M. Jones, *Inorg. Chem.*, **11**, 1715 (1972).
(10) W. M. Riggs, *Anal. Chem.*, **44**, 830 (1972).
(11) C. D. Cook, K. Y. Wan, U. Gelius, K. Hamrin, G. Johansson, E. Olsson, H. Siegbahn, C. Nordling, and K. Siegbahn, *J. Amer. Chem. Soc.*, **93**, 1904 (1971).
(12) W. J. Stec, W. E. Moddeman, R. G. Albridge, and J. R. Van Wazer, *J. Phys. Chem.*, **75**, 3975 (1971).
(13) J. C. Helmer and N. H. Weichert, *Appl. Phys. Lett.*, **13**, 266 (1968).
(14) W. E. Morgan, J. R. Van Wazer, and W. J. Stec, *J. Amer. Chem. Soc.*, **95**, 751 (1973).
(15) W. C. Fernelius, *Inorg. Syn.*, **2**, 104 (1946).
(16) G. Brauer, "Handbook of Preparative Inorganic Chemistry," Vol. I, Academic Press, New York, N. Y., 1963, p 723.
(17) An updated version of a program using a numerical solution of the Hartree-Fock equations: C. Froese, *Can. J. Phys.*, **41**, 1895 (1963).
(18) E. Clementi, "Tables of Atomic Functions," a supplement to a paper appearing in *IBM J. Res. Develop.*, **9**, 2 (1965).
(19) B. J. Lindberg, K. Hamrin, G. Johansson, U. Gelius, A. Fahlman, C. Nordling, and K. Siegbahn, *Phys. Scr.*, **1**, 286 (1970).
(20) U. Gelius, P. F. Heden, J. Hedman, B. J. Lindberg, R. Manne, R. Nordberg, C. Nordling, and K. Siegbahn, *Phys. Scr.*, **2**, 70 (1970).
(21) C. D. Wagner, *Anal. Chem.*, **44**, 1050 (1972).
(22) G. Malmsten, I. Thorén, S. Hogberg, J.-E. Bergmark, S.-E. Karlsson, and E. Rebane, *Phys. Scr.*, **3**, 96 (1971).
(23) T. D. Thomas, *J. Amer. Chem. Soc.*, **92**, 4184 (1970).
(24) M. Pelavin, D. N. Hendrickson, J. M. Hollander, and W. L. Jolly, *J. Phys. Chem.*, **74**, 1116 (1970).
(25) B. J. Lindberg, K. Hamrin, G. Johansson, U. Gelius, A. Fahlman, C. Nordling, and K. Sidgbahn, *Phys. Scr.*, **1**, 286 (1970).
(26) R. Nordberg, R. G. Albridge, T. Bergmark, U. Ericson, J. Hedman, C. Nordling, K. Siegbahn, and B. J. Lindberg, *Ark. Kemi*, **28**, 257 (1968).

TABLE II: Experimental Binding Energies of Various Tin Compounds

Compd	C 1s direct	Measured binding energy, eV: Sn $3d_{3/2}$ Direct	Sn $3d_{5/2}$ Direct	Sn $3d_{3/2}$ Corrected[a]	Sn $3d_{5/2}$ Corrected[a]
K_2SnF_6	286.7	498.0	489.5	496.3	487.8
	287.4	498.7	490.2	496.3	487.8
SnF_2	285.8	496.5	488.1	495.7	487.3
	285.7	496.2	487.9	495.5	487.2
Na_2SnO_3	285.4		486.8		486.4
SnO_2	286.9	497.0	488.7	495.1	486.8
	286.8	496.9	488.5	495.1	486.7
SnO	286.3	497.1	488.7	495.8	487.4
	286.4	496.8	488.5	495.4	487.1
SnS_2	286.5	496.9	488.5	495.4	487.0
SnS	284.6	494.7	486.2	495.1	486.6
$(C_6H_5)_4Sn$	283.5	493.3	485.0	494.8	486.5
	283.4	493.3	484.9	494.9	486.5
$(C_6H_5)_3SnCl$	283.6	494.3	485.8	495.7	487.2
$(CH_2C_6H_5)_3SnCl$	283.6	494.1	485.7	495.5	487.1
$(CH_2C_6H_5)_2SnCl_2$	283.7	494.9	486.5	496.2	487.8

[a] Measurements referenced to hydrocarbon-contaminant C 1s line, assuming a value of 285.0 eV.

TABLE III: Experimental Binding Energies of Various Lead Compounds

Compd	C 1s direct	Measured binding energy, eV: Pb $4f_{5/2}$ Direct	Pb $4f_{7/2}$ Direct	Pb $4f_{5/2}$ Corrected[a]	Pb $4f_{7/2}$ Corrected[a]
PbF_2	286.8	145.8	141.0	144.0	139.2
	286.3	145.3	140.4	144.0	139.1
PbO_2	285.4	143.0	138.3	142.6	137.9
	283.6	141.2	136.4	142.6	137.8
Pb_3O_4	286.7	144.6	139.9	142.9	138.2
PbO	287.0	145.0	140.1	143.0	138.1
	286.2	144.7	139.8	143.5	138.6
PbI_2	286.6	145.3	140.5	143.7	138.9
$(C_6H_5)_2PbCl_2$	285.0	144.4	139.6	144.4	139.6
$(C_6H_5)_3PbCl$	284.6	143.4	138.7	143.8	139.1
$(C_6H_5)_4Pb$	284.3	142.5	137.7	143.2	138.4
	283.7	142.0	137.2	143.3	138.5
PbS	285.0	142.6	137.7	142.6	137.7
Pb	284.9	142.9	138.0	143.0	138.1

[a] Measurements referenced to hydrocarbon-contaminant C 1s line, assuming a value of 285.0 eV.

served,[4] the uncorrected (direct) values always exhibit a larger range of binding energies than is found for the corresponding corrected measurements. Also, as previously noted,[4] it appears that (for reasons which are not clear) the presence of the more electronegative substituents leads to a greater surface-charging correction. Note that the difference between the corrected binding energy of a chosen atom core electron of a given compound and that of another arbitrarily selected compound is termed the chemical shift of the former compound with respect to the latter.

The Ge $2p_{3/2}$ binding energies are reported in Table I for ten germanium compounds of which eight are the

TABLE IV: Experimental Binding Energies of Some Related Carbon and Silicon Compounds

Compd	Measured binding energy, eV: Direct	Corrected[a]
	Si 2p	
K_2SiF_6	106.8	104.8
SiO_2	103.7	103.9
SiS_2	104.4	103.6
$(C_6H_5)_4Si$	98.1	100.9
Si	96.6	99.1
	C 1s	
CO_2		292.1[b]
Na_2CO_3		289.7[b]
C (graphite)		283.8

[a] Measurements referenced to hydrocarbon-contaminant C 1s line, assuming a value of 285.0 eV. [b] Values taken from U. Gelius, *et al.*, *Phys. Scr.*, **2**, 70 (1970).

same as some of the tin compounds in Table II and four are common to both the tin and the lead studies. The Sn $3d_{3/2}$ and $3d_{5/2}$ binding energies are reported in Table II for a series of eleven tin compounds. A previous investigation[27] of the character of the metal atoms in platinum–tin cluster compounds gives Sn $3d_{5/2}$ binding energies which fall in the range expected from the measurements reported herein although none of the compounds are analogous. The binding energy data from two reports[28,29] of a single study of octahedral tin complexes which were referenced in each paper to a different arbitrary value of the same admixed reference compound yielded Sn $3d_{5/2}$ binding energies for K_2SnF_6 which are nominally 1.0 and 0.5 eV higher than the carbon-referenced value reported here-

(27) G. W. Parshall, *Inorg. Chem.*, **11**, 433 (1972).
(28) W. E. Swartz, Jr., P. H. Watts, Jr., J. C. Watts, J. W. Brasch, and E. R. Lippincott, *Anal. Chem.*, **44**, 2001 (1972).
(29) W. E. Swartz, Jr., P. H. Watts, Jr., E. R. Lippincott, J. C. Watts, and J. E. Huheey, *Inorg. Chem.*, **11**, 2632 (1972).

TABLE V: Experimental Binding Energies[a] and Binding Energy Differences for Several Levels of Some Related Germanium, Tin, and Lead Compounds

	Measured binding energy, eV								
		Δ		Δ		Δ		Δ	
				Ge					
Compd	$2p_{1/2}$		$2p_{3/2}$		$3p_{1/2}$		$3p_{3/2}$		
K_2GeF_6	1251.8	(30.9)	1220.9	(1091.7)	129.2	(4.0)	125.2		
GeO_2	1251.6	(31.3)	1220.5 1220.2	(1091.0)	129.5 129.1	(3.8)	125.6 125.4		
$(C_6H_5)_4Ge$	1250.2	(31.1)	1219.1	(1091.7)	127.4	(4.2)	123.2		
				Sn					
	$3p_{1/2}$		$3p_{3/2}$		$3d_{3/2}$		$3d_{5/2}$		
K_2SnF_6	759.0	(41.6)	717.4	(220.8)	496.6	(8.5)	488.1		
SnF_2	758.4	(41.9)	716.5	(221.0)	495.5	(8.3)	487.2		
SnO_2	758.1 758.1	(41.9)	716.1 716.3	(221.1)	495.1 495.1	(8.4)	486.7 486.8		
SnO	758.3	(41.9)	716.4	(221.0)	495.4	(8.3)	487.1		
$(C_6H_5)_4Sn$	758.1	(41.9)	716.2	(221.3)	494.9	(8.4)	486.5		
				Pb					
	$4p_{3/2}$		$4d_{3/2}$		$4d_{5/2}$		$4f_{5/2}$		$4f_{7/2}$
PbF_2	645.3	(209.1)	436.2	(22.1)	414.1	(270.1)	144.0	(4.9)	139.1
PbO_2	644.5	(209.3)	435.2	(22.3)	412.9	(270.3)	142.6	(4.8)	137.8
$(C_6H_5)_4Pb$	644.8	(209.2)	435.6	(22.1)	413.5	(270.2)	143.3	(4.8)	138.5

[a] Measurements referenced to hydrocarbon-contaminant C 1s line, assuming a value of 285.0 eV.

in. These differences from our value may be wholly attributable to the choice of binding energy values for the reference compounds. The only other study[30] involving tin compounds has demonstrated a linear correlation between Mössbauer chemical shifts and Sn 4d binding energies.

The Sn $3d_{3/2}$–$3d_{5/2}$ doublet was found in the present investigation to exhibit an area ratio of 2:3 as predicted[31,32] from a simple free-atom model in which the relative intensity of the two lines is derived from the statistical weights of the two final states (*i.e.* [2(3/2) + 1]:[2(5/2) + 1] = 4:6 or 2:3). Additionally, a constant energy separation of 8.4 ± 0.1 eV was observed for these two peaks over the entire range of compounds in Table II. The series of compounds $(C_6H_5)_4Sn$, $(C_6H_5)_3SnCl$, and $(CH_2C_6H_5)_2SnCl_2$ shows the effect of increasing substitution of chlorine atoms onto tin. Since each of these compounds exhibits an essentially identical[6] carbon 1s environment which yields an intense reference line, the relative shifts of 0.0, +0.7, and +1.3 eV for the Sn $3d_{5/2}$ level may be accurately determined by this method without the usual ambiguity of referencing techniques.

The experimental values of the Pb $4f_{5/2}$–$4f_{7/2}$ doublet appear in Table III for a series of ten related lead compounds. This doublet was found to have a constant energy separation of 4.8 ± 0.1 eV over the entire range of compounds and demonstrated the proper intensity ratio of 3:4. The series of chlorine-substituted lead compounds $(C_6H_5)_4Pb$, $(C_6H_5)_3PbCl$, and $(C_6H_5)_2PbCl_2$, exhibiting relative shifts of 0.0, +0.6, and +1.1 eV, respectively, shows a slight overall reduction in chemical shift when compared to the analogous tin compounds. The observed carbon chemical shift range for the related series of chlorine-substituted methanes[21] CH_4, CH_3Cl, and CH_2Cl_2 with corresponding relative shifts of 0.0, +1.6, and +3.1 eV, respectively, is more than twice as great. Although the compounds in the carbon study were gases, the relative chemical shifts can be taken to be essentially identical[19] with those of the respective solids. Thus, the relative shift for these related group IV-a compounds lies in the following order: carbon ≫ tin > lead.

The analogous carbon and silicon compounds are shown in Table IV along with the respective C 1s and Si 2p binding energies. All of the silicon 2p values have been previously reported,[33] but were repeated in the present study to ensure an accurate comparison with the other measurements taken on the Varian instrument. Two of the carbon 1s values are from previous investigations.[20,34]

In Table V are presented the results of an investigation over a wide energy range on selected germanium, tin, and lead compounds to determine whether or not several energy levels of the same element show the same chemical shift effects. The binding energies reported in Table V are all corrected by referencing to the C 1s line as previously discussed. However, the differences, Δ, shown in parentheses would be the same for the direct measurements since the same surface-charge correction is necessarily applied to all energy levels of a given sample compound. The average differences between the germanium $2p_{1/2}$–

(30) M. Barber and P. Swift, *J. Chem. Soc. D*, 1338 (1970).
(31) C. S. Fadley, D. A. Shirley, A. J. Freeman, P. S. Bagus, and J. V. Mallow, *Phys. Rev. Lett.*, **23**, 1397 (1969).
(32) J. M. Hollander and W. L. Jolly, *Accounts Chem. Res.*, **3**, 193 (1970).
(33) R. Nordberg, H. Brecht, R. G. Albridge, A. Fahlman, and J. R. Van Wazer, *Inorg. Chem.*, **9**, 2469 (1970).
(34) D. N. Hendrickson, J. M. Hollander, and W. L. Jolly, *Inorg. Chem.*, **9**, 612 (1970).

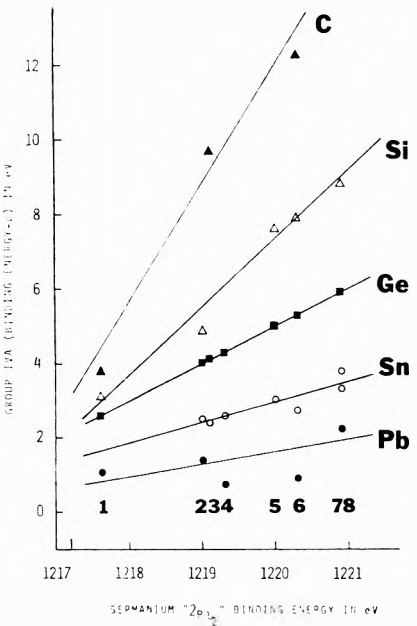

Figure 1. The carbon 1s (β = 280), silicon 2p (β = 96), germanium $2p_{3/2}$ (β = 1215), tin $3d_{5/2}$ (β = 484), and lead $4f_{7/2}$ (β = 137) inner-orbital binding energies *vs.* the germanium $2p_{3/2}$ binding energies. The numbers near the bottom of this figure indicate the position of the binding energies of those compounds having the same number, kind, and arrangement of substituent atoms as the following germanium compounds: 1, Ge; 2, $(C_6H_5)_4Ge$; 3, Na_2GeO_3; 4, GeS; 5, GeS_2; 6, GeO_2; 7, GeF_2; 8, $KGeF_6$. The relative experimental shifts are C, 1.00; Si, 0.58; Ge, 0.32; Sn, 0.17; Pb, 0.10. The β values are simply arbitrary constants, chosen so as to move the binding energies of the different elements closer together on the vertical scale.

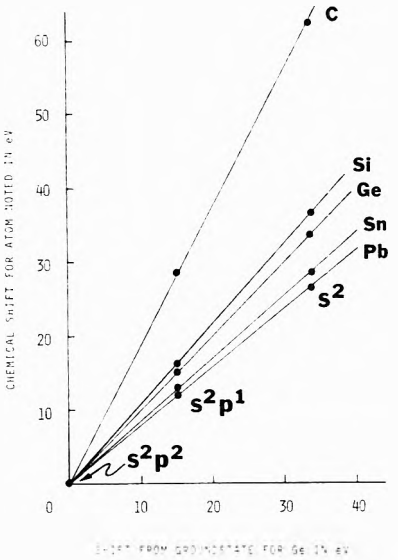

Figure 2. A comparison of the change in inner-orbital energies obtained from atomic SCF calculations of the ground-state atom (with outer electron configuration s^2p^2), the +1 ion (s^2p^1), and the +2 ion (s^2) for each member of the group IV-a elements. The changes in the C 1s, Si 2p, Ge 2p, Sn 3d, and Pb 4f orbital energies were compared with the change in the Ge 2p orbital energy yielding relative shift effects of 1.00, 0.58, 0.53, 0.45, and 0.42, respectively.

$2p_{3/2}$-$3p_{1/2}$-$3p_{3/2}$ levels are 31.1 ± 0.2, 1091.5 ± 0.4, and 4.0 ± 0.2 eV, respectively. Similar differences of 41.8 ± 0.1, 221.0 ± 0.2, and 8.4 ± 0.1 eV were found for the tin $3p_{1/2}$-$3p_{3/2}$-$3d_{3/2}$-$3d_{5/2}$ energy levels. Average values of 209.2 ± 0.1, 22.2 ± 0.1, 270.2 ± 0.1, and 4.8 ± 0.1 eV were observed for the $4p_{3/2}$-$4d_{3/2}$-$4d_{5/2}$-$4f_{5/2}$-$4f_{7/2}$ energy-level differences of lead.

Inspection of Table V shows no systematic variations in the various Δ values from one compound to another for either germanium, tin, or lead, and the observed differences for a given Δ lie within the range to be expected from the experimental error of the binding energy measurements. This finding is experimental evidence to support the idea that the energies of all of the core electrons of any given atom change by the same amount between different chemical environments (*i.e.*, from one molecular structure to another). Our orbital energy SCF calculations on the atoms and ions of carbon, silicon, germanium, tin, and lead show that the Δ values between the different core energy levels are unchanged when going from one state and/or valence electron configuration (including ionized atoms) to another. All of this is in accord with previous experimental and theoretical investigations[4,35,36] which have shown that a chemical shift of any core electron of a given atom is the same as that of its other core electrons. This fact permits meaningful comparisons to be made between chemical shifts of different levels in series of related compounds of different elements.

Qualitative observations of the relative chemical shifts of similar quaternary nitrogen[37] and quaternary phosphorus[38] compounds and a series of similar group VI-a compounds[39] of sulfur, selenium, and tellurium have established a trend of decreasing chemical shift effects upon descending a periodic group. A complete investigation of the group V-a compounds[4,5] has resulted in a determination of the quantitative relative chemical shifts of analogous chemical environments by both theoretical and experimental methods. An investigation[40] of some related compounds of the alkali metal halides which is supported by atomic calculations on the group VII-a elements has shown a similar trend in the shifts of the core electron binding energies.

A quantitative determination of the relative chemical shifts of a series of related group IV-a compounds is presented in Figure 1. In this figure, the binding energies for each compound of the carbon, silicon, germanium, tin, and lead series are plotted against the binding energy of the analogous germanium compound along the abscissa. This procedure necessarily yields a slope of 1.00 for the germanium plot and clearly demonstrates the decreasing chemical shift effects as one proceeds down the periodic group toward larger atomic size. Although the experimental data are plotted against germanium, the results are more easily viewed in the following manner with respect to carbon: C, 1.00; Si, 0.58; Ge, 0.32; Sn, 0.17; Pb, 0.10. These results agree with the previous observations of decreasing chemical shifts with increasing atomic size and also clearly show the very small shift effects observed for the large elements.

Figure 2 is a plot of the free-atom chemical shift as determined from atomic SCF calculations[17] on the ground-

(35) C. S. Fadley, S. B. N. Hagstrom, M. P. Klein, and D. A. Shirley, *J. Chem. Phys.*, **48**, 3779 (1968).
(36) T. A. Carlson in "*Proceedings* of the 1971 International Conference on Electron Spectroscopy," Asilomar, Calif., Tables II and III.
(37) J. J. Jack and D. M. Hercules, *Anal. Chem.*, **43**, 729 (1971).
(38) W. E. Swartz, Jr., and D. M. Hercules, *Anal. Chem.*, **43**, 1066 (1971).
(39) W. E. Swartz, Jr., K. J. Wynne, and D. M. Hercules, *Anal. Chem.*, **43**, 1884 (1971).
(40) L. D. Hulett and T. A. Carlson, *Appl. Spectrosc.*, **25**, 33 (1971).

TABLE VI: Various Determinations of the Range of Chemical Shifts of the Group IV-a Elements

Element	Ratio of $1/r$			SCF atomic shift ratio	Measd shift ratio
	Atomic	Covalent	Ionic (+4)		
C	1.00	1.00	1.00	1.00	1.00
Si	0.69	0.69	0.37	0.58	0.58
Ge	0.66	0.63	0.28	0.53	0.32
Sn	0.56	0.55	0.21	0.45	0.17
Pb	0.52	0.52	0.18	0.42	0.10

state atoms of carbon, silicon, germanium, tin, and lead and their +1 and +2 ions. The chemical shifts of the C 1s, Si 2p, Ge 2p, Sn 3d, and Pb 4f orbital energy levels are plotted against the Ge 2p shift in order to determine the relative chemical shift for the group IV-a atoms in their corresponding valence configurations of s^2p^2, s^2p^1, and s^2. The resulting ratios are C, 1.00; Si, 0.58; Ge, 0.53; Sn, 0.45; and Pb, 0.42. In particular, carbon has a much larger shift than does its nearest neighbor silicon and the overall trend of decreasing shift range with increasing atomic size is maintained. Furthermore, the relative shifts from the free-atom SCF calculations, while decreasing with increasing atomic size, show a definite grouping of silicon and germanium and a second pairing of tin and lead in Figure 2 which is only slightly reflected by the experimental values plotted in Figure 1.

One of the more simple theoretical descriptions of core-level binding energy shifts is the classical charged-shell atomic model[1,35,41] which represents the valence electrons by a spherical "valence shell" of electric charge surrounding but not penetrating the core electrons. If q electronic charges are added or removed from the valence shell of radius r, the potential energy of the inner electron is changed by $\Delta E = q/r$. For a typical mean radius of 1 Å $\simeq$ 2 au, the removal of one electron from the valence shell to infinity results in a reduction of the potential of the core electrons (with a concomitant increase in their binding energy) by about 0.5 au or *ca.* 14 eV. This value is a few electron volts larger than the experimentally observed range of chemical shifts, as would be expected from the concept that generally a total of less than one unit of charge is transferred to the nearby atoms in a molecule or molecular system. Despite the crudeness of this picture, it does correctly predict that the chemical shifts of all core energy levels will be the same, since they reside in a region of constant potential. Also, it establishes a simple explanation for the observed decreasing chemical shift effects with increasing atomic size.

In view of these successes of the simple charged-shell model, it was of interest to compare the observed decreasing shifts with the radii of the group IV-a elements. The interatomic ratios of the reciprocals of the atomic, covalent, and ionic radii[42] of carbon, silicon, germanium, tin, and lead are compared in Table VI with the more rigorous atomic SCF-calculated shift ratios and the experimentally determined values. The first of several interesting observations based on the values of Table VI is the fact that the rigorous, costly, and time-consuming atomic SCF-calculated chemical shift ratios do not differ appreciably from those obtained from the atomic radii. The ratios from the $1/r$ values for the free or covalently bonded atoms are slightly larger than those obtained from the SCF atomic shifts; but the $1/r$ calculation also tends to pair silicon and germanium as well as tin and lead, just as the more rigorous SCF calculations did. Upon comparing the atomic, covalent, and ionic $1/r$ ratios, it is seen that the range of chemical shifts for the heavier elements is the lowest for the ionic case.

Although the values of the $1/r$ ratio for the ionic (+4) species agree rather closely with the measured shifts, especially for germanium, tin, and lead, it seems unreasonable to believe that these group IV-a atoms in their molecular environments exist in an actual +4 oxidation state resulting from the complete loss of four electrons. Alternatively, the difference between the observed experimental chemical shift ratios and the atomic SCF or simple $1/r$ calculated ratios might be accounted for by the increasing ability of the atoms of larger atomic radii with low-lying d orbitals to participate in charge delocalization, as through π bond feedback. If, in fact, electron density were returned to the central atom in the molecule from the more electronegative atoms attached to it, there would be additional reduction of the range of chemical shifts over and above the inherent atomic reduction due to increased atomic size. This contention is supported by a recent He-I photoelectron investigation[43] of the valence orbitals of tetramethyl compounds of the group IV-a elements. Interpretation of the experimental results suggests that a significant amount of stabilization is imparted to certain molecular orbitals as a result of their ability to participate in back bonding to the central atom's vacant d orbitals. The ligand nonbonding orbitals were found to remain essentially constant in energy and the orbitals with metal character decreased steadily in binding energy with the increasingly heavier central atoms. Thus, it is apparent that delocalization of charge through π bonds does play an important role in determining the substituent effects upon the binding energies of the larger atoms, even though a good deal of the decreasing range of chemical shifts with increasing atomic size is an inherent function of the increasing atomic radii.

Acknowledgment. We wish to thank the National Science Foundation (GP-28698X) for partial financial support of this work. Special thanks are extended to the Monsanto Company for the use of their spectrometer and for the cooperation of Dr. James Ogilvie. A gift of several of the germanium compounds from Dwight S. Trehin and J. Adams of Eagle-Picher Industries is deeply appreciated, as is the donation of the updated atomic SCF Hartree-Fock program from Thomas A. Carlson and C. W. Nestor, Jr., of Oak Ridge National Laboratory.

(41) J. M. Hollander and D. A. Shirley, *Annu. Rev. Nucl. Sci.*, **20**, 435 (1970).
(42) R. T. Sanderson, "Chemical Periodicity," Reinhold, New York, N. Y., 1960.
(43) A. E. Jonas, G. K. Schweitzer, F. A. Grimm, and T. A. Carlson, *J. Electron Spectrosc.*, **1**, 29 (1972).

Mass Spectrometric Evidence for the Gaseous Silicon Oxide Nitride Molecule and Its Heat of Atomization

David W. Muenow

Chemistry Department, University of Hawaii, Honolulu, Hawaii 96822 *(Received January 5, 1973)*

Publication costs assisted by The University of Hawaii

The gaseous silicon oxide nitride molecule $Si_2NO(g)$ has been observed with a high-temperature mass spectrometer. Its heat of formation and atomization energy are calculated to be $\Delta H_f°_{298} = -38.1 \pm 10.3$ kcal mol^{-1} and $\Delta H_{atoms}° = 427.4 \pm 17.3$ kcal mol^{-1}, respectively.

Introduction

Silicon oxynitride, Si_2N_2O, has been observed[1] as a mineral in meteorites of the enstatite chondrite type. The presence of this mineral in a meteorite is of importance in terms of origin since it provides an estimate for the conditions of the environment from which it formed.[2] As part of a mass spectrometric study on materials at high temperature the gaseous molecule Si_2NO has been observed and its heat of atomization obtained. Previously, only one other gaseous metal nitride oxide (NUO)[3] has been reported. The lack of molecules of this type in part derives from the ease of oxidation of the corresponding solid metal nitride and the high stability of the nitrogen molecule.

Results and Discussion

Measurements were performed with a 60° sector-field, 15.8-cm radius-of-curvature, first-order, direction-focusing mass spectrometer equipped with a high-temperature Knudsen effusion cell. Ions are produced by an electron impact ion source, and after mass analysis detected and amplified with an electron multiplier and vibrating reed electrometer. The instrument is differentially pumped with two high-speed all-metal vapor diffusion pumps and liquid nitrogen traps and baffles. Details of the basic cell assembly have been previously described.[4] The effusion cell was machined from tantalum and fitted with a graphite crucible and lid. Heating was accomplished by radiation from a tungsten loop resistor wire surrounding the cell, and temperatures measured with a Pt–Pt–10% Rh thermocouple peened into its base. Over the temperature range 1677–1768°K the following isomolecular equilibrium was studied

$$Si_2N(g) + SiO(g) = Si_2NO(g) + Si(g) \qquad (1)$$

The graphite crucible was loaded with small chips of Si_3N_4, powdered silica, boron nitride, and silicon metal. The presence of BN provides a convenient source of nitrogen at high temperatures; metallic silicon ensures a reducing atmosphere. With the cell heated to 1725°K and using 25-V ionizing electrons the main peaks in the mass spectrum were found to be Si_2^+, Si^+, N_2^+, Si_2N^+, Si_2NO^+, and SiO^+. A weak peak at m/e 54 was also observed and is tentatively identified with $SiCN^+$, previously reported.[5]

Assignments were based upon appearance potentials, shutterability, and isotopic-abundance calculations. Appearance potentials were measured by the vanishing-current method using Si^+ (AP = 8.2 eV) and H_2O^+ (AP = 12.6 eV) as standards.[6] The values 11.3 ± 0.5 eV for SiO^+ (m/e 44) and 9.5 ± 0.5 eV for Si_2N^+ (m/e 70) agree closely with those reported previously[7,8] and suggest these ions to be parents. The value 10.8 ± 0.5 eV for Si_2NO^+ (m/e 86) indicates the ion is formed by direct ionization of $Si_2NO(g)$ and not by dissociative ionization of some higher molecular weight species. No shutterable peaks of mass greater than those for the isotopes of Si_2NO^+ (m/e 86, 87, and 88) were observed. Since aluminum oxide is a common impurity in nitrides of boron and silicon and can easily be accommodated in solid solution with Si_3N_4 it was suspected that a portion of measured ion currents for mass peaks m/e 86 and 70 (assigned to Si_2NO^+ and Si_2N^+, respectively) might be due to $Al_2O_2^+$ and Al_2O^+ which produce peaks at these same masses. Neither the isotopic abundances nor previous appearance potential measurements[9] for $Al_2O_2^+$ (9.9 ± 0.5 eV) and Al_2O^+ (7.7 ± 0.2 eV) support this view.

Temperature-dependent, ion-intensity data for Si^+, Si_2N^+, Si_2NO^+, and SiO^+ were obtained using 25-V ionizing electrons at several temperatures in the range 1677–1768°K and were used to calculate the equilibrium constant, K_p, for reaction 1. Instrumental sensitivity was determined using the silver-calibration technique.[10] From JANAF[11] free energy functions for Si(g) and SiO(g), estimated values for $Si_2N(g)$ [−72 cal deg^{-1} mol^{-1} at 1725°K, ref 298°][8] and $Si_2NO(g)$ [−80 cal deg^{-1} mol^{-1} at 1725°K, ref 298°, by analogy with $Al_2O_2(g)$], and the equilibrium constants one derives the corresponding heats of reaction by the third-law method. The results are given in Table I.

Using the average heat of reaction 1 $\Delta H_{298}° = 1.7 \pm 3.3$ kcal mol^{-1}, the dissociation energy of SiO(g), $D_{298}°$ =

(1) C. A. Anderson, K. Keil, and B. Mason, *Science*, **146**, 256 (1964).
(2) W. R. Ryall, and A. Muan, *Science*, **165**, 1363 (1969).
(3) K. A. Gingerich, *Naturwissenschaften*, **24**, 646 (1967).
(4) D. W. Muenow and R. T. Grimley, *Rev. Sci. Instrum.*, **42**, 455 (1971).
(5) D. W. Muenow and J. L. Margrave, *J. Phys. Chem.*, **74**, 2577 (1970).
(6) R. W. Kiser, "Introduction to Mass Spectrometry and its Applications," Prentice-Hall, Englewood Cliffs, N. J., 1962.
(7) D. L. Hildenbrand and E. Murad, *J. Chem. Phys.*, **51**, 807 (1969).
(8) K. F. Zmbov and J. L. Margrave, *J. Amer. Chem. Soc.*, **89**, 2492 (1967).
(9) J. Drowart, G. DeMaria, R. P. Burns, and M. G. Inghram, *J. Chem. Phys.*, **32**, 1366 (1960).
(10) J. L. Margrave, Ed., "The Characterization of High Temperature Vapors," Wiley, New York, N. Y., 1967, pp 222–227.
(11) "JANAF Thermochemical Tables," Dow Chemical Co., Midland, Mich., 1968.

TABLE I: Equilibrium Data for Heat of Reaction 1

Temp, °K	$-\text{Log } K_p$[a]	$-\Delta[G_T^\circ - H_{298}^\circ]/T$, cal deg^{-1} mol^{-1}	ΔH_{298}°, kcal mol^{-1}
1677	0.92	(3)	2.0
1698	0.24	(3)	−3.2
1727	0.88	(3)	1.8
1743	0.97	(3)	2.5
1768	0.42	(3)	−1.9
		Av third-law	1.7 ± 3.3

[a] Assumed relative ionization cross sections and multiplier gains cancel. Relative intensities (1727°K, 25 eV) for Si_2NO^+, Si^+, Si_2N^+, and SiO^+ are 2×10^{-4}, 1.00, 5×10^{-2}, and 1×10^{-2}, respectively.

192.3 ± 2 kcal mol^{-1},[12] the heat of formation of $Si_2N(g)$, $\Delta H_f^\circ{}_{298}$ = 93 ± 5 kcal mol^{-1},[8] and the dissociation energy of $O_2(g)$, D_{298}° = 119 kcal mol^{-1},[12] one calculates for the heat of formation of $Si_2NO(g)$, $\Delta H_f^\circ{}_{298}$ = −38.1 ± 10.3 kcal mol^{-1}. Combined with the dissociation energies of $N_2(g)$ and $O_2(g)$, D_{298}° = 226 ± 2[11] and 119 kcal mol^{-1},[12] respectively, and the heat of sublimation of silicon, $\Delta H_s^\circ{}_{298}$ = 108.4 ± 3 kcal mol^{-1},[13] leads to the atomization energy of $Si_2NO(g)$, ΔH_{atoms}° = 427.4 ± 17.3 kcal mol^{-1}. This may be compared with an estimated value of 444 ± 10 kcal mol^{-1} using 104 kcal mol^{-1} as the lower limit for the mean Si–O bond energy (from the matrix-isolated molecule Si_3O_3 with proposed planar-cyclic structure)[14] and 118 ± 5 kcal mol^{-1} for the mean Si–N bond energy in $Si_2N(g)$ [ΔH_{atoms}° = 236 ± 10 kcal mol^{-1}].[8] Favorable agreement suggests a cyclic rather than linear structure for $Si_2NO(g)$.

Acknowledgment. This work was supported by grants from the Research Corporation and the Hawaii Institute of Geophysics.

(12) L. Brewer and G. M. Rosenblatt, *Advan. High Temperature Chem.*, **2**, 20 (1969).
(13) H. L. Schick, "Thermodynamics of Certain Refractory Compounds," Vol. 1, Academic Press, New York, N. Y., 1966, p 158.
(14) J. S. Anderson and J. S. Ogden, *J. Chem. Phys.*, **51**, 4189 (1969).

COMMUNICATIONS TO THE EDITOR

Direct Observation of the Dibromide Radical Anion Oxidation of Tris(bipyridyl)ruthenium(II). Evidence for a Triplet-to-Triplet Energy Transfer Mechanism in the Photosensitized Redox Decomposition of Cobalt(III) Substrates[1]

Publication costs assisted by The National Science Foundation

Sir: It has very recently been proposed[2] that the $Ru(bipy)_3^{2+}$ photosensitized redox decomposition of cobalt substrates such as $Co(NH_3)_5Br^{2+}$ and Co(HEDTA)Cl^- proceeds predominately by means of electron transfer to these oxidants from the thermally equilibrated charge transfer to ligand triplet excited state, $Ru(bipy)_3^{2+}$ (^3CT),[3] rather than by means of triplet-to-triplet energy transfer as we had earlier proposed for the case of Co(HEDTA)Cl^-.[4] The evidence cited for the former mechanism appears to be the observation that some $Ru(bipy)_3^{3+}$ is a reaction product under some reaction conditions.[2] We have carefully examined the formation of $Ru(bipy)_3^{3+}$ in the $Ru(bipy)_3^{2+}$ sensitized redox decompositions of $Co(NH_3)_5Br^{2+}$, Co(EDTA)$^-$, and Co(HEDTA) X^- (X = Cl, Br, or NO_2); the full report of these studies will be presented elsewhere.[4c] In the present communication we wish to point out that a product analysis is not sufficient to establish a mechanistic hypothesis in systems as complex as these, that radical oxidations of $Ru(bipy)_3^{2+}$ are often very rapid and sometimes observable, and that examination of evidence bearing on the sensitization mechanism indicates that the mechanistic hypothesis of Gafney and Adamson[2c] does not apply to the systems we have investigated.

We have focussed on $Co(NH_3)_5Br^{2+}$ as any acceptor substrate, for purposes of the present report, since the Br_2^- radical anion is a readily formed, easily detected, well-characterized[5] product of the photoredox decomposition of this substrate and since the Br_2^- radical is a powerful and facile oxidant[6,7] which in principle should be able to oxidize $Ru(bipy)_3^{2+}$.

(1) Partial support of this research by the National Science Foundation (Grant No. GP 24053) is gratefully acknowledged.
(2) (a) A. W. Adamson, "Proceedings XIV International Conference on Coordination Chemistry," Toronto, June, 1972, p 240; (b) Abstracts 164th National Meeting of the American Chemical Society, New York, N.Y., August, 1972, INORG 2; (c) H. D. Gafney and A. W. Adamson, *J. Amer. Chem. Soc.*, **94**, 8238 (1972).
(3) (a) J. N. Demas and G. A. Crosby, *J. Mol. Spectrosc.*, **26**, 72 (1968); (b) F. E. Lytle and D. M. Hercules, *J. Amer. Chem. Soc.*, **91**, 253 (1969).
(4) (a) P. Natarajan and J. F. Endicott, *J. Amer. Chem. Soc.*, **94**, 3635 (1972); (b) *ibid.*, in press; (c) *J. Phys. Chem.*, submitted for publication.
(5) J. K. Thomas, *Advan. Radiat. Chem.*, **1**, 103 (1960).
(6) S. D. Malone and J. F. Endicott, *J. Phys. Chem.*, **76**, 2223 (1972).
(7) W. H. Woodruff and D. W. Margerum, *Inorg. Chem.*, in press.

We have found that the $Ru(bipy)_3^{2+}$ sensitized redox decomposition of $Co(NH_3)_5Br^{2+}$ in 1 M H_2SO_4 resulted in the formation of Co^{2+} and $Ru(bipy)_3^{3+}$ in a 1:0.95 ratio when the experiments were run carefully and back reactions were properly taken into account. When the sensitization was performed in 50% 2-propanol the yield of Co^{2+} was increased 85%, but the yield of $Ru(bipy)_3^{3+}$ was decreased 58% (again taking account of back reactions; full details of this work will be reported in ref 4c). These results suggest that the primary redox step produces a radical which can react competitively with 2-propanol and $Ru(bipy)_3^{2+}$; note that the 2-hydroxy-2-propyl radical is known to react efficiently with cobalt(III) substrates.[4c,8,9]

Flash photolysis of $Co(NH_3)_5Br^{2+}$ in acidic solution ($HClO_4$ or H_2SO_4) produces a low yield of the Br_2^- transient due to the combination of photoredox (producing Br·) and photoaquation (producing Br^-) produced by the unfiltered radiation,[10] coupled with the labile equilibrium 1.[6,7,11-13] In the absence of added Br^-, this transient is

$$Br\cdot + Br^- \rightleftharpoons Br_2^- \quad (1)$$

repressed in 50% 2-propanol, indicating an efficient scavenging of Br· (eq 2). We have also observed the decay

$$Br\cdot + (CH_3)_2CHOH \rightarrow Br^- + H^+ + (CH_3)_2\dot{C}OH \quad (2)$$

kinetics of the Br_2^- transient obtained in the flash photolysis of solutions 1 M in H_2SO_4, 1.0×10^{-5} M in $Co(NH_3)_5Br^{2+}$, 1.0×10^{-3} M in Br^-, and with $0 \leq [Ru(bipy)_3^{2+}] < 10^{-5}$ M.

We have found that the pseudo-first-order rate constant for decay of Br_2^- increased in proportion to $[Ru(bipy)_3^{2+}]$ (Figure 1), but the initial yield of Br_2^- was independent of $[Ru(bipy)_3^{2+}]$. The rate constant inferred from these data for the Br_2^- oxidation of $Ru(bipy)_3^{2+}$ (eq 3) is k_3 =

$$Br_2^- + Ru(bipy)_3^{2+} \underset{k_{-3}}{\overset{k_3}{\rightleftharpoons}} \{Ru(bipy)_3^{3+}, Br^-\} + Br^- \quad (3)$$

$(3.1 \pm 0.5) \times 10^9$ M^{-1} sec^{-1}. We have formulated 3 using an ion pair product (eq 4) in order that the reaction 3 be

$$Br^- + Ru(bipy)_3^{3+} \overset{K_0}{\rightleftharpoons} \{Ru(bipy)_3^{3+}, Br^-\} \quad (4)$$

microscopically reversible. The product $Ru(bipy)_3^{3+}$ can in principle oxidize Br^- (the reverse of 3) with an overall rate constant $k_{-3} = K_0 k_{-3}$. We have also investigated this reaction and find at 25° in 1 M H_2SO_4 and excess Br^- that the rate of formation of $Ru(bipy)_3^{2+}$ is pseudo first order, or $[Ru(bipy)_3^{2+}] = [Ru(bipy)_3^{3+}](1 - e^{-\kappa t})$, where κ is a nonlinear function of $[Br^-]$ for $0.1\ M > [Br^-] \geq 6 \times 10^{-3}$ M. When $[Ru(bipy)_3^{3+}]$ was corrected for ion pair formation assuming $K_0 \simeq 20$ M^{-1}, then κ was a second-order function of $[Br^-]$ under the conditions of our experiments; it should be noted that κ was found to be insensitive to variations in K_0 in the range $1\ M^{-1} < K_0 < 100\ M^{-1}$. If the induction period, τ_0 for buildup of $[Br_2^-]$ in these thermal reactions is very short (*i.e.*, less than 1 sec), then a steady-state treatment gives $\kappa \simeq k_{-3}K_0[Br^-]^2$ sec^{-1} with $k_{-3}K_0 = 6.2$ M^{-2} sec^{-1}. Our determination of k_3 in this medium (1 M H_2SO_4) may be used to find that $K_0/K_3 = 2 \times 10^{-9}$ M^{-1} (where $K_3 = k_3/k_{-3}$). This may be compared to a value of $K_0/K_3 = 1.7 \times 10^{-8}$ M^{-1} obtained at zero ionic strength from estimated values of reduction potentials for $Ru(bipy)_3^{3+}|Ru(bipy)_3^{2+}$ ($E^0 = 1.23$ V)[14] and $Br_2^-|Br^-$ ($E^0 = 1.69$ V).[7]

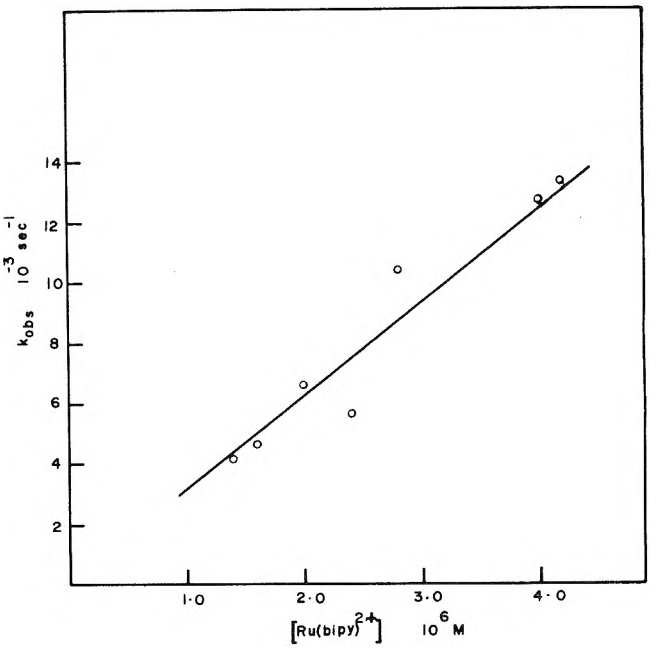

Figure 1. Pseudo-first-order decay rate constants of Br_2^- in the presence of $Ru(bipy)_3^{2+}$ in 1 M H_2SO_4.

In summary, our studies show (1) radicals are produced in the sensitized redox decomposition of $Co(NH_3)_5Br^{2+}$; (2) the primary radicals oxidize $Ru(bipy)_3^{2+}$ at nearly a diffusion-controlled rate; and (3) the product stoichiometry under all medium conditions is accounted for (within 10%) by the $Ru(bipy)_3^{2+}$ triplet sensitized formation of Co^{2+} and Br· followed by competitive scavenging of Br· by Br^-, $Ru(bipy)_3^{2+}$, and 2-propanol. We conclude therefore that at least 90% of the $Ru(bipy)_3^{2+}$ sensitized redox decomposition of $Co(NH_3)_5Br^{2+}$ proceeds by means of a triplet-to-triplet energy transfer mechanism. No evidence has been found to date which indicates that there is any contribution whatsoever from a mechanism involving electron transfer from an excited state of $Ru(bipy)_3^{2+}$.

(8) H. Cohen and D. Meyerstein, *J. Amer. Chem. Soc.*, **94**, 6944 (1972).
(9) (a) E. R. Kantrowitz, M. Z. Hoffman, and K. M. Schilling, *J. Phys. Chem.*, **76**, 2492 (1972); (b) E. R. Kantrowitz, J. F. Endicott, and M. Z. Hoffman, *ibid.*, **75**, 1914 (1971); (c) A. F. Vando, E. R. Kantrowitz, M. Z. Hoffman, E. Papacoustantinou, and J. F. Endicott, *J. Amer. Chem. Soc.*, **94**, 6655 (1972).
(10) A. W. Adamson, *Discuss. Faraday Soc.*, **29**, 163 (1960).
(11) L. I. Grossweiner and M. Matheson, *J. Phys. Chem.*, **61**, 1089 (1957).
(12) M. E. Langmuir and E. Hayon, *J. Phys. Chem.*, **71**, 3308 (1967).
(13) M. Schoeneshoefer and A. Henglein, *Ber. Bunsenges. Phys. Chem.*, **73**, 289 (1969).
(14) D. A. Buckingham and A. M. Sargeson, "Chelating Agents and Metal Chelates," F. P. Dwyer and D. P. Mellor, Ed., Academic Press, New York, N. Y., 1964, Chapter 6.

Department of Chemistry
Wayne State University
Detroit, Michigan 48202

P. Natarajan
J. F. Endicott*

Received August 21, 1972

Nonequilibrium Systems In Natural Water Chemistry

ADVANCES IN CHEMISTRY
SERIES No. 106

Thirteen papers from a symposium by the Division of Water, Air, and Waste Chemistry of the American Chemical Society, chaired by J. D. Hem.

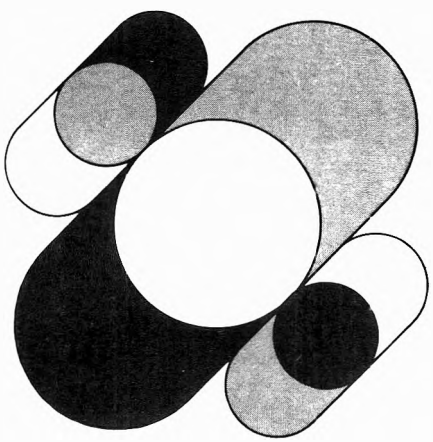

Which is more important: efficient exploitation of our natural resources or a stable ecosystem? What is the relationship between a wide variety of life forms and a healthy environment? What do geology and groundwater flow patterns have to do with the chemical composition of water? How may one predict when a lake will reach equilibrium or tell how long it has supported life?

This volume features:

- principles of water pollution control
- methods of analysis for dissolved chemicals
- mathematical models
- discussion of stratified lakes
- chemical processes in a carbonate aquifer
- decomposition and racemization of amino acids

---

342 pages with index Cloth (1971) $11.00
Postpaid in U.S. and Canada; plus 40 cents elsewhere.
Set of L.C. cards with library orders upon request.

Other books in the ADVANCES IN CHEMISTRY SERIES on water chemistry include:

No. 105 Anaerobic Biological Treatment Processes
Nine papers survey the state of the art of this natural process for waste treatment, with three papers on methane fermentation, others on process control and design. Considers volatile acid formation, toxicity, synergism, antagonism, pH control, heavy metals, light metal cations.
196 pages with index Cloth (1971) $9.00

No. 79 Adsorption from Aqueous Solution
Fifteen papers discuss thermodynamic and kinetic aspects of adsorption phenomena and the results of studies on a variety of adsorbate-adsorbent systems.
212 pages with index Cloth (1968) $10.00

No. 73 Trace Inorganics in Water
Research reports; analytical developments including atomic absorption, flame emission, and neutron activation; and broad reviews, such as effects of trace inorganics on the ice-water system and the role of hydrous manganese and iron oxides on fixing metals in soils and sediments
396 pages with index Cloth (1968) $12.50

No. 67 Equilibrium Concepts in Natural Water Systems
Sixteen papers represent the collaboration of aquatic chemists, analytical chemists, geologists, oceanographers, limnologists, and sanitary engineers, working with simplified models to produce fruitful generalizations and valuable insights into the factors that control the chemistry of natural systems.
344 pages with index Cloth (1967) $11.00

No. 38 Saline Water Conversion—II
Fourteen papers from two symposia; includes recovery of minerals from sea water, minimizing scale formation, wiped thinfilm distillation, diffusion still, solar flash evaporation, osmosis, electrodialysis (3 paper), research in Israel, hydrate process.
199 pages Paper (1963) $8.00

No. 27 Saline Water Conversion
Thermodynamics of desalting, solvent extraction, freezing, centrifugal phase barrier recompression distillation, multistage flash evaporation, ion exchange, osmosis, and electrochemical demineralization.
246 pages Paper (1960) $9.00

Order from: **Special Issues Sales, American Chemical Society**
1155 Sixteenth St., N.W., Washington, D.C. 20036

In Two Volumes

MACROMOLECULAR PHYSICS

Volume 1: **CRYSTALS, STRUCTURE, MORPHOLOGY AND DEFECTS**

by BERNHARD WUNDERLICH

This book presents an in-depth summary of the last 20 years of research on the crystal structure, crystal morphology, and crystal defects in linear high polymers. Although it emphasizes synthetic organic molecules, the book also covers inorganic and biological macromolecules. The book includes enough background material so that it can be used by researchers in several varied disciplines—including biochemistry and inorganic and organic chemistry, as well as solid state physics. It features extensive references to the original literature, about 300 photographs and diagrams, and about 40 tables, most of them newly compiled.

1973, 568 pp., $35.00

NONAQUEOUS ELECTROLYTES HANDBOOK, Volume 1

by G. J. JANZ and R. P. T. TOMKINS

This authoritative handbook provides quick and easy access to tabulated nonaqueous electrolyte data for over 200 solvents and 650 electrolytes in annotated form. It contains extensive cross-referencing by solutes and solvents, and is organized into well-defined areas—solvent physical properties, solvent purification, electrical conductance, diffusion, density, viscosity, and transference numbers.

Contents: Physical Properties of Solvents. Solvent Purification. Electrical Conductance. Diffusion. Density. Viscosity. Transference Numbers. Additional References and Data Sources. Compound Index.

1972, 1108 pp., $55.00

PROGRESS IN SURFACE AND MEMBRANE SCIENCE

Volume 7

(formerly Recent Progress in Surface Science)

edited by J. F. DANIELLI, M. D. ROSENBERG, and D. A. CADENHEAD

Tentative Contents: J. N. ISRAELACHVILI and D. TABOR: van der Waals Forces: Theory and Experiment. Yu. V. PLESKOV: Electric Double Layer on the Semiconductor-Electrolyte Interface. J. G. DASH: Long-Range and Short-Range Order in Adsorbed Films. F. C. GOODRICH: The Hydrodynamical Theory of Surface Shear Viscosity. B. R. MALCOLM: The Structure and Properties of Monolayers of Synthetic Polypeptides at the Air-Water Interface. G. J. SAFFORD and P. S. LEUNG: The Structure and Molecular Dynamics of Water. R. B. KEMP, G. M. W. COOK, and C. W. LLOYD: Glycoproteins in Cell Adhesion.

July 1973, about 275 pp., in preparation

ULTRACENTRIFUGATION OF MACROMOLECULES:

Modern Topics

by J. W. WILLIAMS

This book describes in detail significant recent research on ultracentrifugal analysis and its applications to organic high polymer chemistry and physical biochemistry. It outlines the basic theory of the sedimentation processes that occur in the ultracentifuge and concentrates on the sedimentation behavior of flexible chain macromolecules; self-association of protein and other molecular systems in nonideal solutions; and the combination of sedimentation equilibrium and velocity data as an approach to the analysis of protein self-association.

1972, 136 pp., $9.50

AEROSOLS AND ATMOSPHERIC CHEMISTRY

Proceedings of the American Chemical Society Kendall Award Symposium, Los Angeles, California, March 28–April 2, 1971, honoring Professor Milton Kerker, Clarkson College of Technology, Potsdam, New York

edited by G. M. HIDY

Increased awareness of the impact of aerosols on the environment—as well as the development of new and more sophisticated techniques for measuring aerosol properties—has led to a greater scientific interest in aerosol behavior. This volume presents a wide variety of studies on the physical chemistry of aerosols and their relationship to atmospheric chemistry. A large part of the book is devoted to detailed discussions of the Pasadena Smog Study—a major investigation of Los Angeles carried out at the California Institute of Technology in 1959.

1972, 376 pp., $14.50

PHYSICAL METHODS IN HETEROCYCLIC CHEMISTRY

edited by ALAN R. KATRITZKY

Volume 5—**HANDBOOK OF MOLECULAR DIMENSIONS: X-Ray Bond Angles and Lengths**

by P. J. WHEATLEY

So much progress has been made in the determination of molecular parameters that Volume 5 is devotec entirely to the values of bond lengths and angles obtained by X-ray crystallography. This handbook is a compendium of X-ray structure determinations of molecules and ions containing heterocyclic rings. It consists of a series of entries that lists the values of the more important lengths and angles in the heterocyclic component of each molecular species. Each entry is accompanied by a reference so that the reader can consult the original paper to assess the accuracy of the figures, and also includes the name of the compound used by the authors and the structural formula.

1972, 612 pp., $39.00

In Two Volumes

THE RADIATION CHEMISTRY OF MACROMOLECULES

edited by MALCOLM DOLE

Written by a number of experts in the field, these two volumes offer a complete and extensive survey of the chemical and physical effects of high energy radiations (including high speed electrons, gamma rays, and X-rays) on substances containing molecules of high molecular weight.

They cover all important advances in the field of radiation chemistry of high polymers that have had theoretical or practical significance during the past decade, as well as industrial applications of high energy radiations.

Volume 1

1972, 382 pp., $24.00

Volume 2

1972, 422 pp., $25.00

Two-Volume Set Price: $41.00

prices subject to change without notice